AD-A140 666 CHARGING AND DISCHARGING OF SPACECRAFT THERMAL CONTROL DIELECTRICS(U) MISSION RESEARCH CORP SAN DIEGO CA J D RIDDEL ET AL. 01 AUG 82 MRC/SD-R-105 DNA-TR-81-162 1/2

UNCLASSIFIED DNA001-81-C-0151 F/G 20/3 NL

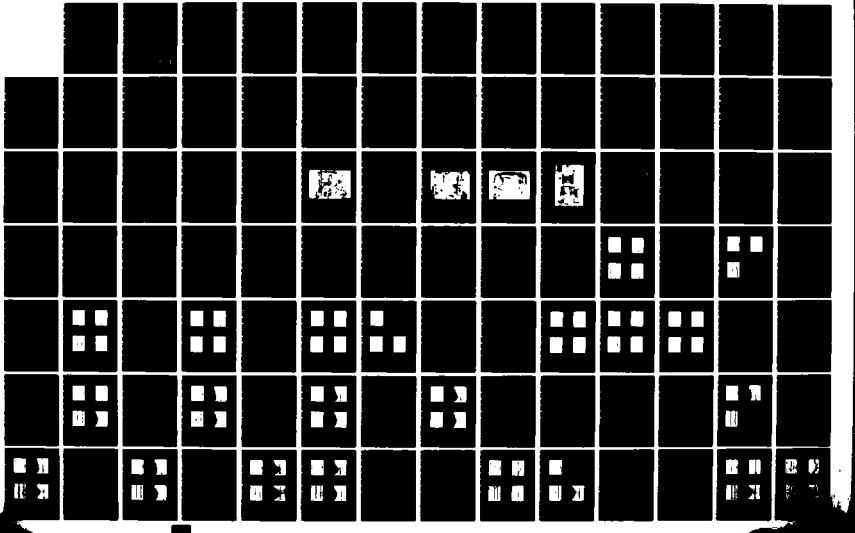

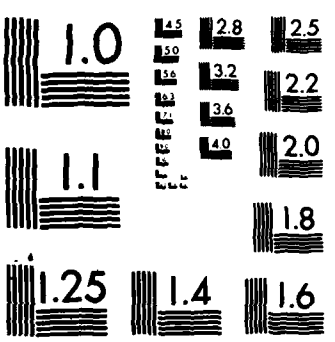

MICROCOPY RESOLUTION TEST CHART
NATIONAL BUREAU OF STANDARDS-1963-A

AD-E301367

AD-A140 666

(12)

DNA-TR-81-162

CHARGING AND DISCHARGING OF SPACECRAFT THERMAL CONTROL DIELECTRICS

J. D. Riddell
B. C. Passenheim
V. A. J. van Lint
B. D. Kitterer
J. P. Vahldieck
N. E. Hall

Mission Research Corporation
5434 Ruffin Road
San Diego, California 92123

1 August 1982

Technical Report

CONTRACT No. DNA 001-81-C-0151

APPROVED FOR PUBLIC RELEASE;
DISTRIBUTION UNLIMITED.

DTIC FILE COPY

THIS WORK WAS SPONSORED BY THE DEFENSE NUCLEAR AGENCY
UNDER RDT&E RMSS CODE B326082466 X99QAXVC00026 H2590D.

Prepared for
Director
DEFENSE NUCLEAR AGENCY
Washington, DC 20305

DTIC
ELECTE
S MAY 1 1984 D
B

84 03 16 019

UNCLASSIFIED

SECURITY CLASSIFICATION OF THIS PAGE (When Data Entered)

REPORT DOCUMENTATION PAGE	READ INSTRUCTIONS BEFORE COMPLETING FORM
1 REPORT NUMBER: DNA-TR-81-162	2 GOVT ACCESSION NO.: AD-A140 666
	3 RECIPIENT'S CATALOG NUMBER:
4 TITLE (and Subtitle): CHARGING AND DISCHARGING OF SPACECRAFT THERMAL CONTROL DIELECTRICS	5 TYPE OF REPORT & PERIOD COVERED: Technical Report
	6 PERFORMING ORG. REPORT NUMBER: MRC/SD-R-105
7 AUTHOR(s): J.D. Riddell, B.C. Passenheim, V.A.J. van Lint, B.D. Kitterer, J.P. Vahldieck, N.E. Hall	8 CONTRACT OR GRANT NUMBER(s): DNA 001-81-C-0151
9 PERFORMING ORGANIZATION NAME AND ADDRESS: Mission Research Corporation, 5434 Ruffin Road, San Diego, California 92123	10 PROGRAM ELEMENT, PROJECT, TASK AREA & WORK UNIT NUMBERS: Task X99QAXVC-00026
11 CONTROLLING OFFICE NAME AND ADDRESS: Director, Defense Nuclear Agency, Washington, D.C. 20305	12 REPORT DATE: 1 August 1982
	13 NUMBER OF PAGES: 184
14 MONITORING AGENCY NAME & ADDRESS (if different from Controlling Office)	15 SECURITY CLASS (of this report): UNCLASSIFIED
	15a DECLASSIFICATION DOWNGRADING SCHEDULE: N/A since UNCLASSIFIED

16. DISTRIBUTION STATEMENT (of this Report)

Approved for public release; distribution unlimited.

17 DISTRIBUTION STATEMENT (of the abstract entered in Block 20, if different from Report)

18 SUPPLEMENTARY NOTES

This work was sponsored by the Defense Nuclear Agency under RDT&E RMSS Code B326082466 X99QAXVC00026 H2590D.

19 KEY WORDS (Continue on reverse side if necessary and identify by block number)

Dielectrics	Glass
Spacecraft Charging	Mylar (Polyethylene Terephthalate)
Electron Radiation	Kapton (Polymide)
Discharge Propagation	Teflon (Polytetrafluoroethylene)
Electrical Conductivity	Spontaneous Discharges

20 ABSTRACT (Continue on reverse side if necessary and identify by block number)

Dielectric spacecraft thermal control materials: Mylar (polyethylene terephthalate), Kapton (polyimide), Teflon (PTFE) and glass second surface mirrors (optical solar reflectors) and solar cell cover glass (fused silica) were exposed to monoenergetic electron beams ranging in energy from 5 to 31 keV and current densities from $\sim$0.1 to $\sim$100 nA/cm^2, at room temperature, in a vacuum of $< 6 \times 10^{-6}$ torr. The charging characteristics, (which depend on conductivity, backscatter and secondary emission) have been documented.

DD FORM 1 JAN 73 1473 EDITION OF 1 NOV 65 IS OBSOLETE

UNCLASSIFIED

SECURITY CLASSIFICATION OF THIS PAGE (When Data Entered)

20. ABSTRACT (Continued)

Conductivity was inferred from slow charge leakage measurements. Numerous spontaneous discharge transient events have been recorded with segmented electrodes under the dielectrics, and a blow-off collector around the dielectric to determine the nature of the discharge (flashover, blow-off, punch-through) and the discharge propagation velocity. This provides direct evidence that some discharges propagate at 1×10^7 cm/s $\leq v \leq 6 \times 10^7$ cm/s (Kapton, Teflon, Mylar) whereas others apparently propagate faster than 2×10^8 cm/s (Glass and Mylar). A variety of discharge patterns were observed under very similar charging conditions.

TABLE OF CONTENTS

Section		Page
	LIST OF ILLUSTRATIONS	2
	LIST OF TABLES	11
I	INTRODUCTION	13
II	SPACECRAFT CHARGING AND DISCHARGING	16
	1. PURPOSE OF THE EXPERIMENT	16
	2. THEORY OF MEASUREMENT	17
	a. Concept Of The Experiment	17
	b. Types of Discharges	17
	c. Subsurface Burrowing With, or Without, Blow-Off	19
	d. Punch Through With Clean-Off	21
	e. Ion-Assisted Flashover (Brush Fire Model)	22
	3. DESCRIPTION OF THE APPARATUS	22
III	EXPERIMENTAL RESULTS	35
	1. KAPTON	35
	2. TEFLON	64
	3. MYLAR	87
	a. Microscopic Examination of Materials after Testing	113
	4. SOLAR CELL COVER GLASS (0.030 cm - 0.012")	117
	5. SECOND SURFACE MIRRORS	144
IV	SUMMARY OF RESULTS	166
	REFERENCES	174
Appendix	GLOSSARY	177

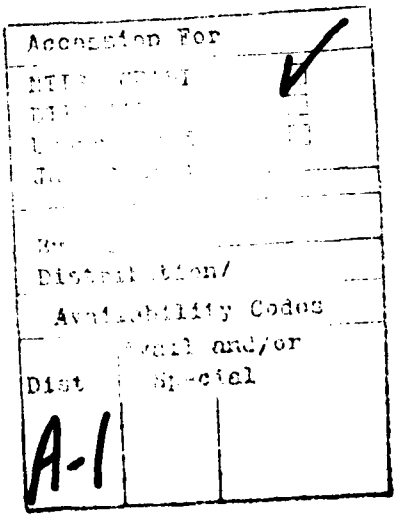

LIST OF ILLUSTRATIONS

Figure		Page
1.	Schematic representation of three kinds of dielectric discharge and the transient electrical signals anticipated from each. The first represents subsurface burrowing of charge with no blow-off. The second is subsurface burrowing of charge with clean-off initiated by a punch through. The third is surface flash-over with blow-off.	18
2a.	Schematic representation of experimental apparatus and electronics. From the top: (1) rastered focused electron gun in a negatively based Faraday cage, (2) the dielectric and noncontacting voltmeter, (3) the segmented electrodes. This figure continues in Figure 2b.	24
2b.	Schematic representation of the transient data acquisition apparatus showing the signal splitters, "first signal trigger" or "gate delay lines" and scopes. The delay lines and inherent delay in each scope resulted in apparent delays of ≈120 ± 10 ns for channels 1-4 and 200 ± 10 ns for channel 5. This figure is continued from Figure 2a.	25
3.	Pictorial representation of the experimental apparatus inside the vacuum bell jar.	28
4.	Photograph of the apparatus (partially assembled) showing (from the top): the grounded acceleration grid (a), the TREK probe (b), on the rotating arm (c), suspended over the sample and segmented back plate (d), the shutter (e), the turn table (f), high voltage electron gun wires (g) and bell jar base plate (h).	29
5.	Photograph of the apparatus from another aspect showing the second acceleration grid (a), above the TREK probe (b), on the swing arm (c), over the sample on the turntable (d), the shutter (e), gun wires (f), and base plate (g). Notice the razor blade clamps.	31
6.	Photograph of the apparatus showing the sample covered with the blow-off collector (slotted for the TREK) and screen.	32
7.	Photograph of the apparatus showing the bell jar (a), electron gun (b), high voltage Faraday cage (c), high voltage gun leads (d), supported on glass rods (e), above the low voltage Faraday cage and blow-off collector (f), surrounding the turntable supporting the sample.	33

LIST OF ILLUSTRATIONS (Continued)

Figure		Page
8.	Reproduction of the 25 cm diameter printed circuit board with its circumferential electrodes. A typical exposure area ≈4 × 8 cm is shown shaded and the 20 cm radius arc electrostatic voltmeter sweeps is shown as a dotted line.	34
9.	Typical potential profiles from a charging sequence for 0.005 cm Kapton exposed to ≈1 nA/cm^2 of 9 keV electrons. Exposure times (in seconds) are indicated.	36
10.	Asymptotic charging of 0.005 cm Kapton with 1.5 nA/cm^2 of 13 kV electrons.	38
11.	Asymptotic potential profile for 0.005 cm Kapton, charging with 1 nA/cm^2 of 18 kV electrons.	39
12.	Decay of potential with time after charging with 1 nA/cm^2 of 13 keV electrons. Shows increase in conductivity due to having room lights on.	40
13.	Another time decay of voltage showing the enhancement of conductivity due to room lights.	42
14.	Decay of potential over two hours after charging with 1 nA/cm^2 at 9 keV.	43
15.	Decay of potential over 1 hour and 20 hours, after charging at 5.3 nA/cm^2 and 18 kV. No lights on.	44
16.	Potential profiles before and after a discharge induced by the TREK probe striking the metal at the edge of the sample.	46
17.	Potential profiles showing two minutes of charging at 21 kV with 7 nA/cm^2, and profile after discharge induced by TREK striking metal at the edge of the sample.	47
18.	Transient record of discharge 11:48 on 0.005 cm Kapton exposed to 21 kV electrons.	48
19.	Potential profiles for 0.005 cm Kapton exposed to 4 nA/cm^2 of 26 kV electrons before and after discharges 3:05, 3:30, and 3:37.	49
20.	Transient record of discharge 3:37 on 0.005 cm Kapton exposed to 26 kV electrons.	50

LIST OF ILLUSTRATIONS (Continued)

Figure		Page
21.	Potential profiles for 0.005 cm Kapton exposed to 75 nA/cm^2 of 26 kV electrons before and after events 3:53, 3:59, and 4:05.	52
22.	Transient record of discharge 4:05 on 0.005 cm Kapton exposed to 75 nA/cm^2 of 26 kV electrons.	53
23.	Actual post-discharge profile and probable pre-discharge profile. Charging with 75 nA/cm^2 of 26 kV electrons.	54
24.	Transient record of discharge 4:44 on 0.005 cm Kapton exposed to 75 nA/cm^2 of 26 kV electrons.	55
25.	Two post-discharge profiles and estimated pre-discharge profile. Charging with 75 nA/cm^2 of 26 kV electrons.	56
26.	Transient record of discharge 4:55 on 0.005 cm Kapton exposed to 75 nA/cm^2 of 26 kV electrons.	57
27.	Transient record of discharge 5:22 on 0.005 cm Kapton exposed to 26 kV electrons.	58
28.	Three post-discharge potential profiles and estimated pre-discharge profile. Charging with 40 nA/cm^2 of 26 kV electrons.	60
29.	Transient record of discharge 5:30 on 0.005 cm Kapton exposed to 40 nA/cm^2 of 26 kV electrons.	61
30.	Transient record of discharge 5:45 on 0.005 cm Kapton exposed to 40 nA/cm^2 of 26 kV.	62
31.	Transient record of discharge 5:50 on 0.005 cm Kapton exposed to 40 nA/cm^2 of 26 kV.	63
32.	Discharge distance versus time after initiation for 23 transient discharge events on 0.005 cm Kapton.	65
33.	Potential profile measurements for 0.013 cm Teflon exposed to monoenergetic electrons of 6 kV, 11 kV, 18 kV, 21 kV, and 23 kV.	66

LIST OF ILLUSTRATIONS (Continued)

Figure		Page
34.	Transient record of discharge 3:17 on 0.013 cm Teflon exposed to 22 kV electrons.	67
35.	Post-discharge 3:17 potential profile and approximate pre-discharge profile charging with ≈ 1 nA/cm^2 of 23 keV electrons.	68
36.	Transient record of discharge 4:35 on 0.013 cm Teflon exposed to 29 kV electrons.	69
37.	Transient record of discharge 4:56 on 0.013 cm Teflon exposed to 29 kV electrons.	71
38.	Two post-discharge potential profiles and probable pre-discharge profile. Charging with 1 nA/cm^2 of 29 kV electrons.	72
39.	Transient record of discharge 5:47 on 0.013 cm Teflon exposed to 29 kV electrons.	73
40.	Decay of voltage overnight, after charging with ≈1 nA/cm^2 at 30 kV.	74
41.	Potential profiles before and after a discharge induced by TREK probe striking the metal at the edge of the sample. Charging with ≈0.5 nA/cm^2 of 23 kV electrons.	75
42.	Potential profiles before and after discharge event 6:04. Charging with 0.5 nA/cm^2 of 23 kV electrons for ≈20 minutes before sweep ⑥. Two minutes of 26 kV electrons before event 6:04 and sweep ⑦.	76
43.	Transient record of discharge 6:04 on 0.013 cm Teflon exposed to 26 kV electrons.	78
44.	Potential profiles shortly before and just after discharge event 6:25. Charging with 0.5 nA/cm^2 of 26 kV electrons.	79
45.	Transient record of discharge 6:25 on 0.013 cm Teflon exposed to 26 kV electrons.	80
46.	Post-discharge profile and estimated pre-discharge profile for event 10:50. Charging at 26 kV with 1 nA/cm^2.	81

LIST OF ILLUSTRATIONS (Continued)

Figure		Page
47.	Transient record of discharge 10:50 on 0.013 cm Teflon exposed to 26 kV electrons.	82
48.	Post-discharge profiles and estimated pre-discharge profile. Charging with 1 nA/cm^2 of 26 keV electrons.	83
49.	Transient record of discharge 11:40 on 0.013 cm Teflon exposed to 26 kV electrons.	84
50.	Transient record of discharge 12:11 on 0.013 cm Teflon exposed to 26 kV electrons.	85
51.	Compilation of the discharge propagation data for 0.013 cm (0.005") Teflon. Discharge distance versus time after initiation.	86
52.	Transient record of discharge 3:33 on 0.0025 cm Mylar exposed to 21 kV electrons.	88
53.	Transient record of discharge 3:25 on 0.0025 cm Mylar exposed to 21 kV electrons.	89
54.	Estimated pre- and actual post-discharge potential profiles. Charging with 2 nA/cm^2 of 21 keV electrons.	91
55.	Transient record of discharge 3:52 on 0.0025 cm Mylar exposed to 21 kV electrons.	92
56.	Transient record of discharge 4:01 on 0.0025 cm Mylar exposed to 21 kV electrons.	93
57.	Post discharge profile for events 4/1/82, 3:52 and 4:01. Since 3:52 involved only a small element of the sample, we think 3:52 is a reasonable approximation of pre-discharge profiles. The maximum potential on Mylar was limited by conductivity.	94
58.	Transient record of discharge 3:14 on 0.0025 cm Mylar exposed to 21 kV electrons.	95
59.	Approximate pre- and actual post-discharge 3:14 potential profiles. Charging with 2 nA/cm^2 of 21 keV electrons.	96

LIST OF ILLUSTRATIONS (Continued)

Figure		Page
60.	Transient record of discharge 5:41 on 0.0025 cm Kapton exposed to 21 kV electrons. Blow-off collector biased +200 V.	98
61.	Transient record of discharge 4:43 on 0.0025 cm Kapton exposed to 21 kV electrons. Blow-off collector biased +200 V.	99
62.	Approximate pre- and actual post-discharge 4:43 potential profiles. Charging with 2 nA/cm^2 of 21 keV electrons.	100
63.	Transient record of discharge 10:02 on 0.0025 cm Mylar exposed to 21 kV electrons.	101
64.	Projected pre- and measured post-discharge (10:02 and 10:38) voltage profiles for 0.0025 cm thick Mylar exposed to ≈1 nA/cm^2 of 21 kV electrons.	102
65.	Transient record of discharge 10:38 on 0.0025 cm Mylar exposed to 21 kV electrons. Blow-off collector biased at -200 V.	103
66.	Transient record of discharge 1:26 on 0.0025 cm Kapton exposed to 22 kV electrons. Channel 2 may reflect a punch-through.	105
67.	Transient record of discharge 1:44 on 0.0025 cm Kapton exposed to 22 kV electrons.	106
68.	Approximate pre-discharge and post-discharge potential profiles. Charging with 2 nA/cm^2 of 21 keV electrons.	107
69.	Transient record of discharge 3:13 on 0.0025 cm Mylar exposed to 22 kV electrons.	108
70.	Two potential profiles taken six days apart, with sample undisturbed between the traces.	109
71.	Discharge distances versus time after initiation for five discharge events on 0.0025 cm Mylar on 3/24/82.	111
72.	Discharge distance versus time after initiation for five discharge events on 0.0025 cm Mylar on 4/2/82.	112
73.	One particular isolated discharge track (TREE) (at 256 and 640X) in a forest of interlaced tracks on a Mylar sample that had experienced 30-50 events.	115

LIST OF ILLUSTRATIONS (Continued)

Figure		Page
74.	Microphotograph at 64X of a typical piece of Mylar that had experienced 30 to 50 discharges. Notice that most but not all tracks conform to a pattern of parallel lines intersecting at about 30°. On closer examination small branches in random directions are also apparent.	115
75.	A photograph at 64X magnification of a portion of a Mylar sample that has experienced 30-50 discharges, showing both regular or linear and dendritic or Lichtenberg-like discharge tracks.	116
76.	Microphotograph of a particular Lichtenberg like discharge site in Mylar at 640X magnification showing the small (≈1 μm) modules along the track.	116
77.	Typical potential profiles from a charging sequence of 0.030 cm solar cell cover glasses, exposed to 0.6 nA/cm^2 of 6 kV electrons. Exposure time (in seconds) are indicated.	118
78.	Charging to asymptotic profile on 0.030 cm cover glass with 3 nA/cm^2 of 11 keV electrons. Charging times in seconds. Delays without charging in minutes.	120
79.	Charging potential profiles on 0.030 cm cover glass with 0.7 nA/cm^2 of 16 keV electrons. Charging times are indicated.	121
80.	Recharging after discharge on 0.030 cm cover glass with 0.6 nA/cm^2 of 26 keV electrons, leading to a discharge.	122
81.	Comparison of potential profiles on 0.030 cm cover glass after a fifteen minute delay without lights and two minute delay with lights.	123
82.	Decay of voltage profile after 10 second charging with 4 nA/cm^2 of 11 kV electrons; 3 minutes between each sweep with beam off.	125
83.	Decay of voltage profile on solar cell cover glass overnight.	126
84.	Enhanced delay conductivity in the non-irradiate portion of solar cell cover glass - with the irradiated current density as a variable.	127

LIST OF ILLUSTRATIONS (Continued)

Figure		Page
85.	Enhanced delayed conductivity in the non-irradiated portion of solar cell cover glass.	128
86.	Charging a 0.030 cm cover glass with 0.5 nA/cm^2 of 16 keV electrons, leading to discharge 3:53.	134
87.	A transient record of discharge 3:53 on 0.03 cm solar cell cover glasses exposed to 0.5 nA/cm^2 of 16 kV electrons.	135
88.	Charging 0.030 cm cover glass at around 0.3 nA/cm^2, 26 kV, leading to discharge 4:42.	136
89.	Transient record of discharge 4:42 on 0.03 cm solar cell cover glass exposed to 26 kV electrons.	138
90.	Charging profiles on 0.03 cm cover glass with 0.3 nA/cm^2, then 0.6 nA/cm^2 of 26 keV electrons, leading to discharge 11:41.	140
91.	Transient record of discharge 11:41 on 0.03 cm solar cell cover glass exposed to 26 kV electron.	141
92.	Charging 0.03 cm cover glass with 1.3 nA/cm^2 of 26 keV electrons, leading to discharge 3:21. Charging times are indicated.	142
93.	Transient record of discharge 3:21 on 0.03 cm solar cell cover glass exposed to 26 kV electron.	143
94.	Perpendicular potential profiles on 0.03 cm cover glass intersecting at point A.	145
95.	Perpendicular sweeps on 0.030 cm cover glass intersecting at point B.	146
96.	Charging profiles for 0.02 cm thick second surface mirrors. Charging with a) 0.4 ± 0.2 nA/cm^2 of 6 keV electrons, then b) 0.3 ± 0.1 nA/cm^2 and 0.55 ± 0.15 nA/cm^2 of 11 keV electrons. Charging times for the sweeps shown were a) 10, 30, 100, 300, 600, 800, 1100 seconds at 6 kV, then b) 30, 100, 300, 600 seconds at ≈0.3 nA/cm^2 and 11 kV, the c) 200, 400, 600, 800, 1100, 1400 seconds at 0.55 ± 0.15 nA/cm^2 and 11 kV.	147

LIST OF ILLUSTRATIONS (Continued)

Figure		Page
97.	Continued charging of 0.02 cm glass mirrors with 2 nA/cm^2 of 16 keV electrons, then a discharge induced by 200 nA/cm^2 of 16 keV electrons.	149
98.	Recharging profiles of 0.020 cm second surface mirrors with 20 nA/cm^2 of 16 keV electrons, leading to discharge 3:04.	150
99.	Transient record of discharge 3:04 on 0.020 cm second surface mirrors exposed to 16 kV electrons.	151
100A.	Diagram of second surface mirror electrode arrangement. Buried charge resides at a , the metal back of the mirror is node b , and the segmented electrodes are at c .	152
100B.	Equivalent circuit for second surface mirrors, showing the buried charge (node a) metal mirror reflectors b , segmented electrodes c and switches d and e to represent punch-through and blow-off, respectively.	152
101.	Asymptotic profiles for 0.020 cm second surface mirrors exposed to 10 nA/cm^2. Beam energy at 11 kV, 12 kV, 13 kV, 14 kV. Discharge with beam at 15 kV.	154
102.	Recharging profiles for 0.020 cm second surface mirrors with 2 nA/cm^2 at 15 kV. Nearly identical asymptotic profiles at 2, 4, 7 nA/cm^2. At 12 nA/cm^2, sample discharged.	156
103.	Post-discharge profiles for 0.020 cm second surface mirrors after events 11:52 and 12:09. Estimate of profile before event 11:52.	157
104.	Transient record of discharge 11:52 on 0.020 cm second surface mirrors exposed to 16 kV electrons.	158
105.	Transient record of discharge 12:09 on 0.020 cm second surface mirrors exposed to 16 kV electrons.	159
106.	Decay of voltage profile on 0.020 cm second surface mirrors after 38 hours.	161
107.	Decay of voltage profile on 0.020 cm second surface mirrors over 138 hours, then 71 hours.	162

LIST OF ILLUSTRATIONS (Concluded)

Figure		Page
108.	Transient record of discharge 11:47 on 0.020 cm second surface mirrors exposed to 16 kV electrons. We believe this is a punch-through or flash-over to the substrate, with no blow-off.	163
109.	Stability of breakdown as a function of beam current and energy. Second surface mirrors.	165

LIST OF TABLES

Table		Page
1	Summary of discharge model characteristics.	23
2	Experiment apparatus.	27
3	Discharge propagation data.	110
4	Discharge propagation data.	110
5	Summary or catalog of events.	168

SECTION I
INTRODUCTION

The earth is surrounded by van Allen radiation belts composed of charged particles trapped by the earth's magnetic field. The exact composition of these belts (electrons, protons, their densities and energies) is constantly changing, varing by several orders of magnitude about the average depending on the orbit or location of the spacecraft, time of day, and recent solar activity. Both the electron and proton flux decrease as energy increases. Typically particle currents on the order of 1 nA/cm^2 with particle energies less than 10 keV impinge on the spacecraft. Spacecraft are usually partially to fully covered with dielectric materials designed to reflect the solar spectrum, (0.2 μm to 2.0 μm) and radiate away what solar power is absorbed, as well as radiate away waste heat from the electronics contained in the satellite. Most satellites derive all, or nearly all, their power from solar cells. Bare solar cells suffer radiation degradation with exposure to the van Allen belts. For that reason, and to protect them from pre-launch environments (dust and humidity), solar cells are covered with thin sheets of glass or fused silica.

There is no question that spacecraft experience dielectric charging to the point of discharge when exposed to space radiation. Furthermore a number of spacecraft malfunctions have been attributed to spacecraft discharge and electron caused ECEMP. The exact potentials and potential gradients on dielectrics depend on a balance between the incident charged particle spectrum, flux, backscatter, secondary electron emission, dielectric conductivity and vacuum ultraviolet photoemission.

The pre-charged condition of spacecraft is also relevant to systems genereated electromagnetic pulse (SGEMP). A negatively pre-charged body when exposed with x-rays will emit more charge, including some comparatively low energy secondary electrons, over greater distances, before space charge limiting occurs than will an initially uncharged body.

The topic of dielectric charging and discharging as applied to spacecraft has been the focus of numerous investigations and analyses over the past five to ten years. Many papers have been published, with perhaps the majority appearing in the annual IEEE Transactions of Space and Nuclear Radiation (the December issue of every year) and the biennial Air Force Geophysics Lab (AFGL) Spacecraft Charging Technology Conference Proceedings. Over the years engineering data on conductivity, secondary emission, scattering, and photoemission have been accumulated, and a number of models have been proposed to explain spacecraft charging, discharging and SGEMP.

The work reported here, and in a companion document titled "Electrical Conductivity of Spacecraft Thermal Control Dielectrics", (Ref. 1) was undertaken to measure the radiation-induced conductivity and the initiation and propagation of discharges for a number of thermal control materials under a range of conditions (such as flux, energy, temperature, and pressure) designed to mimic space exposure.

Section II presents several of the discharge models that have been proposed and the characteristics of the experimental observations one would anticipate from these models. Section II also describes the experimental apparatus and data acquisition system. Section III of the report presents selected data records from this study of Kapton, Teflon, Mylar, solar cell cover glass and second surface mirrors. Usually each record is a transient

---

1. J.D. Riddell, V.A.J. van Lint, B.C. Passenheim, "Charging and Discharging of Satellite Dielectrics," Mission Research Corporation Report, MRC/SD-R-70, January 1981.

(scope) recording of currents sensed by electrodes and a pre- and post-discharge potential profile. Most records are accompanied by a verbal interpretation.

We recognize that the large volume of data presented in this report may be somewhat confusing and difficult to assimilate. First there is a wide variety of observations. There are several different patterns and not all the patterns noted in this work can be fully explained by a single existing model of how discharges initiate and propagate. For this reason we chose to present most of the data with a minimum of manipulation. Each data record is accompanied by a description of what we consider the most relevant features of the record and our interpretation of what model best represents each event. The raw data record, however, is available for the reader, to support or refute a model or supposition not contained in this report.

Table 5, in Section IV, is intended to provide some small assistance to the reader by summarizing some of the more recurrent observations and citing those data records which exhibit these characteristics.

SECTION II
SPACECRAFT CHARGING AND DISCHARGING

1. PURPOSE OF THE EXPERIMENT

The purposes of this experiment were: 1) to measure the charging characteristics of several spacecraft thermal control dielectrics, second surface mirrors, and solar cell cover glasses, under space-like vacuum and irradiation conditions, and 2) to determine the conditions required to initiate and propagate an electrical discharge. We further determined a number of characteristics such as the maximum voltage the dielectric could sustain, the secondary electron "second cross-over" point, bulk field-induced conductivity and maximum potential gradients before and after spontaneous discharge. We also made transient measurements designed to determine the characteristics of spontaneous discharges, such as: the magnitude of the discharge, the propagation velocity, and the overall movement of the charge. This was an attempt to answer such basic questions as: does the discharge initiate and propagate as a surface flash-over, as a bulk punch-through, or subsurface discharge? Was the charge blown-off to the surroundings, or did it recombine with the image charge by going through, or flowing across, the dielectric?

This experiment complements the radiation- and field-induced conductivity experiment previously reported (Ref. 1).

2. THEORY OF MEASUREMENT

a. Concept Of The Experiment

In very general terms, the experiment involved irradiating a thin dielectric with energetic electrons which became imbedded in the sample. This process created a high potential on the surface of the dielectric which was measured periodically. After enough charge had been added, the potential reached a point where it became unstable, and discharged.

Beneath the sample were five metal electrode segments to "sense" the discharge. These electrodes were grounded through 5 Ω resistors, and the current through the resistors was monitored. A unit charge which moved directly from the buried charge layer (near the "front" or irradiated side) to the electrodes on the "back" of the sample - called a "punch-through" - was just a recombination of image charge. The movement resulted in a change in voltage at the surface of the sample, but only a small fraction of that unit charge appeared as current in the external circuit (C_∞/C_{sub} where C_∞ is capacitance to infinity and C_{sub} is the capacitance to the substrate). However, a unit charge which left a portion of the sample, toward anything but the back of the sample, caused a corresponding unit image charge to leave that electrode segment and flow as a current through the external circuit. Around the sample was a plate and screen designed to collect any charge which was emitted into the vacuum above the sample. We refer to this as the "blow-off collector".

b. Types of Discharges

Figure 1 schematically represents three kinds of dielectric discharge and the transient electrical signals anticipated from each.

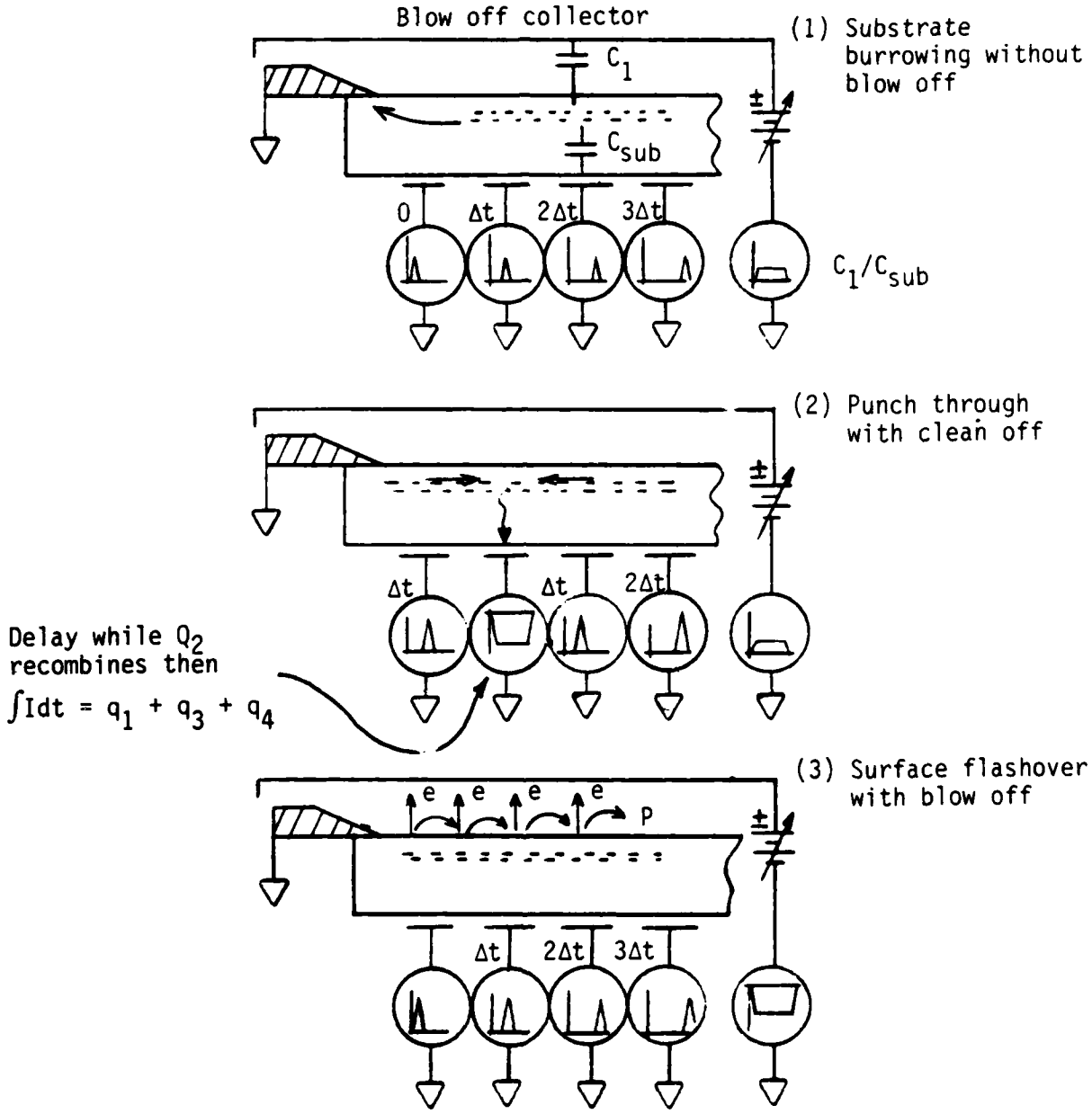

Figure 1. Schematic representation of three kinds of dielectric discharge and the transient electrical signals anticipated from each. The first represents subsurface burrowing of charge with no blow-off. The second is subsurface burrowing of charge with clean-off initiated by a punch through. The third is surface flash-over with blow-off.

c. Subsurface Burrowing With, or Without, Blow-Off

In this kind of discharge the imbedded electrons flow below the surface of the dielectric in channels or tubes producing the well known Lichtenberg figures. Microphotographs of dielectric surfaces showing subsurface mole-hole like structure and also surface tracks has been presented by Balmain, et al., and were observed in Mylar in this investigation. (Ref. 2-4).

The concept of this model is that upon initiation a plasma is formed within the dielectric which provides a conducting channel. The buried charge drains off through the plasma to a grounded conductor at the edge of the sample or to a point where the plasma emerges from the sample and is "blown-off". The discharge is initiated at an edge or at the location with the highest electric field, or weakest dielectric. Within this model, one may assume two charge flow patterns.

In the first version of this model, the discharge is initiated at a high field point or at a weak spot in the dielectric. The discharge then propagates as a column or tube of plasma. At the tip of the column, the fields are very high, and the currents are very concentrated, which generates a lot of Joule heating, which in turn converts more of the material to plasma. In this version, the charge is carried away as soon as it enters the plasma, which is considered to be a good conductor. This scenario might be likened to the propagation of nuclear lightning (Ref. 5) or the collapse of a string of dominoes. Since charge is going away from the tip of the column, a signal on a back surface electrode appears directly under the leading edge of the discharge as it propagates. It is quite possible that at some point, the plasma would break through the surface of the dielectric and charge would be "blown-off". Notice that this break through could also blow a neutral plasma (equal densities of electrons and ions) into this space. Hence, the signal on the blow-off collector could range from large

negative, if nearly all the charge comes out of the sample surface, to very small positive, if all charge flows straight to ground. In the latter case, the only signal on the blow-off collector is the image charge of that fraction of the total charge represented by the ratio of capacitance from the front of the sample to the back of the sample (C_{sub}) versus the capacitance from the front to the blow-off collector (C_1). Some of our observations are consistent with such a model.

A second version of this model seems to fit some other observations. According to this model the discharge burrows very quickly through the sample, leaving in its wake a network of conducting capillaries. If the ability for the charge to make its way out of the sample is constricted, then the potential throughout the plasma would remain essentially the same everywhere, and would drop uniformly with time. For an anlogy, one can imagine a bathtub full of water than has the drain open. The water can rearrange itself to keep level faster than it is draining out, so the water drops everywhere at the same time. For our experimental set-up, this "slow-draining" model would produce, on all segments, signals of comparable magnitude and duration, and beginning simultaneously (or at least within a time small compared to the duration of the event). Again, the blow-off signal could range from large negative to very small positive. This model bears some resemblance to natural lightning model in which an ionized track, called the stepped leader, forms first between a cloud and earth, followed by the main "strokes".

To complete each of these models, we must invoke a mechanism to get the charge from the bulk of the dielectric into the plasma channel. We suspect, and this is often supported by visual observation of discharges, that the discharge channels branch into smaller and smaller channels. Eventually the entire sample is completely laced with tiny capillaries. Presumably, the charges embedded in the dielectric around these capillaries feel very strong fields (and possibly a fair amount of thermal activation) which

allows the buried charge to move into the plasma channel without heating the solid dielectric to the extent required to generate a plasma. Numerous theories and some measurements support field-enhanced conductivity. Thus, the entire sample can be nearly completely discharged without turning the whole buried charge layer into a plasma.

d. Punch-Through With Clean-Off

In this model, the discharge is initiated at a weak spot in the dielectric, burning a trail from the buried charge layer to the back electrode. It then propagates radially, either subsurface or at the surface, to cover the rest of the buried charge layer. The charge from much, or all, of the sample drains off through the punch-through site to the rear electrode under that site. As with the preceeding model, the propagating discharge will be first seen either in a) the adjacent segmented electrode, or b) simultaneously on all electrodes other than the one under the punch-through site; the pattern of the signals depending on whether charge from the vicinity of the punch-through must first be removed before neighboring charge can move (dominoe model) or charge over the entire sample area moves in concert but is restricted in getting out (draining tub model).

The signal on the electrode where the punch-through initiated is initially small as the real and image charge recombines. Thereafter that signal becomes larger and negative, from the real flow of negative electrons from other areas on the sample to that electrode. It persists while the charge originally over the other electrodes flows to ground through the punch-through channel. As with the previous model, the blow-off signal can be anything from very small positive to large negative. In this case, however, the signal cannot be as large as the total charge moved on the sample, because of the charge that "punched-through".

e. Ion-Assisted Flashover (Brush-Fire Model)

This discharge model was independently proposed by MRC and TRW in the 1979 Spacecraft Charging Technology Conference (Ref. 6) and more recently by Inouye et al., (Ref. 7). In this model the discharge is initiated as blow-off or punch-through at a high field point or at a weak spot in the dielectric. The initial discharge releases nearby trapped electrons, and also produces a few ions which are emitted into the vacuum area above the dielectric. Such ions are attracted toward the negatively charged dielectric even as the released electrons are swept away. The collision of the positively charged ions with the negatively charged dielectric frees more electrons and ions. The electrons mostly blow off, while the ions tumble across the dielectric as a propagating wave front at a comparatively slow rate ($\approx 10^7$ cm/s). In this model the charge released propagates radially from the point of initiation, and the blow-off collector signal is mostly negative, (i.e., it is collecting the blow-off electrons) and persists the entire duration of the discharge.

The data presented here should be examined with these models in mind in order to distinguish which (if any) of them are most probable. The summary of these models is presented in Table 1 to clarify how they could be distinguished when looking at the data.

3. DESCRIPTION OF THE APPARATUS

The experimental apparatus used in this investigation is schematically represented in Figure 2. Mono-energetic electrons of energies from

6. B.C. Passenheim and V.A.J. van Lint, "Charging and Discharging Teflon," pg. 52 in the 1980 Spacecraft Charging Technology Conference Proceedings, NASA pub. 2182, AFGL-TR-81-0270.

7. G.T. Inouye, "Brushfire Arc Discharge Model," pg. 133 of the 1980 Spacecraft Charging Technology Conference Proceedings, NASA pub. 2182, AFGL-TR-81-0270.

TABLE 1. SUMMARY OF DISCHARGE MODEL CHARACTERISTICS.

Model	Back Surface Sensors	Blow-off Collector	First Appears
Subsurface Burrowing	All Positive polarity (charge removal)	Small positive, long (capacitive), or any size negative, possibly delayed (real charge)	Either at initiation site or simultaneously everywhere.
Punch-Through	Negative (after delay) at initiation site, Positive elsewhere	Small positive, long (capacitive), or negative, less than total charge, possibly delayed	Either at neighbor of initiation site or simultaneously everywhere
Ion-Assisted Flashover (brush-fire)	Positive polarity (charge removal)	Large Negative, long (total charge available)	At initiation site

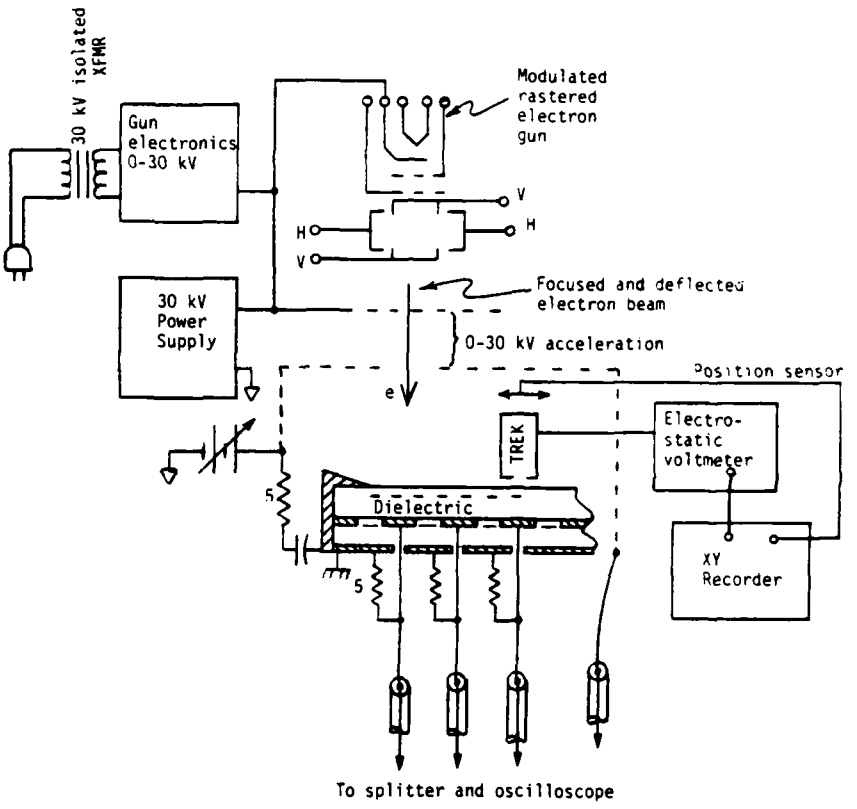

Figure 2a. Schematic representation of experimental apparatus and electronics. From the top: (1) rastered focused electron gun in a negatively based Faraday cage, (2) the dielectric and noncontacting voltmeter, (3) the segmented electrodes. This figure continues in Figure 2b.

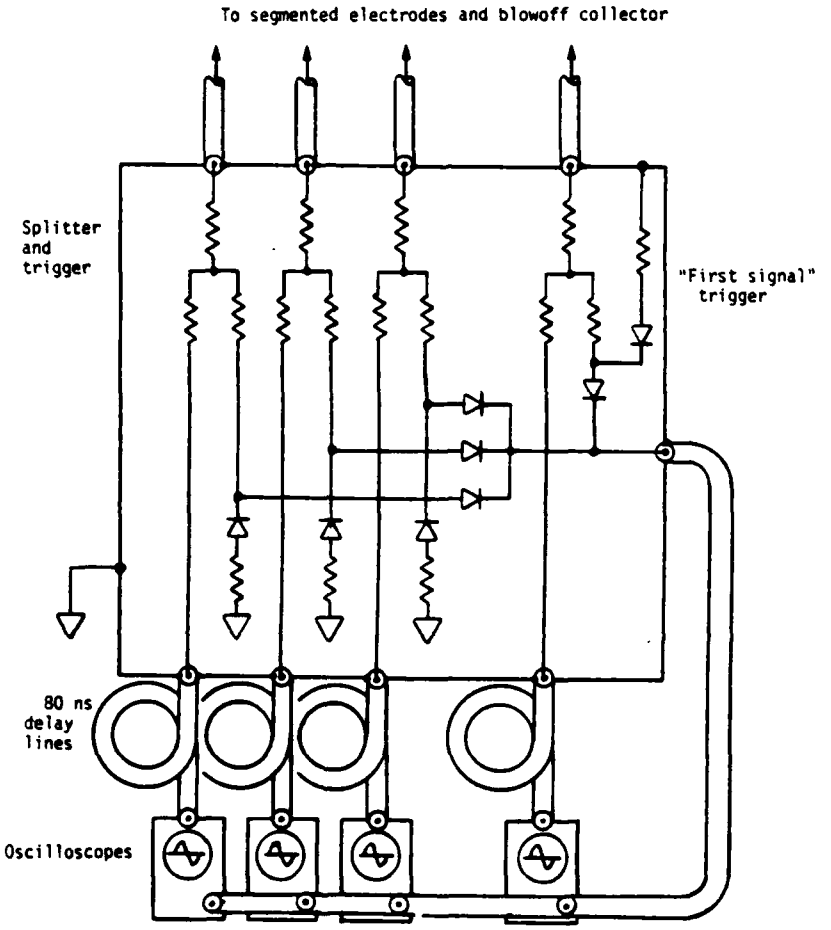

Figure 2b. Schematic representation of the transient data acquisition apparatus showing the signal splitters, "first signal" trigger, "or" gate delay lines and scopes. The delay lines and inherent delay in each scope resulted in apparent delays of ~ 120 ± 10 ns for channels 1 - 4 and 200 ± 10 ns for channel 5. This figure is continued from Figure 2a.

-5 to -31 kV were provided by a biased, modulated, rastered electron gun schematically represented at the top of Figure 2. The focused and deflected electron beam was accelerated across the 5 cm gap between two grids. The electron gun was contained in one (window-screen) Faraday cage. A screened enclosure completely surrounded the dielectric sample, serving as a second Faraday cage to preclude further deflection of the electrons after acceleration (except by the sample). The dielectric sample shown in the center of the figure was 25 cm (10") in diameter and rested horizontally on a printed circuit (PC) board. This double-clad PC board had been etched to leave concentric rings around the circumference which provided the electrodes for the back of the sample. The PC board rested on a turntable so that different portions of the sample could be irradiated at a different times. The dielectric was pressed to the PC board support plate with clamps around the periphery. The dielectric potential was periodically sampled by sweeping a TREK non-contacting electrostatic voltmeter over the sample and recording the profile on an XY recorder. The TREK location is represented by the horizontal displacement, (X), the TREK voltage by the vertical displacement (Y). Each of the circumferential electrodes was attached to ground through a 5 Ohm resistor, and the signals induced on the electrodes were transmitted to the external instrumentation via 50 Ω coaxial cables. All five electrodes and the blow-off collector passed through a divide-by-2 splitter box. Half of each signal continued on through approximately 80 ns delay lines to be displayed on oscilloscopes. The other half of each signal was combined in a diode "or-circuit" to provide a "first-signal" trigger to all the oscilloscopes simultaneously on the arrival of the first impulse. The experimental apparatus employed in this investigation are listed in Table 2.

Figure 3 is a pictorial representation of the experimental apparatus inside the vacuum bell jar, labeling the various pieces which are also apparent in the ensuing photographs. Figure 4 is a photograph of the apparatus partially assembled emphasizing the sample holding turntable and the TREK probe. At the top of this figure is the grounded acceleration grid

TABLE 2. EXPERIMENT APPARATUS.

Vacuum System (VEECO)
- Controller
- Gauges (thermocouple and ion)
- Vacuum Rotary Feed-thrus (Ferro-fluidic)
- Electrical Feed-thrus

Electron Gun
- Intensity/Focus/Deflection
- High Voltage (Spellman 30 kVDC Supply)
- Z Axis Intensity
- (TRS80 Controlled)
- Pattern Monitor
  - (Sodium salicylate and CRT)

Current Measurement
- Keithly Pico ampmeter (4145)
- Segmented Shutter
- Sweeping Faraday Cup

Potential Measurement
- TREK Electrostatic Voltmeter (Model 340 HV)
- Position Sensor (resistive bridge)
- X-Y Recorder (d,V) Hewlett-Packard 7046A)

Transient Measurements
- 6 Scope channels (Tektronix 7844 and 7603)
- 5 segments
- 1 blowoff collector

Variables
- V, J, J(xy)
- Edge/no edge
- Material

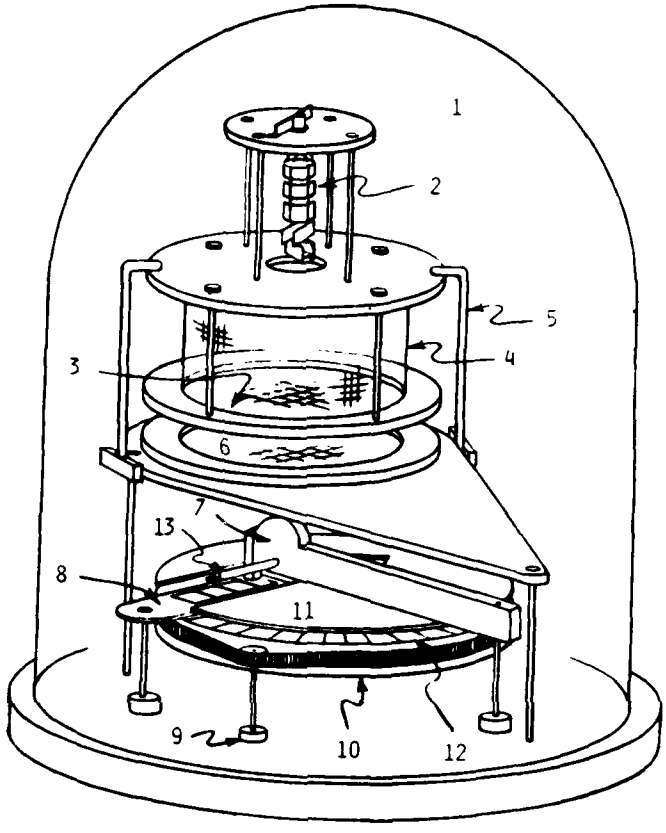

1. Bell jar
2. Electron gun
3. 0-30 kV acceleration grid
4. High voltage cage
5. Glass rod standoff's
6. Grounded acceleration grid
7. Electrostatic voltmeter on rotary feed through
8. Shutter on rotary feed through
9. Turn table drive feed through
10. Turn table
11. Aperture plate and blow-off collector
12. Sample edge clamps (razor blades)
13. Sweeping Faraday Cup

Figure 3. Pictorial representation of the experimental apparatus inside the vacuum bell jar.

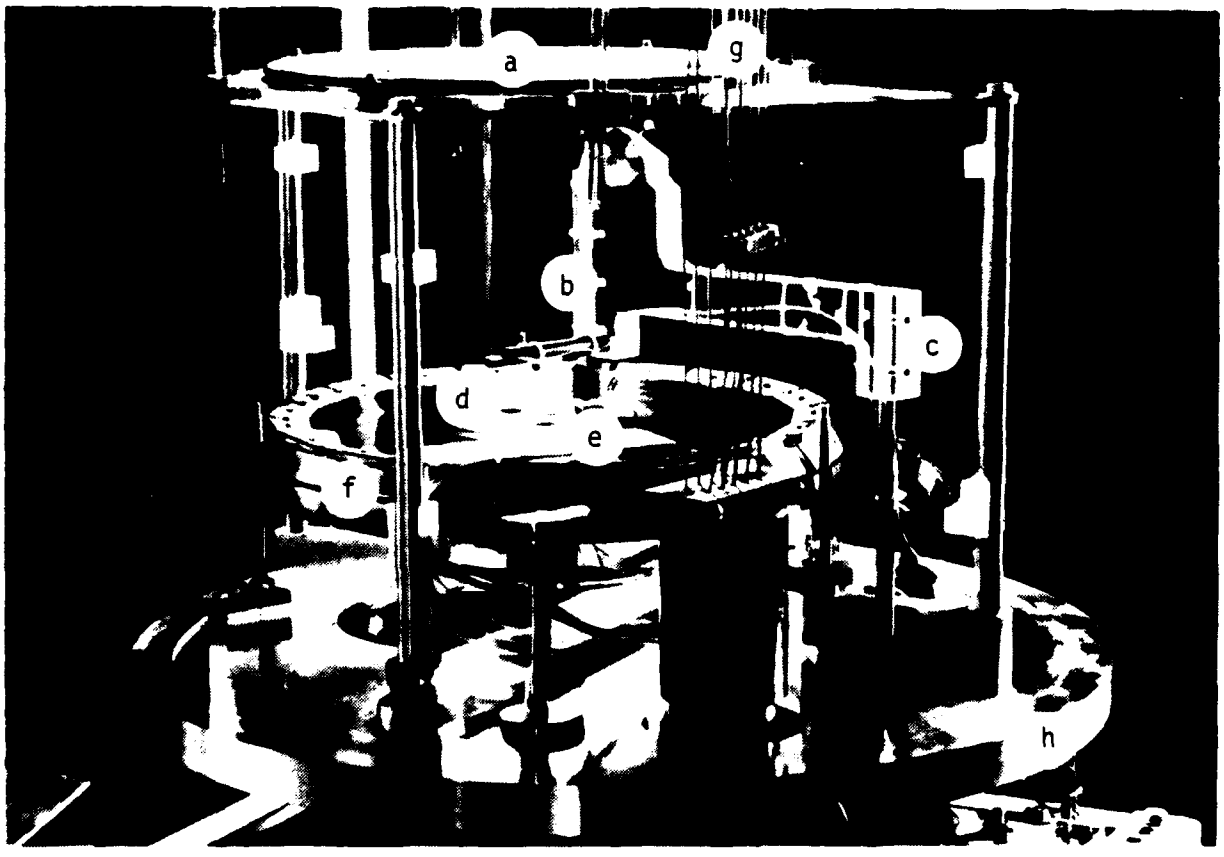

Figure 4. Photograph of the apparatus (partially assembled) showing (from the top): the grounded acceleration grid (a), the TREK probe (b), on the rotating arm (c), suspended over the sample and segmented back plate (d), the shutter (e), the turn table (f), high voltage electron gun wires (g) and bell jar base plate (h).

which was a stainless steel screen of 0.0025 cm (0.001") woven wire with greater than 90% transparency. Also apparent in this figure is the rotating swing-arm, supporting the TREK probe and the sweeping Faraday cup; the rotating shutter; and the turntable rotator. The circumferential electrodes are just visible through the transparent sample which is held in place with 20 clamps made of single-edge razor blades around the periphery.

Figure 5 is a photograph of the same apparatus from another aspect. Again the second acceleration grid is visible at the top of the picture. The TREK on its swinging arm is in the center of the picture. The segmented shutter for monitoring the electron beam is seen to the right of the figure. The turntable, with the transparent sample, circumferential electrodes and edge clamp appears in the center of the figure. All this apparatus is supported on and clamped to the base plate of the vacuum system.

Figure 6 is another photograph of the apparatus from approximately the same aspect as the preceding photograph with the blow-off collector plate and Faraday cage screen installed.

Figure 7 is a photograph of the apparatus assembled, but with the bell jar removed, from an aspect which is approximately that of Figure 3. In this photograph the bell jar is located in the upper left hand corner. The electron gun and high voltage Faraday cage are at the top. The grounded Faraday cage and sample are at the bottom center surrounding the TREK, shutter and turntable. The bell jar support plate is at the bottom.

Figure 8 is a photograph of the segmented printed circuit board with a typical irradiation area and the TREK sweep included.

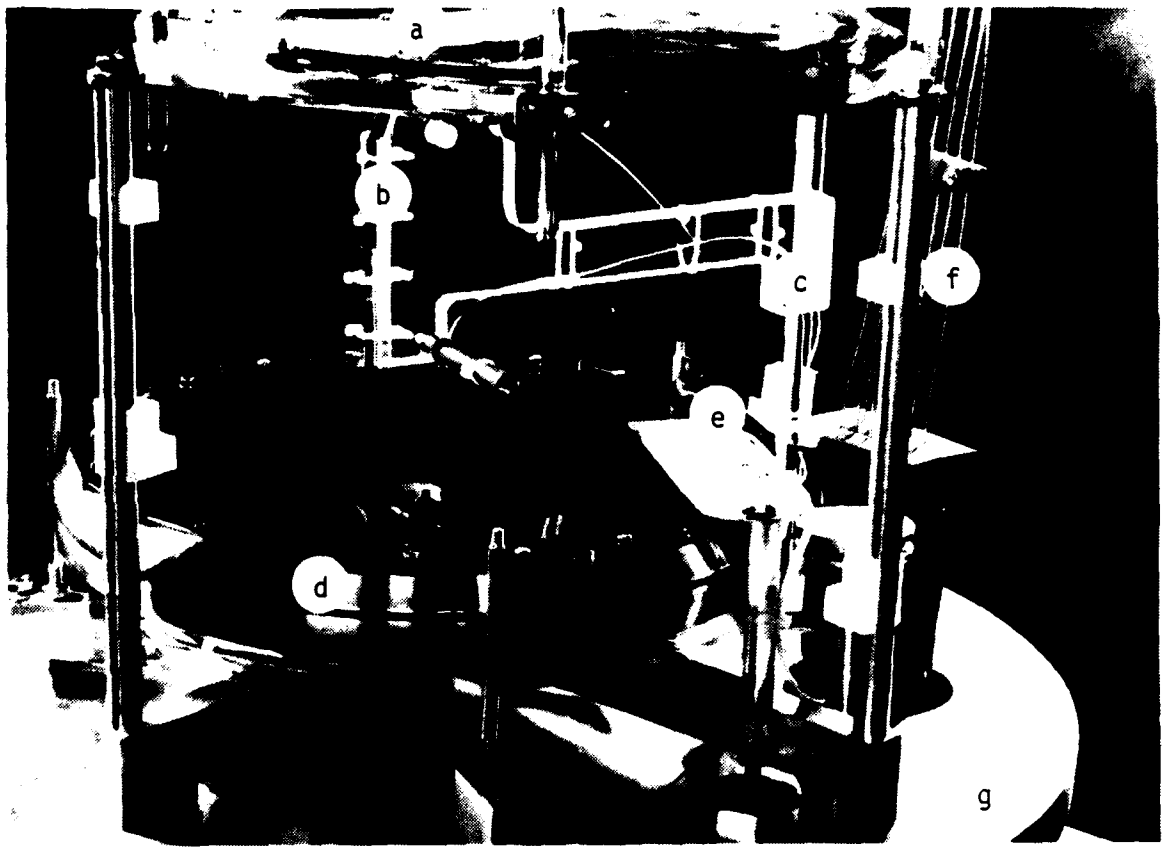

Figure 5. Photograph of the apparatus from another aspect showing the second acceleration grid (a), above the TREK probe (b), on the swing arm (c), over the sample on the turntable (d), the shutter (e), gun wires (f), and base plate (g). Notice the razor blade clamps.

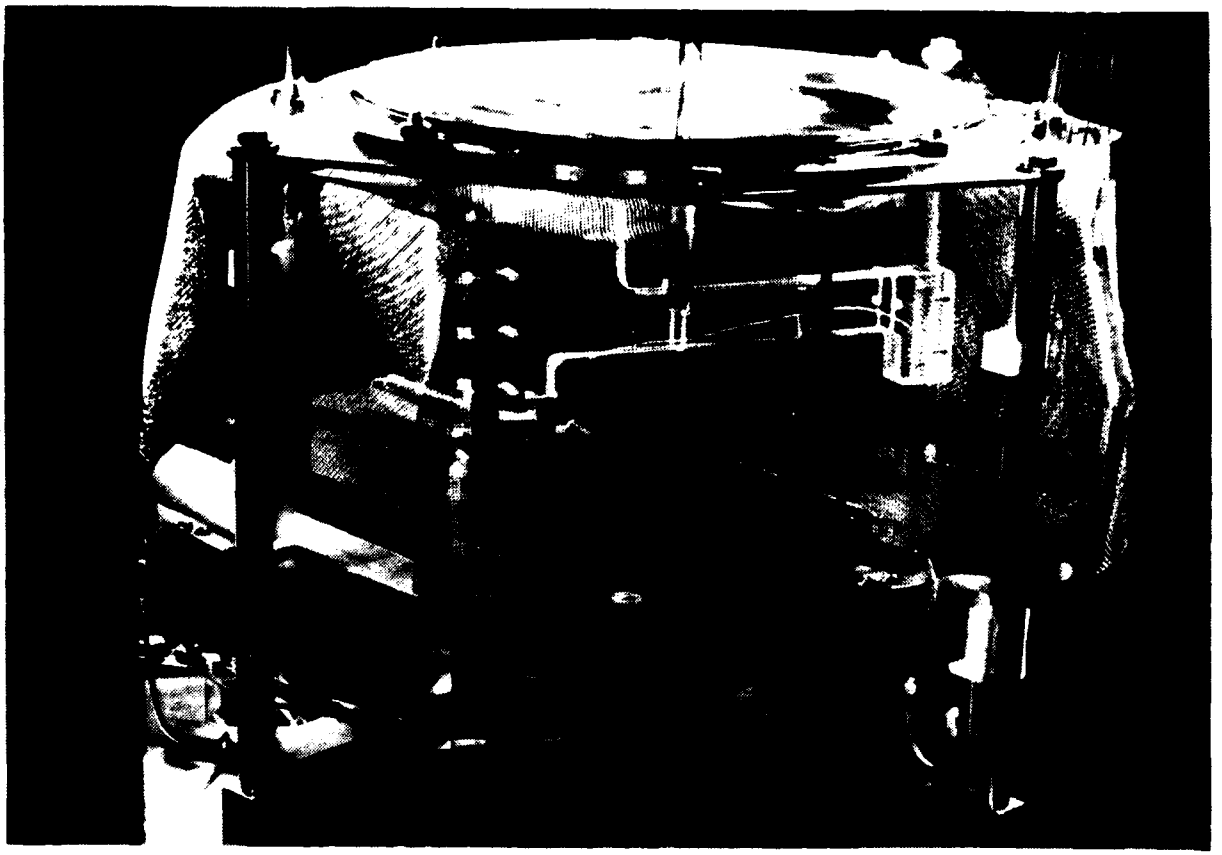

Figure 6. Photograph of the apparatus showing the sample covered with the blow-off collector (slotted for the TREK) and screen.

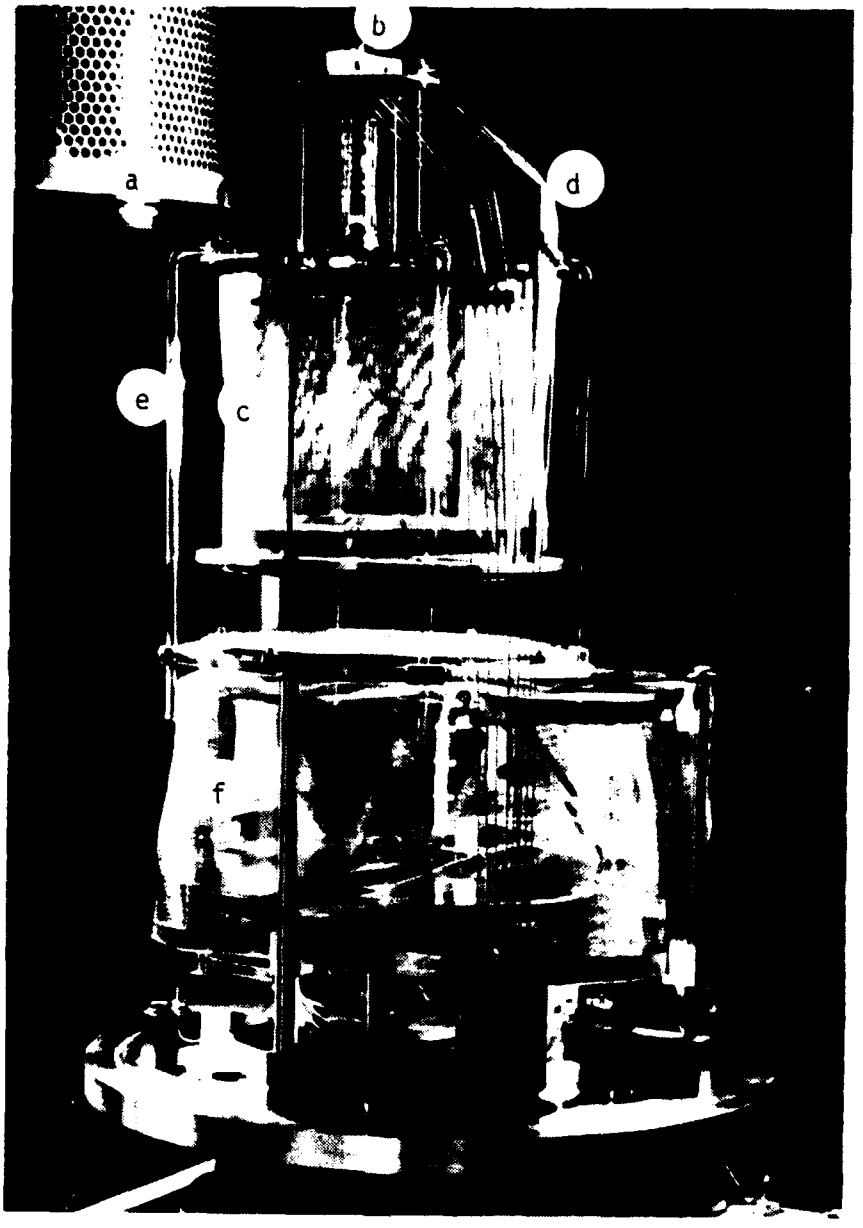

Figure 7. Photograph of the apparatus showing the bell jar (a), electron gun (b), high voltage Faraday cage (c), high voltage gun leads (d), supported on glass rods (e), above the low voltage Faraday cage and blow-off collector (f), surrounding the turntable supporting the sample.

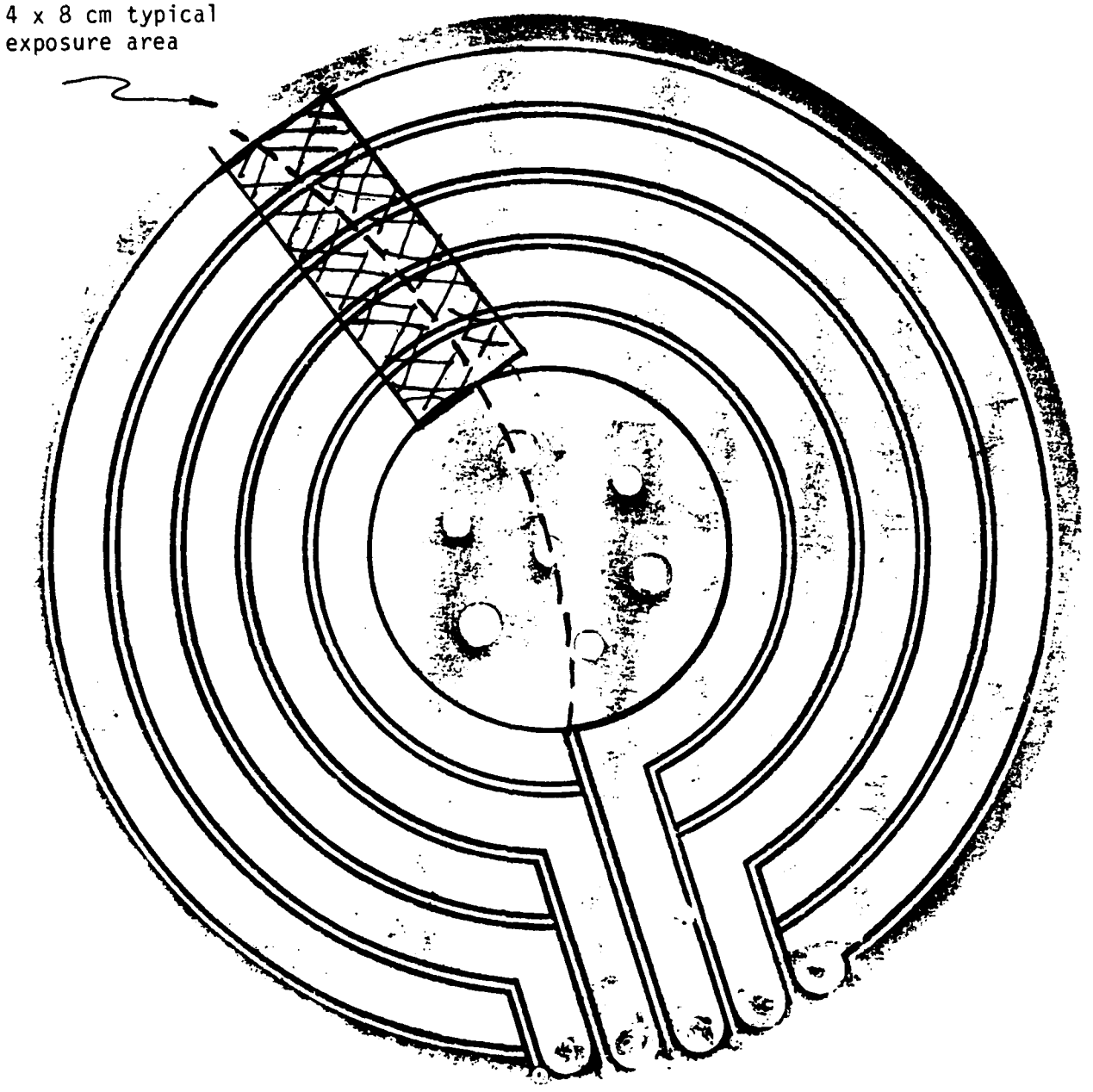

Figure 8. Reproduction of the 25 cm diameter printed circuit board with its circumferential electrodes. A typical exposure area ≈4 × 8 cm is shown shaded and the 20 cm radius arc electrostatic voltmeter sweeps is shown as a dotted line.

SECTION III
EXPERIMENTAL RESULTS

1. KAPTON

Figure 9 is a typical charging sequence for 0.005 cm (0.002") Kapton exposed to 1 nA/cm^2 of 9 keV photoelectrons. This trace shows the potential as a function of position as measured with a Trek probe which swings on a 20 cm pivoted arm describing an arc across the dielectric surface. This family of profiles is a result of charging for 3, 10, 30, 100, 300, 600 and 900 seconds. Apparently the center of the sample from ≈ -5 to +5 cm was accidentally charged by electrons oversprayed or scattered during the gun tuning process. The part of the sample which was intentionally irradiated, from ≈ 5 to 13.5 cm was protected with mechanical shutter during the tuning process. The gaps between the segmented electrodes are clearly distinguished by the double humped peaks. This results because the capacitance between the buried charge and ground is less over the fiberglass than over the circumferential electrodes, so equal charge density results in higher voltage. The double nature of the peak results because there is a thin grounded ring of copper between each electrode. Thus, the TREK is sweeping over a wide copper electrode, then a thin strip where the copper, has been removed exposing fiberglass, then a thin strip of copper, then another thin strip of fiberglass, then the next wide copper electrode.

This sample attained an asymptotic voltage of ≈ 7.2 kV which is 1.8 kV less than the charging potential. Note: The highest profile is probably slightly less than the asymptotic form, because the time involved would have been excessively long at this current density. At higher

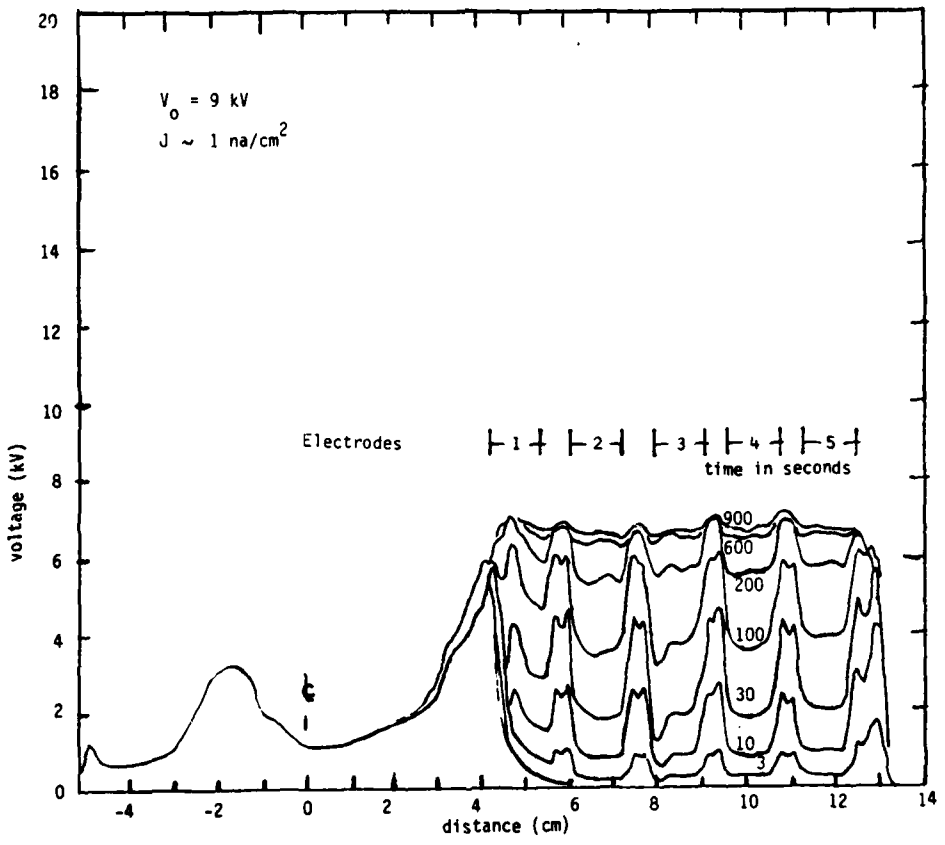

Figure 9. Typical potential profiles from a charging sequence for 0.005 cm Kapton exposed to ≈1 nA/cm^2 of 9 keV electrons. Exposure times (in seconds) are indicated.

currents, the voltage over the copper eventually rose to match the peaks and produced a smooth profile.

Figure 10 shows the end of a charging sequence for 0.002" Kapton using 1.5 nanoamp/cm^2 of 13 kV electrons (10 min. and 20 min. of charging). This sample attained an asymptotic voltage of ≈ 11.2 kV, also 1.8 kV less than the charging potential.

Figure 11 shows an asymptotic profile for 0.002" Kapton irradiated with ≈ 1 nA/cm^2 of 18 keV electrons. This sample achieved a peak asymptotic potential of about 14.6 kV which is 3.4 kV less than the charging voltage. At low charging voltages the sample equilibrium potential is probably established by the second cross-over point where secondary emission equals incident current which we would infer to be ≈ 1.8 kV. At higher potentials and low currents the equilibrium potential in Kapton is probably dominated by field enhanced conductivity which is reported to have a functional form (Ref. 8).

$$\sigma = \sigma_0 \left\{ \frac{2 + \cosh\left(\beta_F E \delta / 2kT\right)}{3} \right\} \frac{2kT}{eE\delta} \left(\sinh \frac{eE\delta}{2kT} \right)$$

where

$\beta_F = \sqrt{e^3/\pi\varepsilon\varepsilon_0} = 1.22 \times 10^{-23}\ e^{-3/2}$

δ = defect-defect separation

σ is conductivity

E is electric field

k is Boltymann's constant (1.38×10^{-23} joules/K)

e is an electron charge (1.6×10^{-19} coul)

T is absolute temperature

Figure 12 shows the potential profile for 0.002" thick Kapton as a function of time and illumination after irradiation. The four traces were taken at

8. V. Adamec and J.H. Calderwood, "Electrical Conduction in Dielectrics at High Fields," J. Phys. D, 8, 551, (1975).

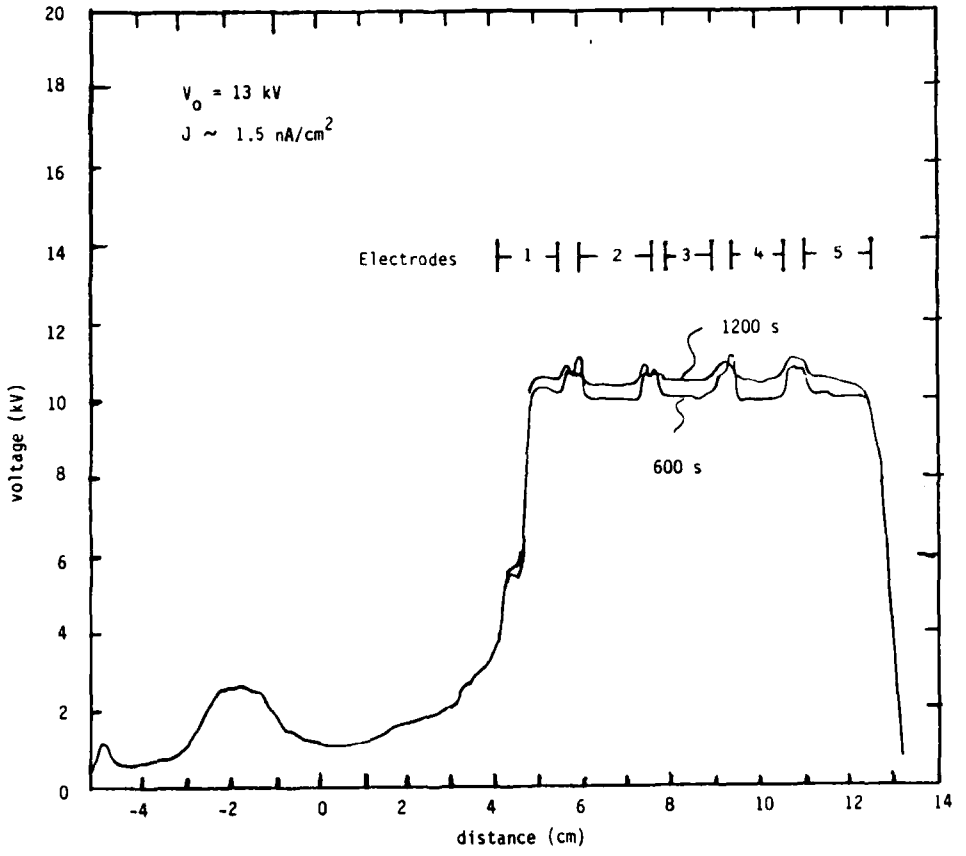

Figure 10. Asymptotic charging of 0.005 cm Kapton with 1.5 nA/cm^2 of 13 kV electrons.

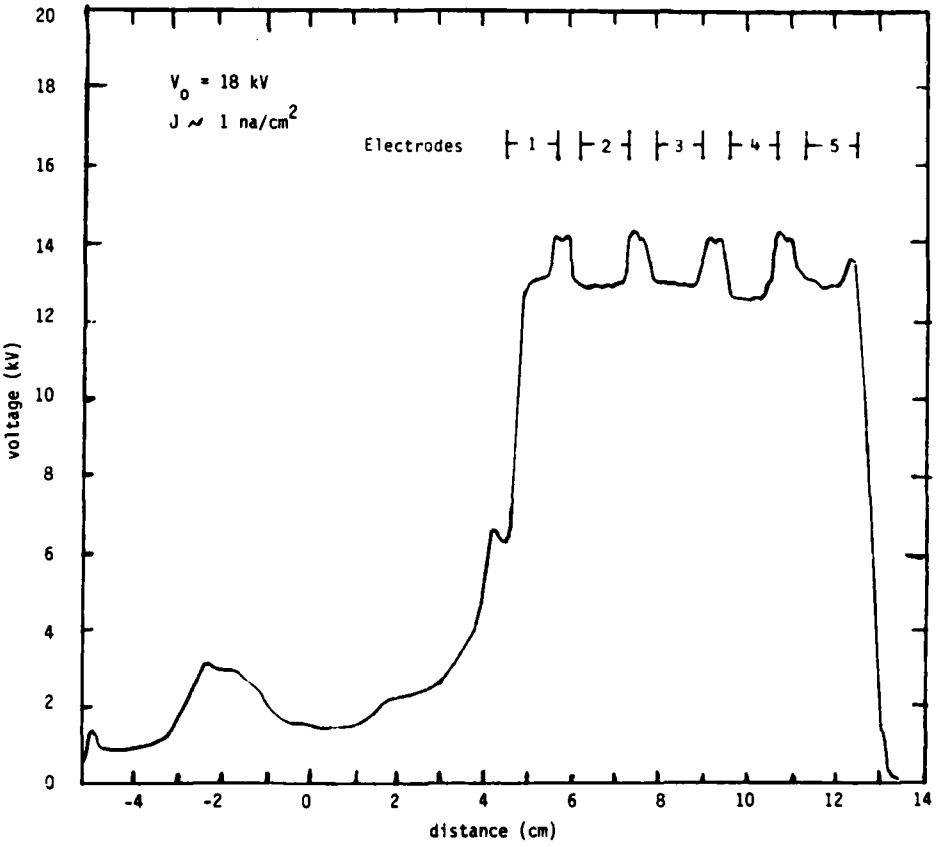

Figure 11. Asymptotic potential profile for 0.005 cm Kapton, charging with 1 nA/cm^2 of 18 kV electrons.

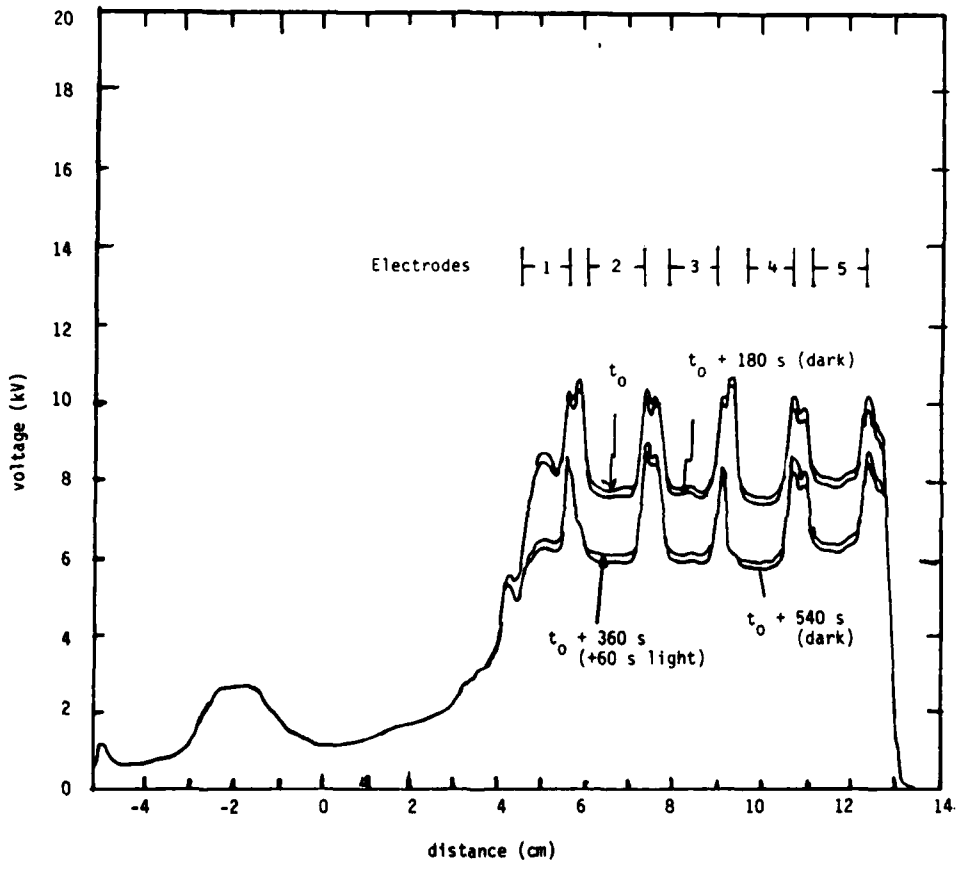

Figure 12. Decay of potential with time after charging with 1 nA/cm^2 of 13 keV electrons. Shows increase in conductivity due to having room lights on.

equally spaced time intervals of 3 minutes. The sample had been charged with 1 nA/cm^2, 13 kV electrons. The sample was in the dark between Trace 1 and Trace 2, and between Trace 3 and 4. The sample was illuminated for 1 minute with ordinary fluorescent room lights filtered by the bell jar and blow off screen for 1 minute between Trace 2 and 3. Although we have no direct measurement, we estimate this irradiance must have been less than 10^{-2} W/cm^2 with virtually no ultraviolet. From this data we find the dark conductivity to be $\approx 3.5 \times 10^{-17}$ (ohms cm)$^{-1}$. Conductivity during illumination is $\approx 1 \times 10^{-15}$ (ohms cm)$^{-1}$. It is interesting to note that the accidental charge which had been deposited 6 or 7 hours earlier during the electron gun tuning, located between -5 and +5 cm is apparently not subject to this photo-enhanced photoconductivity.

Figure 13 is another example showing the decay of voltage with lights on and with lights off. The sample had been left with no irradiation for ≈2 hours after charging with ≈3 nA/cm^2 at 19 kV. The time elapsed between each trace is the same. In addition, between the two upper traces, room lights were on for 30 seconds; between the two middle traces, twice as much light was on for 60 seconds; between the last two, no light was on.

Figure 14 shows two potential profiles for a sample which had previously been charged to an asymptotic voltage of ≈ 7.2 kV by a 1 nA/cm^2, 9 kV beam. These two profiles were taken approximately 2 hours apart. From these data one would infer a dark conductivity of $\approx 2.4 \times 10^{-17}$ (ohm cm)$^{-1}$.

Figure 15 shows two potential profiles taken approximately 1 and 20 hours after charging. From these data one would infer a conductivity of $\approx 4.4 \times 10^{-17}$ (ohm cm)$^{-1}$ during the first 60 minutes. The conductivity is 3.6×10^{-18} (ohm cm)$^{-1}$ during the next 17 hours and a conductivity of 4.8×10^{-18} (ohm cm)$^{-1}$ during the period from 17 to 20 hours after charging.

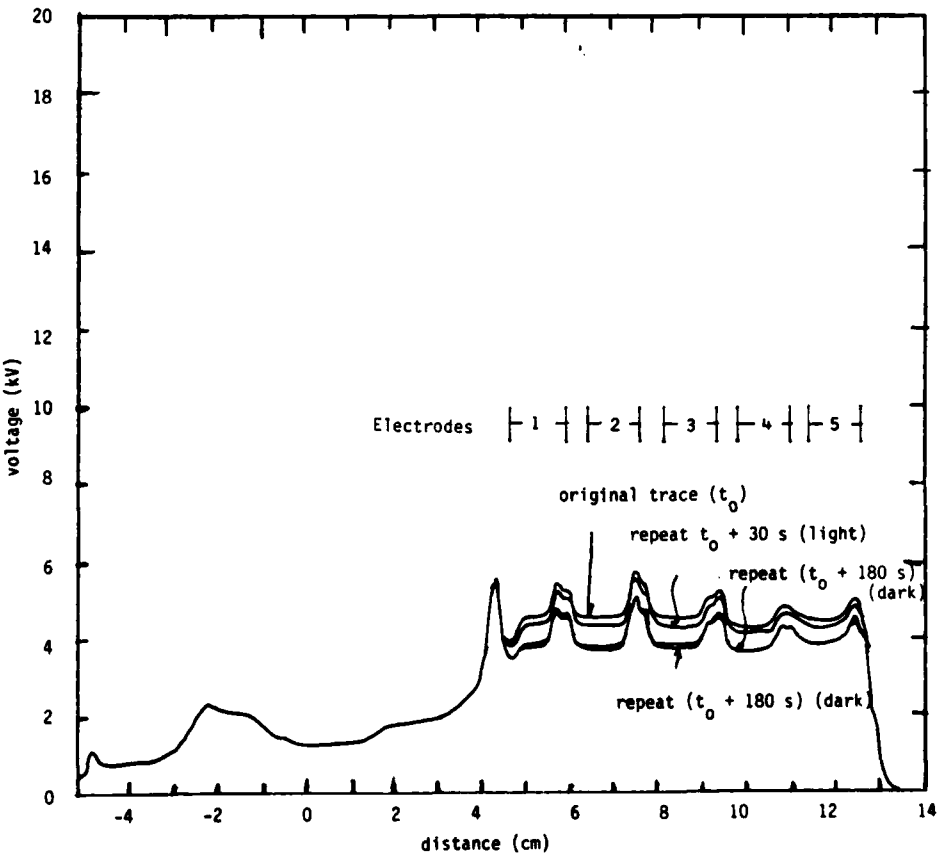

Figure 13. Another time decay of voltage showing the enhancement of conductivity due to room lights.

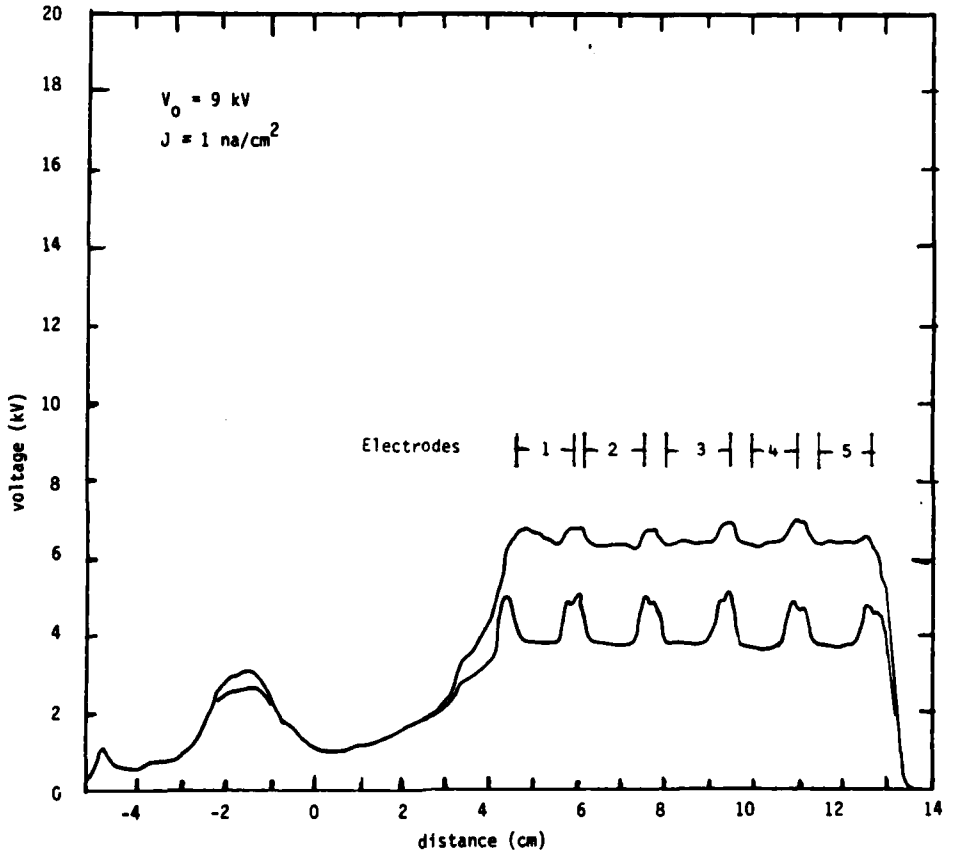

Figure 14. Decay of potential over two hours after charging with 1 nA/cm^2 at 9 keV.

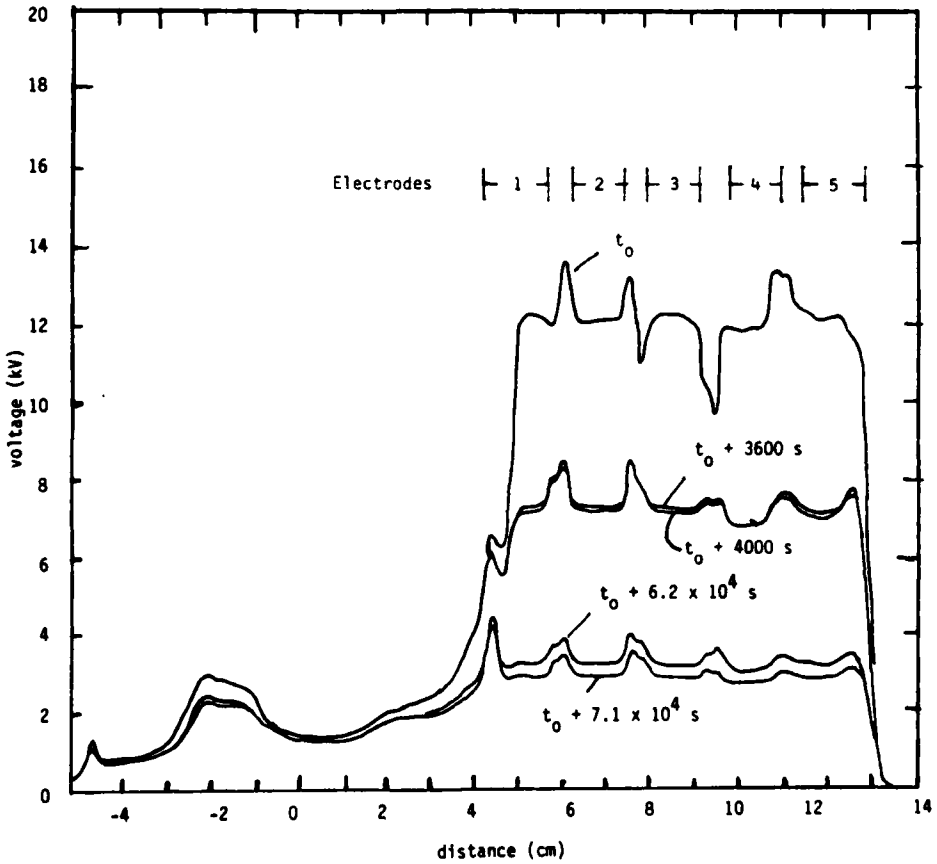

Figure 15. Decay of potential over 1 hour and 20 hours, after charging at 5.3 nA/cm^2 and 18 kV. No lights on.

Figure 16 through 18 show the potential distribution for 0.002" Kapton charged with 4 nA/cm^2 electrons of energy 20 keV. The sample had achieved a potential of ≈ 16 kV over the low capacitance gaps and approximately 11-12 kV over the grounded electrodes before the TREK induced a discharge. Shown on Figure 17 is a potential profile after discharge 11:48. The transient data records are indicated in Figure 18. This sample lost approximately 0.6 μC/cm^2 moderately uniformly across the entire sample surface. Figure 18, the transient signal, shows that the discharge is seen first in segment 5 and progresses sequentially thru segments 4, 3, 2, and 1. From this data record alone, one would infer a propagation velocity of ≈ 10^7 cm/s.

Figure 19 shows three potential profiles for 0.002" Kapton after three different discharges. Before Trace 22, the sample had been charging for more than 8 minutes with 4 nA/cm^2 at 26 kV, when it discharged. Charge can be seen to be missing from over electrodes 4 and 5. A 5 s irradiation at ≈75 nA/cm^2 and 26 kV filled in most of that missing charge and caused a discharge over electrode 1 which we can see in Trace 23. Both these sweeps show preferential discharges over the low capacitance regions between the back surface electrodes. For instance, Trace 22 has a peak at ≈6 cm and a valley at ≈9 cm, while Trace 23 has a valley at ≈6 cm and a peak at ≈9 cm. 5 seconds more at 70 nA/cm^2 caused a discharge which cleared the charge off almost all the sample except over Ch 1. The discharge which occurred just before Trace 24 is shown in Figure 20.

Figure 20 shows transient record of the discharge on 0.005 cm (0.002") Kapton charged at about 70 nA/cm^2 with 26 kV electrons to potential of ≈ 11±1 kV before discharge. These data records clearly show propagation of a discharge from segment 5, the outer edge defined by the razor blade clamp, toward the center of the sample (toward segment 1). This record alone would indicate a propagation velocity of ≈ 1.2 x 10^7 cm/s. The blow-off collector record indicates that the majority of the charge removed from the dielectric surface was collected by the blow-off collector.

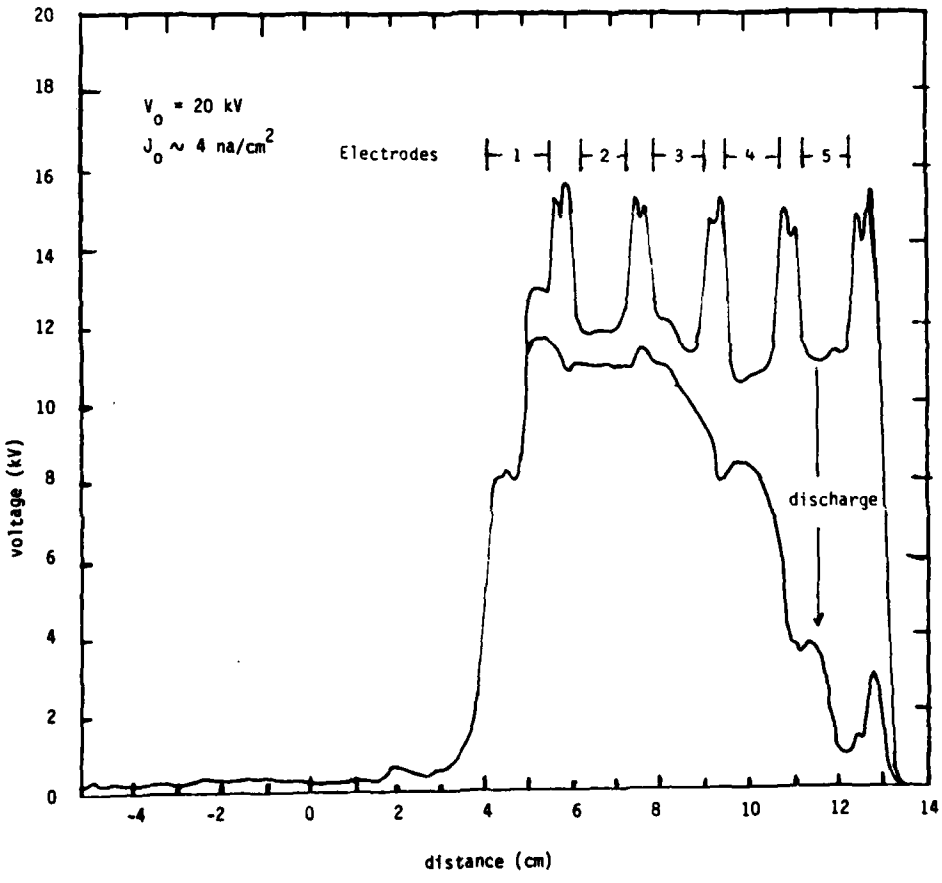

Figure 16. Potential profiles before and after a discharge induced by the TREK probe striking the metal at the edge of the sample.

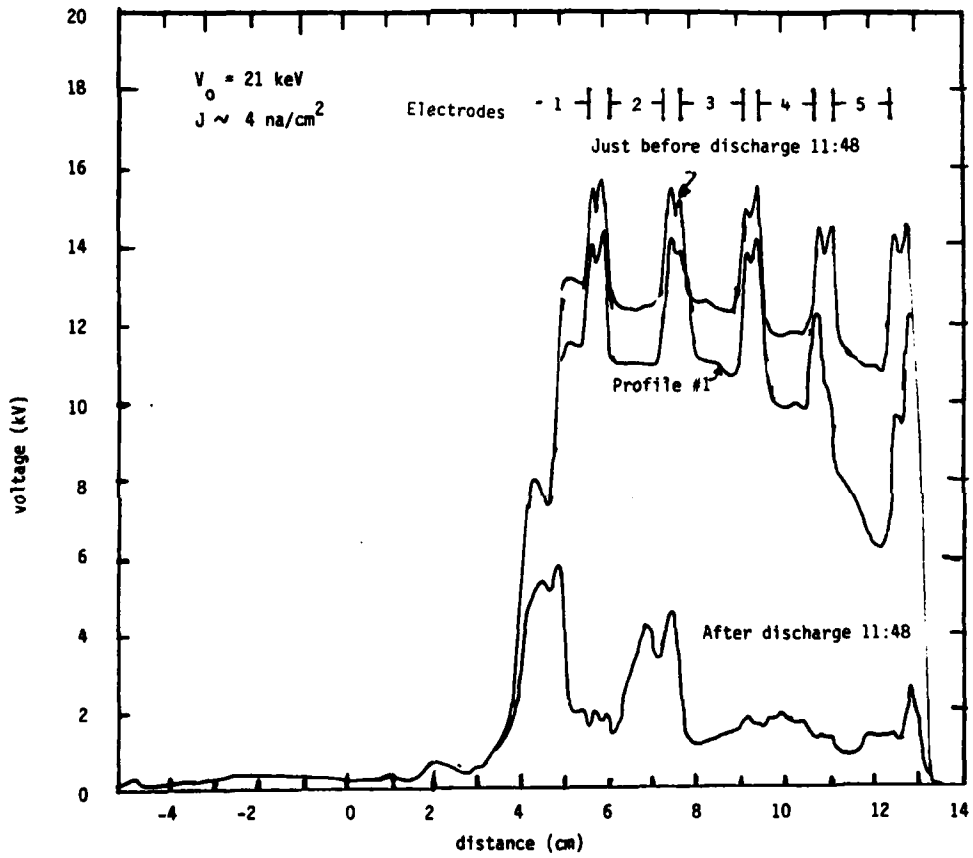

Figure 17. Potential profiles showing two minutes of charging at 21 kV with 7 nA/cm^2, and profile after discharge induced by TREK striking metal at the edge of the sample.

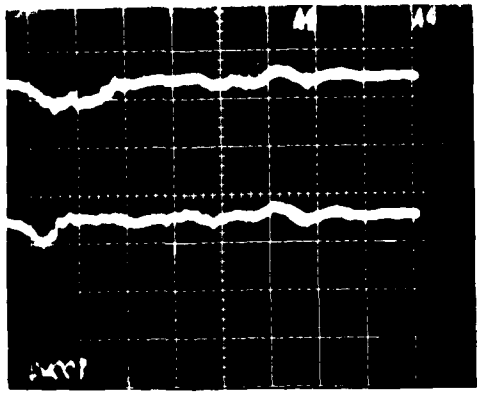

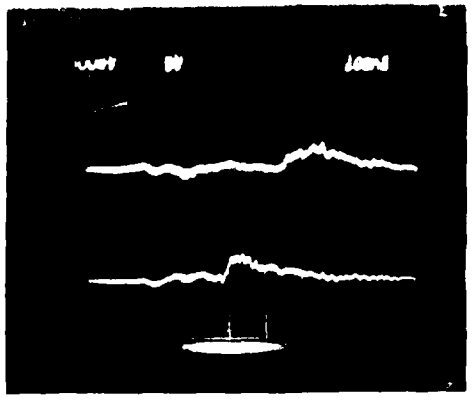

Material: Kapton
Charging Voltage: 26 kV

Date: 4/14/82
Time: 11:48

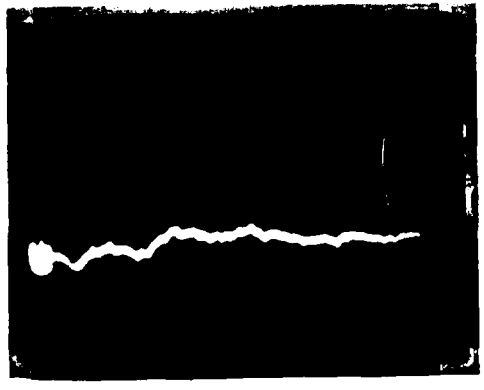

Figure 18. Transient record of discharge 11:43 on 0.005 cm Kapton exposed to 21 kV electrons.

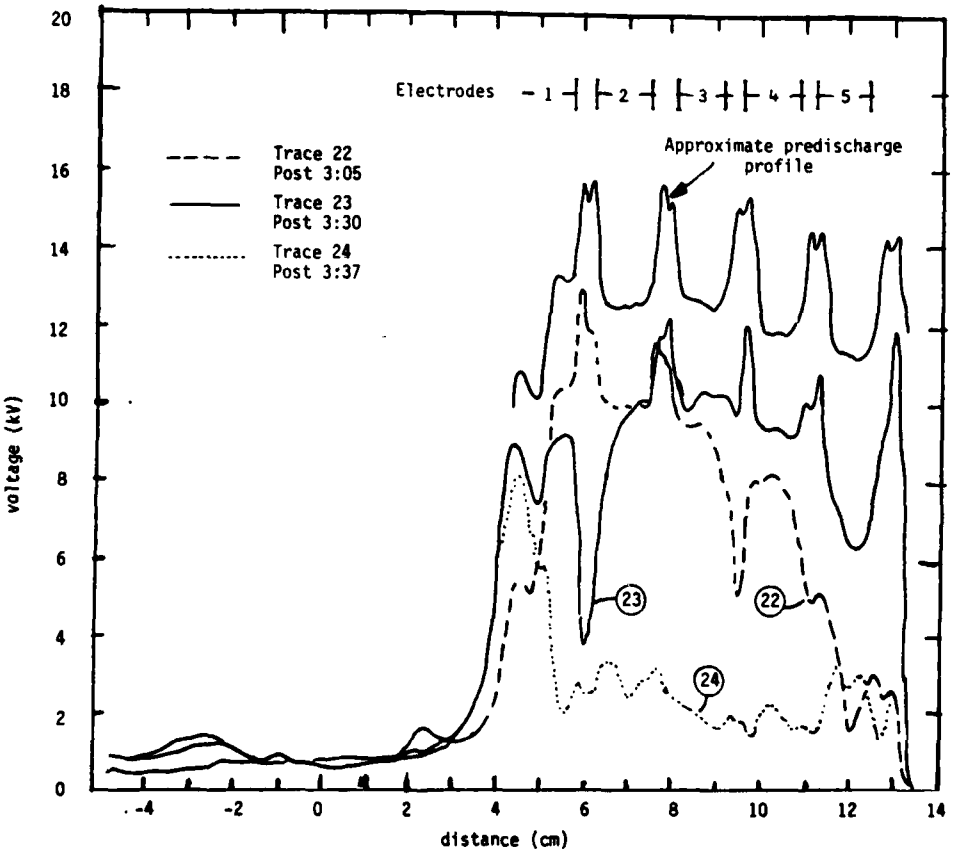

Figure 19. Potential profiles for 0.005 cm Kapton exposed to 4 nA/cm^2 of 26 kV electrons before and after discharges 3:05, 3:30, and 3:37.

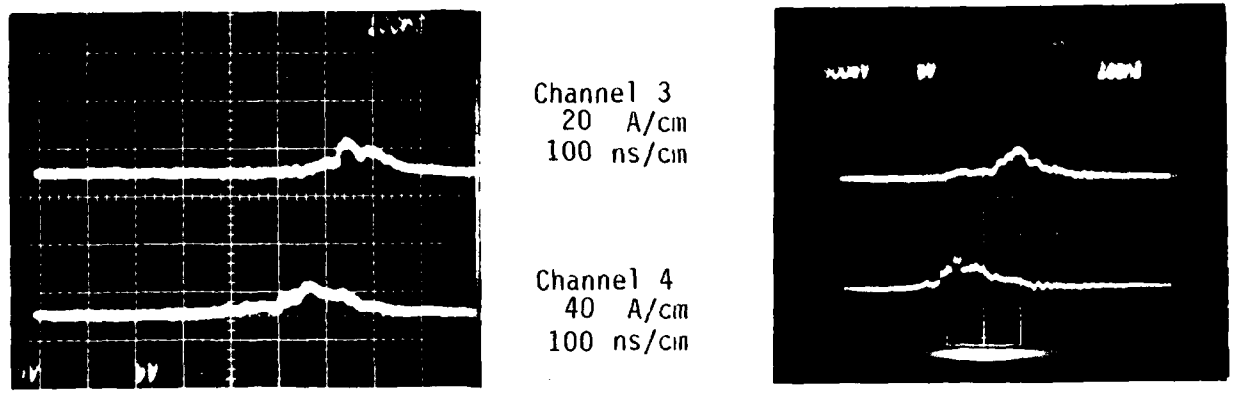

Material: Kapton
Charging Voltage: 26 kV

Date: 4/14/82
Time: 3:37

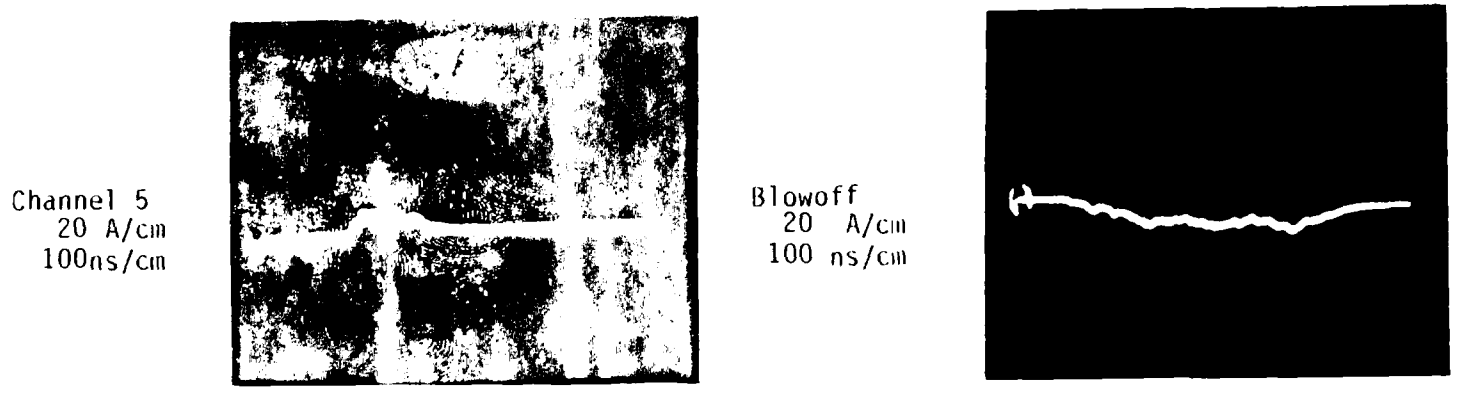

Figure 20. Transient record of discharge 3:37 on 0.005 cm Kapton exposed to 26 kV electrons.

Figure 21 shows potential profiles associated with the charging and discharge of 0.002" Kapton charged at ≈75 nA/cm^2 with 26 kV electrons. Between Trace 26 and 27, the beam was on for almost 8 seconds, ending with a discharge which apparently affected only the charge over electrode 5. Then the beam was on for almost 10 seconds, when discharge 4:05 occurred. Trace 28 represents the voltage profile obtained immediately after discharge 4:05. Notice that the discharge resulted in potential valleys in the portions of the sample over the dielectric, which had previously been peaks. This discharge was visually noted to be dim, relative to other discharges, but covered the entire sample.

Figure 22 is the transient record of discharge 4:05. The blow-off collector shows substantial charge was emitted from the dielectric, but the signals induced on the segmented electrodes 1 through 4 are small and slow. This is because the principal charge motion was in the gaps between the electrodes and persists for the time it takes the discharge to propagate across the width of the sample (about 4 cm).

Figure 23: the potential profiles before and after a discharge here represent another example of a sample which is preferentially discharged (event 4:44) in the high voltage regions above the dielectric stripes.

Figure 24 This transient record also shows long duration, low amplitude signals whose timing is uncertain. Again the blow-off collector shows substantial negative charge collected.

Figure 25 shows a set of post discharge potential profiles for events 4:55 and 5:22. Notice that whereas event 4:55 uniformly discharged the sample surface, event 5:22 involves principally the areas over electrodes 3, 4, and 5. These observations are supported by the transient data in Figures 26 and 27. In event 4:55, signals are clearly seen in all five electrodes while in event 5:22, the signals on electrodes 3, 4, and 5 are significantly greater than on electrodes 1 and 2. The blow-off collector intercepted about 8μC

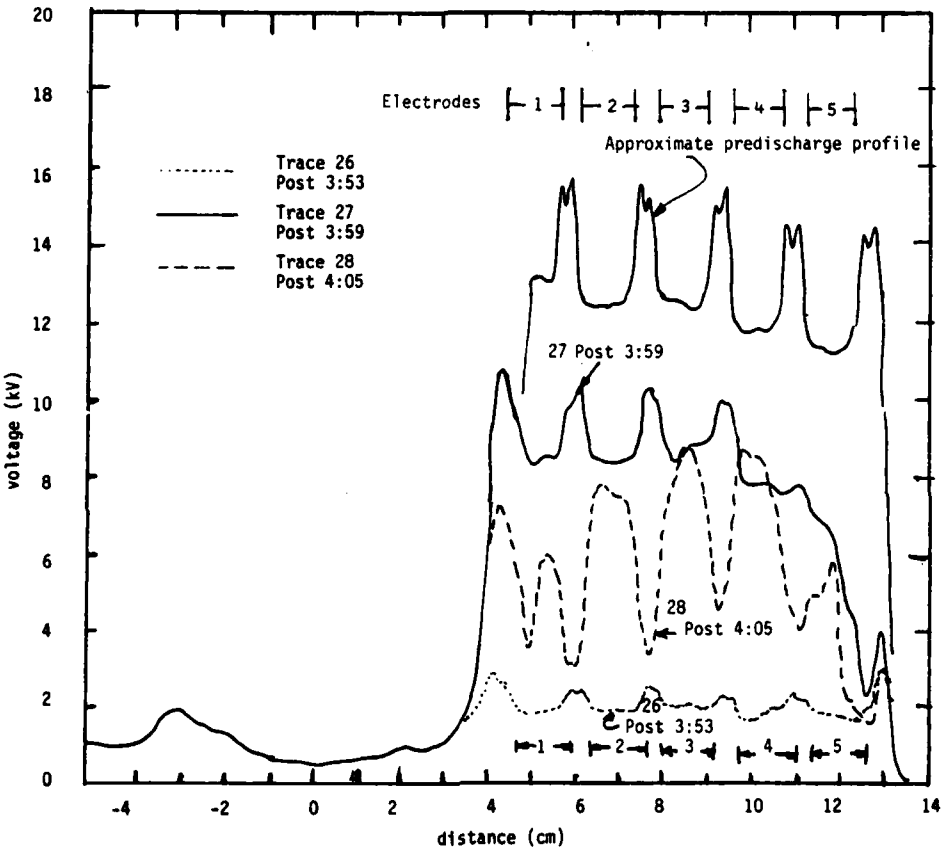

Figure 21. Potential profiles for 0.005 cm Kapton exposed to 75 nA/cm^2 of 26 kV electrons before and after events 3:53, 3:59, and 4:05.

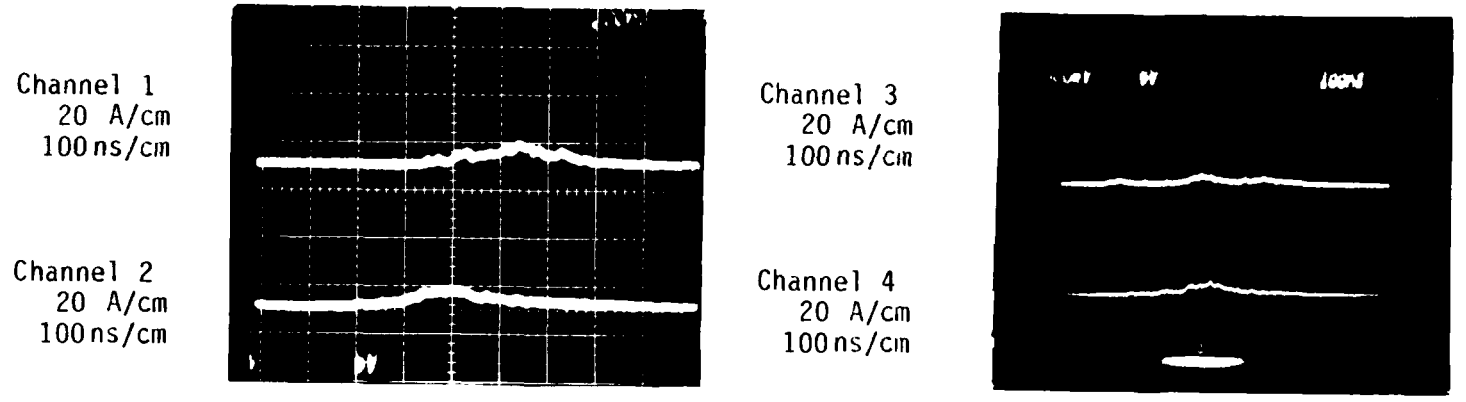

Material: Kapton
Charging Voltage: 26 kV

Date: 4/14/82
Time: 4:05

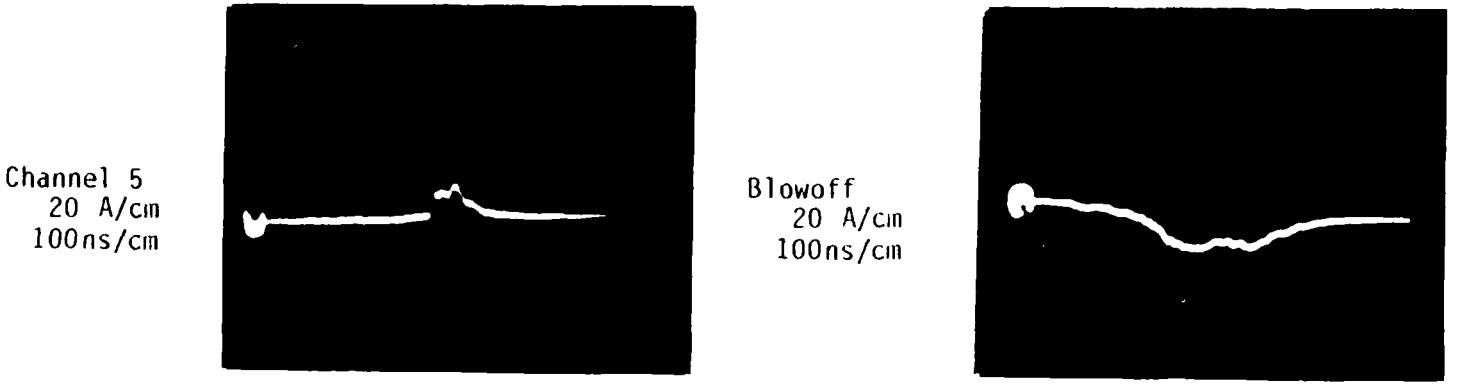

Figure 22. Transient record of discharge 4:05 on 0.005 cm Kapton exposed to 75 nA/cm^2 of 26 kV electrons.

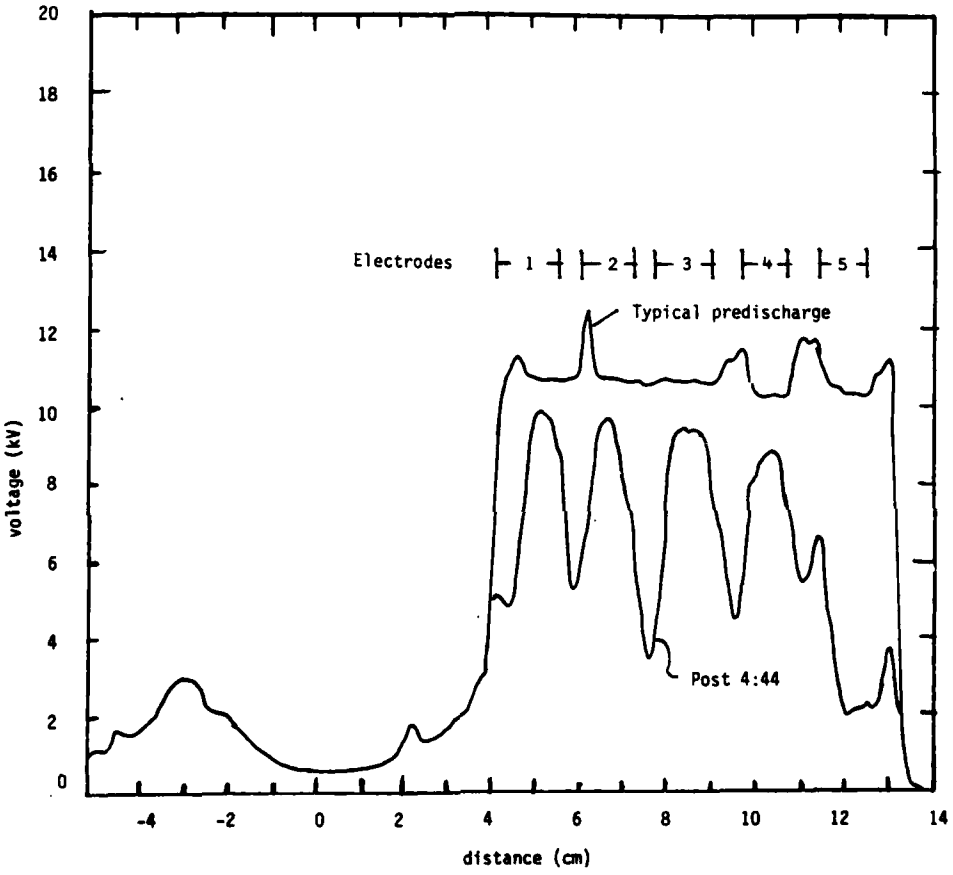

Figure 23. Actual post-discharge profile and probable pre-discharge profile. Charging with 75 nA/cm^2 of 26 kV electrons.

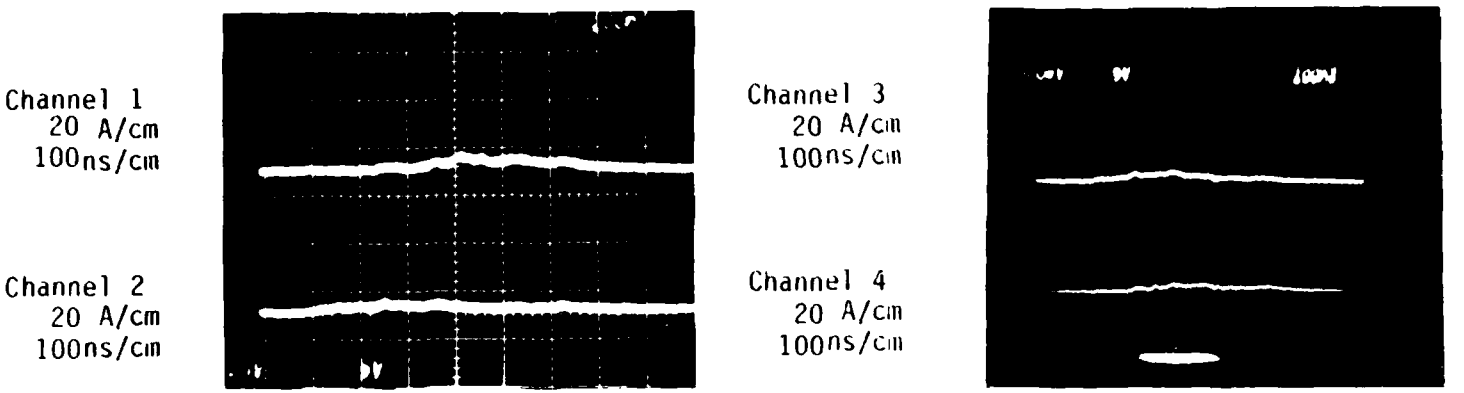

Material: Kapton
Charging Voltage: 26 kV

Date: 4/14/82
Time: 4:44

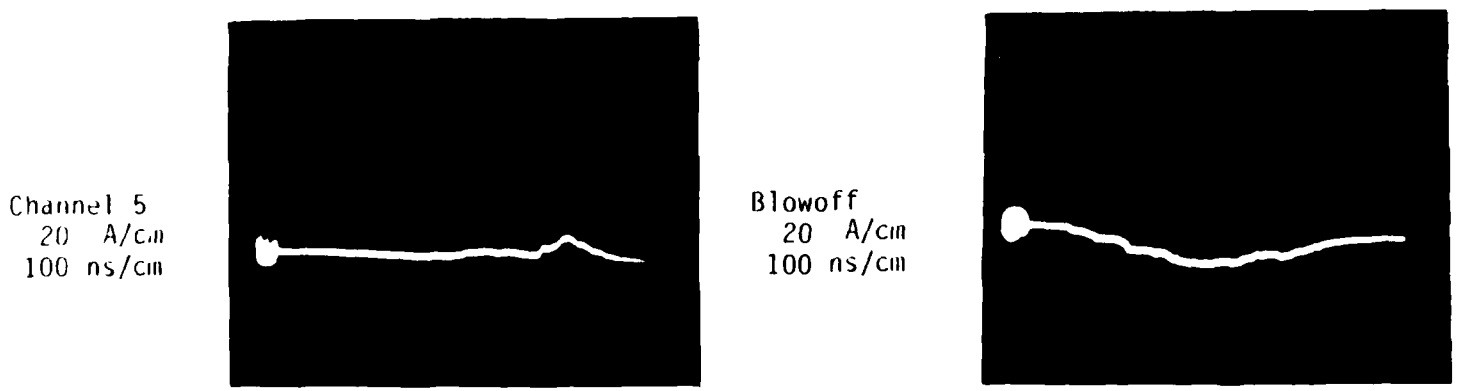

Figure 24. Transient record of discharge 4:44 on 0.005 cm Kapton exposed to 75 nA/cm^2 of 26 kV electrons.

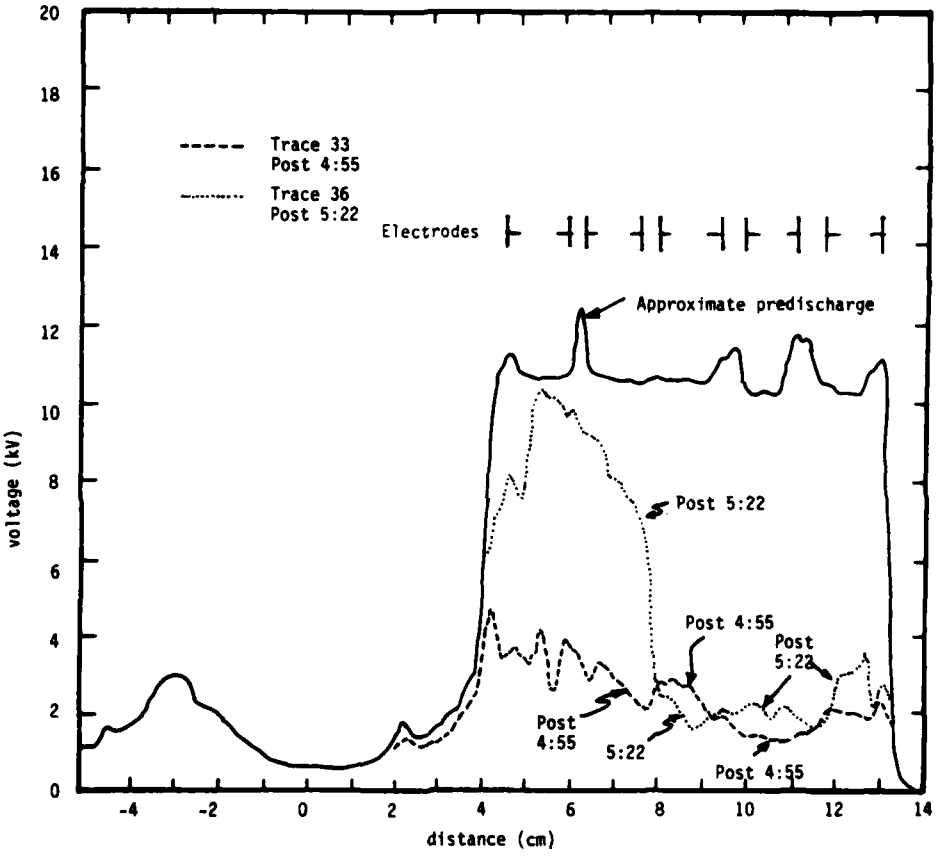

Figure 25. Two post-discharge profiles and estimated pre-discharge profile. Charging with 75 nA/cm^2 of 26 kV electrons.

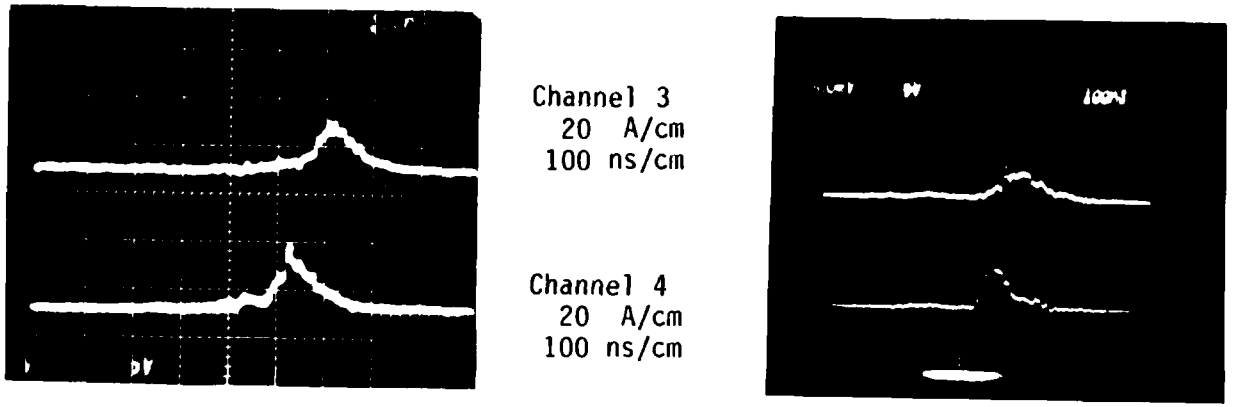

Material: Kapton
Charging Voltage: 26 kV

Date: 4/14/82
Time: 4:55

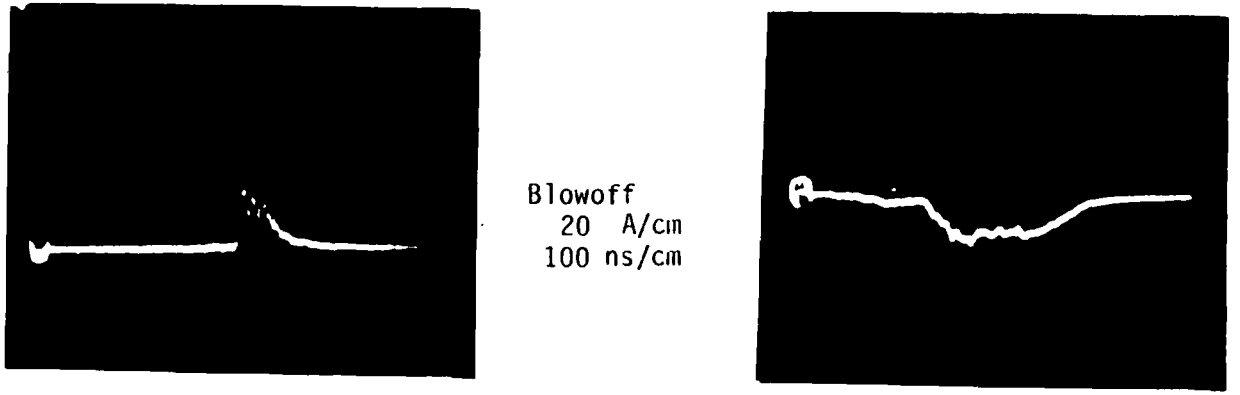

Figure 26. Transient record of discharge 4:55 on 0.005 cm Kapton exposed to 75 nA/cm^2 of 26 kV electrons.

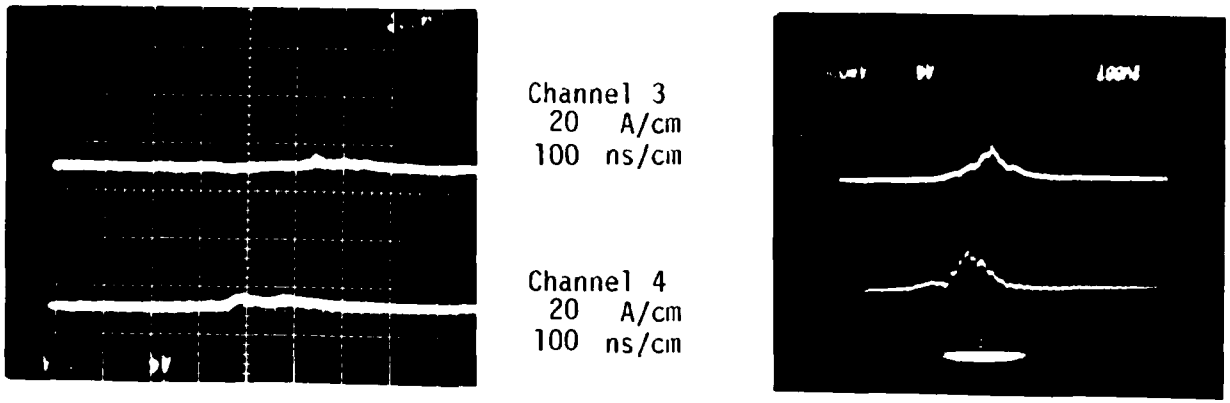

Material: Kapton
Charging Voltage: 26 kV

Date: 4/14/82
Time: 5:22

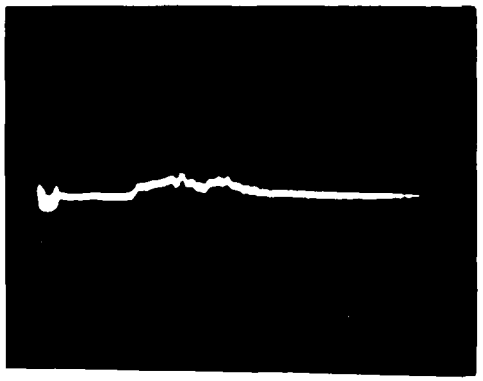

MISSING

Figure 27. Transient record of discharge 5:22 on 0.005 cm Kapton exposed to 26 kV electrons.

of charge in the 4:55 event. We infer about 10-12 μC of charge was lost from CΔV of Figure 25. Visual observation of the 5:22 event showed a Lichtenburg figure structure with the trunk originating on the razor blade edge.

Figure 28 shows potential profiles for 0.005 cm (0.002") Kapton charged with approximately 40 nA/cm^2 of 26 kV electrons before and after events 5:30, 5:45 and 5:50. The transient record for event 5:30 is shown in Figure 29. It clearly shows a discharge propagating from the outer toward the inner segments at a rate of approximately 10^7 cm/s resulting in post discharge profile 5:30 on Figure 28. Visually event 5:30 looked about the same as for 5:22 (i.e., a Lichtenberg figure with the trunk at the metal dielectric boundary), while event 5:45 appeared to be several Lichtenberg figures heading across the sample parallel to the electrodes (see also Figure 30) and event 5:50 looked like Lichtenberg branches going out in all directions from a bright spot in the middle of the sample (see also Figure 31).

Figure 30 shows discharge event 5:45 which propagates from segment 1 or 2 (the inside about 5 cm from the center of the dielectric) towards the ouside (metal dielectric boundary at 13 cm) at $\approx 10^7$ cm/s. The long duration, low amplitude signals on segments 2, 3, 4 are characteristic of the horizontal discharges. About 10 μC negative charge is collected by the blow-off collector. From Figure 28 (CΔV) we infer 7.5 μC of charge left the sample.

Figure 31 is the transient record of discharge event 5:50 which resulted in the post discharge profile 41 on Figure 28. This record clearly shows discharge propagation from the outer edge (metal dielectric at ≈13 cm) to the inner edge, and collection of about 8 μC negative charge by the blow-off collector. From Figure 28 (CΔV) we infer ≈12 μC of charge left the sample.

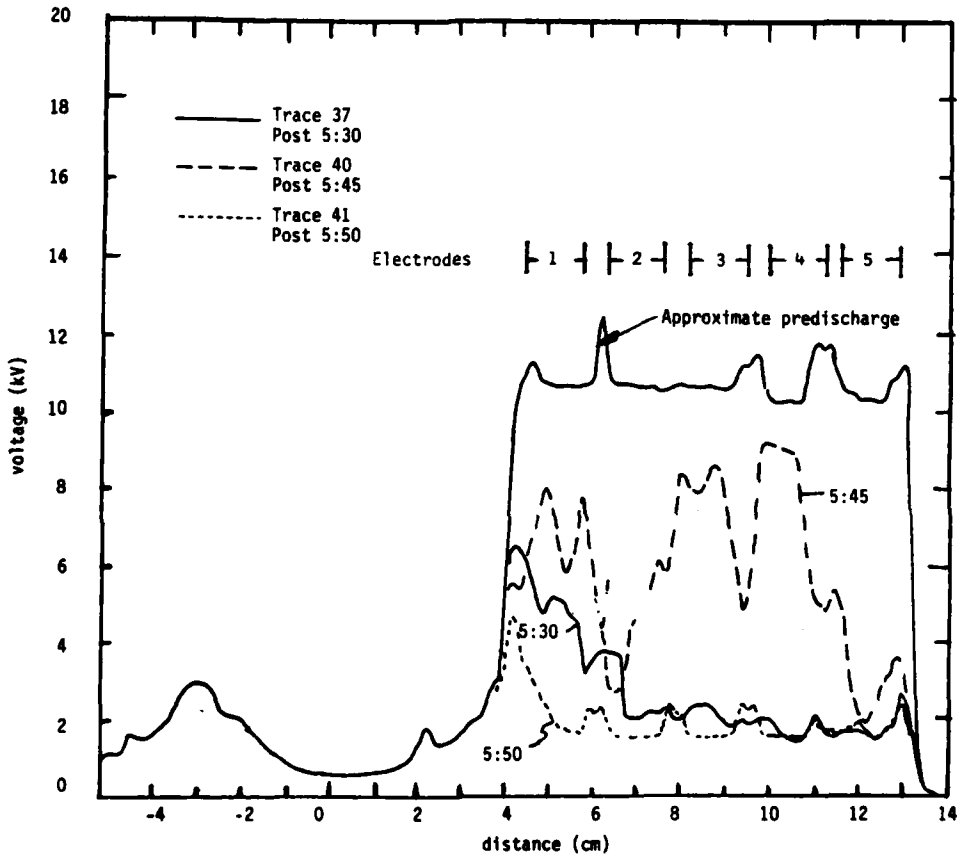

Figure 28. Three post-discharge potential profiles and estimated pre-discharge profile. Charging with 40 nA/cm^2 of 26 kV electrons.

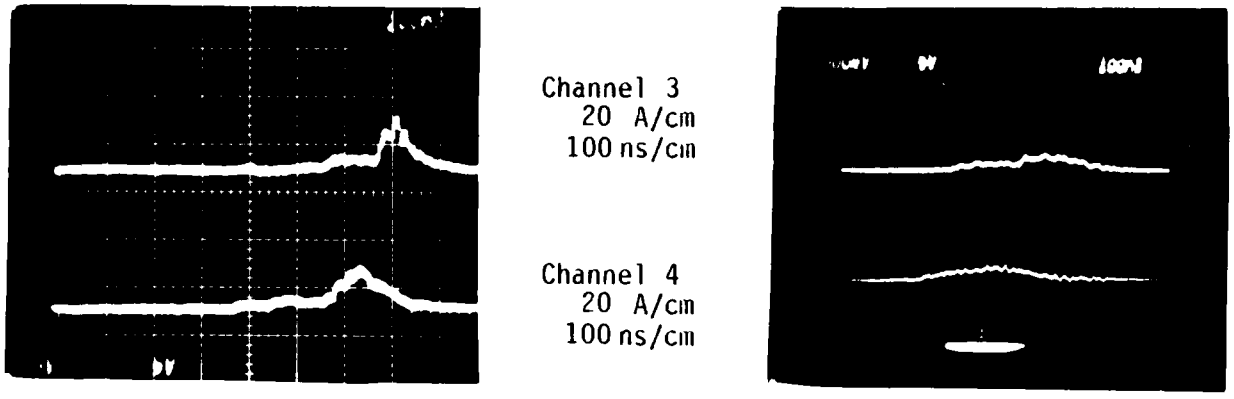

Material: Kapton
Charging Voltage: 26 kV

Date: 4/14/82
Time: 5:30

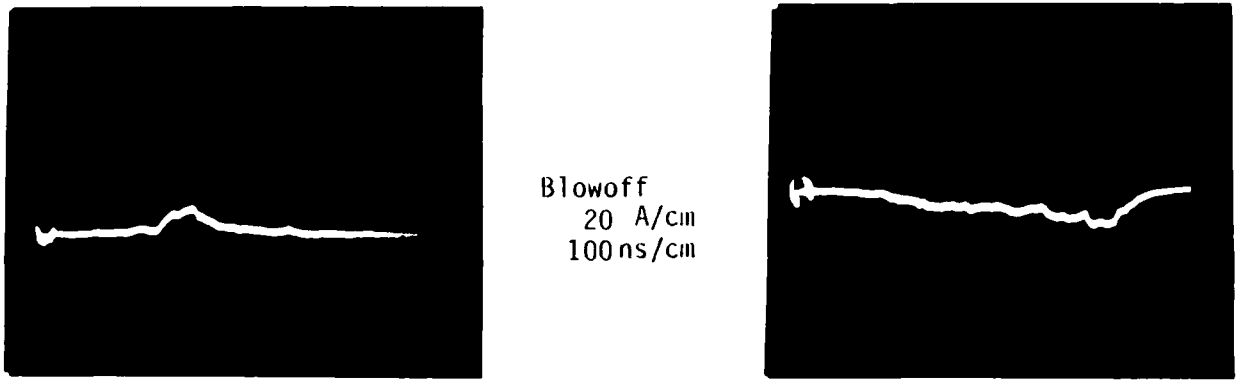

Figure 29. Transient record of discharge 5:30 on 0.005 cm Kapton exposed to 40 nA/cm^2 of 26 kV electrons.

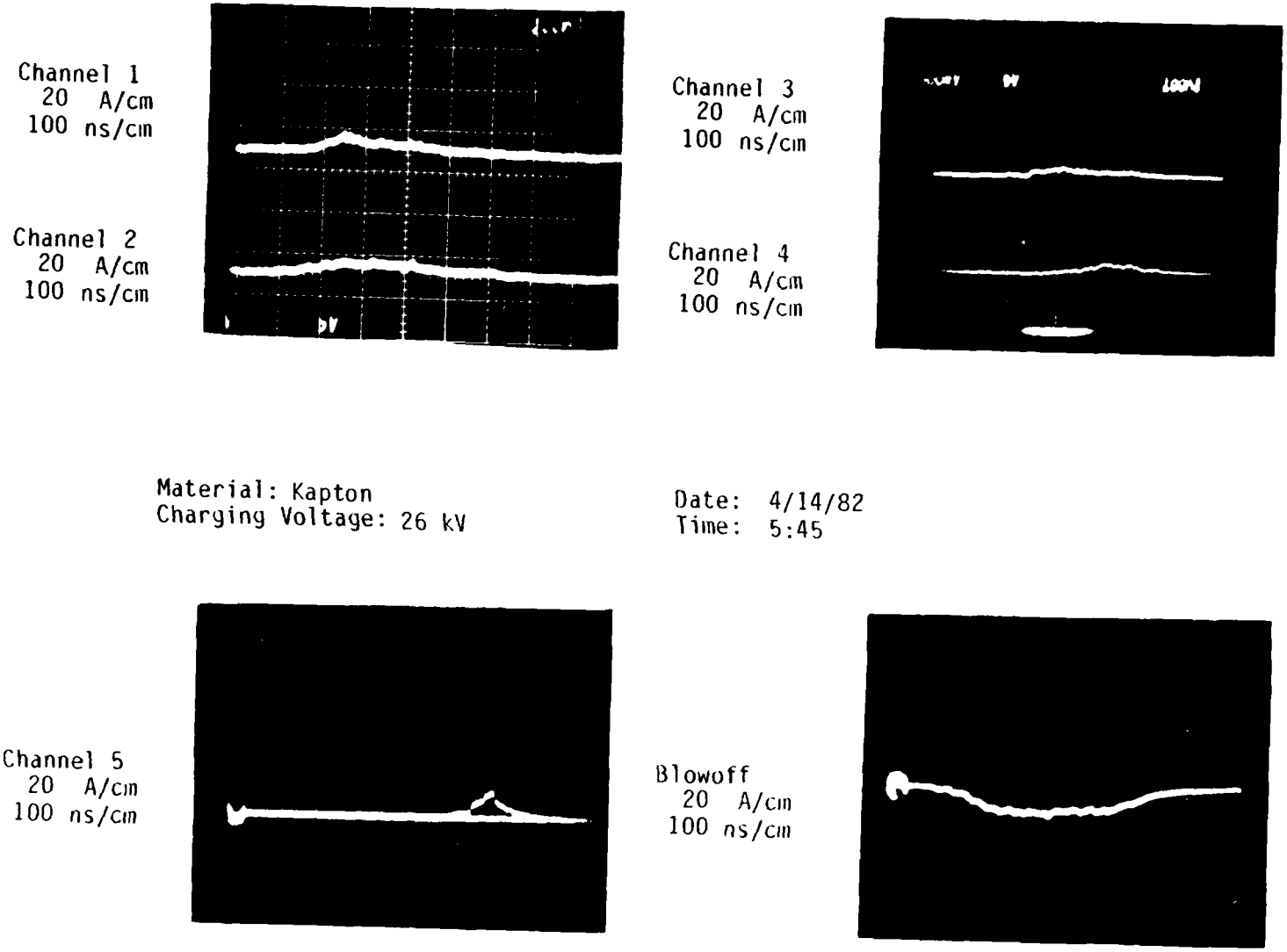

Figure 30. Transient record of discharge 5:45 on 0.005 cm Kapton exposed to 40 nA/cm^2 of 26 kV.

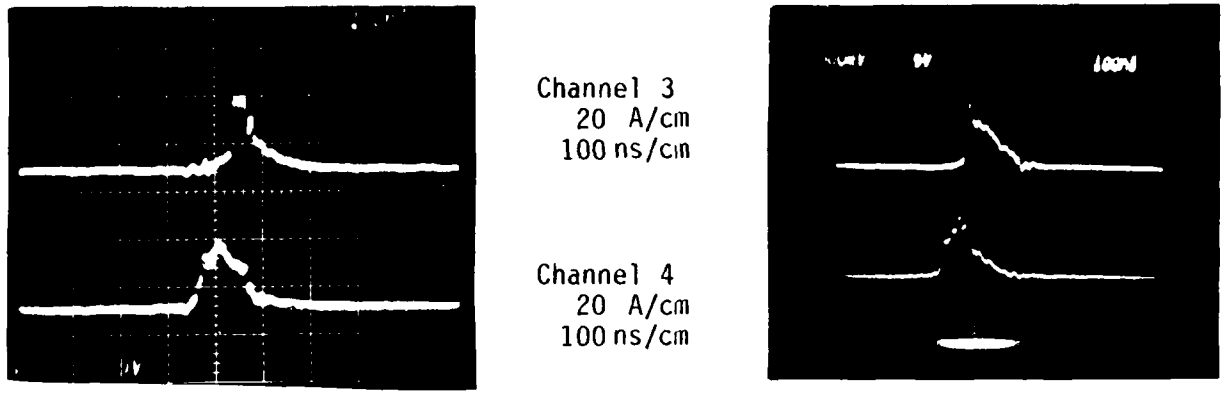

Material: Kapton
Charging Voltage: 26 kV

Date: 4/14/82
Time: 5:50

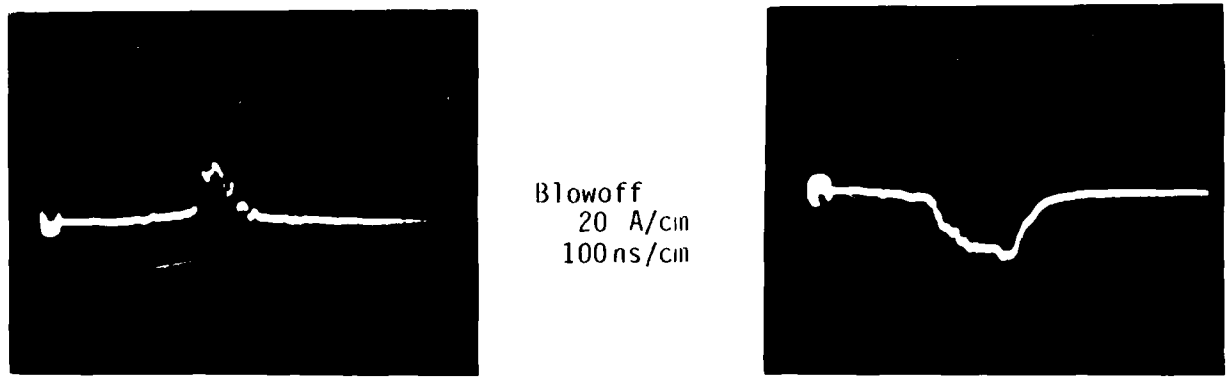

Figure 31. Transient record of discharge 5:50 on 0.005 cm Kapton exposed to 40 nA/cm^2 of 26 kV.

Figure 32 Approximately 23 transient discharge records were examined in an attempt to infer the propagation velocity of a discharge in Kapton. Figure 32 represents the average results for the 7 clearest propagation measurements. From this data we infer an average propagation velocity of $1.7 \pm 0.3 \times 10^7$ cm/s for 0.005 cm (0.002") Kapton.

2. TEFLON

Figure 33 shows the compilation of 5 charging studies of 0.013 cm (0.005") Teflon with monoenergetic electrons of 6 kV, 11 kV, 18 kV, 21 kV and 23 kV. Teflon approached the asymptotic potentials of 4, 9.2, 16, and 18.4 and 20.5 ± .5 kV, thus indicating its unity secondary cross-over point is ≈ 2 kV.

Figure 34 shows the transient data record 4/6/82, 3:17. This data record is somewhat difficult to interpret. It may indicate that the discharge initiated adjacent to Band 4, propagating rather slowly toward 5 and toward 1. However, the discharge amplitude as recorded in Bands 2-5 is smaller than one would infer by comparing the pre- and post-radiation voltage profiles as shown in Figure 35. Notice also that Figure 35 shows the charge is preferentially removed from the areas between electrodes 2, 3, 4, and 5. We have noted other examples where slow, low amplitude signals induced on the capacitive sensors were related to preferential charge removal from the bands separating the electrodes, as opposed to the surface over the sensing electrodes. We propose two possible explanations for why there was less charge appearing on the electrodes than seems to be missing from the voltage difference. First is that the signal actually persisted for too long and at too low an amplitude to be seen on an oscilloscope with these settings. The second possibility is that much of the charge punched through the sample, and hence was not seen in the external circuit.

Figure 36 shows transient data record 4/6/82, 4:35. The sample had been charged with 29 kV electrons. This data gives the appearance of a propagation which initiates at, or between, electrodes #1 and 2 propagating toward

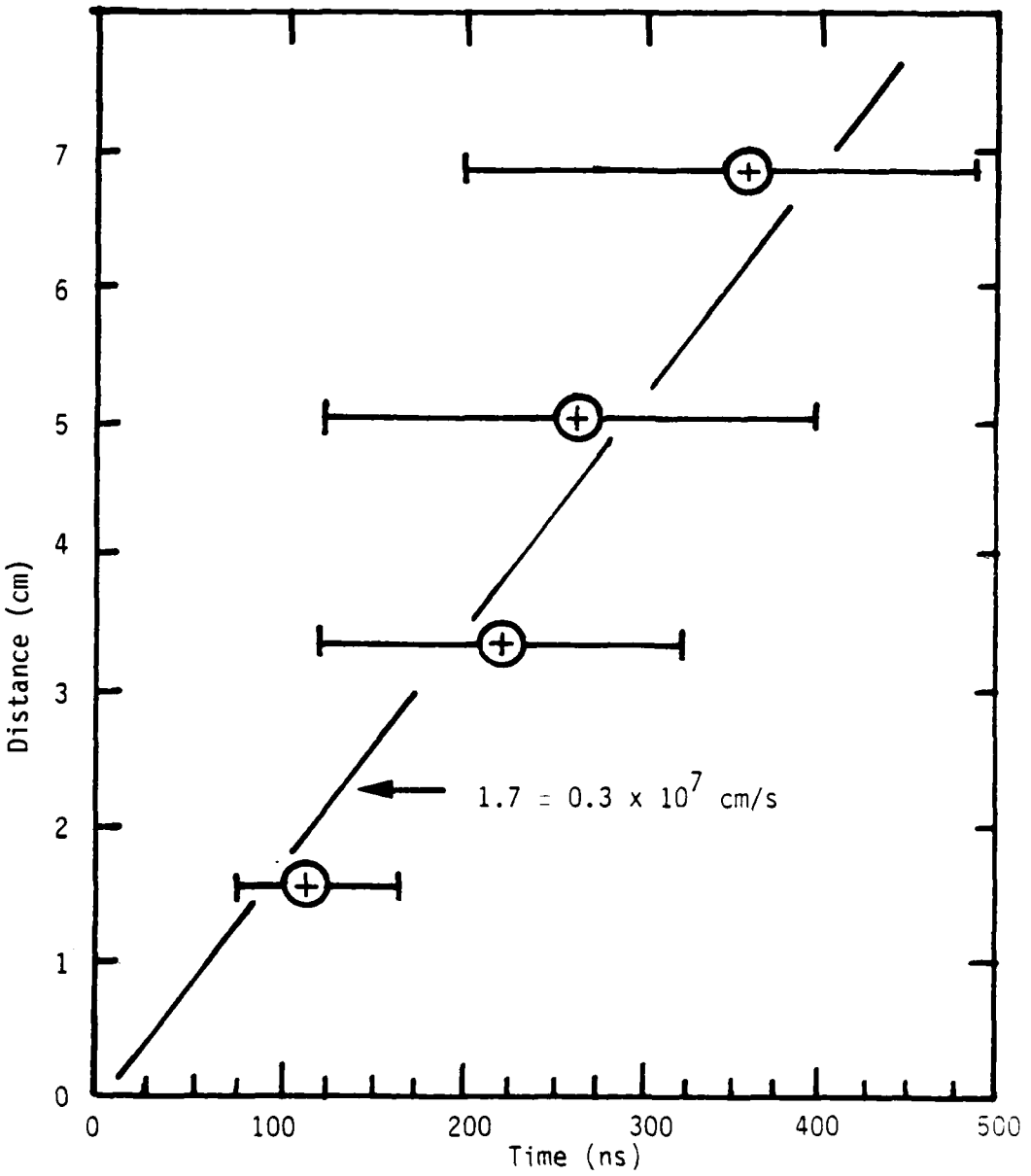

Figure 32. Discharge distance versus time after initiation for 23 transient discharge events on 0.005 cm Kapton.

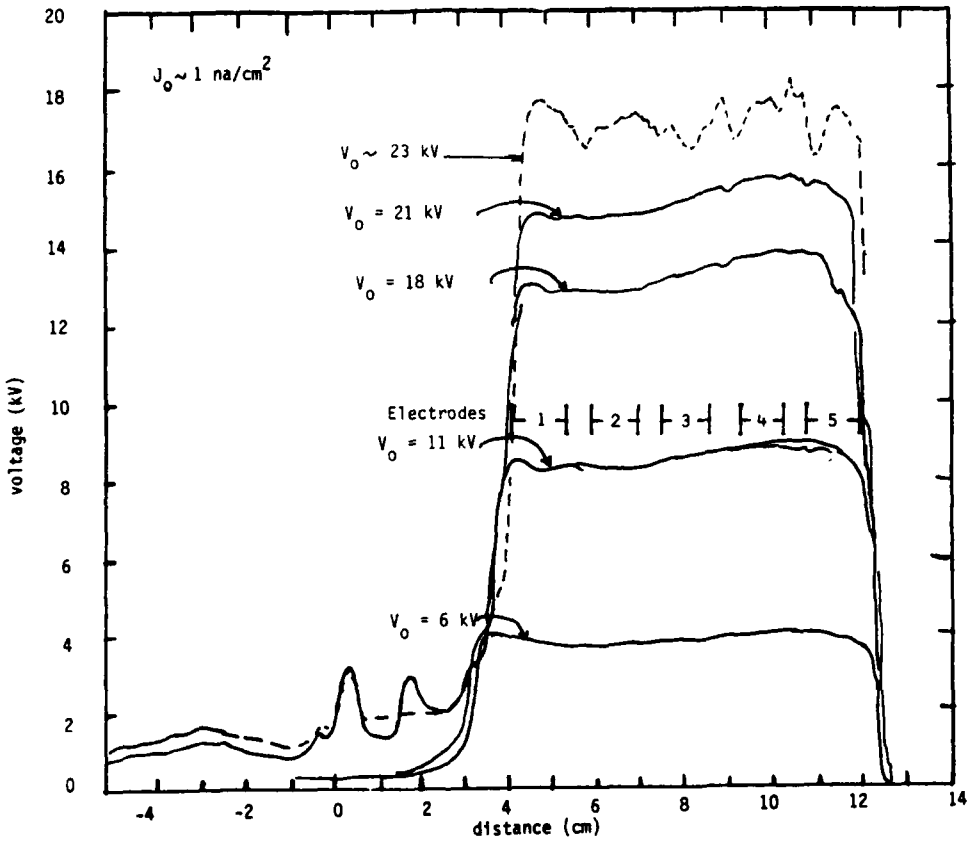

Figure 33. Potential profile measurements for 0.013 cm Teflon exposed to monoenergetic electrons of 6 kV, 11 kV, 18 kV, 21 kV, and 23 kV.

Channel 1
20 A/cm
100 ns/cm

Channel 2
20 A/cm
100 ns/cm

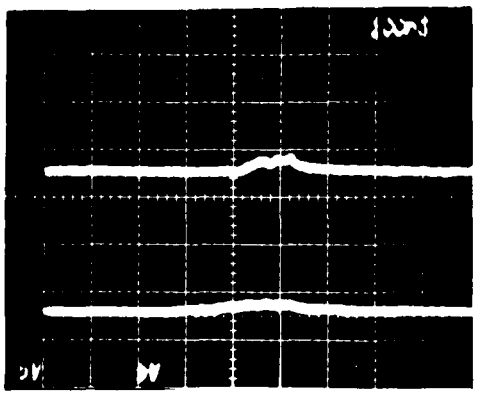

Channel 3
20 A/cm
100 ns/cm

Channel 4
20 A/cm
100 ns/cm

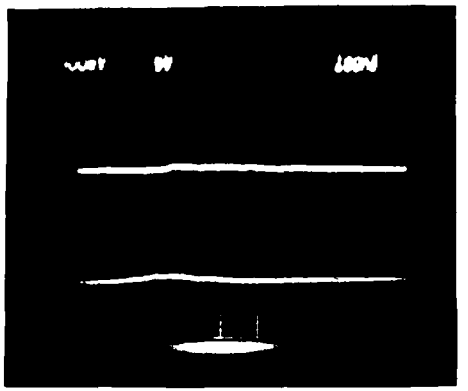

Material: Teflon
Charging Voltage: 22 kV

Date: 4/6/82
Time: 3:17

Channel 5
20 A/cm
100 ns/cm

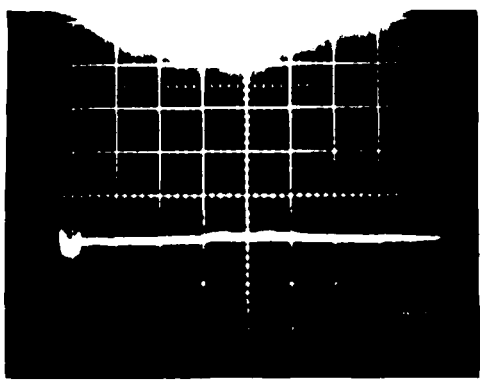

Blowoff
20 A/cm
100 ns/cm
probably NG

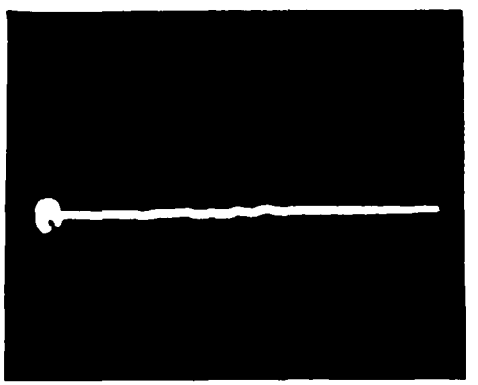

Figure 34. Transient record of discharge 3:17 on 0.013 cm Teflon exposed to 22 kV electrons.

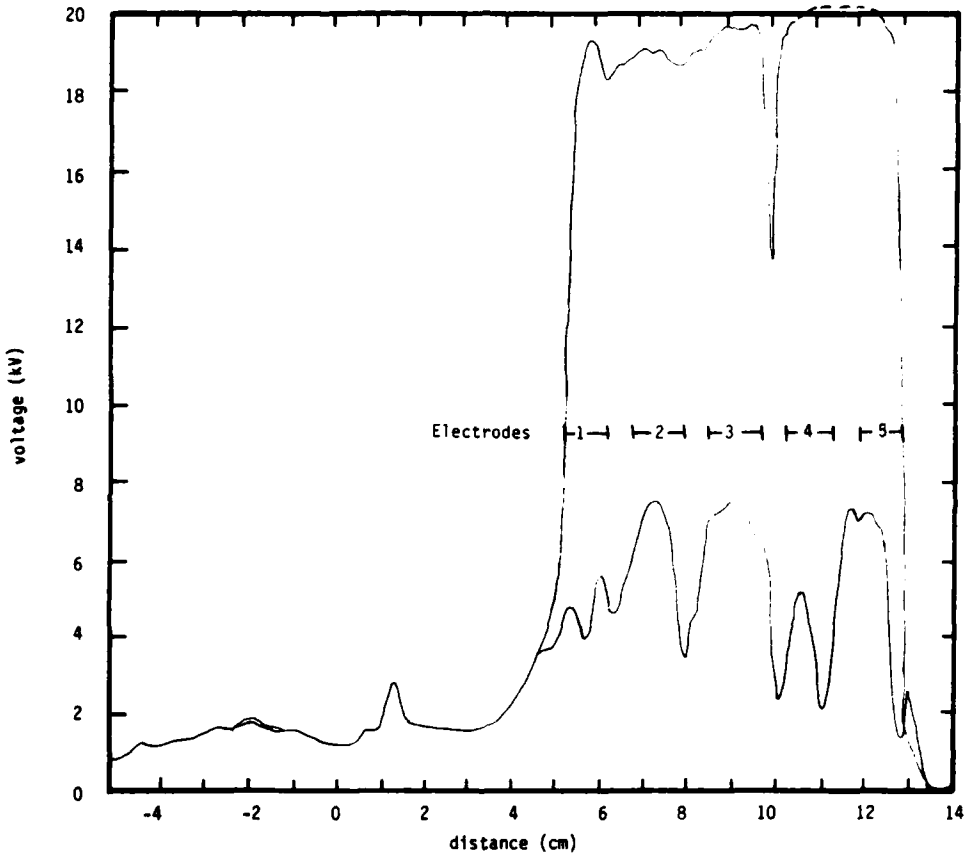

Figure 35. Post-discharge 3:17 potential profile and approximate pre-discharge profile charging with ≈ 1 nA/cm^2 of 23 keV electrons.

Channel 1
8 A/cm
100 ns/cm

Channel 2
8 A/cm
100 ns/cm

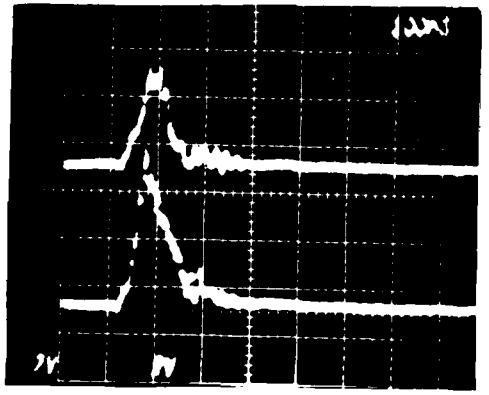

Channel 3
8 A/cm
100 ns/cm

Channel 4
8 A/cm
100 ns/cm

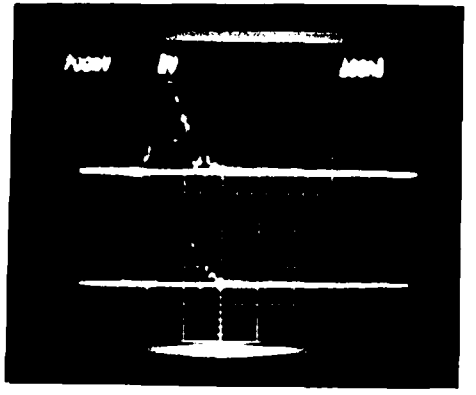

Material: Teflon
Charging Voltage: 29 kV

Date: 4/6/82
Time: 4:35

Channel 5
8 A/cm
100 ns/cm

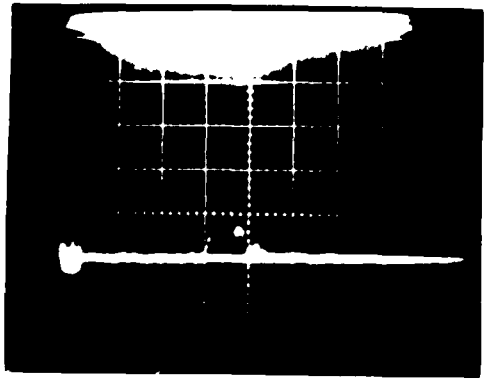

Blowoff
8 A/cm
100 ns/cm
probably NG

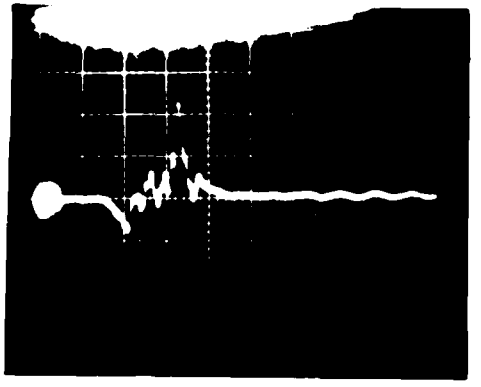

Figure 36. Transient record of discharge 4:35 on 0.013 cm Teflon exposed to 29 kV electrons.

electrode 5 at a velocity of $\approx 6 \times 10^7$ cm/s. Unfortunately, we suspect the data recordings on the blow-off collector are not valid (we think it may have been shorted - see note at end of this section). The transient currents on Figure 36 suggest ≈16 μC were removed from areas above electrodes 1-4 whereas we estimate from $\Delta Q = C\Delta V$ that about 14 μC of charge was removed.

Figure 37 shows a discharge which propagated from electrode 5, the dielectric-metal boundary, for a sample which had been charged at 29 kV. This discharge propagates at a velocity of $\approx 3.7 \times 10^7$ cm/s. In this case the apparent charge loss from the transient records, Figure 37, and before and after voltage profiles are very nearly the same ($\Delta Q/A \approx 0.3 \times 10^{-6}$ coul/cm^2). Figure 38 shows the "probable" pre- and actual post-discharge profiles for event 4:35 and event 4:56. Notice that, contrary to the data of Figure 35, these discharges removed charge in nearly equal measure over all portions of the sample.

Figure 39 shows a discharge propagating from the dielectric metal boundary toward the inside of the sample at a rate of $\approx 2 \times 10^7$ cm/s. Unfortunately, the blow-off collector signal is considered unreliable on this figure.

Figure 40 shows the result of leaving a sample in a pre-charged condition (peak voltage 11.7 kV) for 14 hours (overnight). These data indicate a dark conductivity of 2.9×10^{-19} Ω^{-1} cm^{-1} over a period of 5.2×10^4 s.

Figure 41 shows the potential profile before and after a lateral discharge in which the charge is preferentially removed from the dielectric between the capacitive bands. This discharge is interesting because the discharge was initiated by a spark from the TREK to the metal at the end of the sample, but the charge was largely removed from bands running across the sample perpendicular to the TREK sweep and up to 8 cm away.

Figure 42 shows the potential profiles of Teflon charged with 23 kV electrons before and after an event which occurred at 6:04, on 4/8/82. After

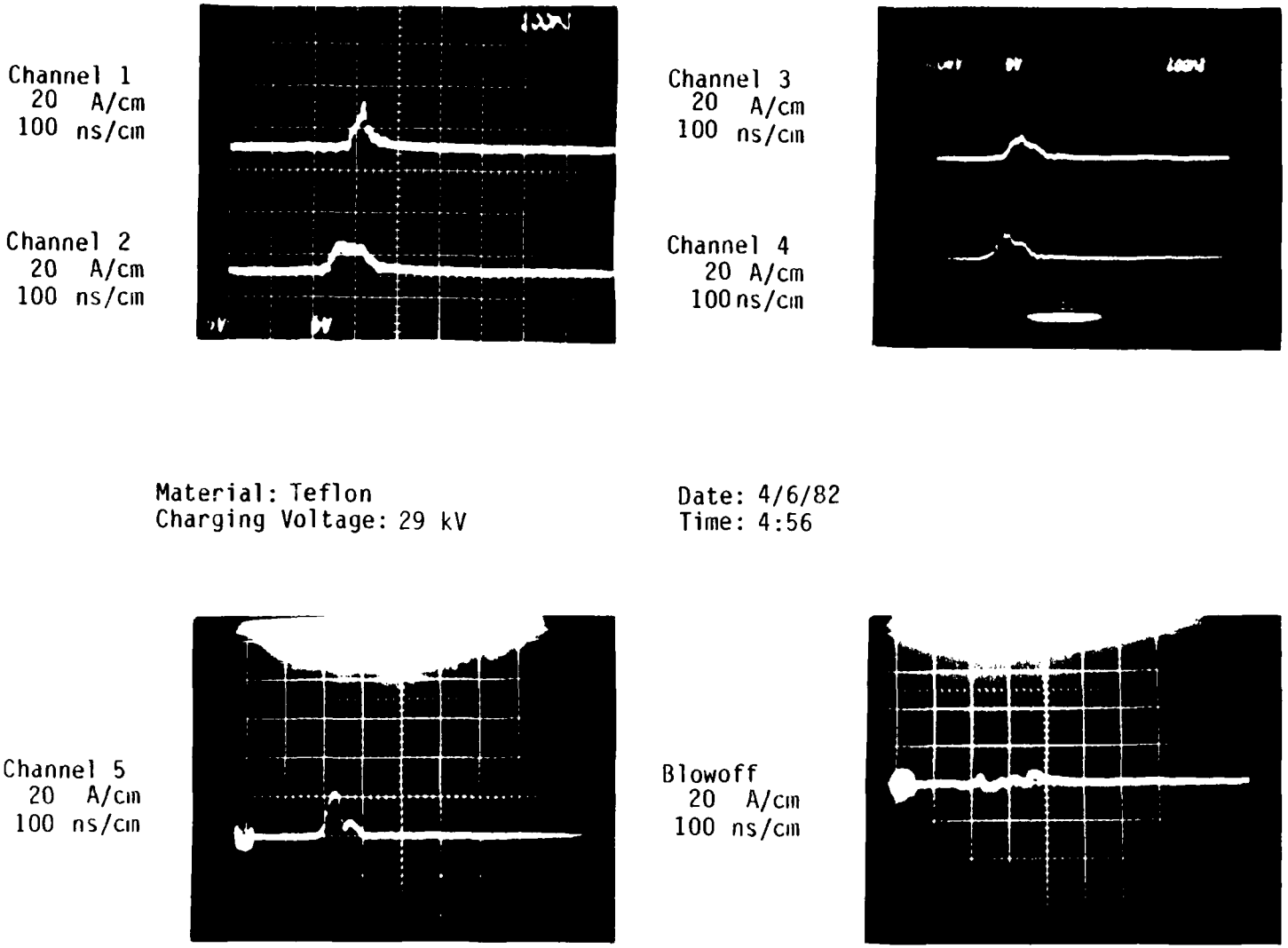

Figure 37. Transient record of discharge 4:56 on 0.013 cm Teflon exposed to 29 kV electrons.

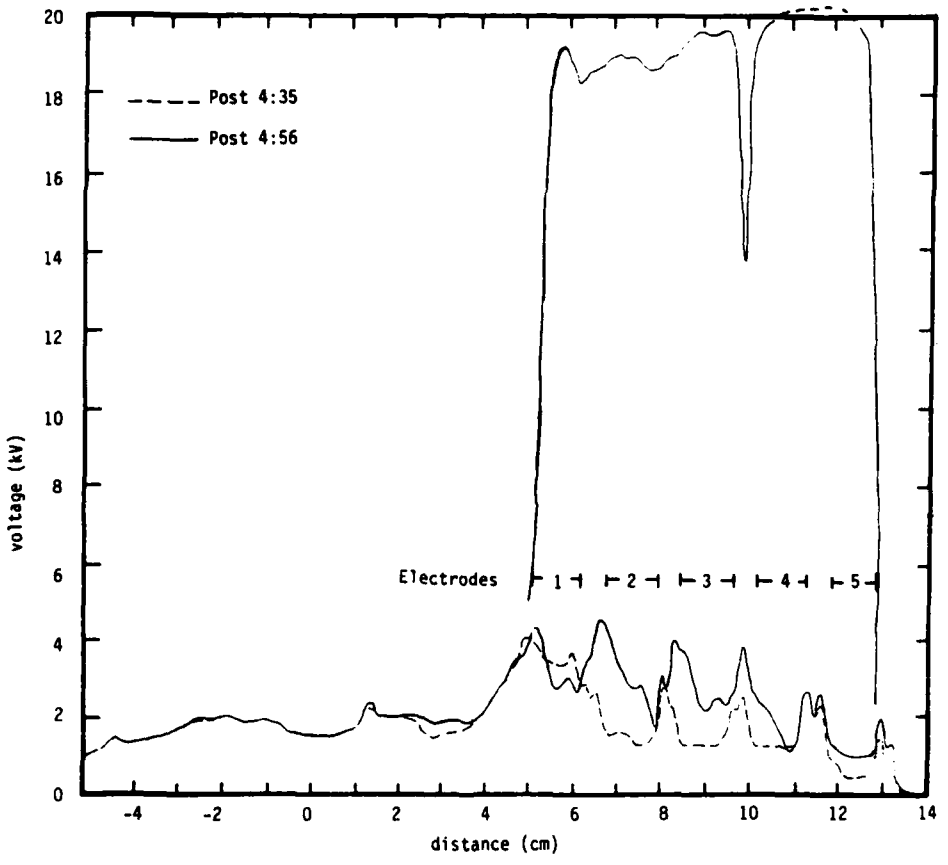

Figure 38. Two post-discharge potential profiles and probable pre-discharge profile. Charging with 1 nA/cm^2 of 29 kV electrons.

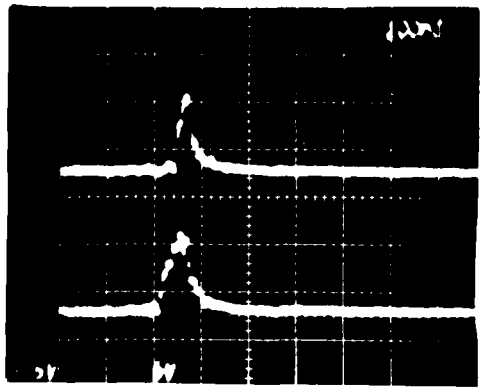

Channel 1
20 A/cm
100 ns/cm

Channel 2
20 A/cm
100 ns/cm

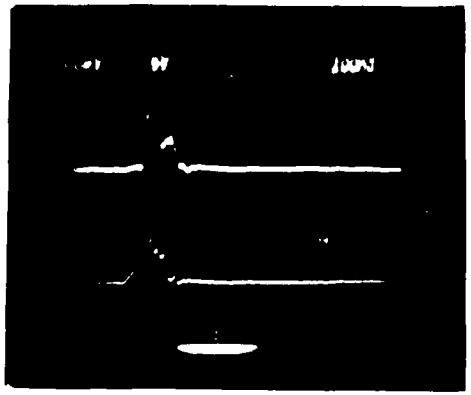

Channel 3
20 A/cm
100 ns/cm

Channel 4
20 A/cm
100 ns/cm

Material: Teflon
Charging Voltage: 29 kV

Date: 4/6/82
Time: 5:47

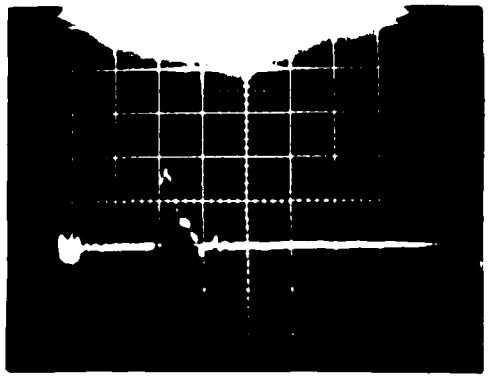

Channel 5
20 A/cm
100 ns/cm

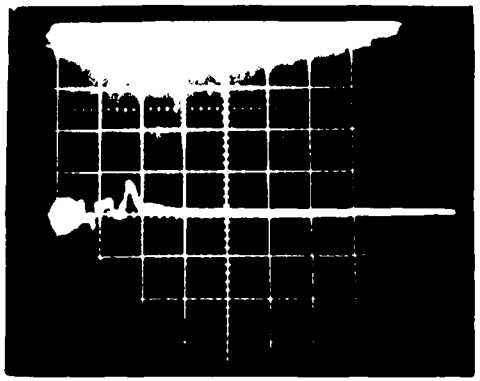

Blowoff
20 A/cm
100 ns/cm
probably NG

Figure 39. Transient record of discharge 5:47 on 0.013 cm Teflon exposed to 29 kV electrons.

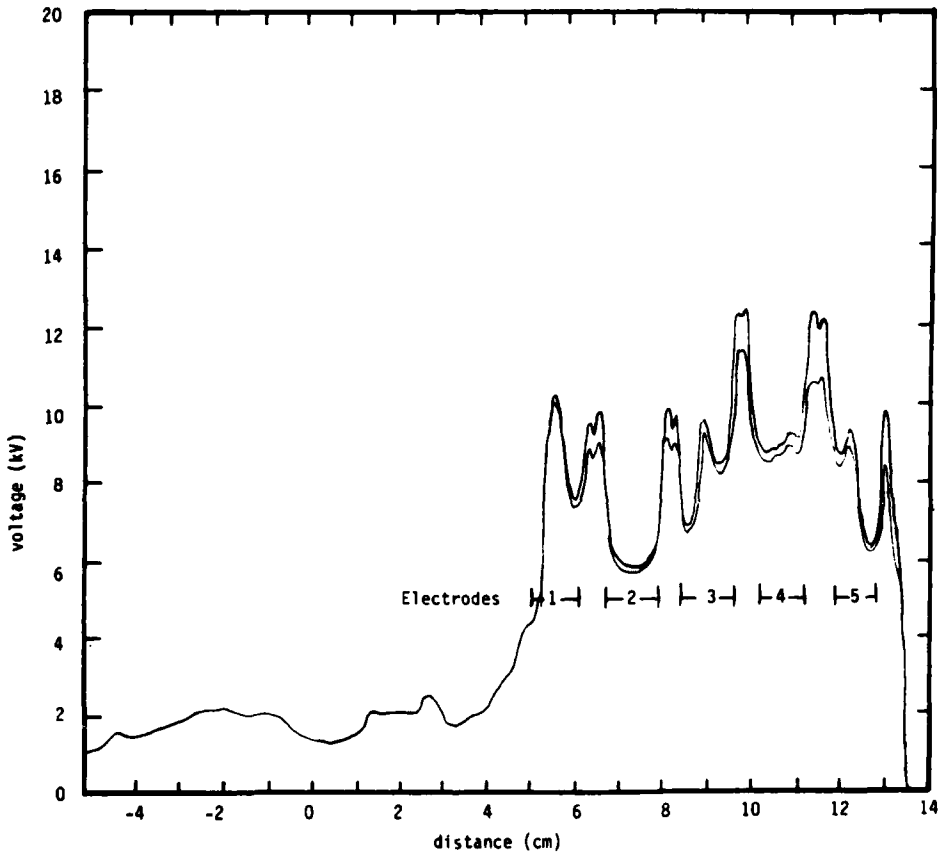

Figure 40. Decay of voltage overnight, after charging with ≈1 nA/cm^2 at 30 kV.

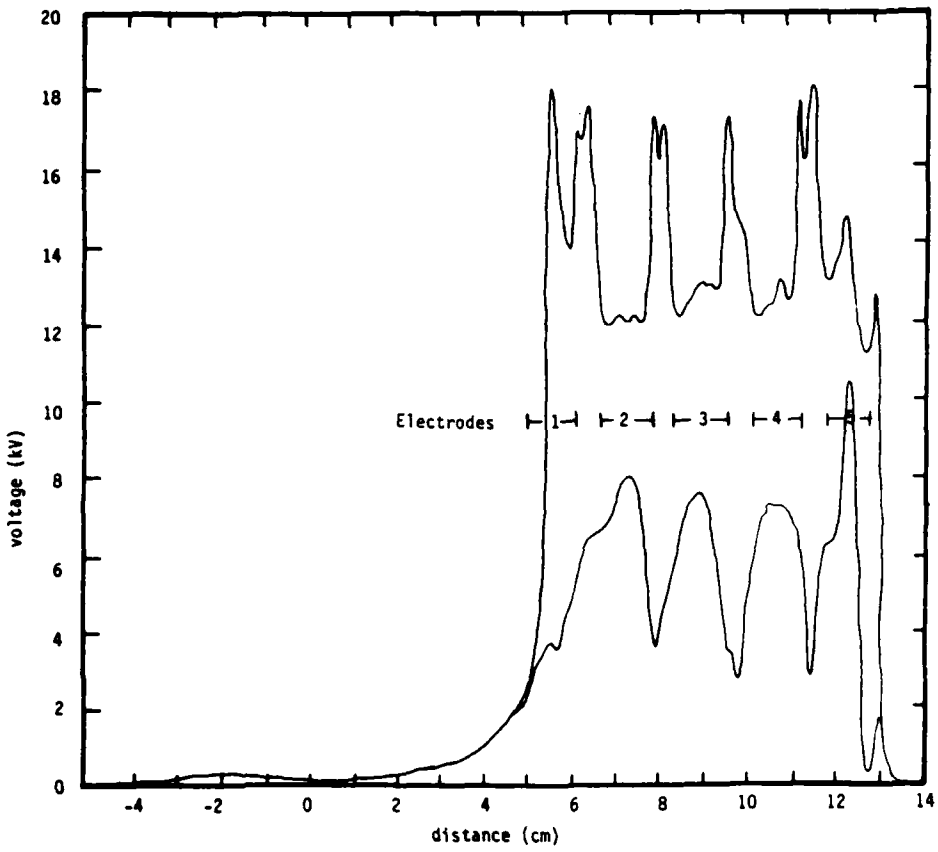

Figure 41. Potential profiles before and after a discharge induced by TREK probe striking the metal at the edge of the sample. Charging with ≈0.5 nA/cm^2 of 23 kV electrons.

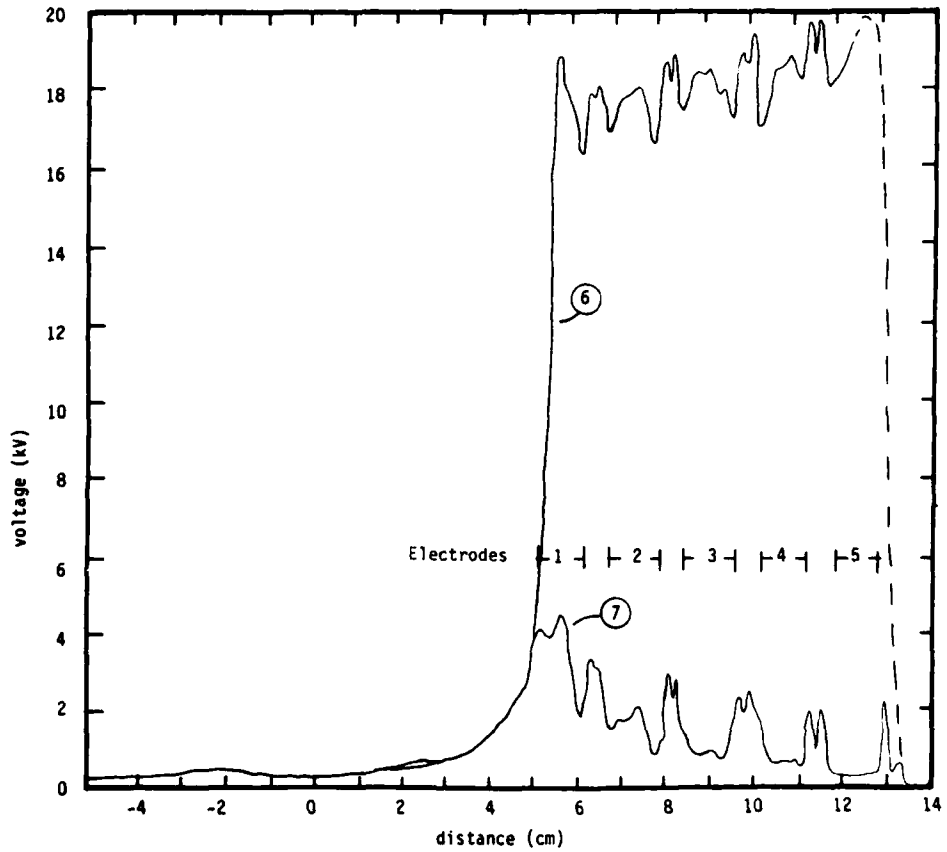

Figure 42. Potential profiles before and after discharge event 6:04. Charging with 0.5 nA/cm^2 of 23 kV electrons for ≈20 minutes before sweep ⑥. Two minutes of 26 kV electrons before event 6:04 and sweep ⑦.

Trace 6, the beam was on at 26 kV for 2 minutes at ≈0.5 nA/cm^2, which caused a spontaneous discharge. Figure 43 shows the transient data record from that event showing the discharge propagating from electrode 5 (the metal dielectric edge) toward electrode 1 (open dielectric) at a rate of ≈4 x 10^7 cm/s.

Figure 44 shows the potential profile of Teflon charged with 26 kV electrons for 12 minutes, resulting in a potential of nearly 20 kV. Two more minutes of charging caused spontaneous discharge event 6:25.

Figure 45 shows the discharge event 6:25, on 4/8/82. It propagated from the metal-dielectric boundary towards the center at a rate of ≈3.8 x 10^7 cm/s.

Figure 46 shows the "approximate" pre- and actual post-discharge potential profiles for a sample which had been charged for 9 minutes with 26 kV electrons at ≈1 nA/cm^2. The transient data for event 10:50, on 4/9/82 is shown in Figure 47. This record shows a propagation from the metal-dielectric boundary towards the center of the sample at a rate of ≈ 3.4 x 10^7 cm/s.

Figure 48 shows the pre- and post-discharge potential profiles for events which occurred at 11:40 and 12:11 on 4/9/82. At 11:40, the sample had been charged at ≈1 nA/cm^2 for 6 minutes with 26 kV electrons; at 12:11, it had been charged for ≈9 minutes. The transient records that accompany these are shown in Figures 49 and 50. Figure 49 shows a propagation from the dielectric-metal boundary toward the center of the sample at a rate of about 3.4 x 10^7 cm/s. Figure 50 shows a similar propagation. It should be noted that event 12:11 occurred 45 seconds after the impinging electron beam had been turned off.

Figure 51 shows a compilation of discharge propagation data. From these data one would infer a propagation velocity of ≈ 4.1 ± 0.8 x 10^7 cm/s. To

Channel 1
20 A/cm
100 ns/cm

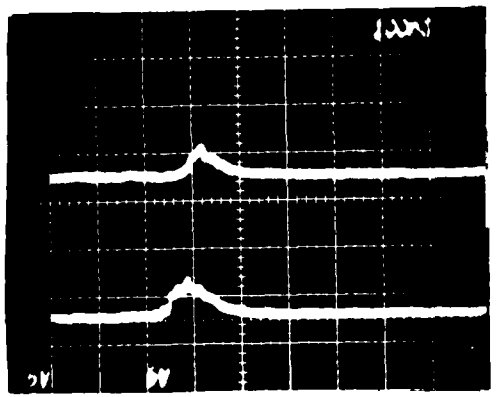

Channel 3
20 A/cm
100 ns/cm

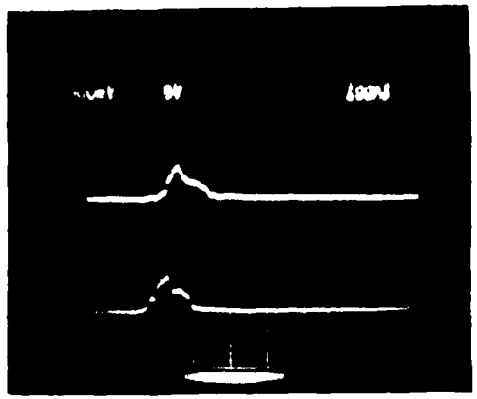

Channel 2
20 A/cm
100 ns/cm

Channel 4
20 A/cm
100 ns/cm

Material: Teflon
Charging Voltage: 26 kV

Date: 4/8/82
Time: 6:04

Channel 5
A/cm
ns/cm

NO FILM

Blowoff
20 A/cm
100 ns/cm
probably NG

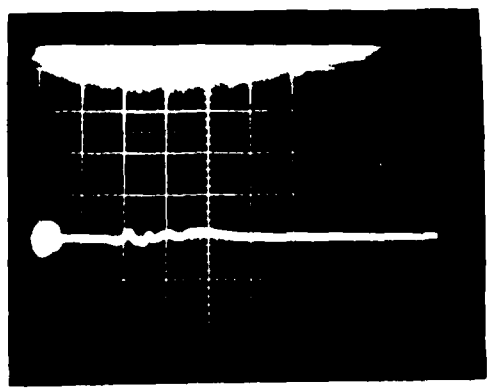

Figure 43. Transient record of discharge 6:04 on 0.013 cm Teflon exposed to 26 kV electrons.

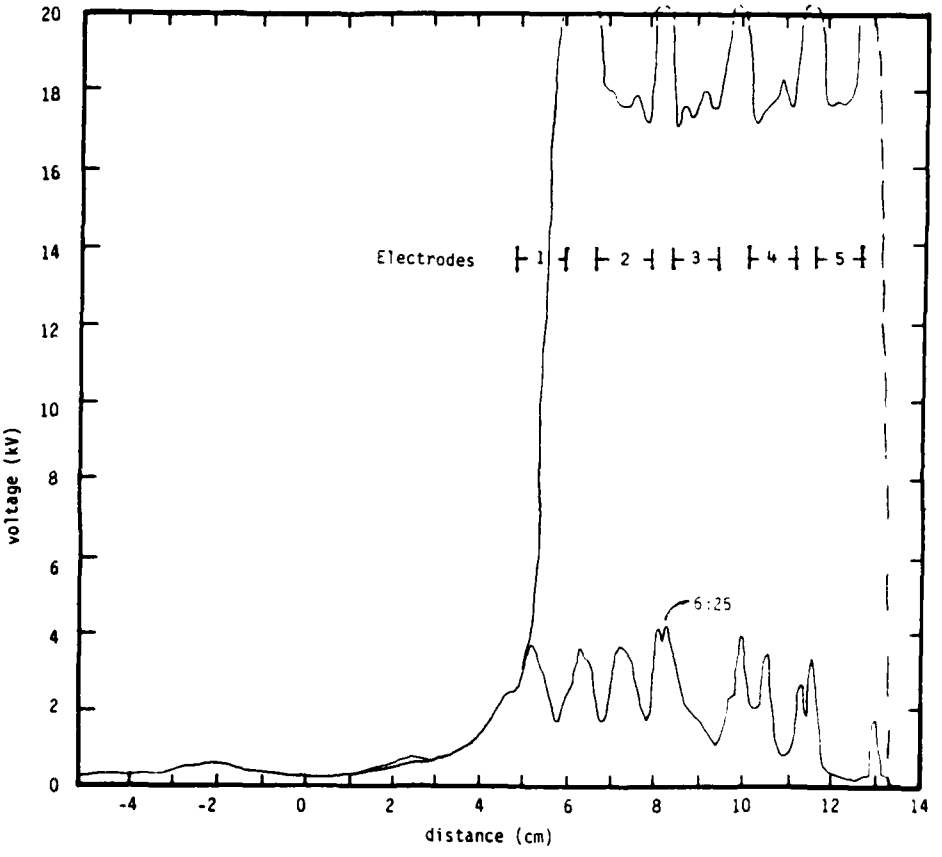

Figure 44. Potential profiles shortly before and just after discharge event 6:25. Charging with 0.5 nA/cm^2 of 26 kV electrons.

Channel 1
20 A/cm
100 ns/cm

Channel 2
20 A/cm
100 ns/cm

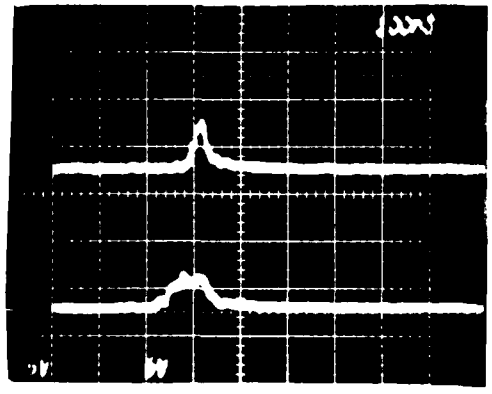

Channel 3
20 A/cm
100 ns/cm

Channel 4
20 A/cm
100 ns/cm

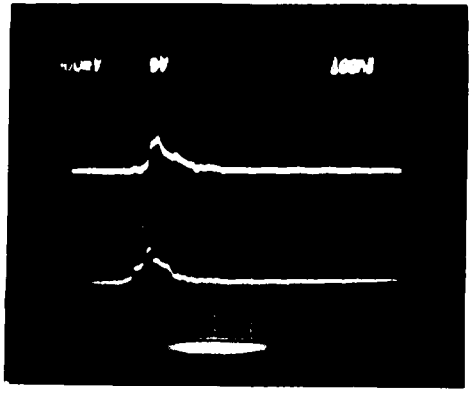

Material: Teflon
Charging Voltage: 26 kV

Date: 4/8/82
Time: 6:25

Channel 5
20 A/cm
100 ns/cm

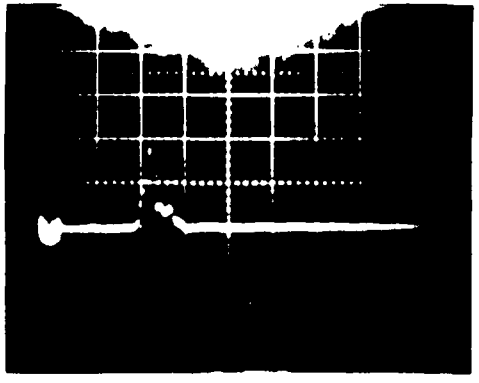

Blowoff
20 A/cm
100 ns/cm
probably NG

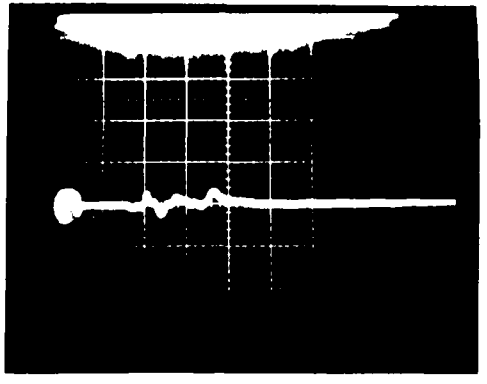

Figure 45. Transient record of discharge 6:25 on 0.013 cm Teflon exposed to 26 kV electrons.

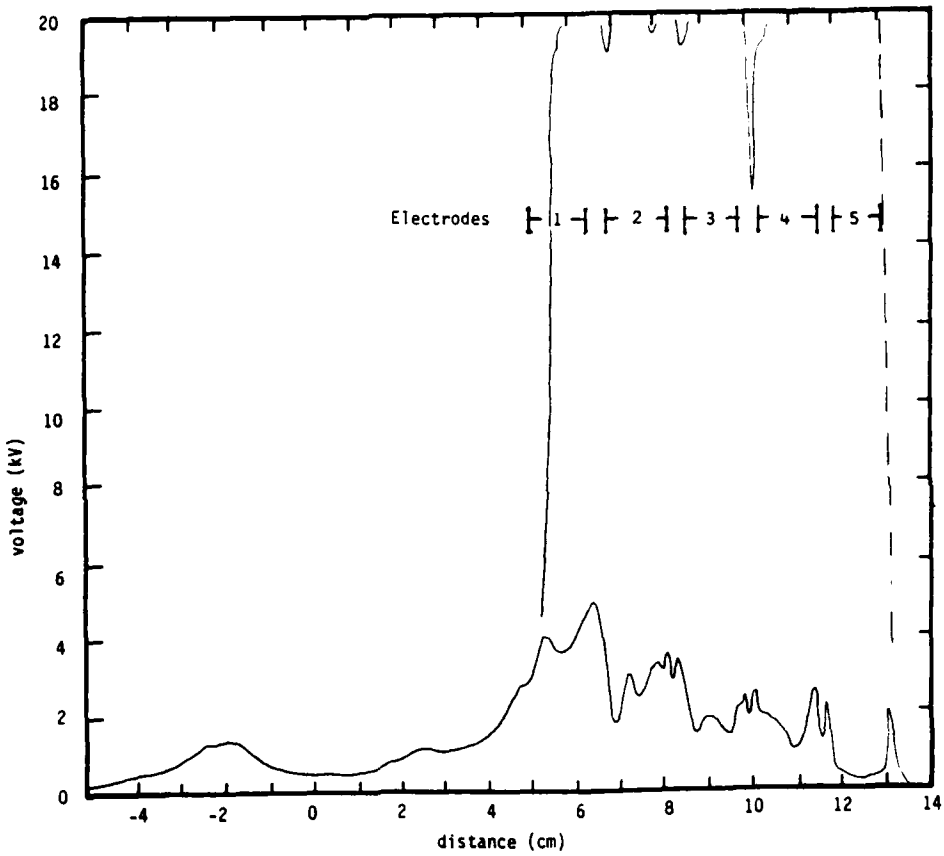

Figure 46. Post-discharge profile and estimated pre-discharge profile for event 10:50. Charging at 26 kV with 1 nA/cm^2.

Channel 1
20 A/cm
100 ns/cm

Channel 2
20 A/cm
100 ns/cm

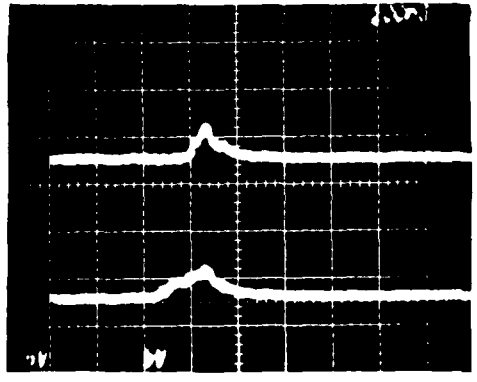

Channel 3
20 A/cm
100 ns/cm

Channel 4
20 A/cm
100 ns/cm

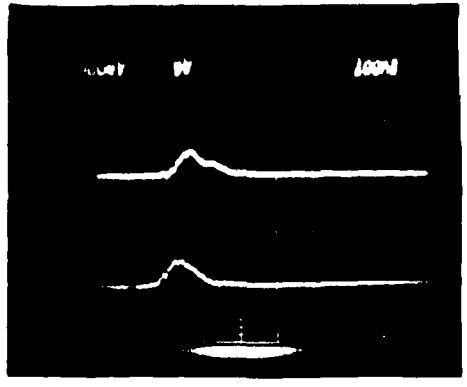

Material: Teflon
Charging Voltage: 26 kV

Date: 4/9/82
Time: 10:50

Channel 5
20 A/cm
100 ns/cm

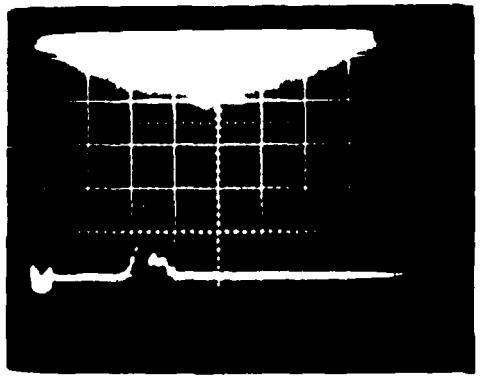

Blowoff
20 A/cm
100 ns/cm
probably NG

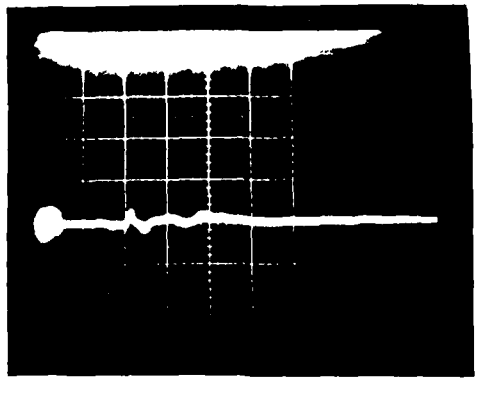

Figure 47. Transient record of discharge 10:50 on 0.013 cm Teflon exposed to 26 kV electrons.

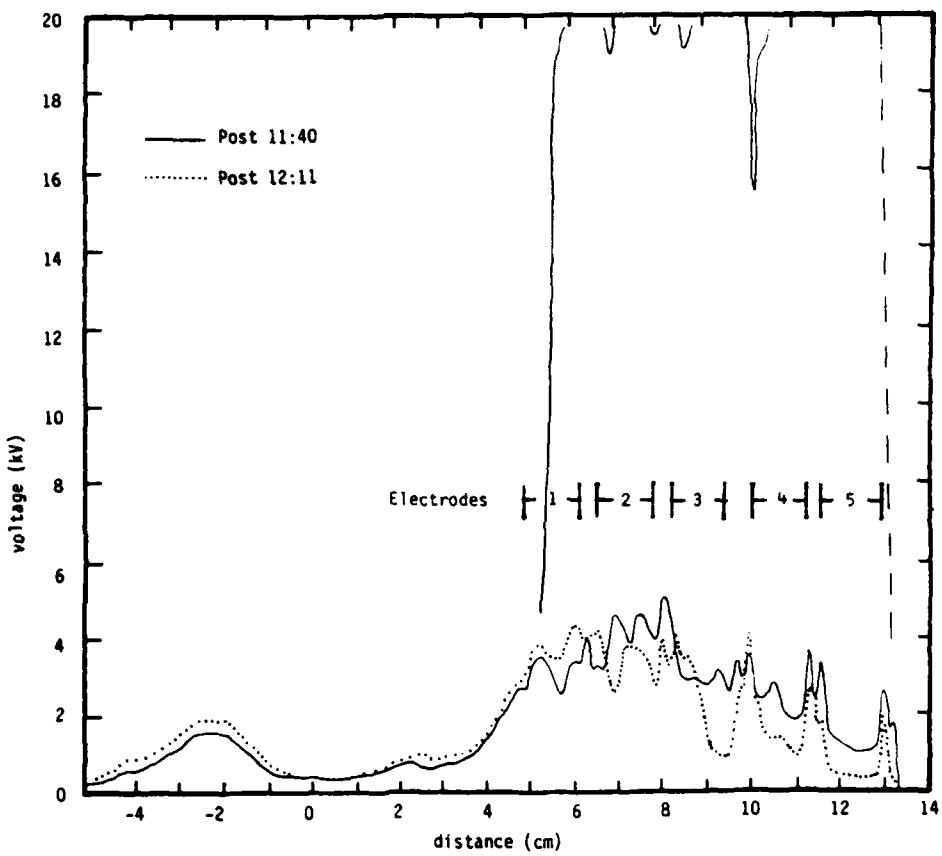

Figure 48. Post-discharge profiles and estimated pre-discharge profile. Charging with 1 nA/cm^2 of 26 keV electrons.

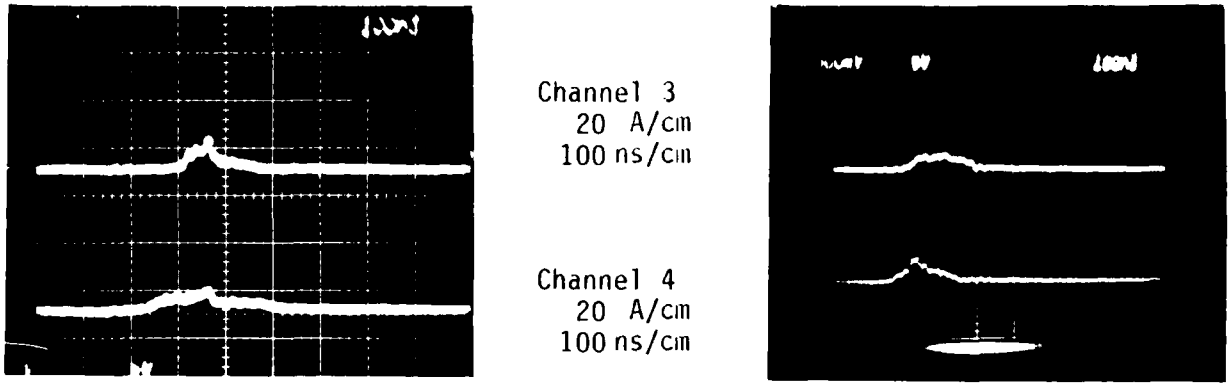

Channel 1
20 A/cm
100 ns/cm

Channel 2
20 A/cm
100 ns/cm

Channel 3
20 A/cm
100 ns/cm

Channel 4
20 A/cm
100 ns/cm

Material: Teflon
Charging Voltage: 26 kV

Date: 4/9/82
Time: 11:40

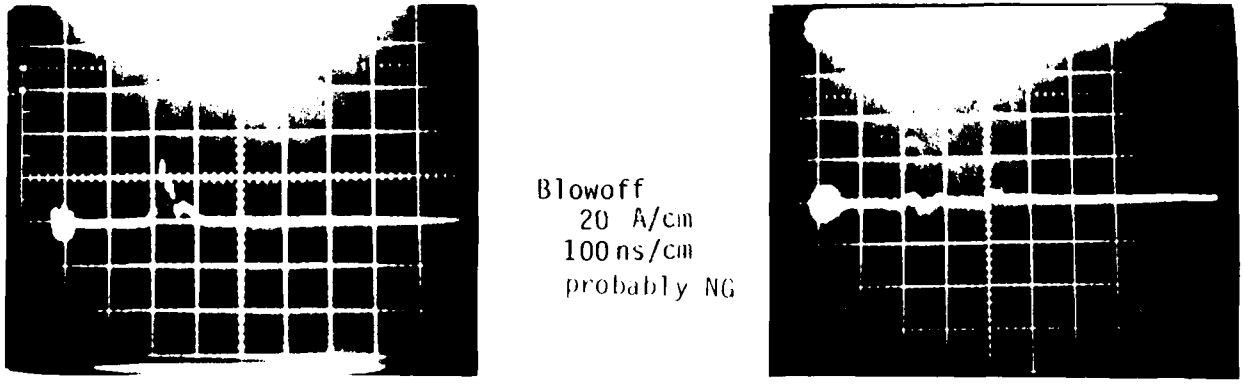

Channel 5
20 A/cm
100 ns/cm

Blowoff
20 A/cm
100 ns/cm
probably NG

Figure 49. Transient record of discharge 11:40 on 0.013 cm Teflon exposed to 26 kV electrons.

Channel 1
20 A/cm
100 ns/cm

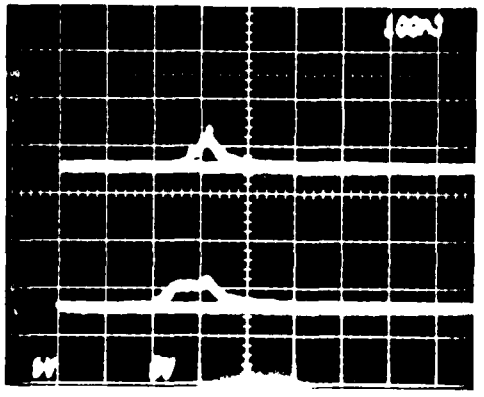

Channel 3
20 A/cm
100 ns/cm

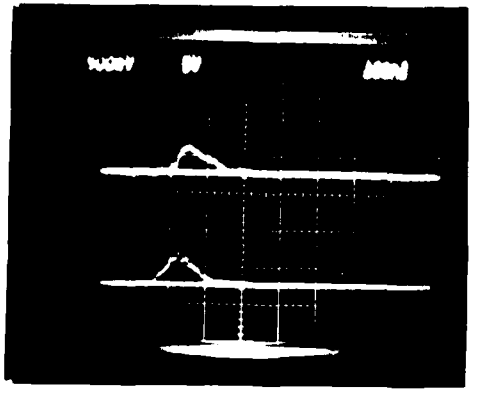

Channel 2
20 A/cm
100 ns/cm

Channel 4
20 A/cm
100 ns/cm

Material: Teflon
Charging Voltage: 26kV

Date: 4/9/82
Time: 12:11

Channel 5
20 A/cm
100 ns/cm

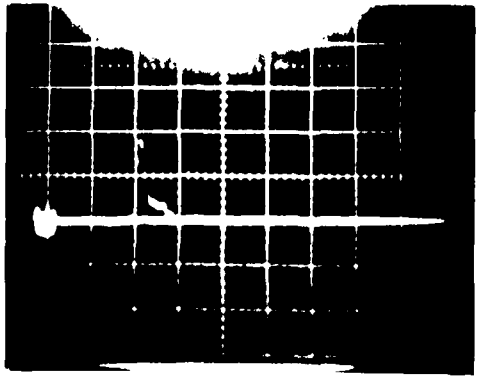

Blowoff
20 A/cm
100 ns/cm
probably NG

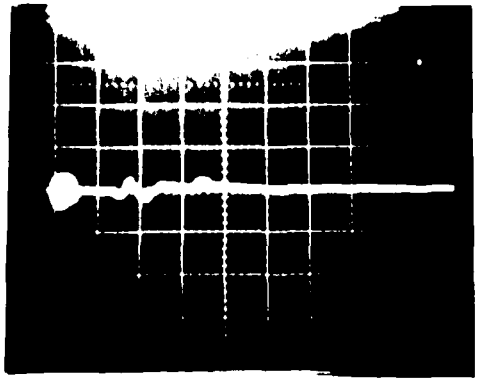

Figure 50. Transient record of discharge 12:11 on 0.013 cm Teflon exposed to 26 kV electrons.

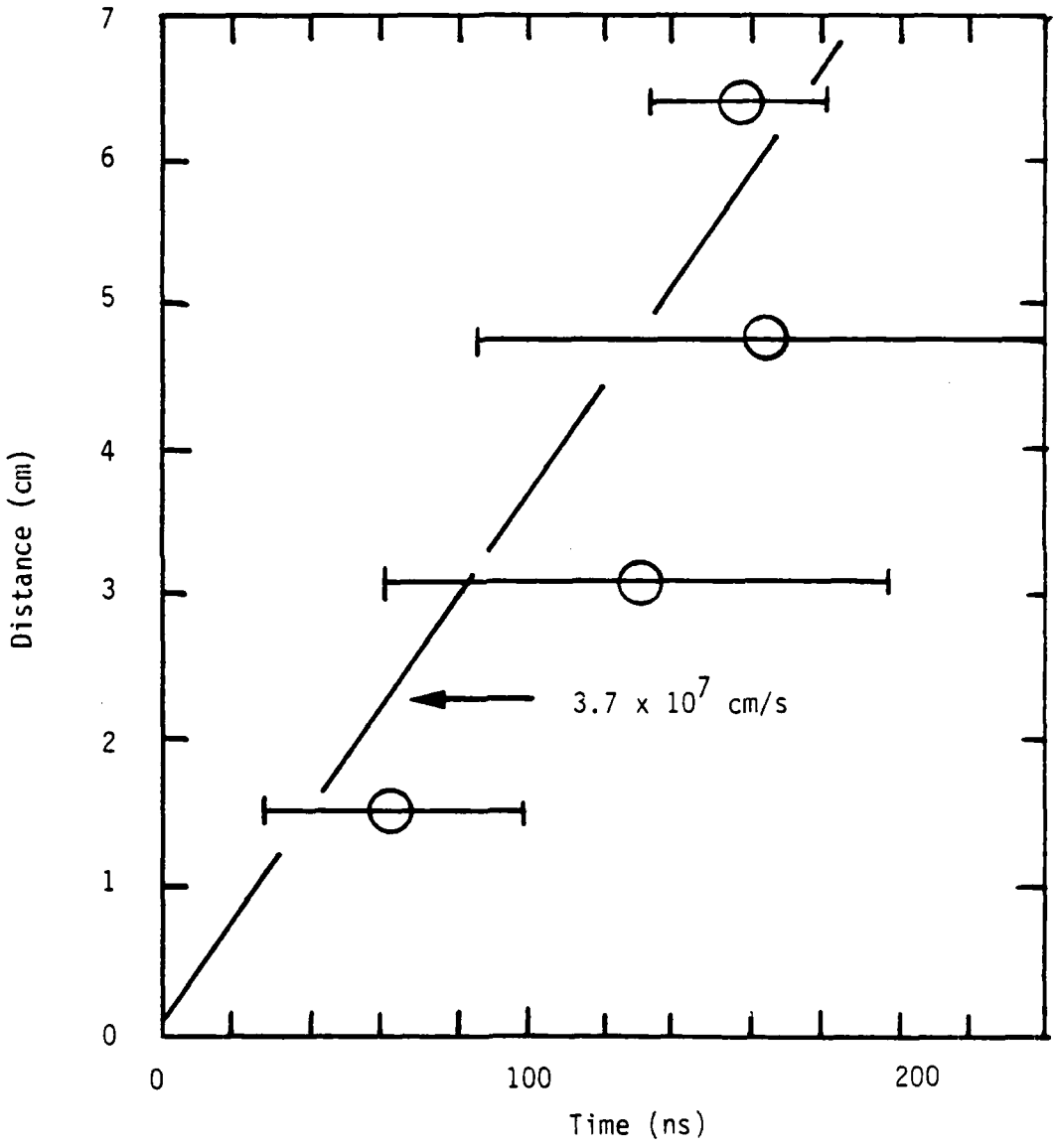

Figure 51. Compilation of the discharge propagation data for 0.013 cm (0.005") Teflon. Discharge distance versus time after initiation.

develop this figure we registered the time when the signal first appeared on each channel and plotted that on the abscissa (X scale). Each data point represents the average of all the "reasonable" arrival times for each given channel. The ordinate (y scale) represents the center-to-center distance between the sensing electrode and the electrode where a signal first appeared. The error bars indicate the standard deviation of the arrival times. This does not represent a measurement uncertainty. It represents the observation that there was considerable event to event variation.

A note concerning the blow-off collector: we have no direct evidence that the blow-off collector was shorted. However, on reviewing the data we noticed that on this sample, the blow-off collector never registered a net charge. When visually observing the discharges though, we had noted that the sodium salicylate on the blow-off collector plate had fluoresced, which we assume was caused by energetic particles arriving. Hence, we resolve this contradiction by supposing that the blow-off collector had somehow made direct contact with ground, and that charge did, in fact, get blown-off, but went straight to ground without being recorded.

3. MYLAR

The first several figures in this section exhibit some of the discharge characteristics observed for precharged Mylar. Figure 52 shows a discharge (4/1/82, 3:33) which initiates at the outer-most ring, or dielectric-metal boundary, and propagates in a more-or-less continuous fashion to the innermost electrode. Notice that substantial blow-off is observed which corresponds to collection of ≈6.4 μC of charge. While the discharge propagation velocity is somewhat discontinuous, it is ≈1 x 10^7 cm/s for this record.

Figure 53 (4/1/82, 3:25) is a record of an extremely small discharge which occurred only at the metal-dielectric boundary. The potential profiles

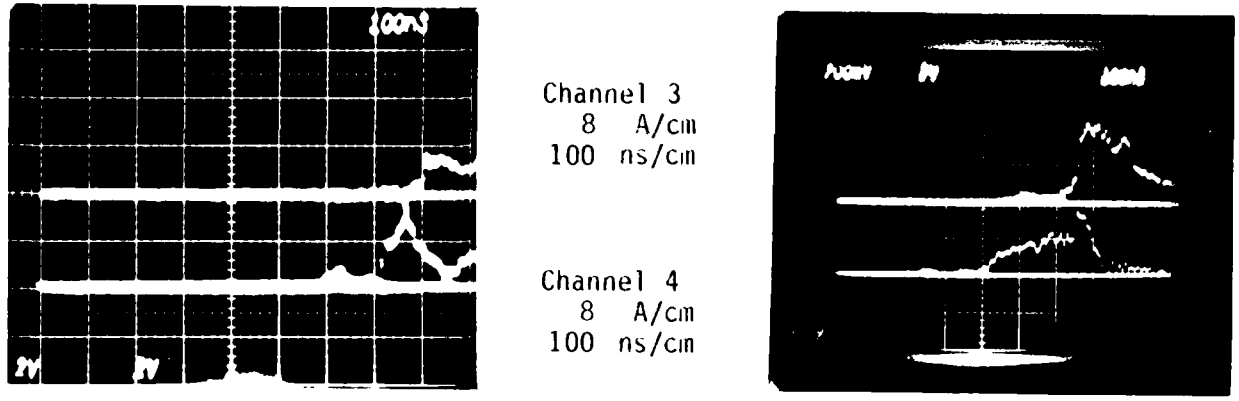

Material: Mylar
Charging Voltage: 21 kV

Date: 4/1/82
Time: 3:33

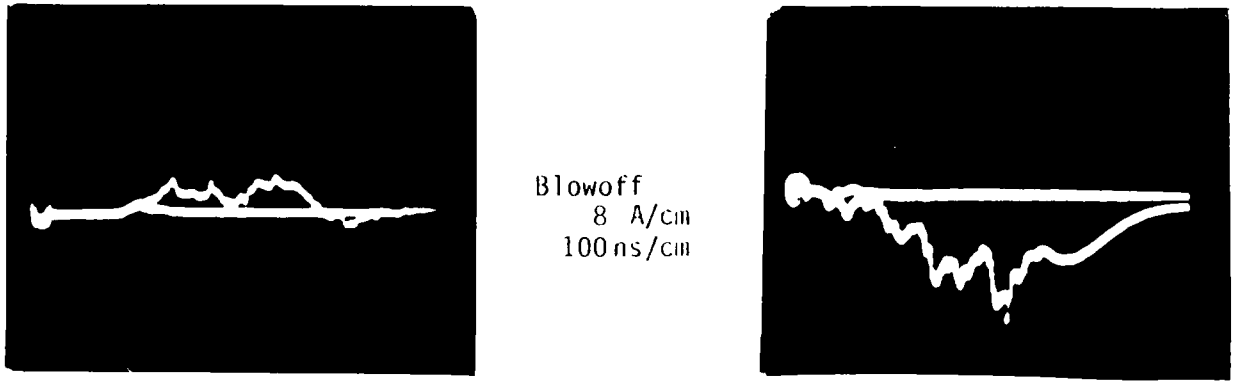

Figure 52. Transient record of discharge 3:33 on 0.0025 cm Mylar exposed to 21 kV electrons.

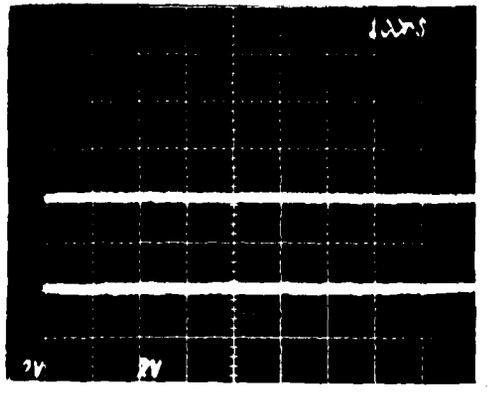

Channel 1
8 A/cm
100ns/cm

Channel 2
8 A/cm
100 ns/cm

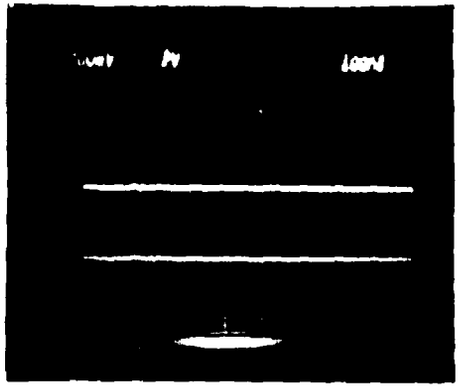

Channel 3
8 A/cm
100 ns/cm

Channel 4
8 A/cm
100 ns/cm

Material: Mylar
Charging Voltage: 21 kV

Date: 4/1/82
Time: 3:25

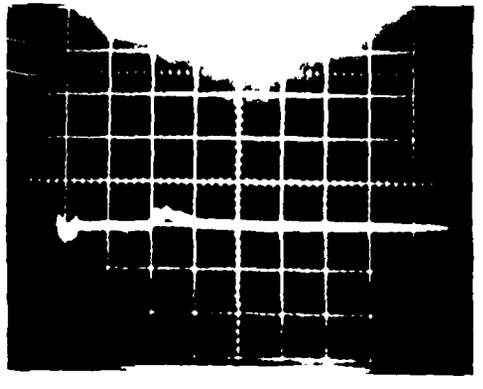

Channel 5
8 A/cm
100 ns/cm

Blowoff
8 A/cm
100 ns/cm

MISSING

Figure 53. Transient record of discharge 3:25 on 0.0025 cm Mylar exposed to 21 kV electrons.

taken immediately after each of these two discharges is shown in Figure 54. Unfortunately we didn't actually measure the potential profile just before the small discharge (3:25). The "typical" predischarge profile was obtained later. We suspect the actual pre-discharge profile was not much different than post 3:25 and that later the "aged" sample supported higher voltages. Clearly the large discharge (3:33) removed a lot more charge than discharge 3:25. Approximately 8 μC of charge were removed based on $C\Delta V$ measurements.

Figure 55 also is another record of a very small event which discharged only near the metal dielectric boundary. Figure 56 shows another transient record of a propagating discharge. One might infer a propagation velocity of $\approx 2.5 \times 10^7$ cm/s from this record, based on time of arrival of the discharge pulse. Again notice that the blow-off collector indicates the collection of negative charge. The post-discharge potential profile for these two records is shown in Figure 57. As before the large discharge removed approximately 5 microcoulombs.

Figure 58 (4/1/82, 3:14) is the transient record of a discharge which propagates in a peculiar fashion. This discharge initiates over segment #5, near the dielectric-metal boundary and appears next in the adjacent segment, #4, 150 nanoseconds later. It is comparatively insignificant in segment #3 until approximately 720 nanoseconds, which is after it appeared in the innermost segments #2 and #1. Again the blow-off collector is large and negative, indicating the collection of about 4 μC of charge. In other words nearly all the charge which was removed from the dielectric was blown off to the collector. Figure 59 shows the approximate pre-discharge potential profile (obtained by extrapolating from previously measured profiles to the moment of discharge) and (exact) post-discharge potential profile for this event (3:14). There is also evidence from this record also that charge was removed more from the area over segments 1, 2, 4, and 5 than 3.

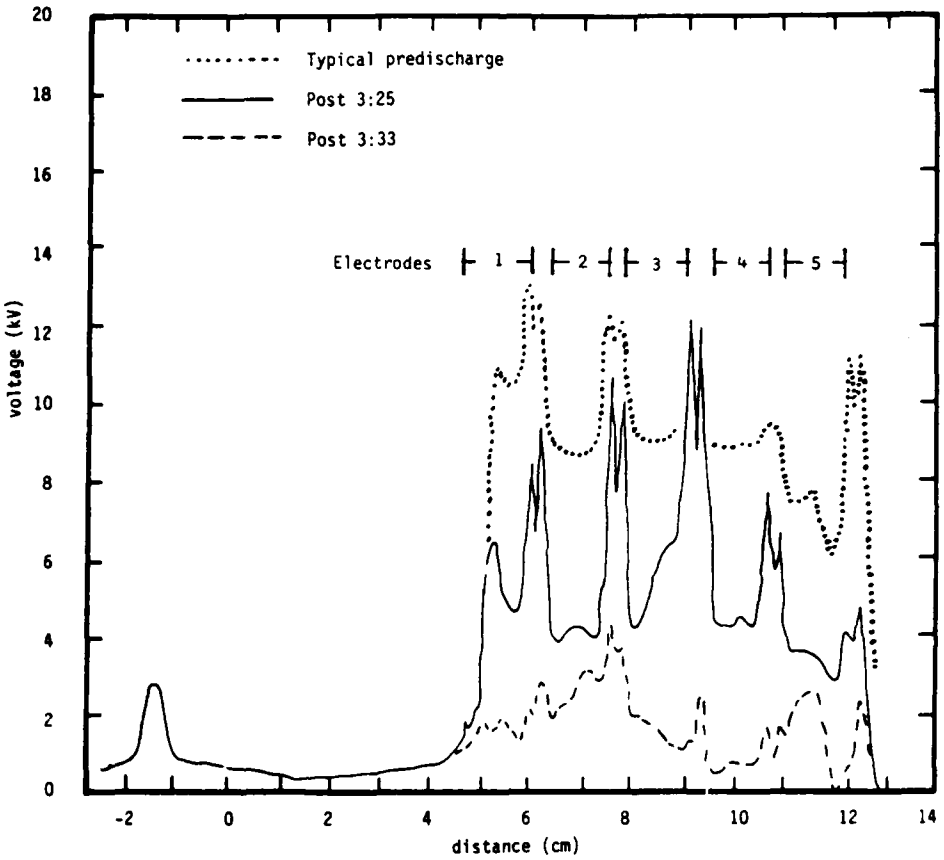

Figure 54. Estimated pre- and actual post-discharge potential profiles. Charging with 2 nA/cm^2 of 21 keV electrons.

Channel 1
8 A/cm
200 ns/cm

Channel 2
8 A/cm
200 ns/cm

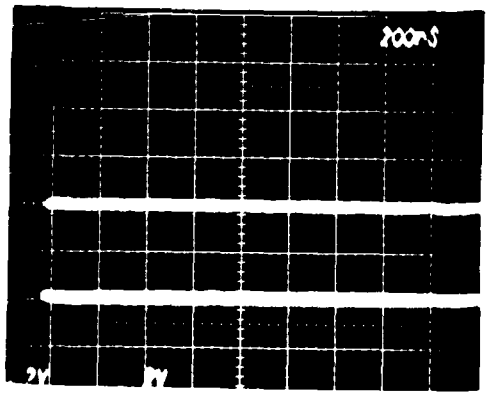

Channel 3
8 A/cm
200 ns/cm

Channel 4
8 A/cm
200 ns/cm

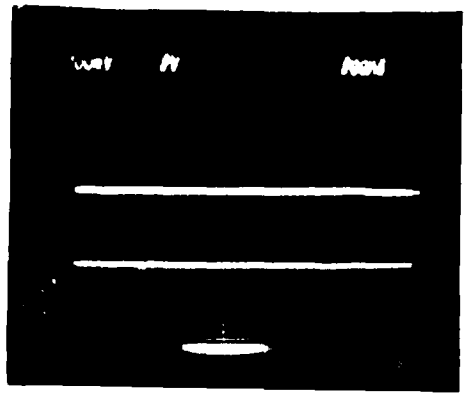

Material: Mylar
Charging Voltage: 21 keV

Date: 4/1/82
Time: 3:52

Channel 5
8 A/cm
200 ns/cm

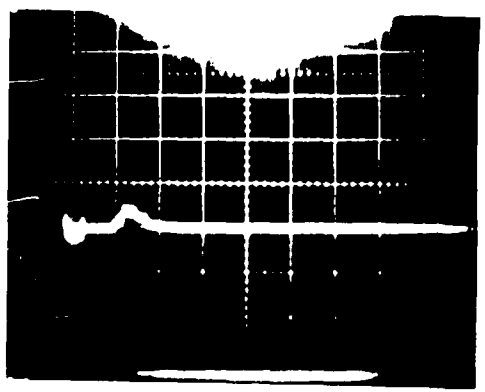

Blowoff
8 A/cm
200ns/cm

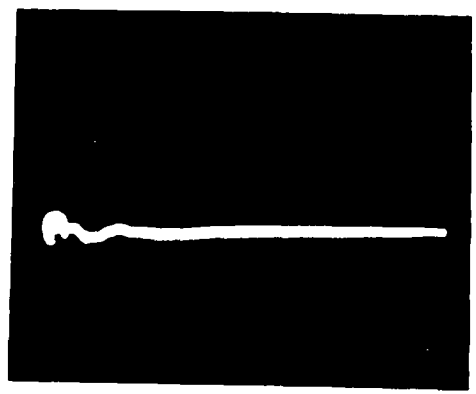

Figure 55. Transient record of discharge 3:52 on 0.0025 cm Mylar exposed to 21 kV electrons.

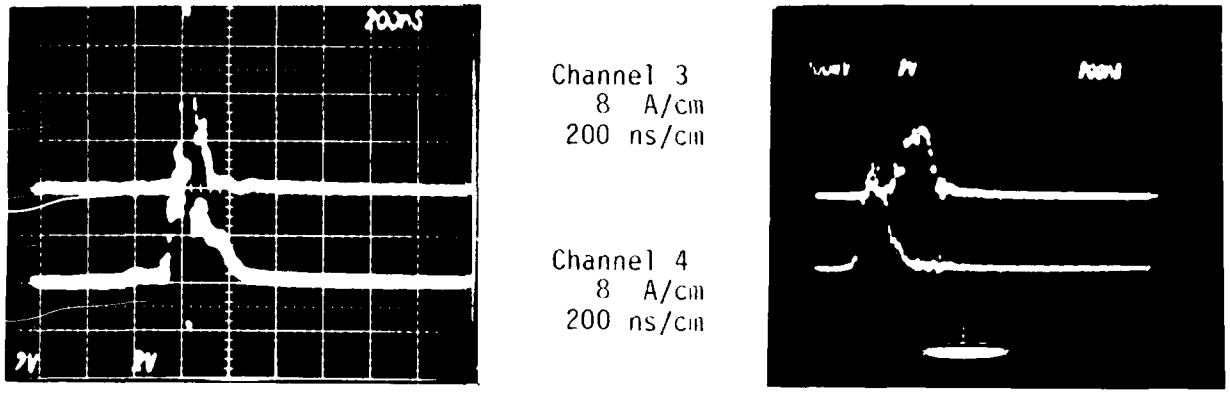

Figure 56. Transient record of discharge 4:01 on 0.0025 cm Mylar exposed to 21 kV electrons.

AD-A140 666 CHARGING AND DISCHARGING OF SPACECRAFT THERMAL CONTROL DIELECTRICS(U) MISSION RESEARCH CORP SAN DIEGO CA J D RIDDEL ET AL. 01 AUG 82 MRC/SD-R-105 DNA-TR-81-162 2/2

UNCLASSIFIED DNA001-81-C-0151 F/G 20/3 NL

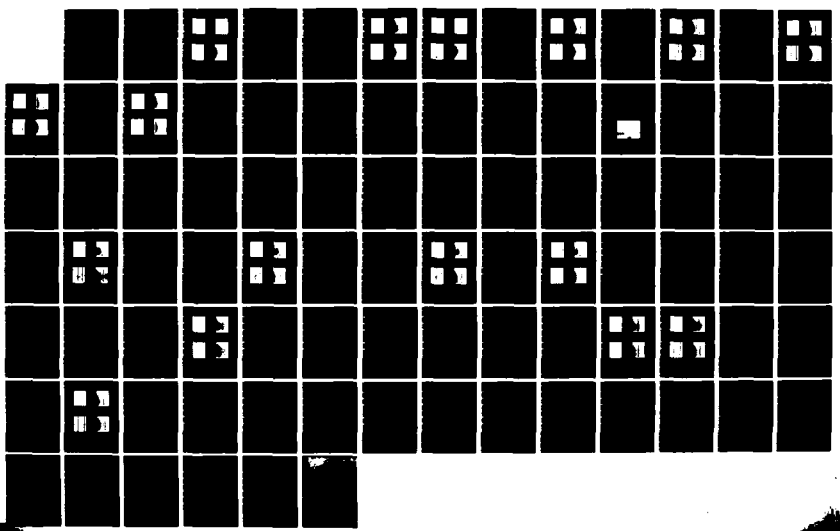

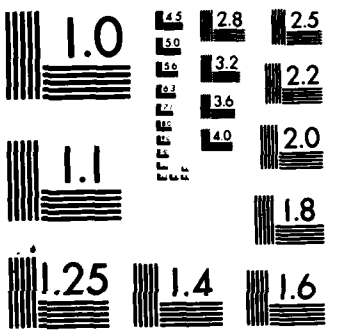

MICROCOPY RESOLUTION TEST CHART
NATIONAL BUREAU OF STANDARDS-1963-A

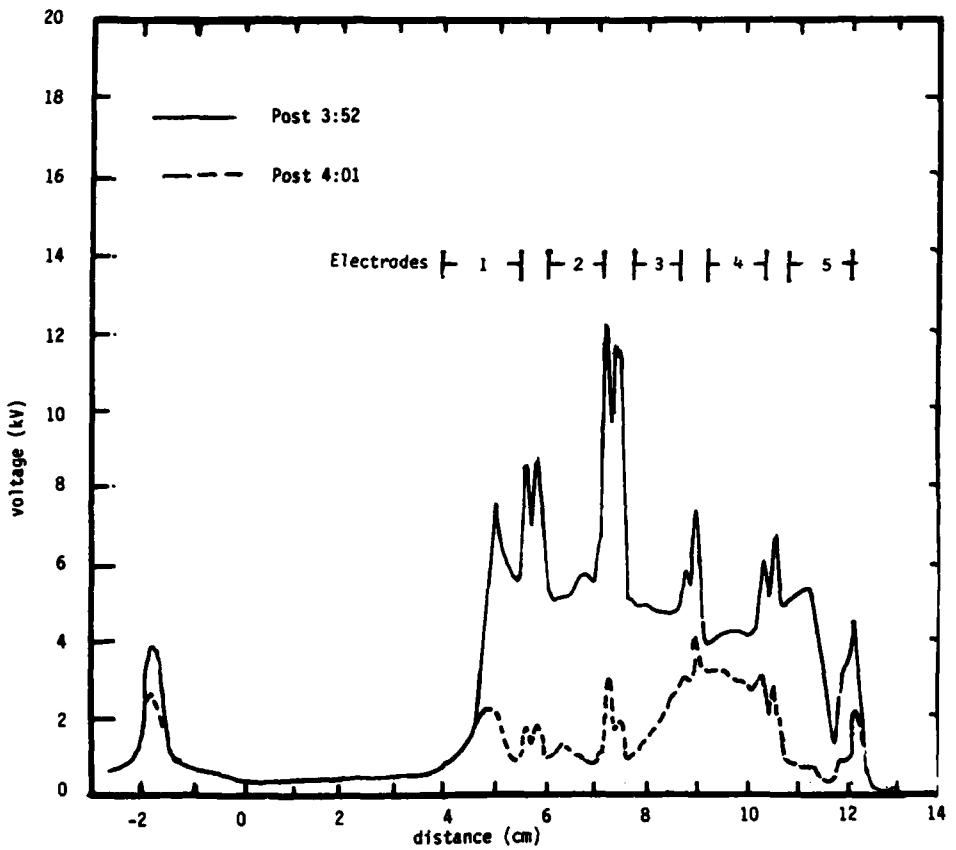

Figure 57. Post discharge profile for events 4/1/82, 3:52 and 4:01. Since 3:52 involved only a small element of the sample, we think 3:52 is a reasonable approximation of pre-discharge profiles. The maximum potential on Mylar was limited by conductivity.

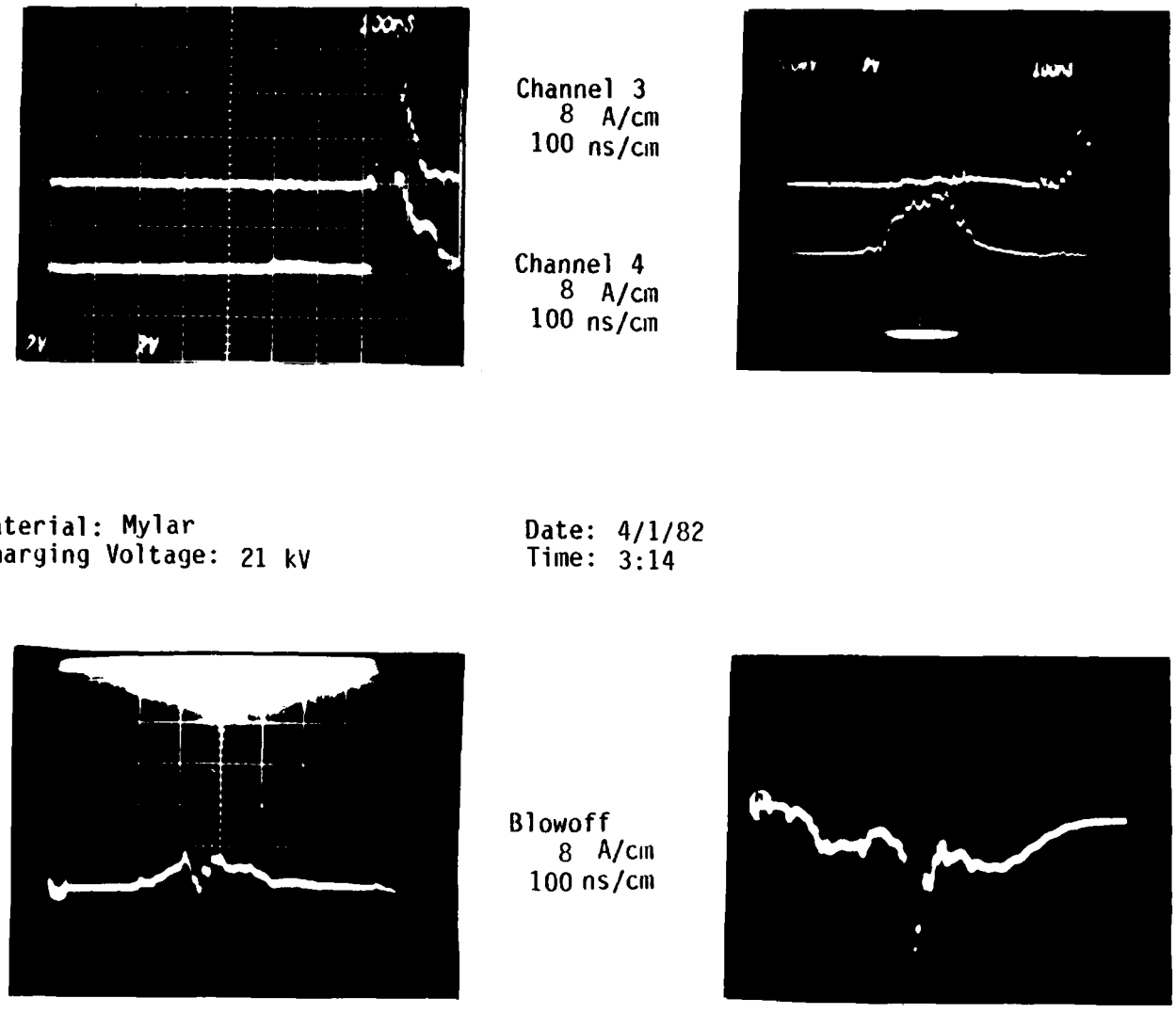

Figure 58. Transient record of discharge 3:14 on 0.0025 cm Mylar exposed to 21 kV electrons.

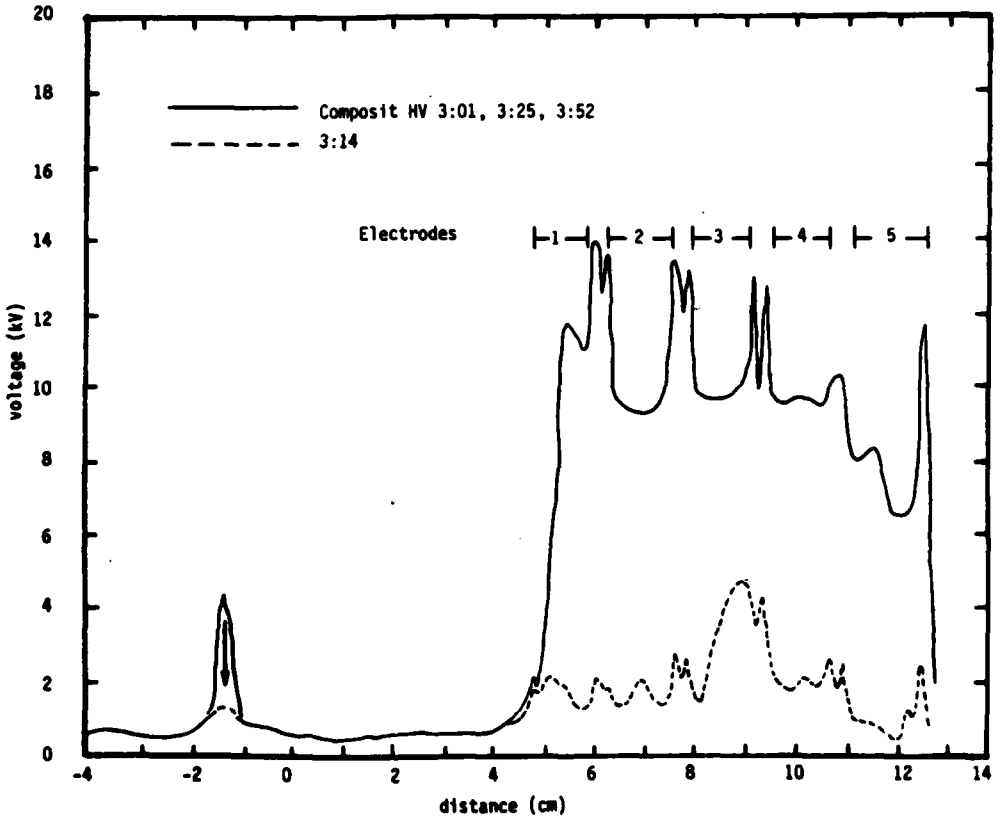

Figure 59. Approximate pre- and actual post-discharge 3:14 potential profiles. Charging with 2 nA/cm^2 of 21 keV electrons.

Figures 60 (4/1/82, 5:41) and 61 (4:43) show discharges with another character. In these events the discharge appears nearly simultaneously over all five segmented electrodes, which would correspond to a propagation velocity in excess of 3×10^8 cm/s. These discharges persist, however, for ≈200 nanoseconds. Notice that in these cases the blow-off collector had been biased +200 volts and that the large negative blow-off collector signal represents the collection of more than 30 microcoulombs of negative charge. This is somewhat puzzling since that is more than 5 times the amount of charge lost by the sample as determined with the before and after potential profile ($\Delta Q = C\Delta V$) shown in Figure 62. One possible explanation is conduction through, or charge separation of, a neutral plasma in the space above the charged dielectric.

Figure 63 shows the transient record of the propagating discharge (10:02) involving only the surface over segment 5. Notice that the blow-off collector signal is small and negative. That only segment 5 discharged is substantiated by the post 10:02 profile of Figure 64, which shows a reduced sample potential principally in the area of segment 5 (11-13 cm).

Figure 65 (10:38) shows another nearly simultaneous discharge over the entire sample surface. In this case the blow-off collector had been biased to -200 volts in an attempt to suppress the blow-off electrons and collect ions (should any be present). There is a prompt negative signal on the blow-off collector, simultaneous with the transient signal on the segmented electrodes followed by a long persistent positive signal which may be due to conduction through a plasma, or the collection of positive ions. The net charge under this signal is probably about 200 μC, which is very large compared to the charge loss (≈ 30 μC) inferred from the potential profile before and after (10:38) shown in Figure 63. This would seem to confirm the hypothesis that the discharge generates a neutral plasma which either provides a conducting path between the blow-off collector and ground or separates into positive and negative charges which are collected by the blow-off collector according to its bias. Other authors have asserted a plasma is

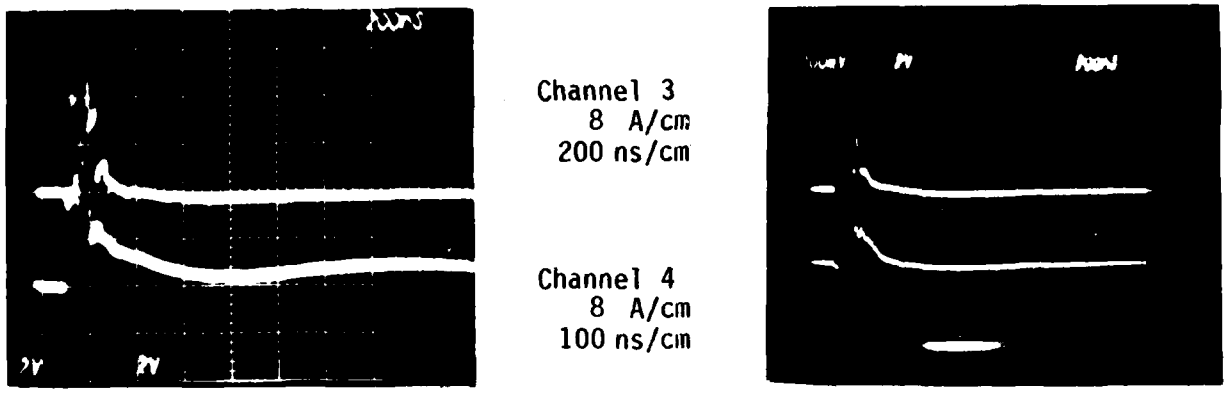

Material: Mylar
Charging Voltage: 21 kV

Date: 4/1/82
Time: 5:41

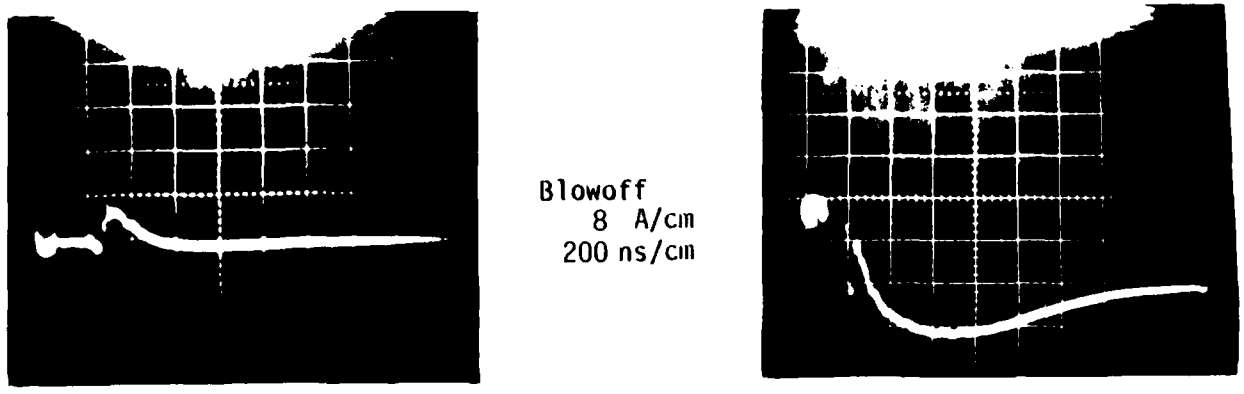

Figure 60. Transient record of discharge 5:41 on 0.0025 cm Kapton exposed to 21 kV electrons. Blow-off collector biased +200 V.

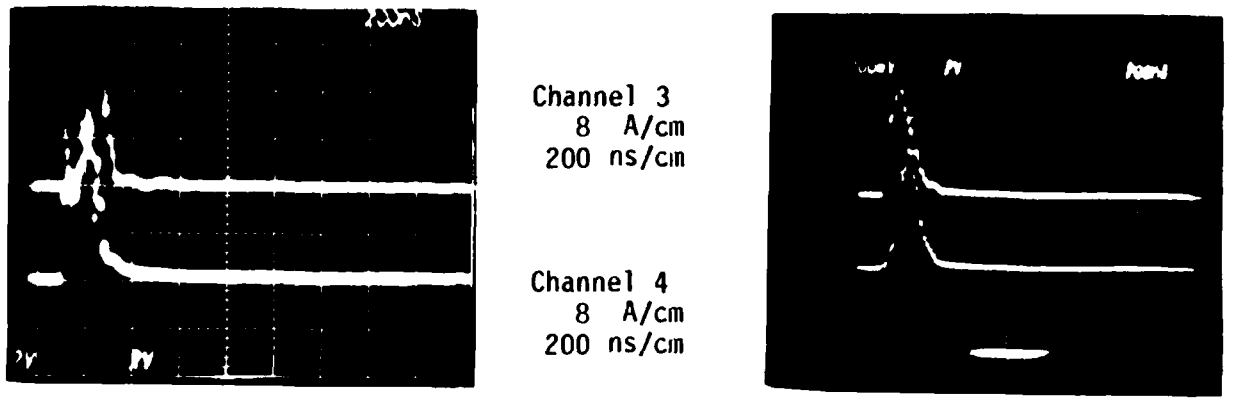

Figure 61. Transient record of discharge 4:43 on 0.0025 cm Kapton exposed to 21 kV electrons. Blow-off collector biased +200 V.

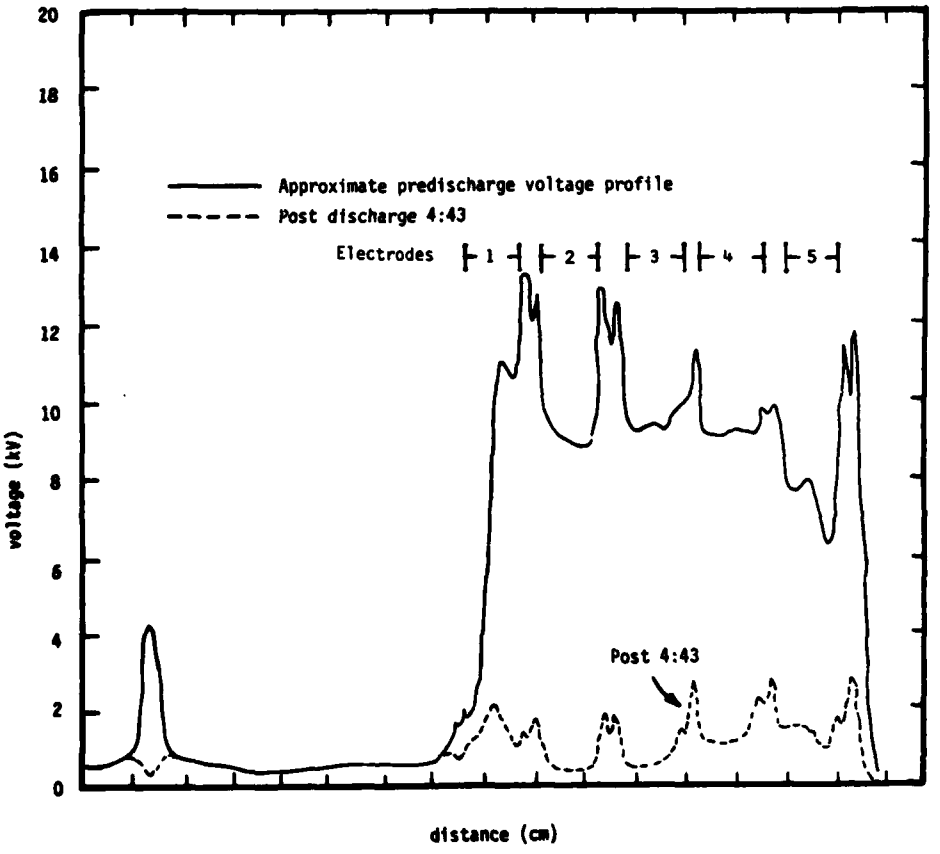

Figure 62. Approximate pre- and actual post-discharge 4:43 potential profiles. Charging with 2 nA/cm^2 of 21 keV electrons.

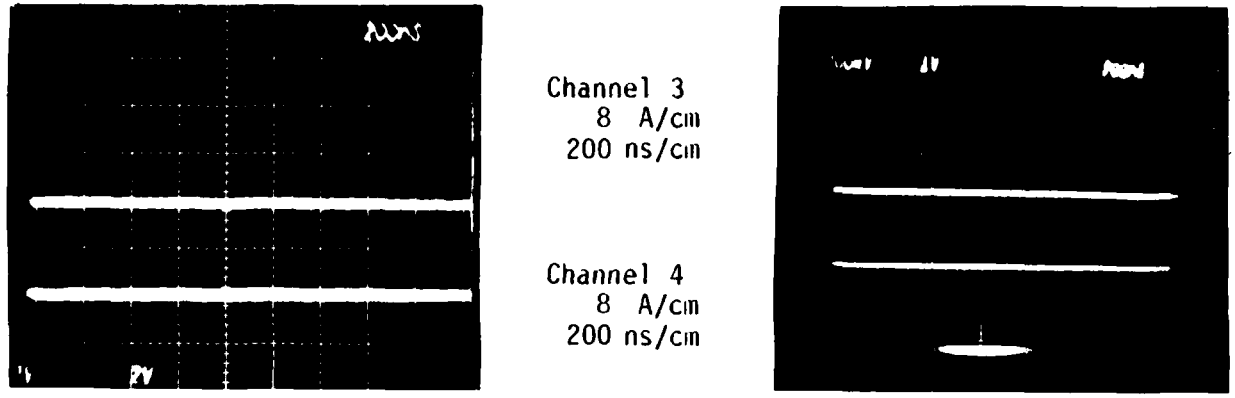

Material: Mylar
Charging Voltage: 21 kV

Date: 4/2/82
Time: 10:02

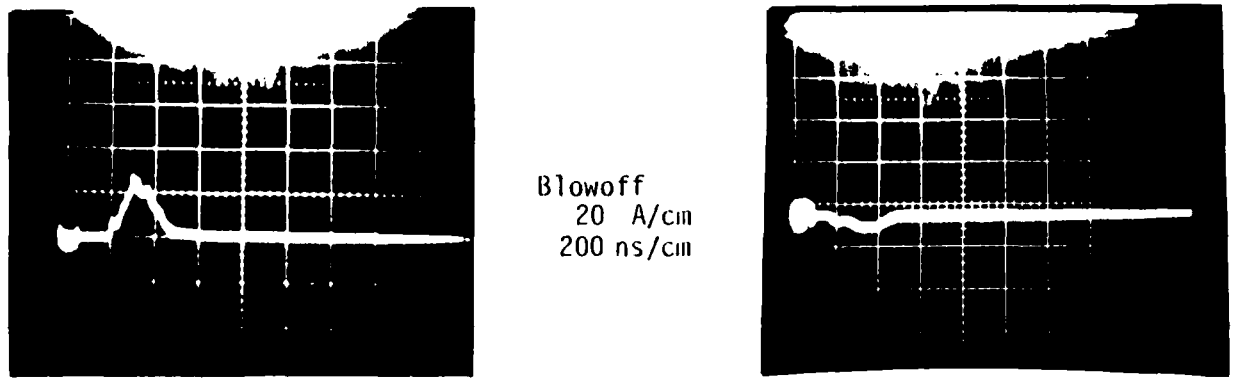

Figure 63. Transient record of discharge 10:02 on 0.0025 cm Mylar exposed to 21 kV electrons.

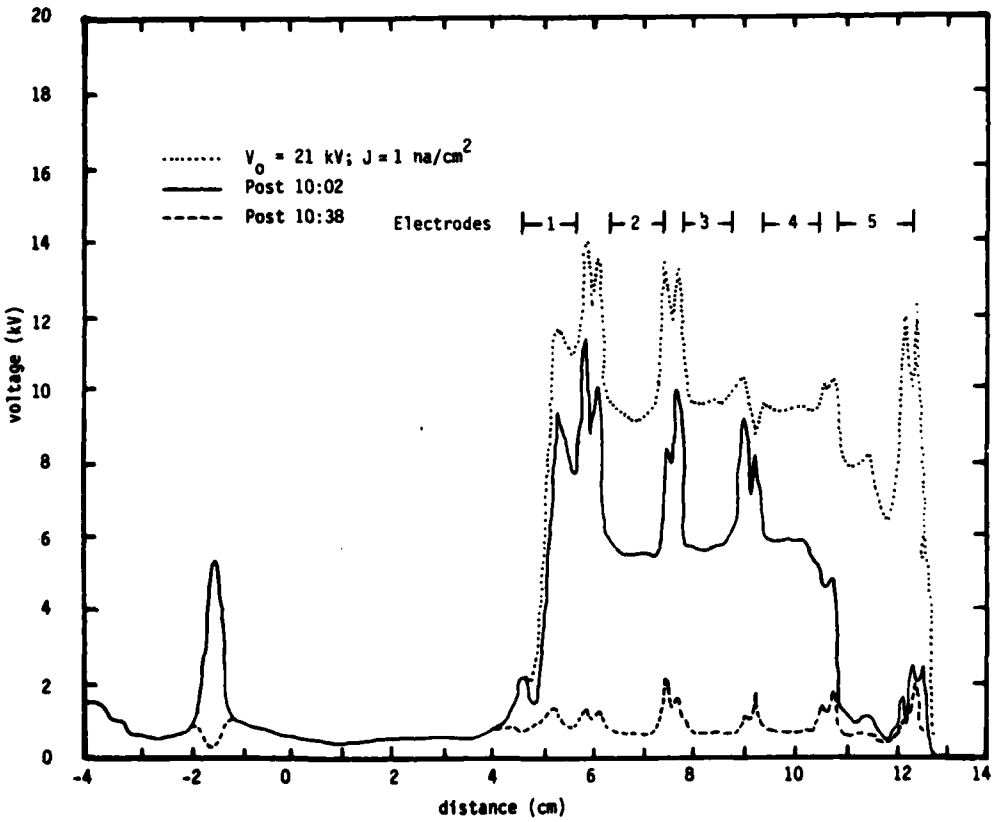

Figure 64. Projected pre- and measured post-discharge (10:02 and 10:38) voltage profiles for 0.0025 cm thick Mylar exposed to ≈ 1 nA/cm^2 of 21 kV electrons.

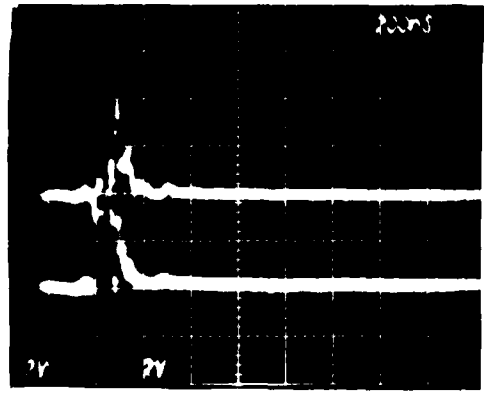

Channel 1
8 A/cm
200 ns/cm

Channel 2
8 A/cm
200 ns/cm

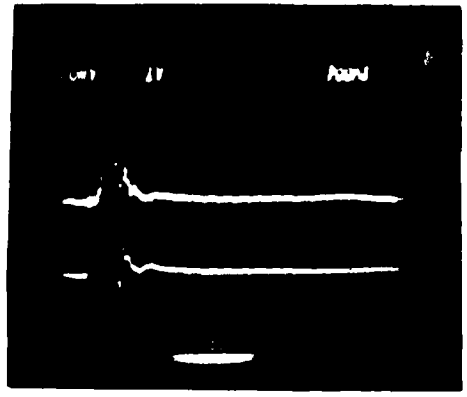

Channel 3
8 A/cm
200 ns/cm

Channel 4
8 A/cm
200 ns/cm

Material: Mylar
Charging Voltage: 21 kV

Date: 4/2/82
Time: 10:38

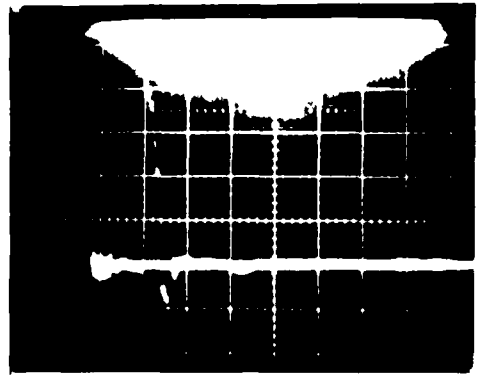

Channel 5
8 A/cm
200 ns/cm

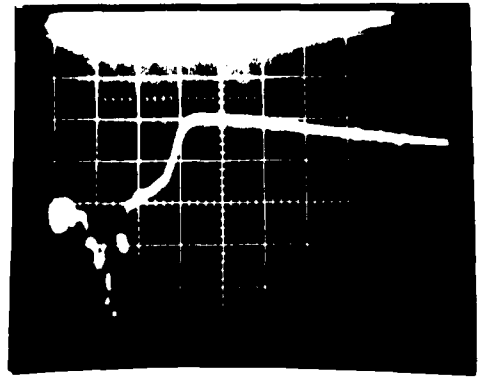

Blowoff
20 A/cm
200 ns/cm

Figure 65. Transient record of discharge 10:38 on 0.0025 cm Mylar exposed to 21 kV electrons. Blow-off collector biased at -200 V.

associated with discharges (Ref. 9), and a back-of-the-envelope calculation indicates that there is enough energy in the discharge to produce the amounts of charge collected by the blow-off collector.

Figure 66 shows another discharge event (4/2/82, 1:26) which appears nearly simultaneously over the entire 3 by 8 cm sample area. Notice that the signals on all segmented electrodes are positive (characteristic of electrons leaving the sample surface) except for segment 2 which is negative, and therefore may represent a punch-through. In this case the blow-off collector shows a bipolar signal which is initially negative (collecting electrons) and subsequently positive (ordinary type, i.e. not collecting ions), though the blow-off collector was not biased.

Figure 67 shows another nearly simultaneous discharge (1:44) (although segment 1 senses current 40 nanoseconds after segment 2). This event also exhibits a bipolar blow-off signal, but also shows a late time negative going trace on electrode 5. A negative-going signal on electrode 5 would represent negative charges returning to the electrode or positive charges leaving. Figure 68 shows the pre- and post-discharge voltage profiles for these two events.

Figure 69 shows a data record which represents (a) one discharge (3:13) which propagates in a discontinuous fashion or (b) two separate discharges. The record shows a signal first appearing on segment 5 (the metal-dielectric boundary) coincident with a small negative blow-off collector signal and followed ~ 260 ±20 nanoseconds later by charge motion over segments 1 through 4.

Figure 70 shows two potential profiles taken approximately 6 days apart. From these data one may infer that the dark conductivity of mylar charged to approximately 1 kilovolt is no greater than 2×10^{-19} $(\text{ohms/cm})^{-1}$.

---

9. A.R. Fredrickson, "Bulk Charging and Breakdown in Electron-Irradiated Polymers," pg. 33 of the 1980 Spacecraft Charging Technology Conference Proceedings, NASA pub. 2182.

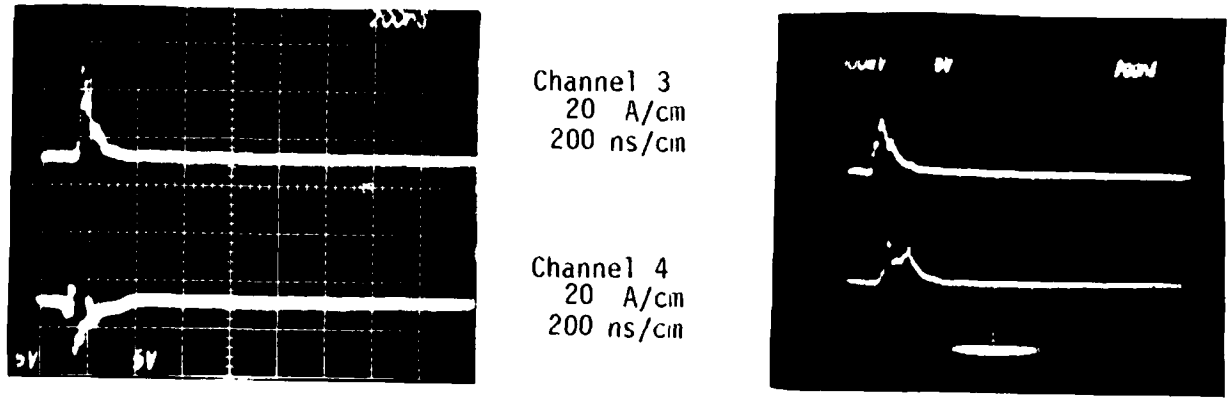

Material: Mylar
Charging Voltage: 22 kV

Date: 4/2/82
Time: 1:26

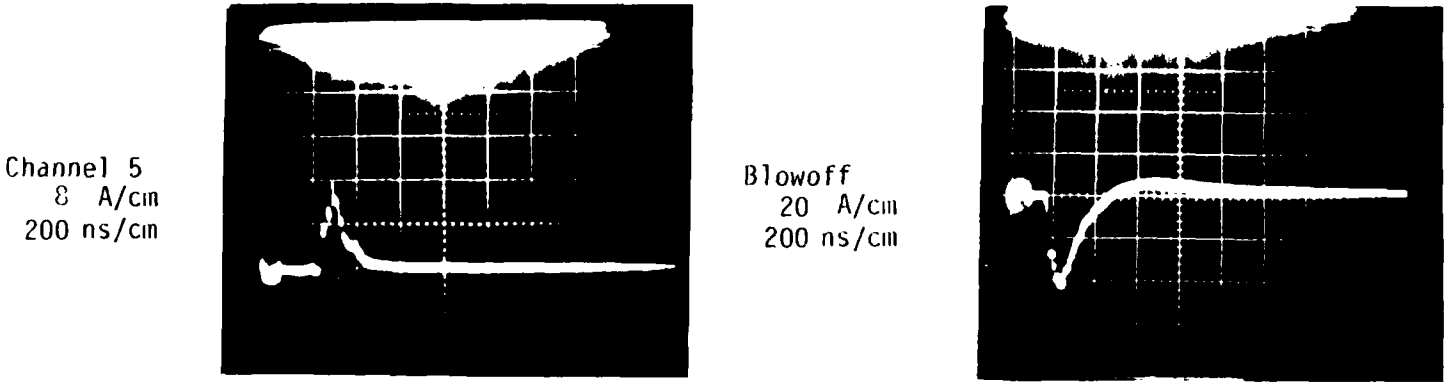

Figure 66. Transient record of discharge 1:26 on 0.0025 cm Kapton exposed to 22 kV electrons. Channel 2 may reflect a punch-through.

Channel 1
20 A/cm
100 ns/cm

Channel 2
20 A/cm
100 ns/cm

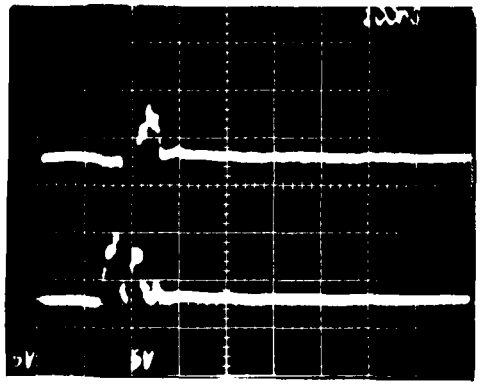

Channel 3
20 A/cm
100 ns/cm

Channel 4
20 A/cm
100 ns/cm

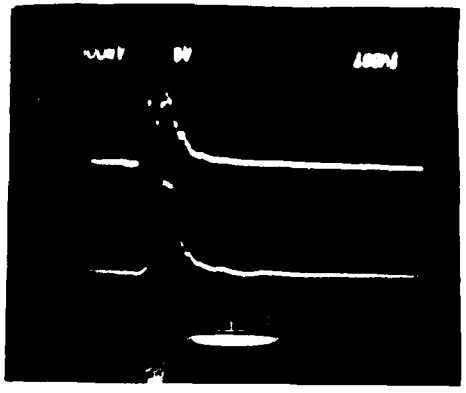

Material: Mylar
Charging Voltage: 22 kV

Date: 4/2/82
Time: 1:44

Channel 5
20 A/cm
100 ns/cm

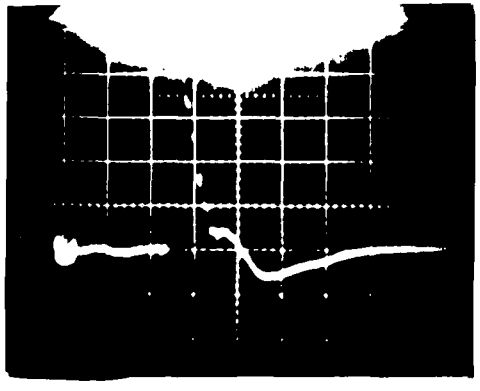

Blowoff
20 A/cm
100 ns/cm

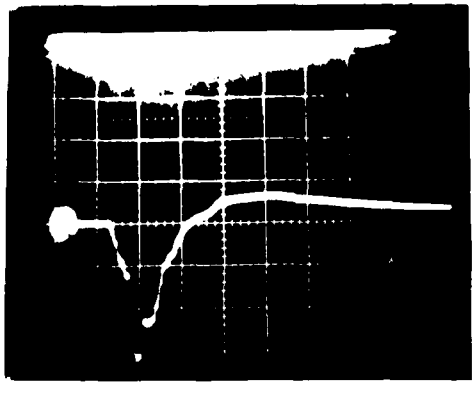

Figure 67. Transient record of discharge 1:44 on 0.0025 cm Kapton exposed to 22 kV electrons.

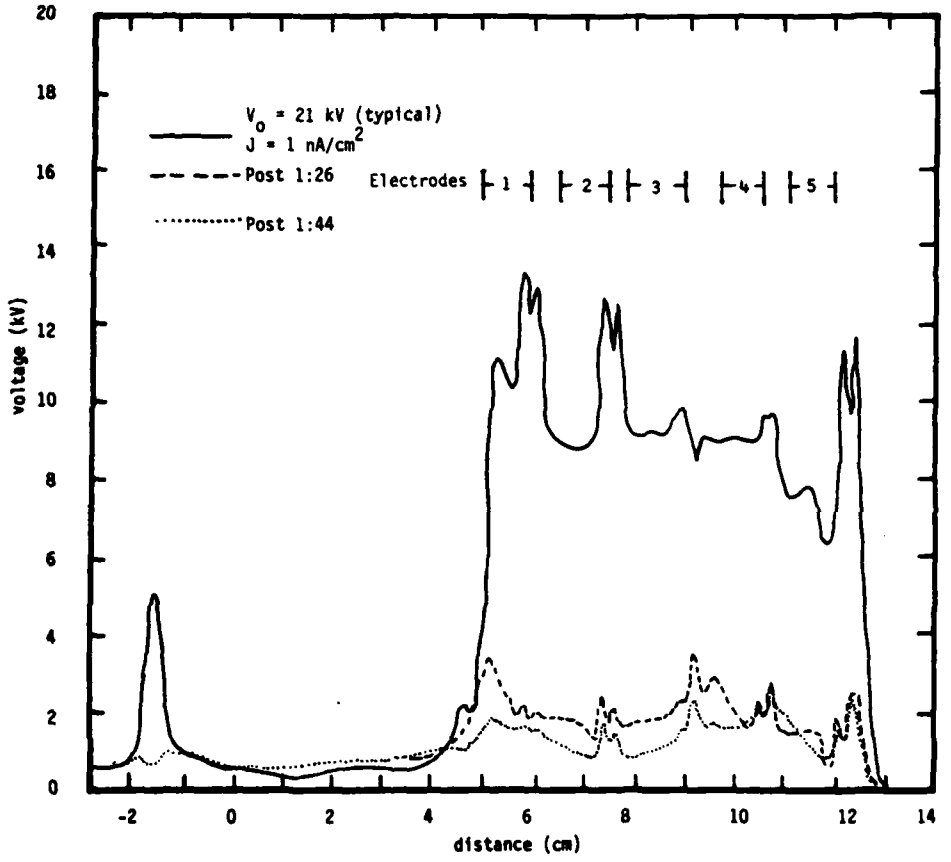

Figure 68. Approximate pre-discharge and post-discharge potential profiles. Charging with 2 nA/cm^2 of 21 keV electrons.

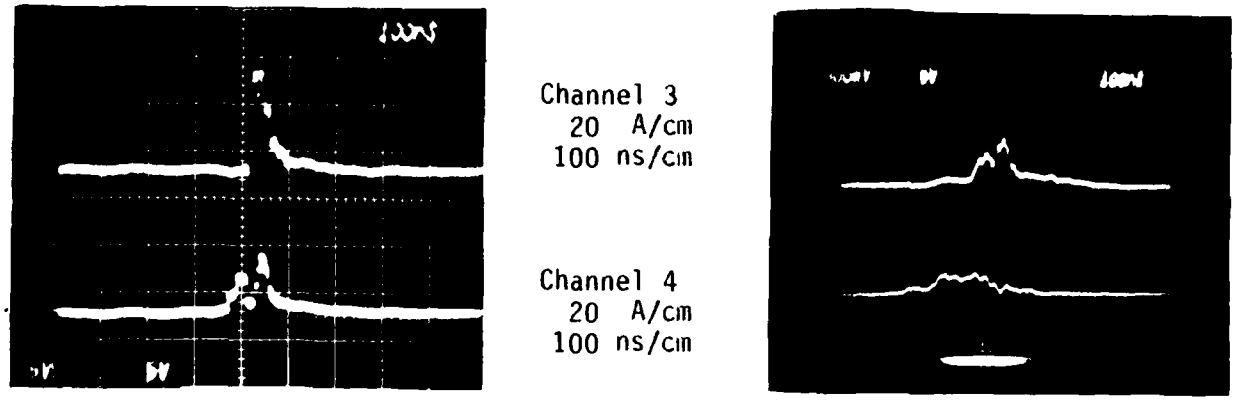

Material: Mylar
Charging Voltage: 22 kV

Date: 4/2/82
Time: 3:13

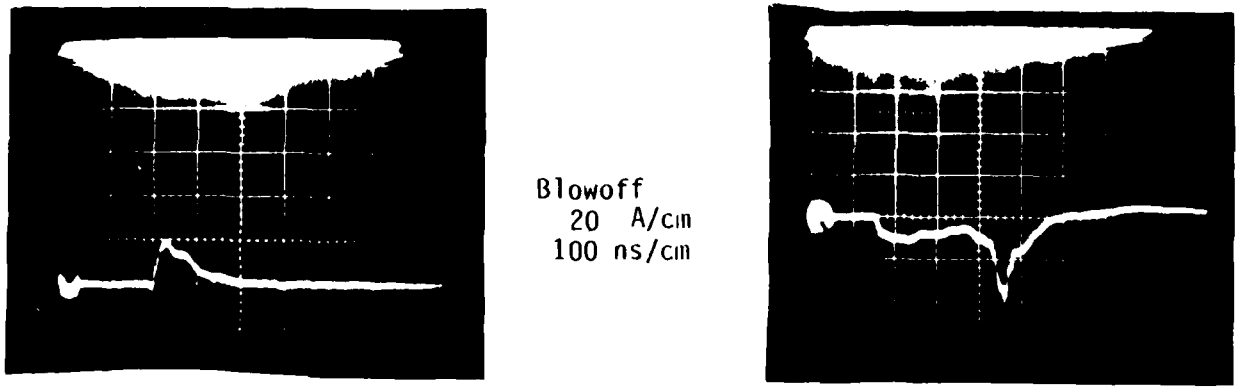

Figure 69. Transient record of discharge 3:13 on 0.0025 cm Mylar exposed to 22 kV electrons.

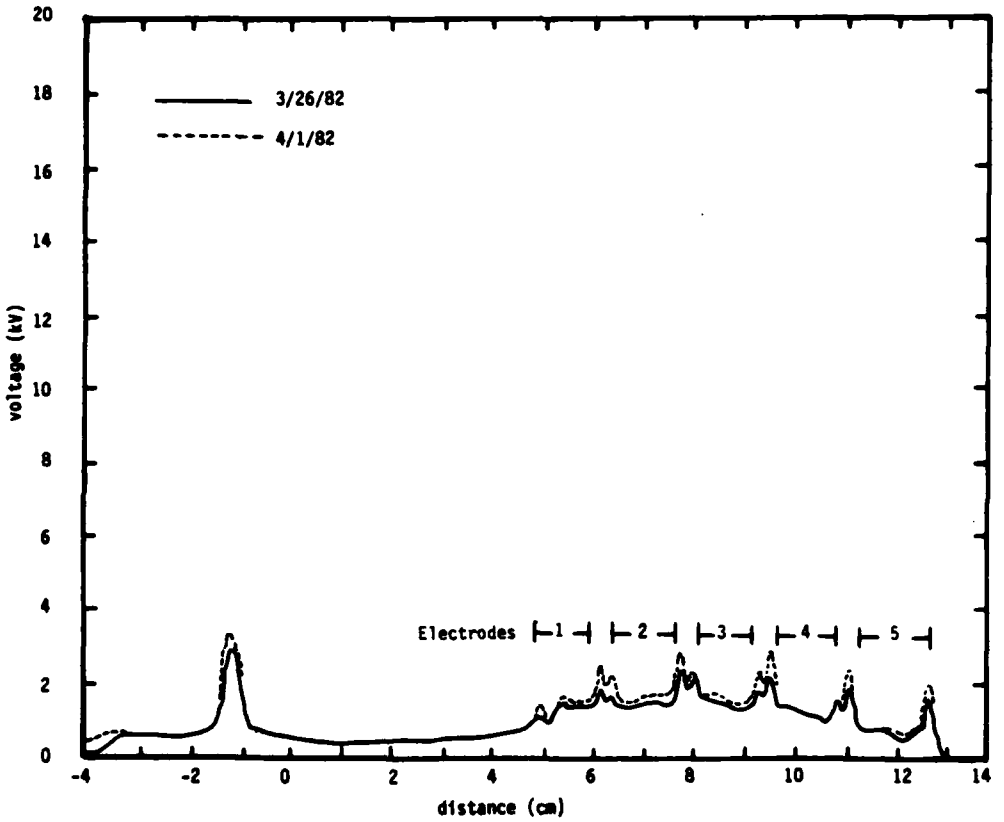

Figure 70. ...o ...itial profiles taken six days apart, with sample ... disturbed between the traces.

Table 3 is a summary of data from some selected transient discharge data records on Mylar on March 23 and 24, 1982.

TABLE 3. DISCHARGE PROPAGATION DATA.

Event I.D.	Starting Location (electrode)	Time in ns to reach location 1.6 cm	3.2 cm	4.9 cm	6.5 cm
2:54	5	30	70	--	160
3:23	5	70	110	200	250
11:29	5	100	280	-NG-	320
2:34	5	100	320	300	300
4:22	5	40	100	--	--
avg. ± std. dev.		70±30	176±100	250±50	257±60

These data and one particular discharge (3:23) are plotted in Figure 71. The average velocity is about 2.3×10^7 cm/s.

Table 4 is a summary of data from some selected transient discharge data records on Mylar taken on April 1 and 2, 1982. This is a different portion of the same Mylar sample.

TABLE 4. DISCHARGE PROPAGATION DATA.

Event I.D.	Starting Location (electrode)	Time in ns to reach location 1.6 cm	3:2 cm	4.9 cm	6.5 cm
3:14	5	150	720*	580	600
3:33	5	260	500	580	680
4:01	5	80	280	435	475
11:41	5	180	280	375	555
2:35	5	100	300	310	400
avg ± std dev.		150±60	420±170	460±110	540±100

*Questionable

These data are plotted in Figure 72. The average velocity is 1.2×10^7 cm/s.

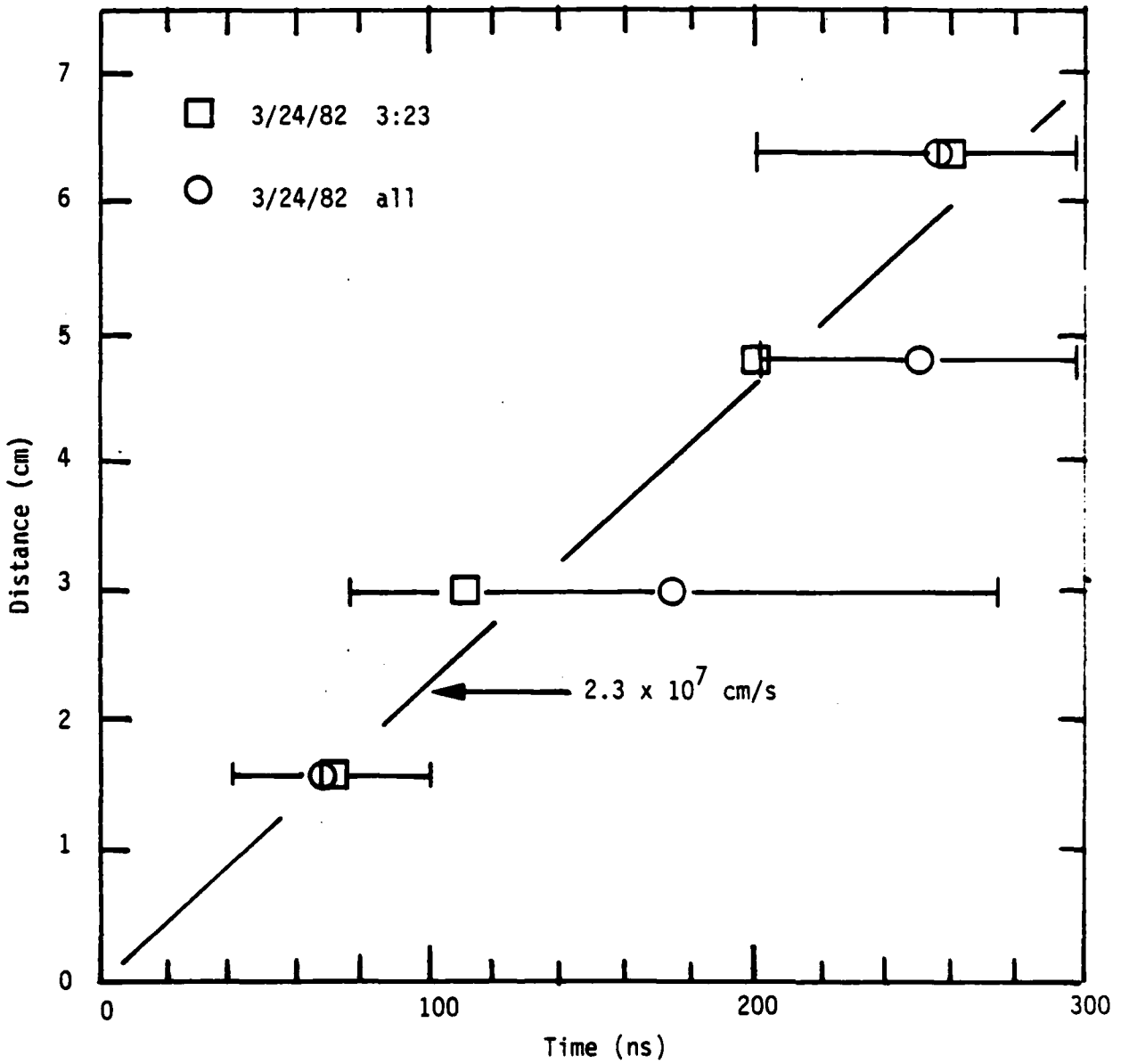

Figure 71. Discharge distances versus time after initiation for five discharge events on 0.0025 cm Mylar on 3/24/82.

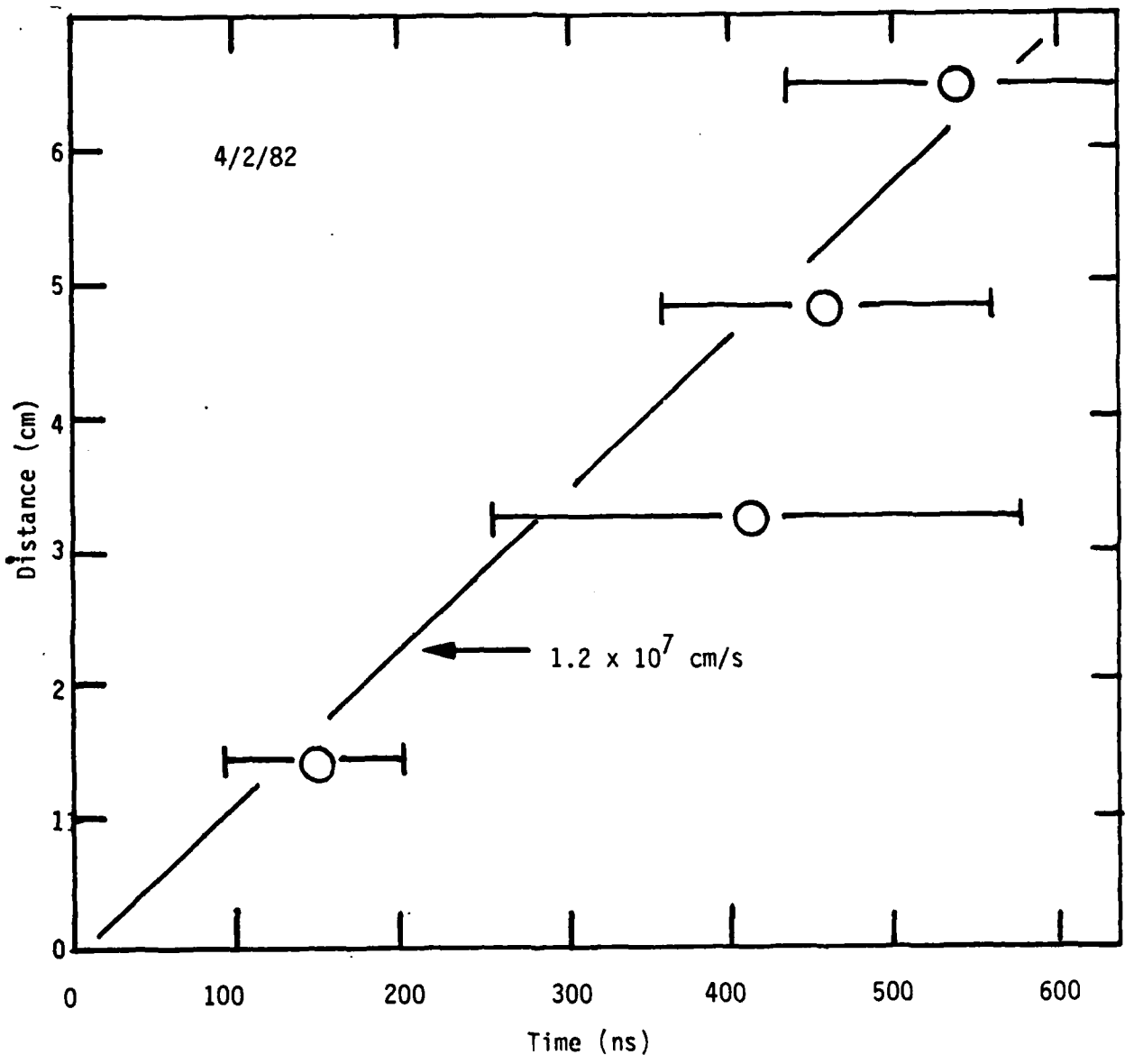

Figure 72. Discharge distance versus time after initiation for five discharge events on 0.0025 cm Mylar on 4/2/82.

Notice that while both sets of records show considerable shot to shot variation in apparent velocity, the average velocities differ by about a factor of two and the data spread just barely overlap. We suspect this is a reflection on anisotropic sample characteristics. Gossland, et al., (Ref. 2) and Wilkenfeld (Ref. 10) have noted a tendency for discharges to run along defects in the dielectric. We suspect the part of the sample irradiated 3/23/82 was oriented with its predominant defects across the segmented sensing electrodes while the part of the sample irradiated on 4/2/82 had defects oriented at an angle with respect to the electrodes (i.e., @ ~60°).

a. Microscopic Examination of Materials after Testing

Each of the materials was examined under a microscope after the test series. The microscope used was a Zeiss reflected light microscope with magnifications of 64X, 256X, and 640X, with polarizers and interference objectives to increase visibility and contrast. We only found evidence of discharge-related damage on the Mylar sample. On the other samples, there was no visible difference between the irriadated areas and the non-irradiated areas.

On the Mylar sample, virtually the entire area of all three exposure areas was interlaced with branching tracks, which bore a resemblence to Lichtenberg figures. After each exposure region had been exposed to 10 to 50 discharges, there were essentially no areas larger than a square millimeter within the exposure area, which did not have any discharge tracks. In some areas major tracks were only 30 μm apart.

By comparing the observed tracks with a scale of known dimensions we estimate that the discharge channels were less than 1 micron in width.

10. J. Wilkenfeld presentation at the 1980 Spacecraft Charging Technology Conference (not published in the proceedings).

Generally it was impossible to find a beginning or end to any track: the surface was just covered with an interconnected network. At one point we did find an isolated track, about 0.15 mm long, (Figure 73) with numerous branches, but that was the exception rather than the rule. In Figure 74 we see than many of the tracks intersect or branch at very specific angles. We attribute this to scratches or manufacturing defects which were on the material before the test series. Evidently, there is some tendency of the discharges to follow scratches. However, as Figure 75 illustrates, this tendency was far from absolute, and often seemingly random, "tree-root", patterns were mixed in with "parallel" type discharges. Furthermore, we followed one scratch from outside the exposure area, where there was no evidence of discharging, across the exposure area to the other side. This was certainly one of the larger scratches, to be visible over about 6 cm. Within the exposure area, there were places where the discharge had clearly followed the scratch, but mostly the density of discharge tracks was at least as high in the area around the scratch as at the scratch itself.

In one region, where there was an especially high density of "tree-root" type tracks, we examined the tracks with the 640X magnification, and discovered tiny nodules along the discharge tracks (Figure 76). Unfortunately, the nodules were just barely within the resolving power of the light microscope, and barely show on the photogragh. Nonetheless, as best we could tell, the nodules were roughly spherical, and about 1 μm in diameter. They were scattered about every 10 μm along the discharge channels. They seemed mostly to be adjacent to the tracks - that is, touching but usually not centered on the channel. They were seen both on major "trunks" as wells as on the very fine capillaries.

By moving the sample relative to the focal point of the microscope, it was possible to get an idea of the relative depths of features in the sample. The apparent thickness of the sample was 15 ± 3 μm, which is smaller than the actual 25 μm thickness because of the index of refraction

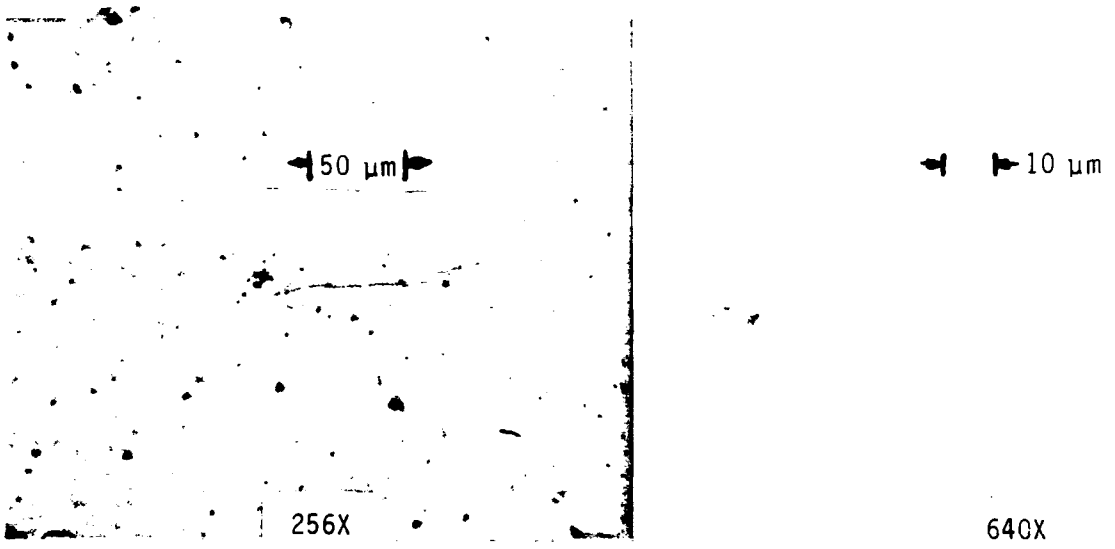

Figure 73. One particular isolated discharge track (TREE) (at 256 and 640X) in a forest of interlaced tracks on a Mylar sample that had experienced 30-50 events.

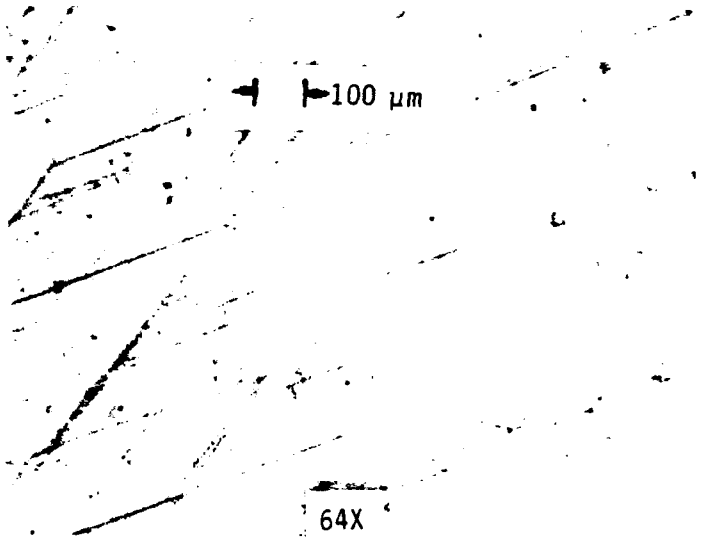

Figure 74. Microphotograph at 64X of a typical piece of Mylar that had experienced 30 to 50 discharges. Notice that most but not all tracks conform to a pattern of parallel lines intersecting at about 30°. On closer examination small branches in random directions are also apparent.

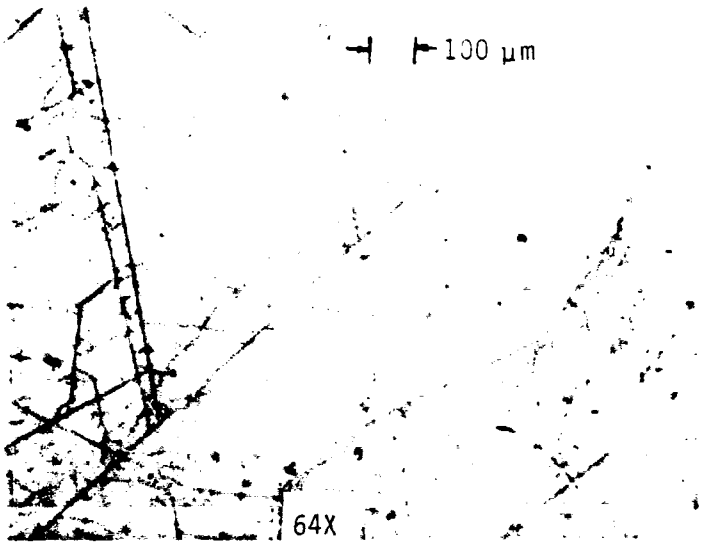

Figure 75. A photograph at 64X magnification of a portion of a Mylar sample that has experienced 30-50 discharges, showing both regular or linear and dendritic or Lichtenberg-like discharge tracks.

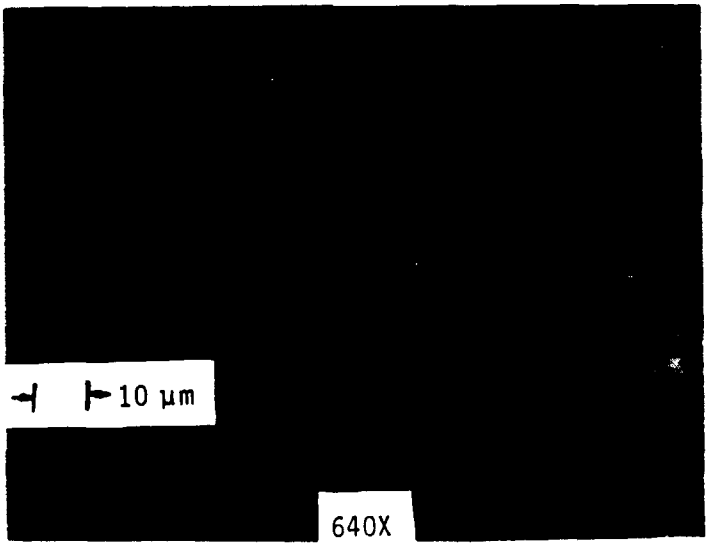

Figure 76. Microphotograph of a particular Lichtenberg like discharge site in Mylar at 640X magnification showing the small (≈1 µm) modules along the track.

of the dielectric. Using this same technique we determined the depth of the discharge tracks below the surface to be less than 3 μm, with no evidence that they ever extended below that depth. This is in keeping with the average range of a 20 kV electron being ≈4 × 10^{-4} gm/cm^2.

Our conclusion from the observations are that the type of discharges which created these tracks occur either on the surface of the dielectric or just below the surface. Furthermore, this type of discharge does seem to occur in discrete channels, rather than propagating across the entire dielectric in one continuous wave front. Also, the channels do branch into ever smaller and smaller capillaries, so that removing charge from the rest of the area not included in a channel need only occur over relatively short distances.

These observations are essentially identical to those presented by Gossland, Balmain and Treadaway in Reference 2. However, we wish to add that Mylar was the only material which displayed this type of damage, though all the materials were exposed and experienced discharges under nearly identical conditions.

4. SOLAR CELL COVER GLASS (0.030 cm - 0.012")

Figure 77 shows accumulation of charge (voltage) on a 0.030 cm thick solar cell cover glass with successive irradiations with 6 kV electrons. Note that the scale here is 10 kV full scale. Traces were taken after 3, 10, 30, 100, 300 and 600 sec of irradiation at 0.6 nA/cm^2. The asymptotic voltage varies from ≈ 1 kV to 3.4 kV, and every sweep, including the asymptotic one, shows a higher potential at the sides than in the middle. We suspect that much of this structure is due to variations in the thickness of the silicon rubber cement between the cover glass and the printed circuit board underneath. This shape turned out to be relatively independent of incident current from 1 nA/cm^2 to more than 10 nA/cm^2.

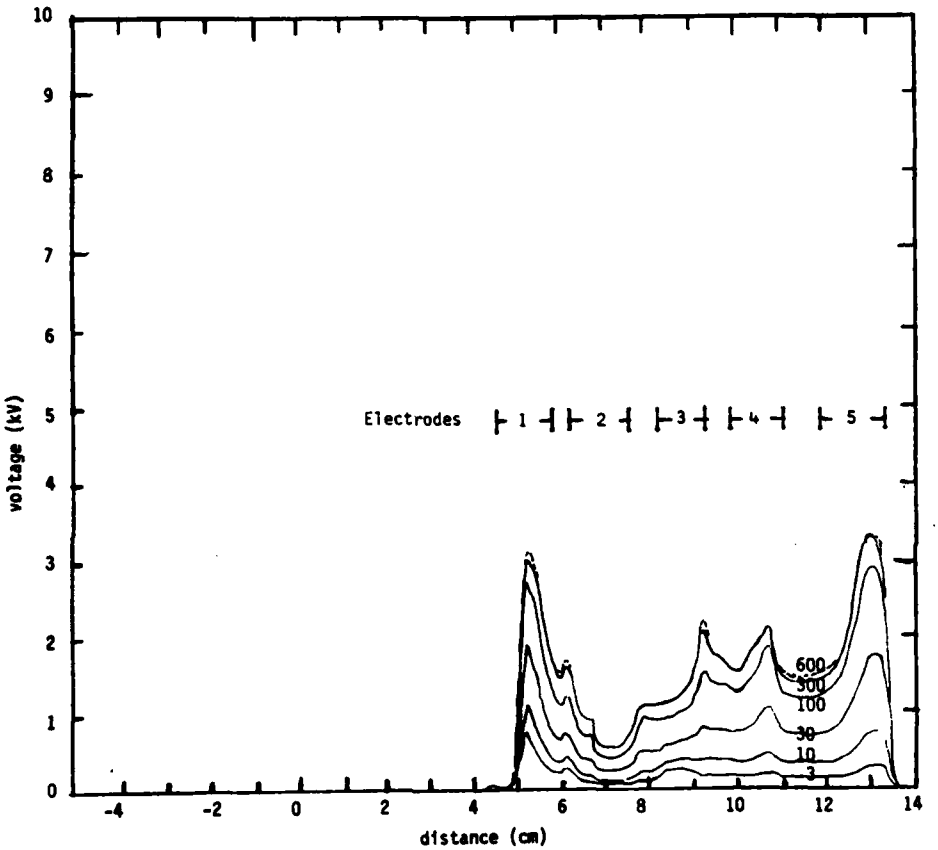

Figure 77. Typical potential profiles from a charging sequence of 0.030 cm solar cell cover glasses, exposed to 0.6 nA/cm^2 of 6 kV electrons. Exposure time (in seconds) are indicated.

Figure 78 shows the accumulation of charge on cover glass irradiated with 3 nA/cm^2 of 11 keV electrons. The beam was on 30 s between Traces 25 and 26, then there was a 6 minute delay between Trace 26 and 28. Between Traces 28 and 29, the beam was on 70 s more. Between Trace 29 and 30, the beam was on 200 s. Note that the asymptotic profile, Trace 30, has a peak at 8.1 kV, and again, the peak is at the edge, not in the middle.

Figure 79 shows the accumulation of charge on a cover glass exposed to 0.7 nA/cm^2 of 16 keV electrons after 3, 10, 30 and 105 s of irradiation. The vertical scale here is 20 kV full scale. The two sharp valleys in Traces 2 and 3 at 9 cm and 11 cm are a) the edge between the two cover glasses, and b) a crack in one of the cover glasses, respectively. Evidently, these gaps lost charge more rapidly than did the bulk of the material. Trace 6 is presumably an asymptotic form. Notice that the highest potential is at ≈ 12,000 V, which is 4 kV below the incident energy.

Figure 80 shows the build-up of charge, after a discharge, with 0.6 nA/cm^2 of 26 keV electrons. Between Traces 8 and 9, the beam was on 1 minute, between 9 and 10 the beam was on 30 s, followed by a 15 minute delay. The fact that Traces 9 and 10 are almost identical shows that charge leaked away at about 1/30 the rate of charging which implies the conductivity of glass under these conditions was ($2 \times 10^{-17} < \sigma < 4 \times 10^{-17}$ $(\Omega cm)^{-1}$). Between Traces 10 and 11, the beam was on for another 30 s of charging; between 11 and 12, and 12 and 13, the beam was on 1 minute each. Withough further addition of charge, the sample discharged while the TREK was over it.

Figure 81 shows the results of an investigation to see if Solar Cell Cover Glass showed the same kind of photo-sensitive conductivity that Kapton exhibited. For this purpose, the sample was charged with 6 kV electrons for more than 1/2 hour at ≈ 10 nA/cm^2 resulting in profile 13. Then there was a 20 minute delay (resulting in Trace 14). From these data we infer $\sigma \approx 3.3 \times 10^{-17}$ $(\Omega\text{-cm})^{-1}$. Then the room lights were left on for 2 minutes before measuring Trace 15. With Kapton, that amount of light would have produced a

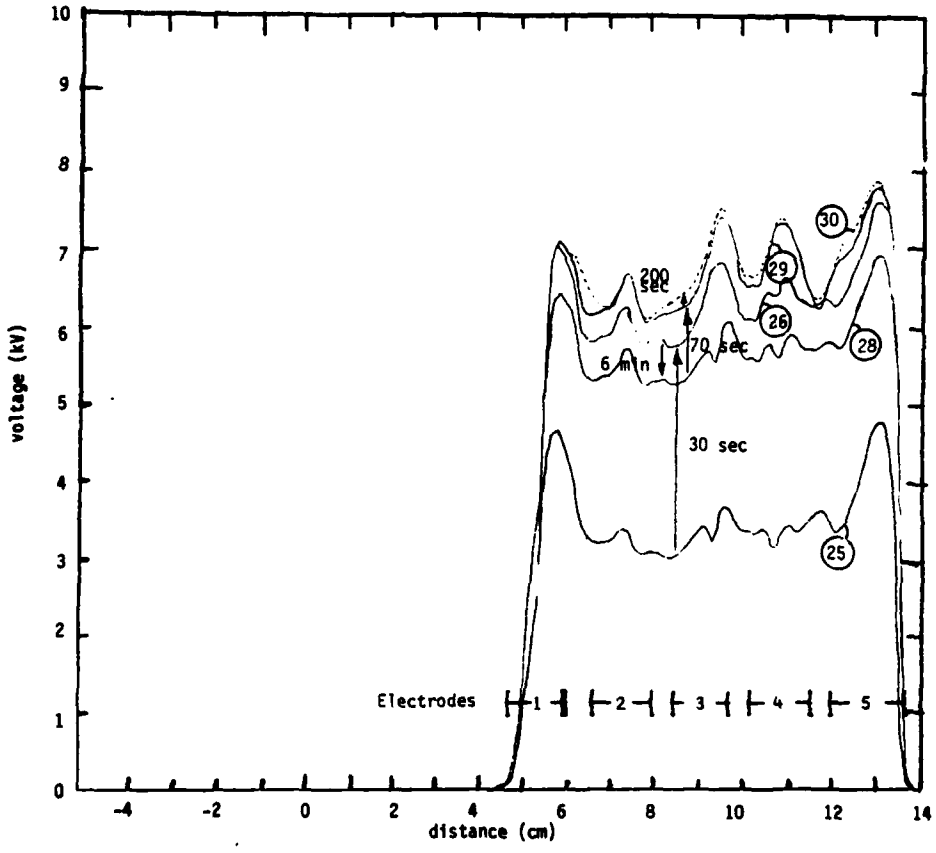

Figure 78. Charging to asymptotic profile on 0.030 cm cover glass with 3 nA/cm^2 of 11 keV electrons. Charging times in seconds. Delays without charging in minutes.

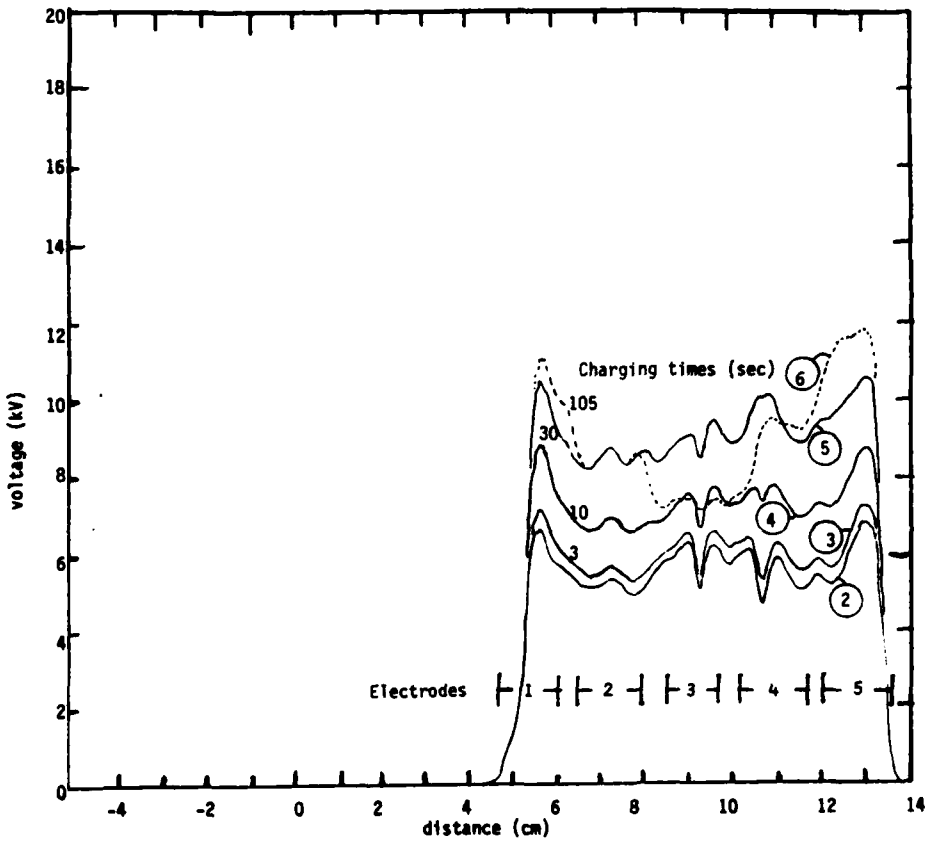

Figure 79. Charging potential profiles on 0.030 cm cover glass with 0.7 nA/cm^2 of 16 keV electrons. Charging times are indicated.

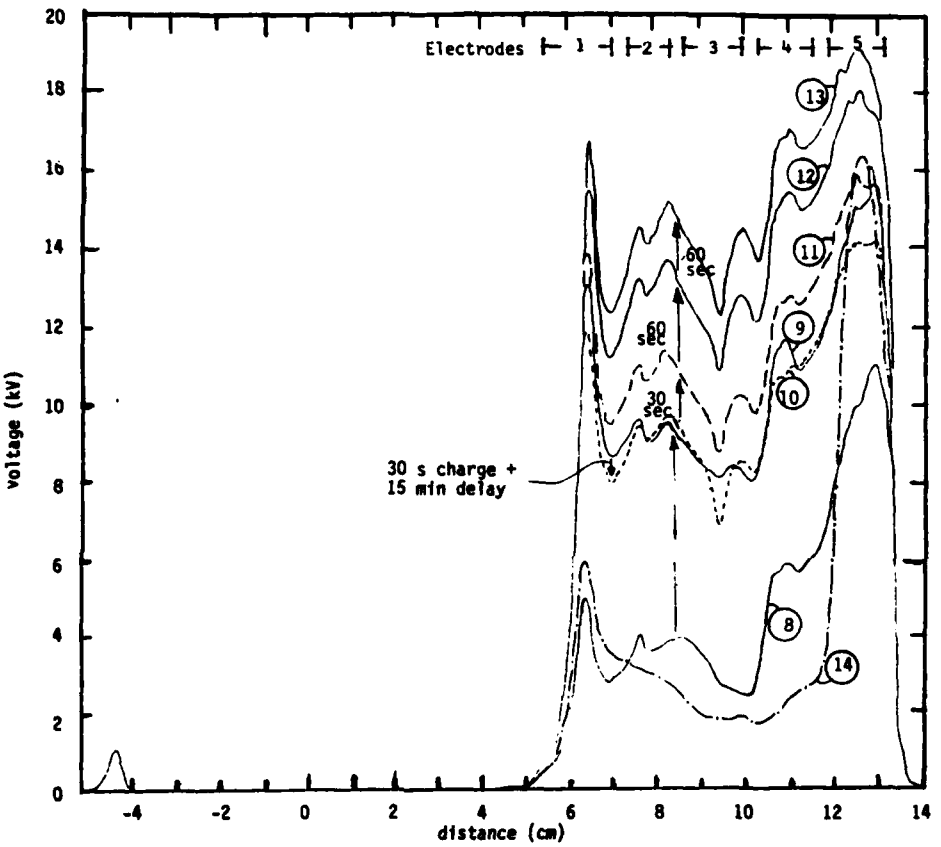

Figure 80. Recharging after discharge on 0.030 cm cover glass with 0.6 nA/cm^2 of 26 keV electrons, leading to a discharge.

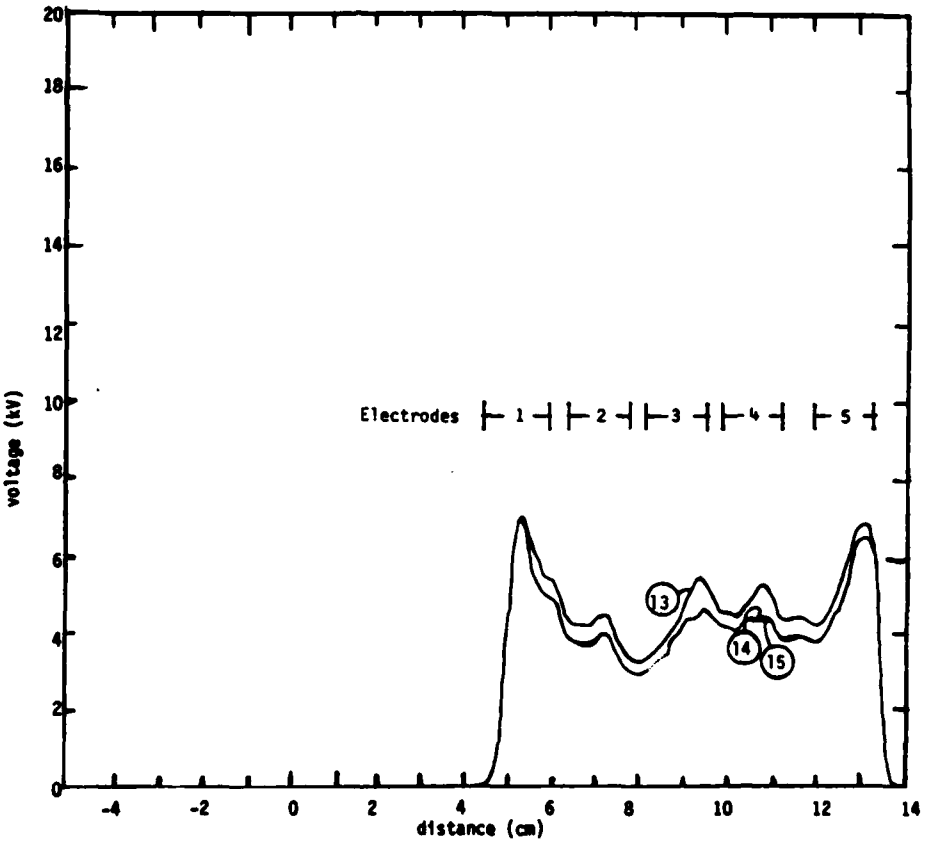

Figure 81. Comparison of potential profiles on 0.030 cm cover glass after a fifteen minute delay without lights and two minute delay with lights.

very substantial drop in voltage, but with the solar cell glass there was no change. That means cover glass is not nearly as photoconductive as Kapton.

Figure 82 gives a good example of what we have labeled delayed enhanced conductivity in non-irradiated material. This describes conductivity which is generated by the beam in the region beyond an electron range. In this case, the sample was charged with 11 keV electrons at 4 nA/cm^2, then the voltage was measured repeatedly at equal time intervals. One can see that profiles taken at equal time intervals get closer and closer together as the time after irradiation goes by. This means conductivity $\sigma(\Omega cm)^{-1}$ is gradually decreasing. Since

$$\sigma = \frac{\varepsilon}{V} \frac{dV}{dt}$$

where ε is the dielectric constant (about 3×10^{-13} farad/cm), V is voltage and t is time. We estimate σ decreases from about 1×10^{-16} to 5×10^{-17} $(\Omega cm)^{-1}$ in this series of mesurements.

Figure 83 shows the extent of voltage sagging for 15 hours after the beam had been on at $\approx$ 0.07 nA/cm^2. Comparison with T-4 shows that "enhanced non-irradiated conductivity" is much smaller after the sample has been exposed to lower current densities ($\sigma \approx 5 \times 10^{-19}$ Ohm^{-1} cm^{-1}). A compilation of all the data on "non-irradiated conductivity" of solar cell cover glass is given in Figures 84 and 85.

This data represents the conductivity in the dielectric beyond the electron range to the conducting substrate as inferred from the loss of stored charge as a function of time after radiation ceased (i.e., $\sigma \approx \frac{\varepsilon}{V} \frac{dV}{dt}$) Figures 84 and 85 represent a compilation of data from seven sets of profiles. The horizontal error bars represent the fact that we are deriving conductivity by taking the difference between potential profile measurements made at widely separated times, so the numerical value of conductivity is averaged over that measurement period. In other words, the error bars start

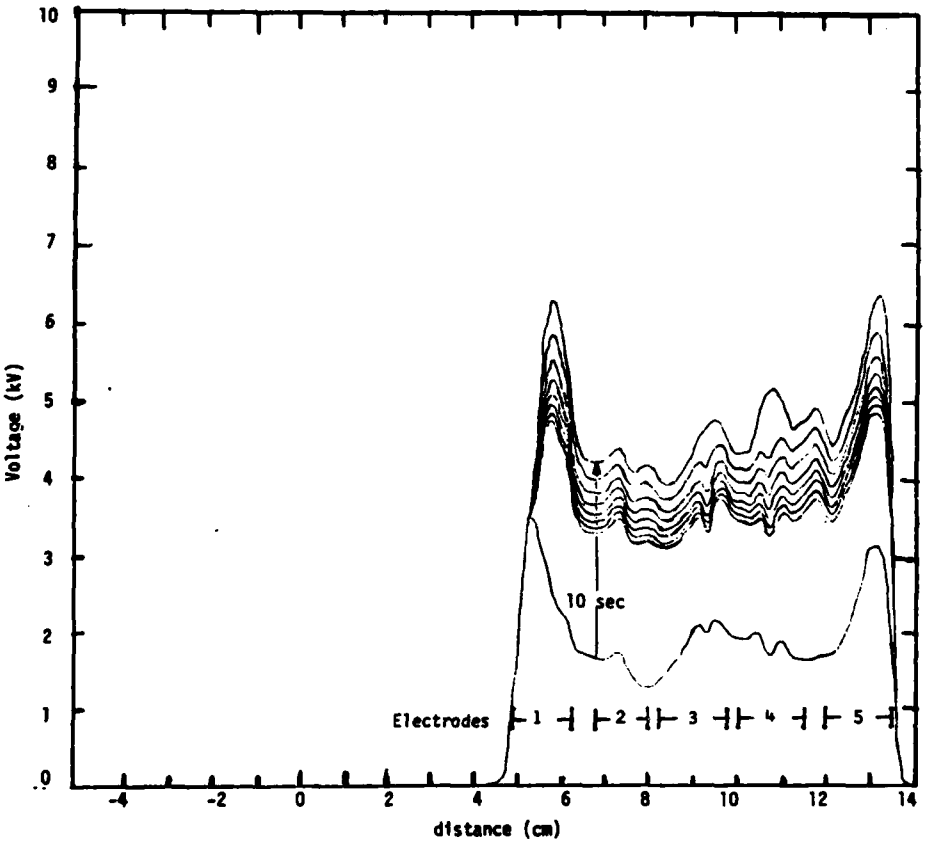

Figure 82. Decay of voltage profile after 10 second charging with 4 nA/cm^2 of 11 kV electrons; 3 minutes between each sweep with beam off.

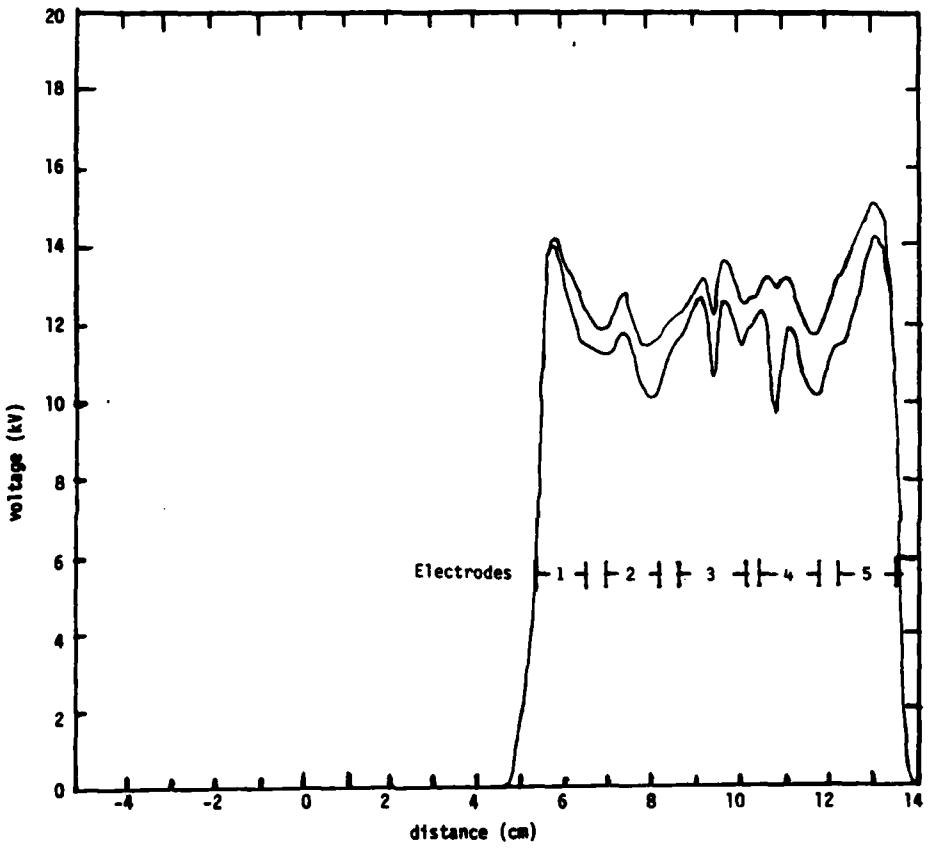

Figure 83. Decay of voltage profile on solar cell cover glass overnight.

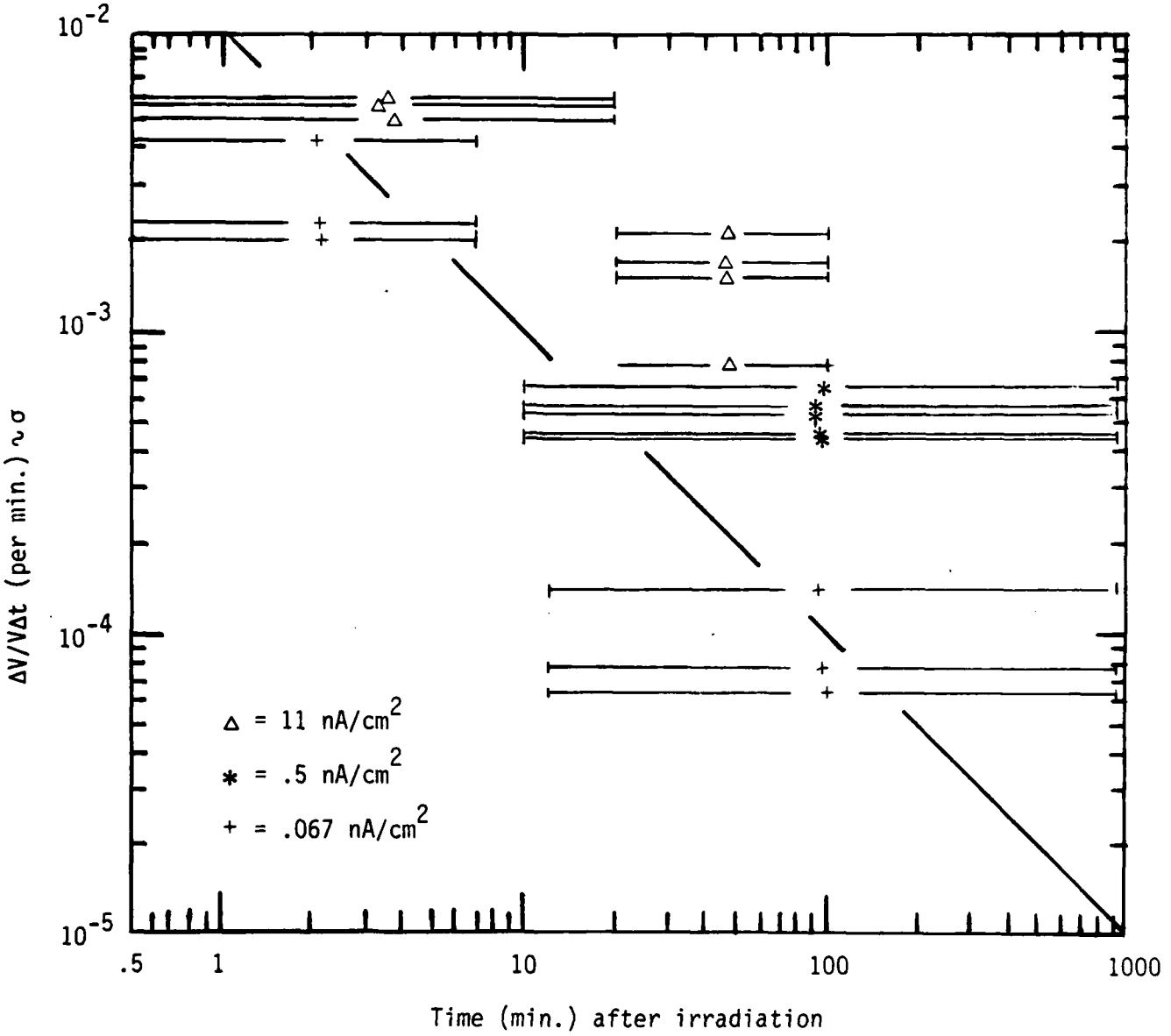

Figure 84. Enhanced delay conductivity in the non-irradiate portion of solar cell cover glass - with the irradiated current density as a variable.

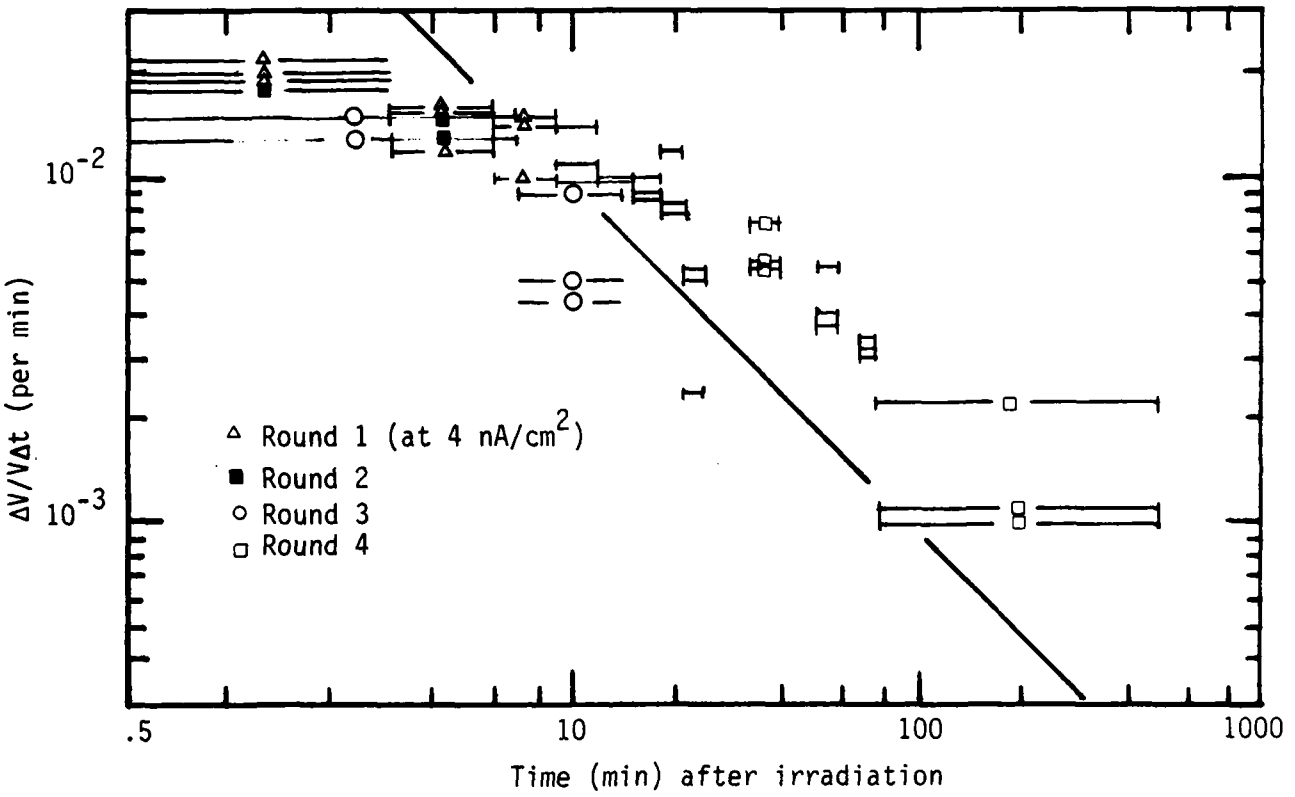

Figure 85. Enhanced delayed conductivity in the non-irradiated portion of solar cell cover glass.

at the time of one profile and end at the time of the next, while the conductivity is inferred from the change in voltage between the two profiles. The vertical spread of data (at a given current density) are a result of the fact that different areas on the sample displayed different apparent conductivities. Gross, Sessler and West (Ref. 11) reported delayed conductivites in the irradiated region of their Teflon samples which decreased as t^{-1} where t is the time after the end of irradiation. The present data is not so clearly defined that we would assert a t^{-1} dependence, however, we have superimposed a t^{-1} line on the data for comparison purposes. We note that Gross, et al., were discussing the delayed conductivity in the irradiated part of their samples, whereas we think we are observing enhanced delayed conductivity in the dielectric beyond the electron's range, where the ionization was previously thought to be negligible.

Our interpretation of these observations is as follows: first, the maximum asymptotic potential which the sample achieved was nearly 3 kV below the incident energy, a value which is much larger than any secondary emission unity cross-over point previously reported (Ref. 12). On the other hand, the asymptotic potential did increase with increasing incident electron energy. The shape of the potential profile also leads us to believe that secondary emission is not the limiting factor, because a secondary-limited profile typically has comparatively little structure except for rounded shoulders, while the glass shows peaks at the edges. The reason for rounded shoulders is that the secondary emission coefficient increases, as the the angle of incidence becomes more oblique. Thus, unity cross-over occurs at a lower potential on the sample near the edges where the electrons

---

11. B. Gross, G.M. Sessler, J.E. West, "Charge Dynamics for Electron Irradiated Polymer Foil Electrets," J. Appl. Phys., 45, 3841 (1974).

12. J.A. Wall, E.A. Burke and A.R. Fredrickson, "Results of Literature Search on Dielectric Properties and Electron Interaction Phenomena Related to Spacecraft Charging," pg. 581 of the 1977 Proceedings of the Spacecraft Charging Technology Conference, AFGL-TR-77-0051 or NASA TMX-73537.

are deflected the most (and hence have the most oblique angle of incidence). Combining these observations therefore, we are compelled to infer that the limitation of the asymptotic potential is due to conductivity through the bulk of the material.

Further, we observed that the asymptotic potential profile was essentially unchanged when incident current was changed by more than a decade. This leads us to suspect the potential profile is established by a conductivity which increases to accomodate any current, since at equilibrium

$$\frac{dQ}{dt} = J_{inc} - \sigma E = C \frac{dV}{dt} = 0$$

where Q is charge (coulombs), J is current density (amp/cm^2), σ is conductivity $(\Omega cm)^{-1}$, E is electric field (V/cm), C is capacitance (farads), V is voltage, and t is time. (That implies $\sigma = J_{inc}/E$ no matter what J_{inc} is.)

Next, we observed that the voltage tended to sag after the beam was turned off, thus substantiating the existence of a conductivity through the sample. That "delayed" conductivity was seen to decay on a time scale of tens of minutes after the beam was turned off. Also, the rate at which the voltage sagged was much higher after the beam had been on at hgher current densities, which further supports the concept of a conductivity that is proportional to incident current density.

Drawing all these observations together, we suggest that there is a conductivity through the bulk of the material (which we did not suspect before these measurements). This conductivity is apparently generated by the electron beam and is proportional to current density in the beam, <u>even though</u> it is in the portion of the sample beyond the range of the electrons. This conductivity is much smaller when the beam is off than when the beam is

on. Furthermore, the current, conductivity, and secondary emission establish an equilibrium voltage between 3 and 5 kilovolts below the incident energy of the beam.

To express this mathematically we write a current continuity equation. For a given incident current, J_{inc}, some current will be back emitted by scatter and secondary electrons, some will be conducted through the sample, and the remainder causes the material to charge up

$$J_{inc} = \sigma \frac{V}{d} + f_s J + C \frac{dV}{dt}$$

Where σ is conductivity, V is the voltage at the front of the sample (relative to the back which is at ground), C is the capacitance of the sample, d is the thickness of the sample, and f_s is the secondary emission coefficient, which depends on the energy of the electrons (V_o-V) as they strike the sample. For energetic electrons,

$$f_s \approx \frac{K_s}{(V_o - V)}$$

where V_o is the energy of the beam, V is the sample potential and K_s is an empirical constant. At equilibrium, the last term ($dV/dt \to 0$) becomes zero as the sample no longer charges. The equation can be rewritten as

$$V^2 - (V_o + \frac{Jd}{\sigma}) V + (V_o - K_s) \frac{Jd}{\sigma} = 0$$

which has the quadratic solution

$$V = \frac{\left[V_o + \frac{Jd}{\sigma} \pm \sqrt{\left(V_o - \frac{Jd}{\sigma} \right)^2 + 4Jd \frac{K_s}{\sigma}} \right]}{2}$$

for V to be independent of J, σ must be proportional to J. Furthermore, the equilibrium voltage will depend on the thickness of the sample (including any glue holding it down), just as the early-time potential will (because $C = \varepsilon A/d$). Also, the equilibrium voltage will not always be the same amount below the incident energy, because of the V_0 in the first term.

We would like to suggest here an example of a model that might be constructed to fit the patterns described above. The details of charge trapping and untrapping, mobility, migration, thermal activation, etc., have been discussed at length in the literature. Without depending on any one of these models specifically, let us suppose that as the electrons come to rest in the sample, they are free to move for a time. As the field builds up, the free electrons move in the field towards the rear electrode, into the area beyond the range of the electron beam. These free electrons continue to move, either by tunneling, untrapping and retrapping, hopping, or some other mechanism, until they either pass out of the back plane of the sample, or fall into traps so deep that their release time is long compared to our observation times. Thus, the total current at equilibrium is determined by the number of free electrons available (which is proportional to incident current) minus the number that get permanently trapped (which is a function of field, material, and thickness). Hence, beginning with an uncharged ("virgin") sample, at first, charge would just stick in the sample and raise the voltage and field. As the field built up, more and more charges would begin drifting thorugh the sample, slowing the rate of potential rise. Simultaneously, the secondary emission increases, as the difference between the surface potential and incident electron energy decreases, further slowing the rate of charge build-up. At some voltage, well below the secondary emission unity second cross-over, the fraction of the incident current which is re-emitted by secondary emission is just equal to the fraction of the incident current which is being trapped permanently in the sample (the remaining current flows through the sample as conduction current).

This model predicts a charging profile that : 1) is independent of incident current density (because both conductivity and secondary emission are proportional to current density); 2) stays below the charging voltage by some amount greater than the secondary unity second cross-over voltage; and 3) sags after the beam is turned off, due to "leftover" conduction that is a) proportional to the proceeding beam current and b) decays with time after radiation ceases. To account for the shape of the asymptotic profile, we recall that the cover glasses were held in place with silicon rubber cement (RTV or Silastic) which has considerable variation in thickness. We believe that the silicon rubber was thicker at the edges.

Returning to the discharge data, Figure 86 shows a set of charging profiles with the beam at ≈0.5 nA/cm^2 and 16 kV. One minute of charging separates each of the higher traces, then there was ≈ 50 s of charging after Trace 16 before the discharge. Hence, Trace 16 must have been very close to the actual profile when the discharge happened. Trace 17 was taken after event 3:53, and shows about 70% of the charge had gone away, though less is missing on electrode 5 than on the other channels.

Figure 87 shows the transient records for event 3:53. Much more current appears on channels 2 and 3 than on the others. Furthermore, the signal is simultaneous to within the resolution of the pictures, except on channel 1. Channel 1 exhibits noise when the other channels have signals, but net charge does not start to move until almost 200 ns later. Note that the sample only covers about half as much of electrode 1 as it covers of the other electrodes. Also, Channel 2 shows about 0.1 A for the first 100 ns then jumps to 0.6 A. The blow-off collector shows that it collected approximately the sum of the charges which left the 5 back electrodes, though its tail persists longer than the signals on the back electrodes.

Figure 88 shows a set of charging profiles and a post-discharge profile. The beam was at 26 kV and about 0.3 nA/cm^2. The beam was on for 80 s, 60 s and 120 s, and then on 110 s as indicated before discharge event 4:42 which

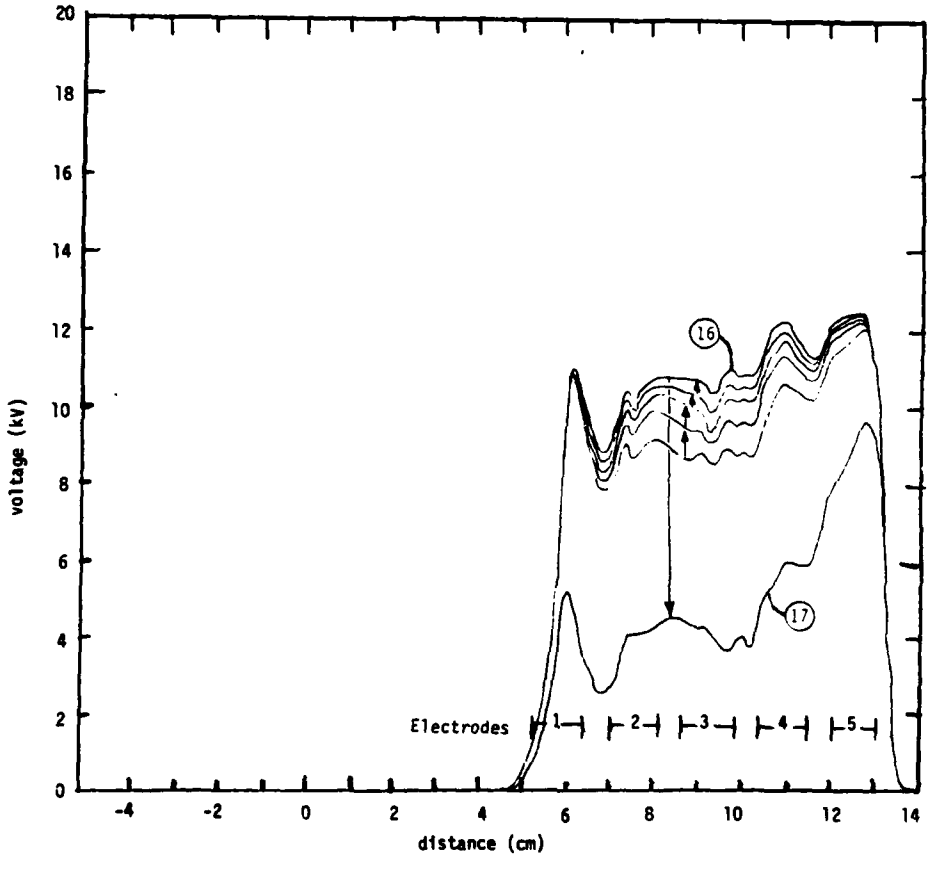

Figure 86. Charging a 0.030 cm cover glass with 0.5 nA/cm^2 of 16 keV electrons, leading to discharge 3:53.

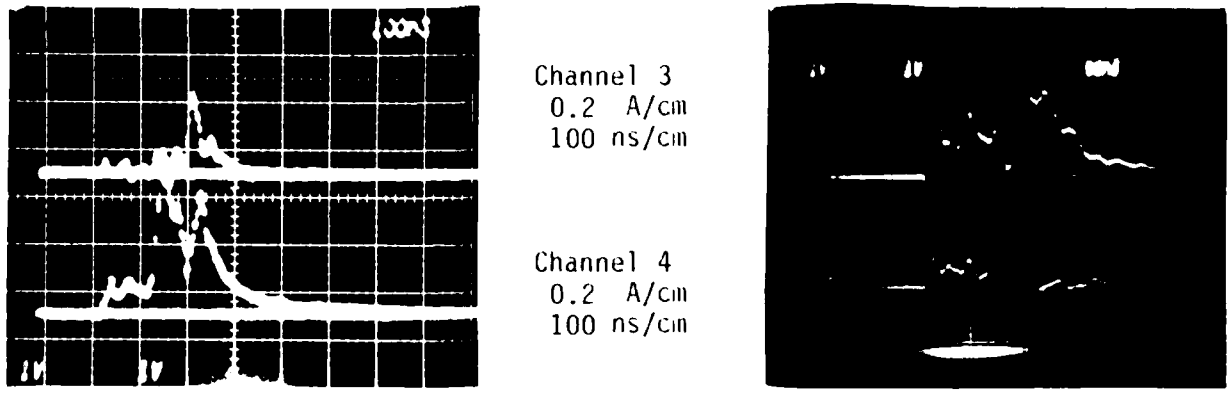

Material: Solar Cell Cover Glass
Charging Voltage: 16 kV

Date: 4/27/82
Time: 3:53

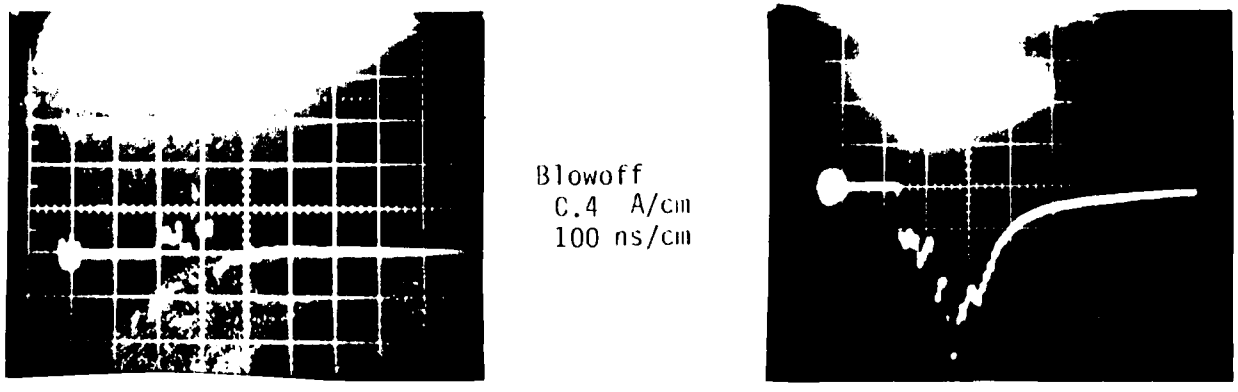

Figure 87. A transient record of discharge 3:53 on 0.03 cm solar cell cover glasses exposed to 0.5 nA/cm^2 of 16 kV electrons.

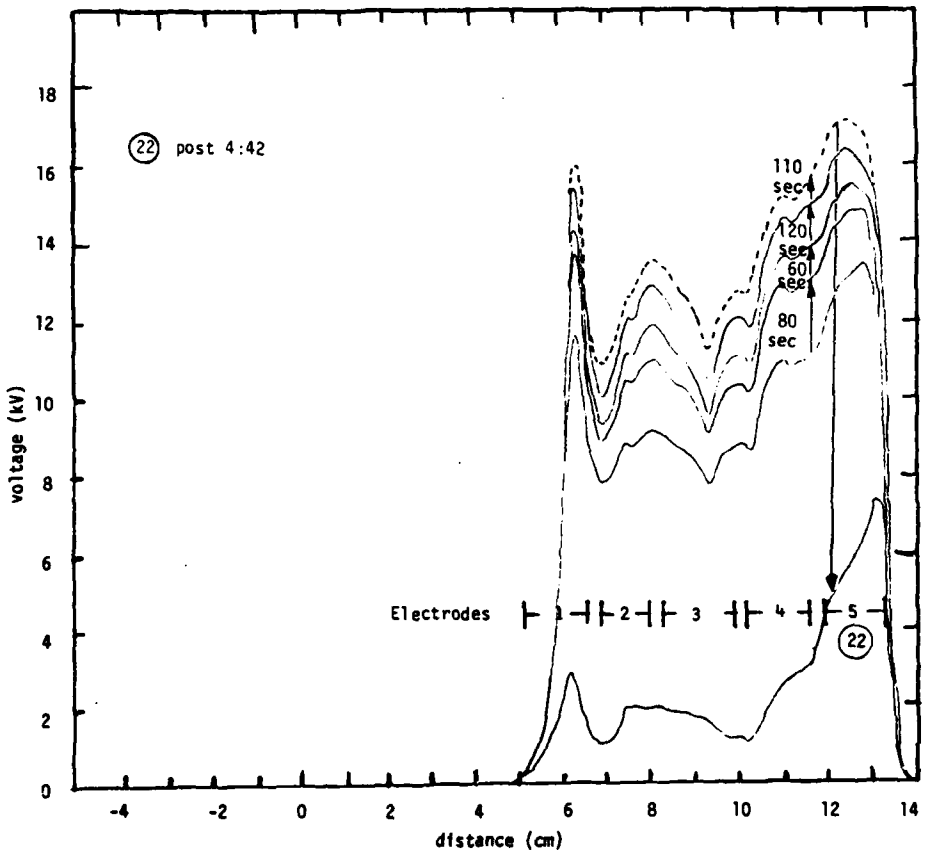

Figure 88. Charging 0.030 cm cover glass at around 0.3 nA/cm^2, 26 kV, leading to discharge 4:42.

preceeded Trace 22. The dashed line represents an estimation of the approximate condition of the sample before discharge. Before this discharge the sample sustained considerably higher voltages than it had before the preceeding discharge (Figure 86). This could be a consequence of the increase in charging voltage, aging of the sample, or decrease in charging current density (this decreased current was accidental, so we don't know exactly how much it dropped). After discharge 4:42, the potential was considerably lower than after discharge 3:53, so the total charge removed is much greater. This is substantiated by the larger transient currents indicated in the transient record for discharge 4:42 shown in Figure 89.

Figure 89 shows the transient records for discharge event 4:42. Unfortunately, the signals were so large that they go off scale and are difficult to resolve (especially after reproduction). However, many of the features of the previous discharge are apparent. The signals appear simultaneously on all channels except 1, which probably starts about 100 ns later. The signals on channels 2 and 3 are much larger than on the others. This might just be an indication that the glue behind the sample was thinner there and so the capacitance was larger, and hence there was more charge at the same voltage. The signal on the blow-off collector looks just like the preceeding one, scaled up by a factor of ≈ 2. The one feature that's different is the ringing in the tail of the signal on channels 1 and 2. The frequency is 50 MHz, and it persists for more than 200 ns. We were subsequently able to generate ringing at this frequency in the circuit itself with this sample, by pulsing one of the electrodes with a pulse of 50 or 100 times more amplitude than the ringing. We believe this is because the metalization on the back of the second surface mirrors caused capacitive coupling between channels which was not adequately decoupled by the grounded strips between the electrodes. Such ringing appeared at 25-100 MHz at least one channel on 9 out of 15 discharges records. Ringing at approximately 10 MHZ appeared on the blow-off collector on 3 discharges.

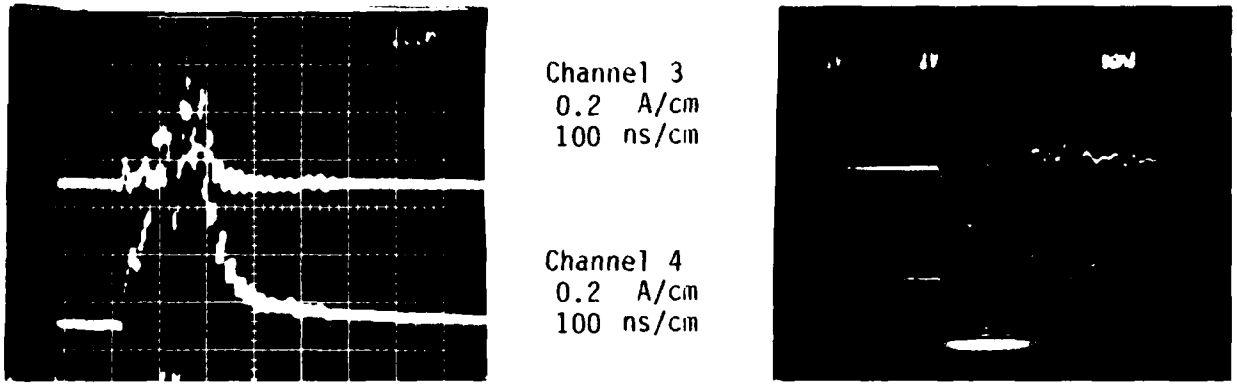

Material: Cover Glass
Charging Voltage: 26 kV

Date: 4/27/82
Time: 4:42

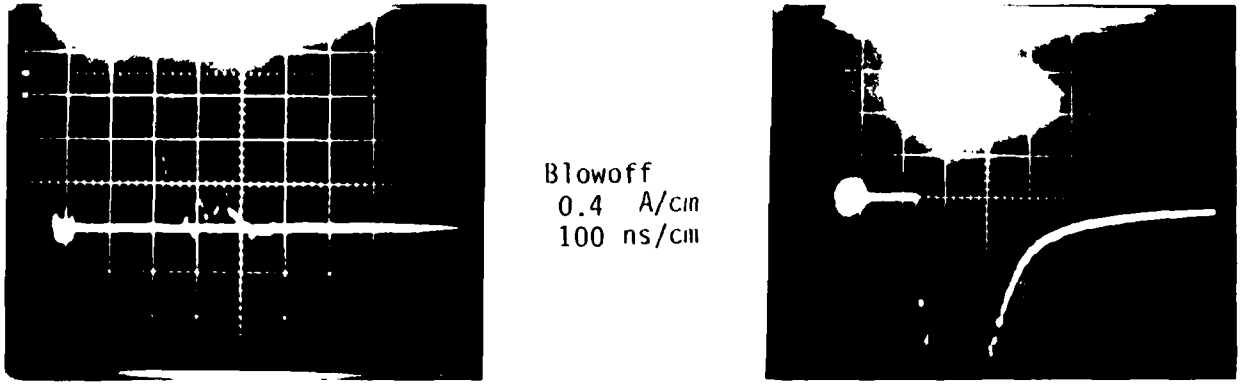

Figure 89. Transient record of discharge 4:42 on 0.03 cm solar cell cover glass exposed to 26 kV electrons.

Figure 90 shows charging with 26 kV electrons at a current density of ≈0.3 nA/cm^2 then 0.6 nA/cm^2, followed by a discharge. Between Sweeps 2, 3, 4, and 5 the beam was on at 0.3 nA/cm^2 for 30 s, 1 min, and 1 min, respectively, and between 5 and 6, at 0.6 nA/cm^2 for 30 s. The beam was then on ≈30 s more before event 11:41. Our best estimate of the pre-discharge potential is indicated by the dashed trace. The traces show ≈2 μC missing altogether, although less charge is missing over segment 5.

Figure 91 is the transient record of event 11:41, and resembles the two previous ones very much. Here again we see a signal that arrives at the same time on channels 2 through 5, and another signal (perhaps) that appears ≈100 ns later on channels 1, 2, and 3. The blow-off collector also shows an early charge movement followed by a jump in current at ≈ 100 ns. The back surface electrodes added together recorded ≈ 20% of the charge which left the sample, and the blow-off collector recorded ≈ 30% of the charge which left the sample (as inferred from the drop in voltage on Figure 90).

Figure 92 shows another charging pattern and post-discharge trace. The beam was on at 1.3 nA/cm^2, and 26 kV for 1 min between Traces 22 and 23, and 54 s after 23 before discharge event 3:21.

Figure 93 is the transient record for event 3:21. This event looks very much like event 4:42 (Figure 89), except that channels 4 and 5 both show a definite bipolar signal. The negative part indicates either a) charge which had previously left the sample returned, or b) charge from another portion of the sample arriving. The amount of negative charge represented would change the potential above that electrode by 250 V. The blow-off signal is much larger, but also shorter, and again only accounts for about 20% of the missing charge.

On none of the solar cell cover glass discharges did we observe a discharge that appeared to propagate from one electrode to the next, even though the charge is rather uniformly removed (i.e., the transient signals

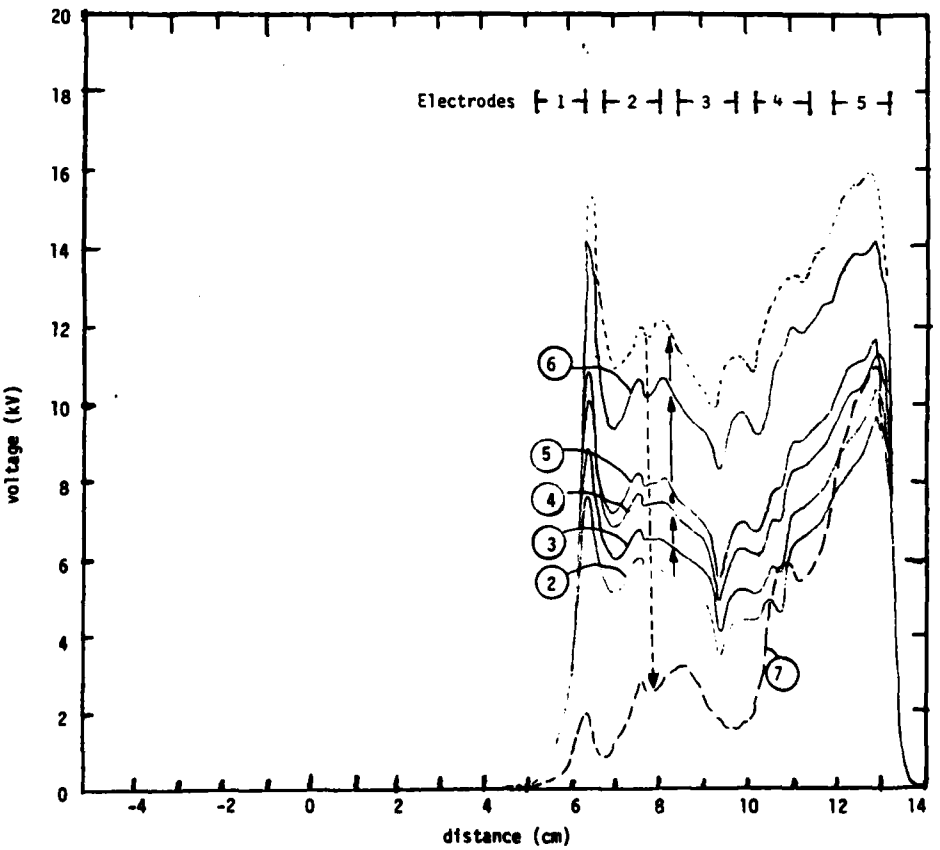

Figure 90. Charging profiles on 0.03 cm cover glass with 0.3 nA/cm^2, then 0.6 nA/cm^2 of 26 keV electrons, leading to discharge 11:41.

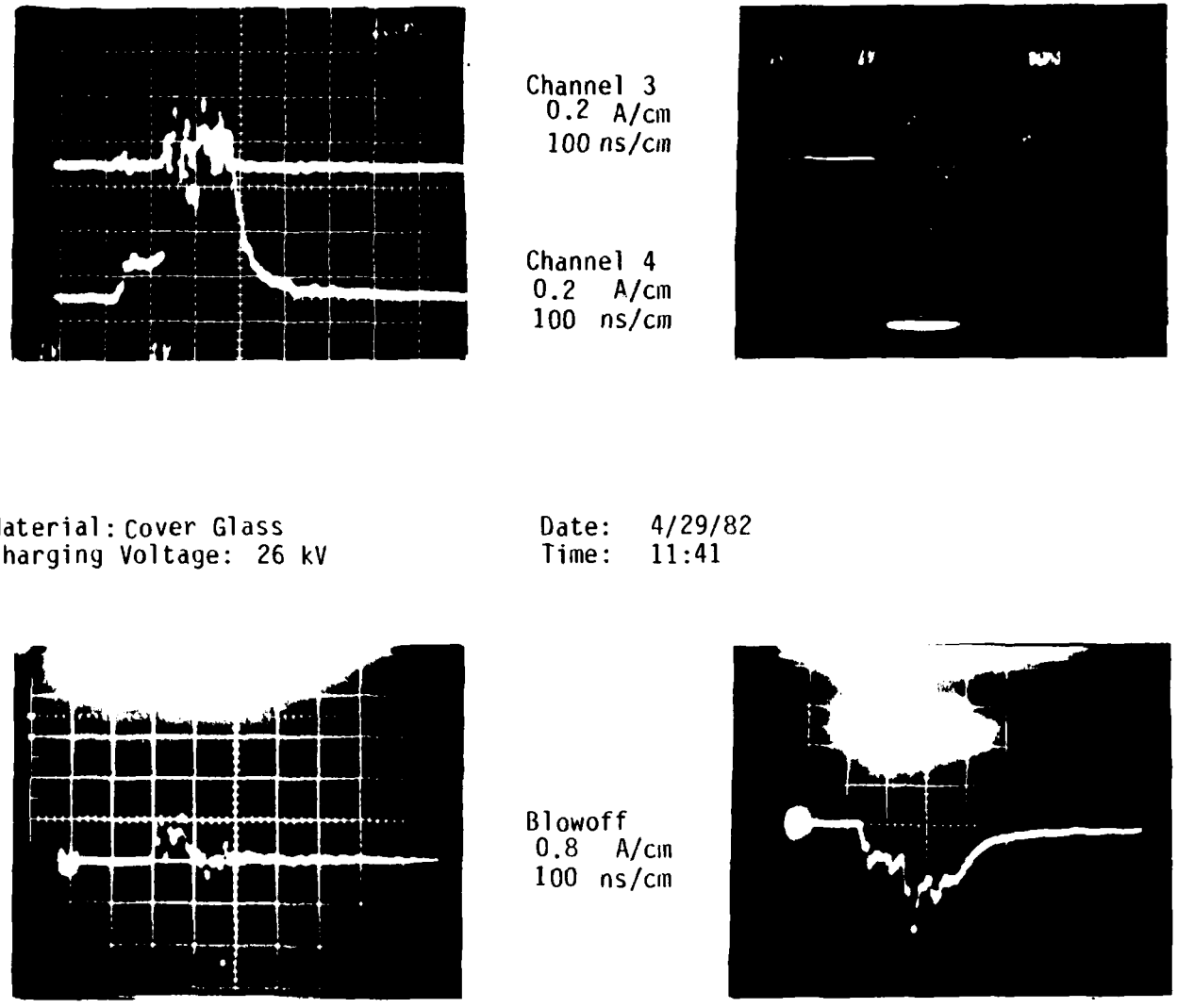

Figure 91. Transient record of discharge 11:41 on 0.03 cm solar cell cover glass exposed to 26 kV electron.

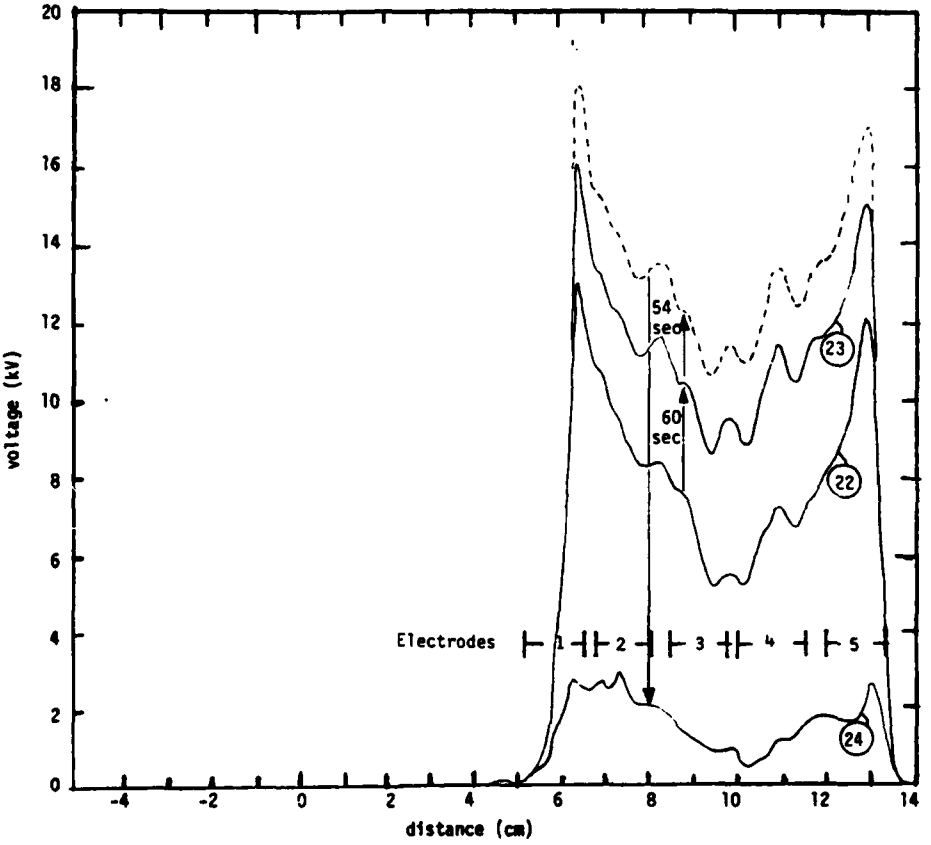

Figure 92. Charging 0.03 cm cover glass with 1.3 nA/cm^2 of 26 keV electrons, leading to discharge 3:21. Charging times are indicated.

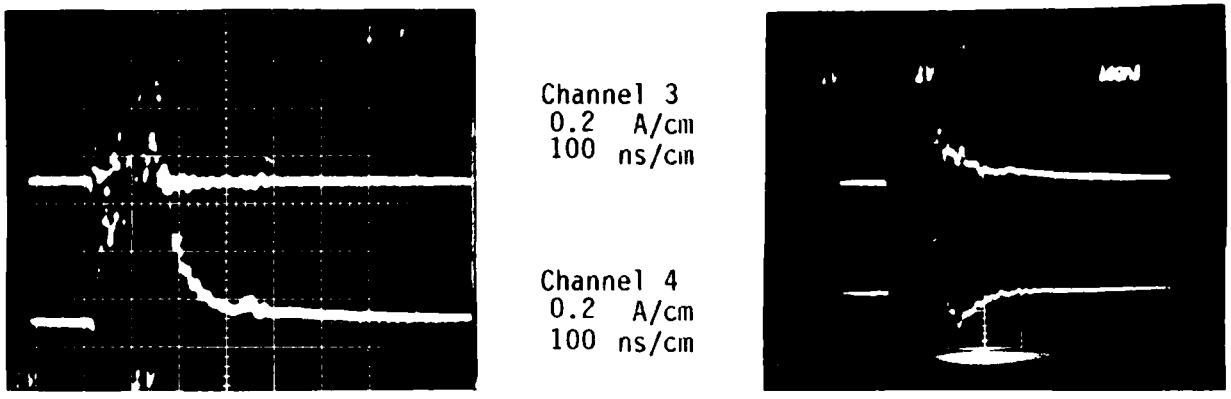

Material: Cover Glass
Charging Voltage: 26 kV

Date: 4/24/82
Time: 3:21

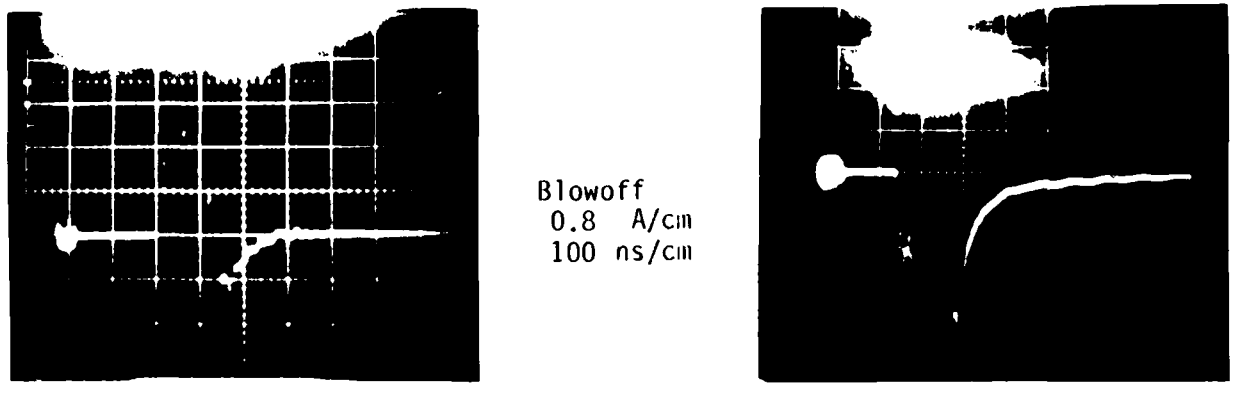

Figure 93. Transient record of discharge 3:21 on 0.03 cm solar cell cover glass exposed to 26 kV electron.

were all simultaneous to within about ±20 ns). This says that if a propagation velocity can be associated with discharges on solar cell cover glass, it must be faster than 2 or 3 x 10^8 cm/s. The only discharges we were able to observe visually appeared as bright points of light, on or near the boundary between the 2 covers, which was over electrode segment 3.

Figure 94 shows sweeps in two perpendicular directions. The lower trace represents a standard radial trace. We then moved the TREK probe to point A and rotated the turntable to take a profile in the circumferential direction. The point A is the same X-Y position on both sweeps.

Figure 95 is the same as Figure 94 but over a different part of the sample. The very small differences between the 2 radial potential profiles (Figure 94 and 95) is because the beam was inadvertantly on at very low current between the sweeps.

5. SECOND SURFACE MIRRORS

The 0.020 cm thick mirrors we tested were cemented to the segmented printed circuit (PC) board electrodes with a very thin layer of beeswax. The metalized side had been coated by the manufacturer (Optical Coating Labs, Inc., Santa Rosa, CA) with a thin coating to protect the metallization from deterioration. The mirrors were used in "as is" condition, with the metalized side placed down (toward the electrodes).

Figure 96 shows the charging pattern with 6kV electrons at 0.4 ± 0.2 nA/cm^2 (current was dropping during sequence), and 11 kV electrons at 0.5 ± 0.1 nA/cm^2. The pattern here does not reflect the segmented electrode structure noted in nonmetallic samples because of the metallization on the back of the sample itself. The asymptotic profile is at least 3 kV below the incident energy, but shows every sign of being limited by secondary emission. The peak on the left of the first few traces is from charge which spilled over the end of the shutter while we were tuning the beam. The

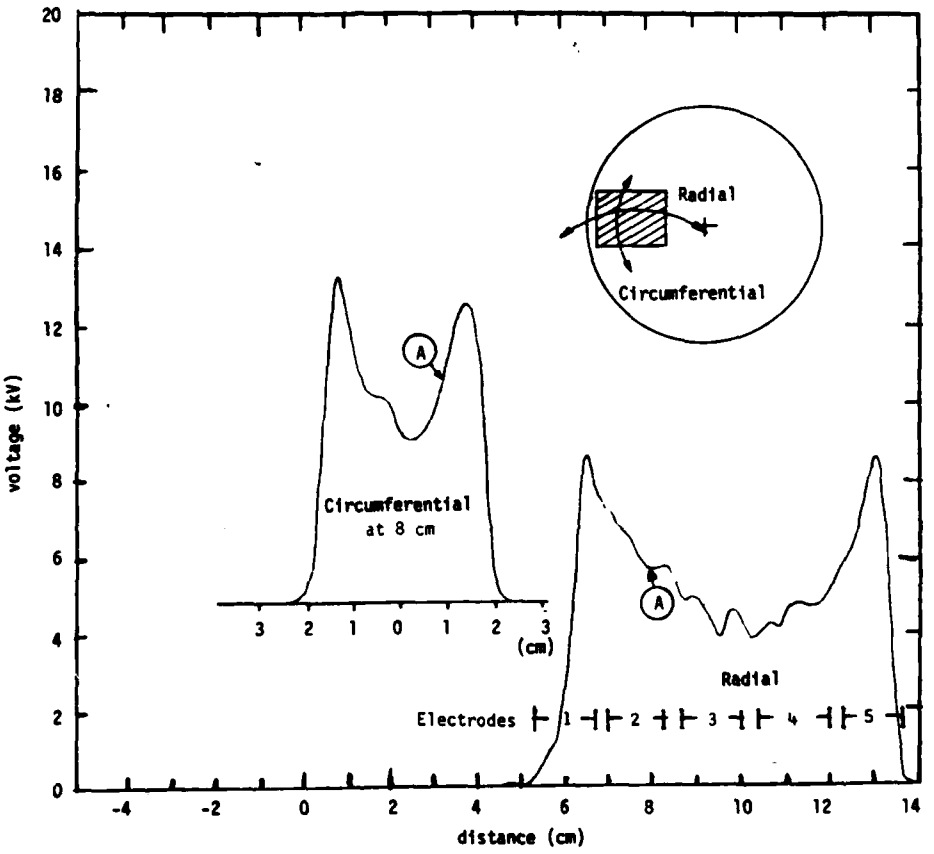

Figure 94. Perpendicular potential profiles on 0.03 cm cover glass intersecting at point A.

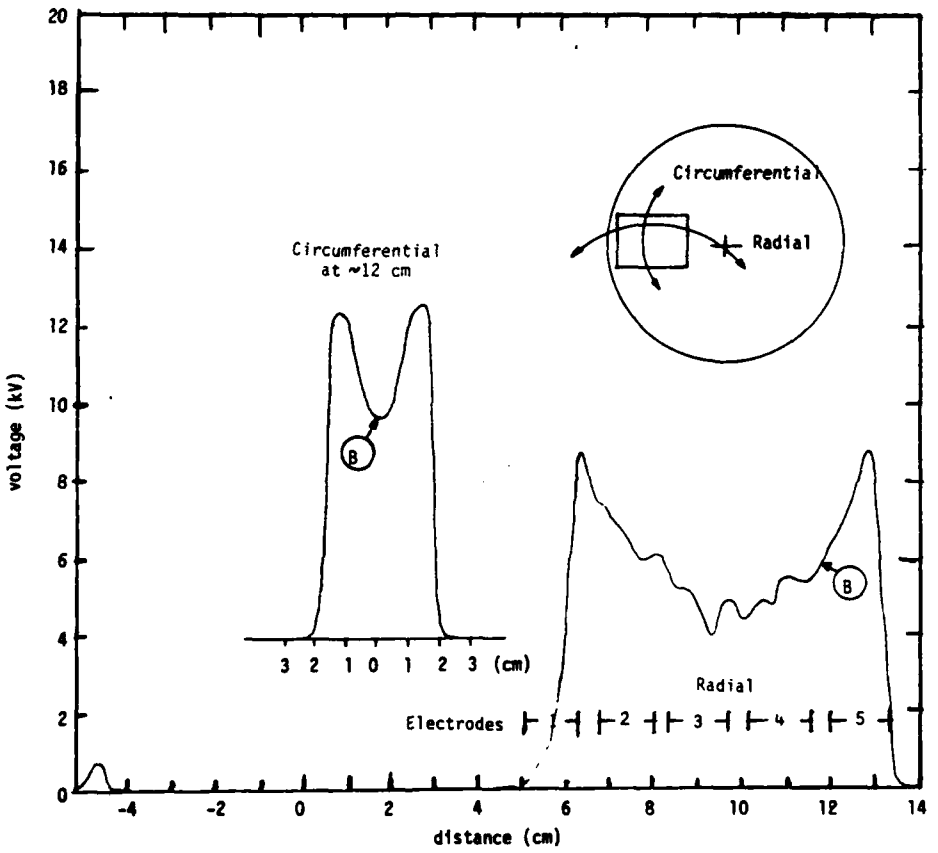

Figure 95. Perpendicular sweeps on 0.030 cm cover glass intersecting at point B.

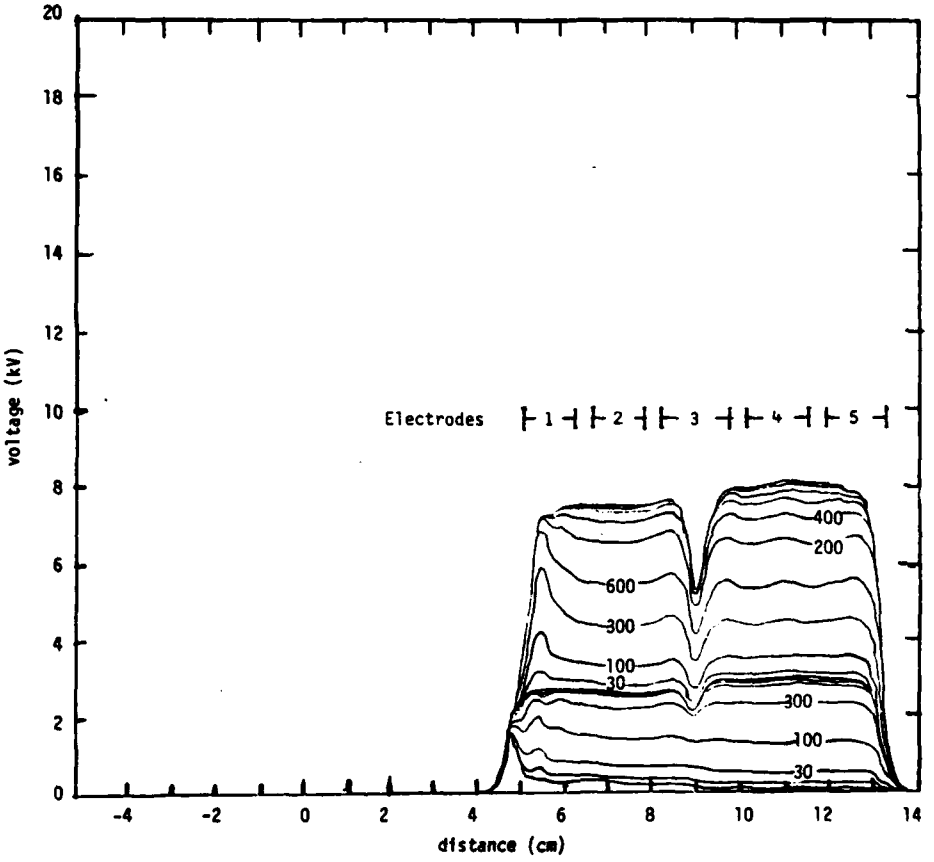

Figure 96. Charging profiles for 0.02 cm thick second surface mirrors. Charging with a) 0.4 ± 0.2 nA/cm^2 of 6 keV electrons, then b) 0.3 ± 0.1 nA/cm^2 and 0.55 ± 0.15 nA/cm^2 of 11 keV electrons. Charging times for the sweeps shown were a) 10, 30, 100, 300, 600, 800, 1100 seconds at 6 kV, then b) 30, 100, 300, 600 seconds at ≈0.3 nA/cm^2 and 11 kV, the c) 200, 400, 600, 800, 1100, 1400 seconds at 0.55 ± 0.15 nA/cm^2 and 11 kV.

peak on the left during the 11 kV charging is of unknown origin, though we suspect it is due to non-uniformities in the beam. The valley in the middle is at the edge between the 2 mirrors. This minimum gets deeper as the voltage gets higher around it. It is conceivable that there is actually a zero potential there which is too narrow for the TREK to resolve. Lastly, notice that the potential on the left half of the sample is lower than the potential on the right half. This is probably because the TREK sweeping arc is such that the probe is much closer to the edge of the mirror on the left half of its sweep than on the right half.

Figure 97 shows charging at 11 kV to restore the asymptotic profile, then further charging at 16 kV, 2 nA/cm^2. After the asymptotic profile was achieved, we turned the current up to 200 nA/cm^2 and the sample discharged. The asymptotic profile shows about the same shape as before, and has its maximum at $\approx$ 2.6 kV below the beam energy.

Figure 98 shows recharging at 16 kV, 20 nA/cm^2, leading to a discharge. Between Traces 17, 18, 19, and 20, the beam was on 3.7 s, 9.1 s and 13.6 s, respectively. The beam was then on 25 s before discharge 3:04. The profile before the discharge was probably very similar to Trace 20, because comparison with the previous figure shows that Trace 20 is very close to the asymptotic profile.

Figure 99 shows discharge event 3:04 which was associated with the preceeding potential profiles. To correctly interpret these records, we need to keep in mind that there is a metal plane between the buried charges and the electrodes (See Figure 100). Mirror 1 covers electrodes 1, 2, and half of 3; mirror 2 covers electrodes 4, 5, and half of 3 (Figure 100A). Therefore, for each unit of charge which goes from mirror 1 to ground (i.e., is blown off, which we represent by closing switch ⓔ in the equivalent circuit of Figure 100B) approximately 40% appears on electrode 1, 40% appears on segment 2, and 20% appears on segment 3. Similarly, charge leaving mirror 2 going to ground has 20% appear on segment 3, 40% appear on segment 4, 40%

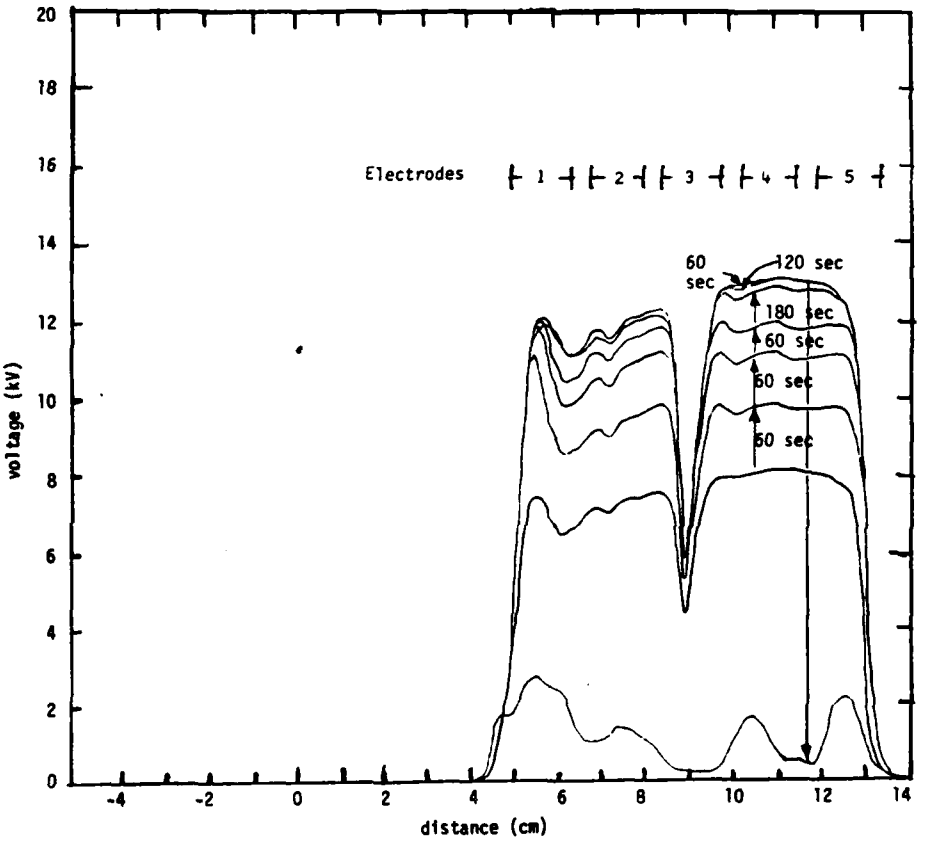

Figure 97. Continued charging of 0.02 cm glass mirrors with 2 nA/cm^2 of 16 keV electrons, then a discharge induced by 200 nA/cm^2 of 16 keV electrons.

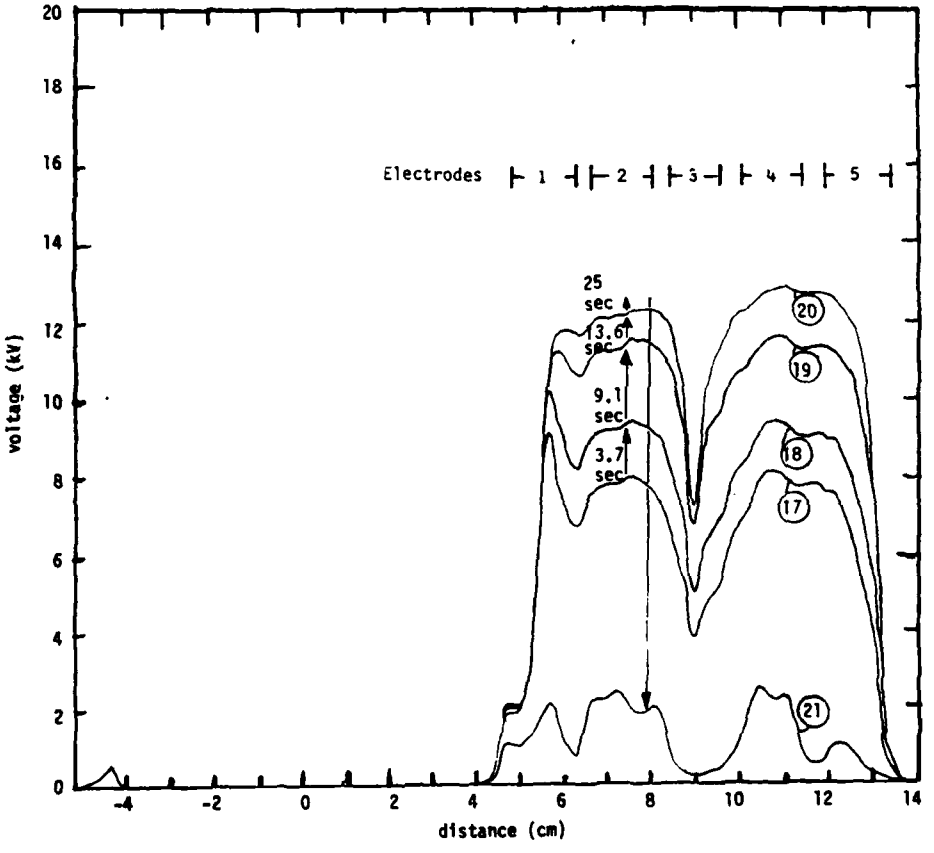

Figure 98. Recharging profiles of 0.020 cm second surface mirrors with 20 nA/cm^2 of 16 keV electrons, leading to discharge 3:04.

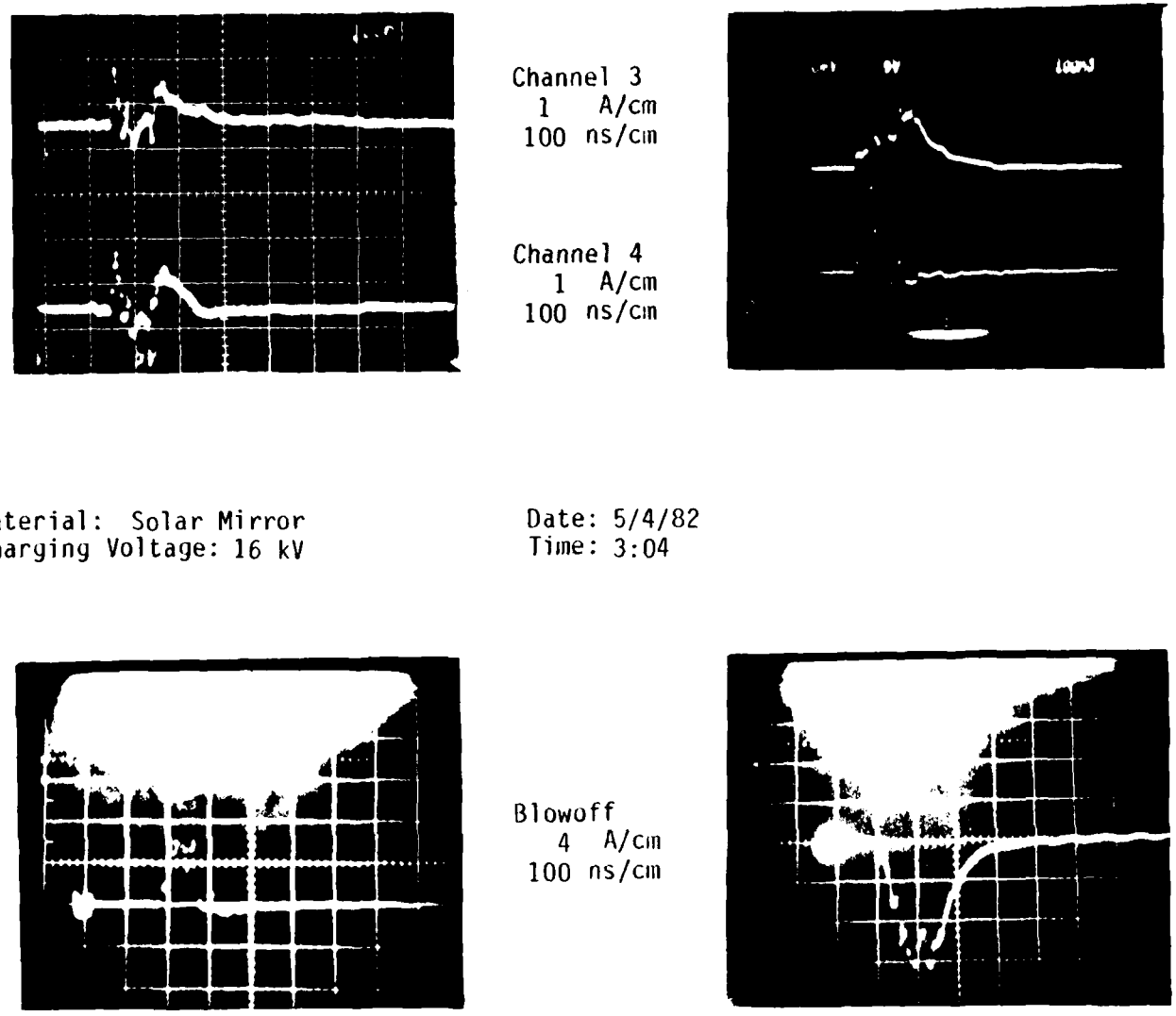

Figure 99. Transient record of discharge 3:04 on 0.020 cm second surface mirrors exposed to 16 kV electrons.

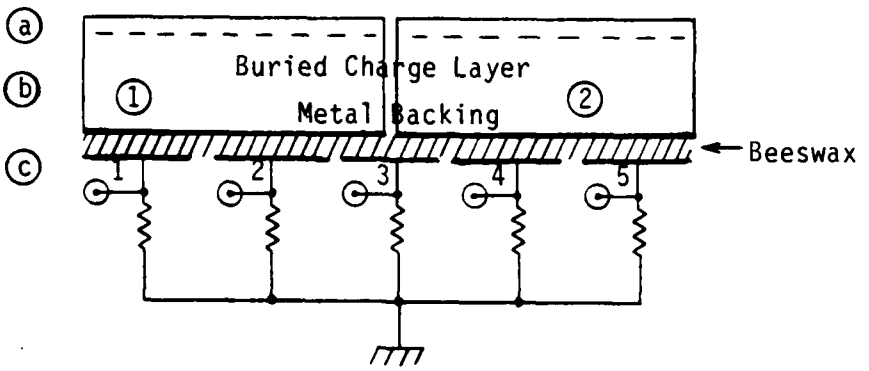

Figure 100A. Diagram of second surface mirror electrode arrangement. Buried charge resides at (a), the metal back of the mirror is node (b), and the segmented electrodes are at (c).

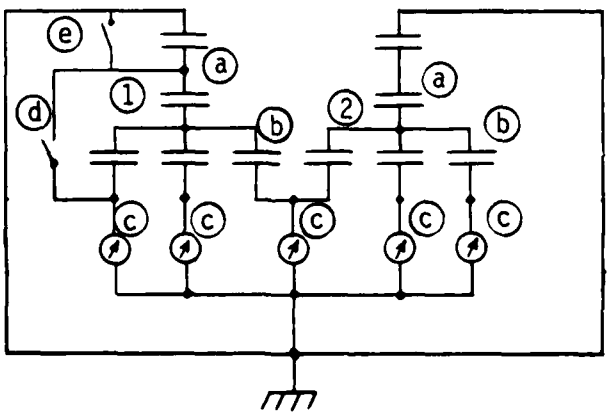

Figure 100B. Equivalent circuit for second surface mirrors, showing the buried charge (node (a)) metal mirror reflectors (b), segmented electrodes (c) and switches (d) and (e) to represent punch-through and blow-off, respectively.

appear on segment 5. On the other hand, if charge punches through the sample, or runs around the edge to the electrode, 40% of that charge is recombining with its image charge. The image charge for the rest is on the other electrodes. So, if charge leaves mirror 1 and goes directly onto channel 1, 60% appears as a negative signal on Channel 1, 40% appears positively on channel 2 and 20% appears positively on Channel 3 (we represent this in Figure 100B by closing switch ⓓ). Mirror 2 behaves analogously. We were concerned about signals on one channel coupling to another to produce spurious signals (i.e., in ways other than those indicated above), but (as mentioned for solar cell cover glass) pulse tests showed that any coupling is less than a few percent of the original signal.

Referring back to Figure 99, Channels 4 and 5 both show a current pulse starting at zero time and lasting for ≈100 ns, Channels 1 and 2 show small transients coincident with the beginning of the signals on 4 and 5 (t_0), followed by a pulse beginning about t_0 = 100 ns and persisting for about 100 ns. Our interpretation is that Mirror 2 discharged first, taking ≈100 ns to discharge. Mirror 1 exhibited some small prompt activity, but most of its charge took 100 ns to start leaving. Channel 3 is essentially an average of both other signals. The blow-off collector collected ≈ 2/3 of the charge which we calculate to have been on the sample (which might be within our error bars for how much charge was available). Channel 5 alone recorded less than 10% of what the blow-off collector recorded. The visual observation of the discharge was 5 or 6 tiny bright points of light along the edge of the sample and one or two others in the middle.

Figure 101 shows asymptotic potential profiles for second surface mirrors charged with 10 nA/cm^2 of 11 kV, 12 kV, 13 kV, and 14 kV electrons. The profiles are just 1 kV apart, with the maximum being 2800 V below the beam voltage for each profile. The 13 kV profile is actually two indistinguishable profiles, the beam was on 60 s before the first record and another 60 s before the second. After charging at 14 kV, the beam was turned on for an additional 14 s at 15 kV before a discharge occurred.

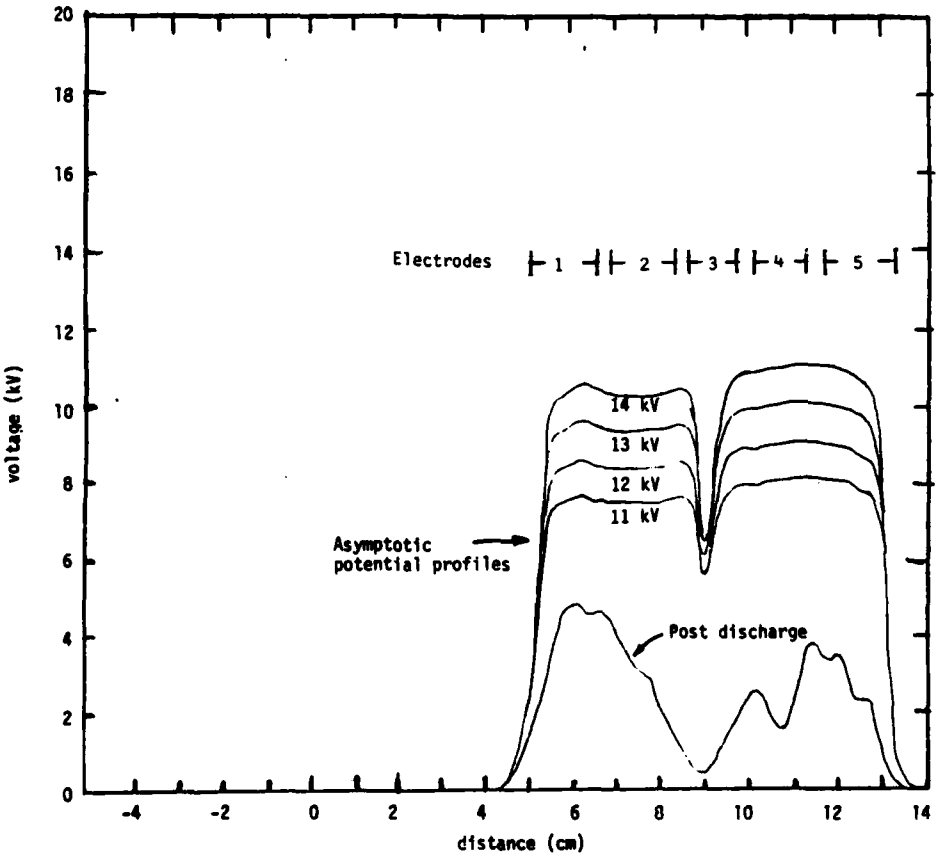

Figure 101. Asymptotic profiles for 0.020 cm second surface mirrors exposed to 10 nA/cm^2. Beam energy at 11 kV, 12 kV, 13 kV, 14 kV. Discharge with beam at 15 kV.

Figure 102 shows the results of charging at 16 kV, with 2 nA/cm^2 current densities. After the profile reached asymptotic form, current was raised to 4 nA/cm^2, then 7 nA/cm^2, then 12 nA/cm^2. The beam was then on 2 min, 20 s when the sample discharged. There was no visible difference between the asymptotic profiles at different currents. The discharge removed most of the charge on the sample.

Trace 14 of Figure 103 shows a profile after discharge event 11:52, which followed 22 s of charging with 16 kV electrons at 10 nA/cm^2. Clearly, the sample discharged at a much lower voltage than one would expect from the previous data, and much less charge was involved, than in the preceeding discharge. This is confirmed by the transient record. After Trace 14, the 16 kV beam was on for 30 s when discharge event 12:09 happened. The pre-discharge profile was probably considerably higher than before discharge 11:52, because the charging started from a higher base potential and charged longer. Again, the transient record shows considerably more charge than the preceeding discharge.

Figure 104 shows transient records from event 11:52. In this event, Channels 4 and 5 show no signal, from which we infer that mirror 2 did not participate in the event at all. Channels 1, 2, and 3 show similar positive signals to begin the event, lasting about 50 ns. Then, channel 1 goes strongly positive, and channels 2 and 3 go negative. We interpret this to mean that the event began as a "blow-off" and then became a "punch-through" or "flash-over" (around the edge) onto electrodes 2 and 3. The blow-off collector supports this interpretation, showing a negative signal for the first 50 ns, and then very little. Visually, the event appeared as a few tiny bright points along the joint between the two mirrors.

Figure 105 shows transient records for event 12:09. This record is a little more difficult to interpret. Channels 4 and 5 look almost identical, and indicate a blow-off lasting ≈ 300 ns. Channel 3 suggests a "punch-through" or "flash-over" directly to the electrode, which was large enough to more

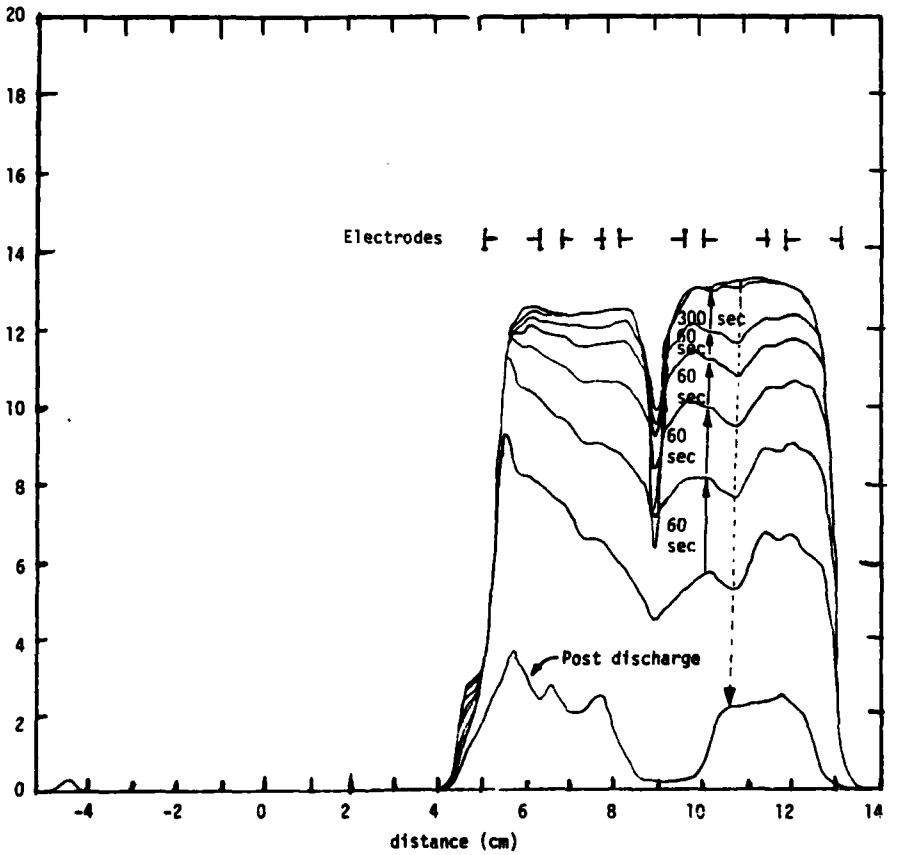

Figure 102. Recharging profiles for 0.020 cm second surface mirrors with 2 nA/cm^2 at 15 kV. Nearly identical asymptotic profiles at 2, 4, 7 nA/cm^2. At 12 nA/cm^2, sample discharged.

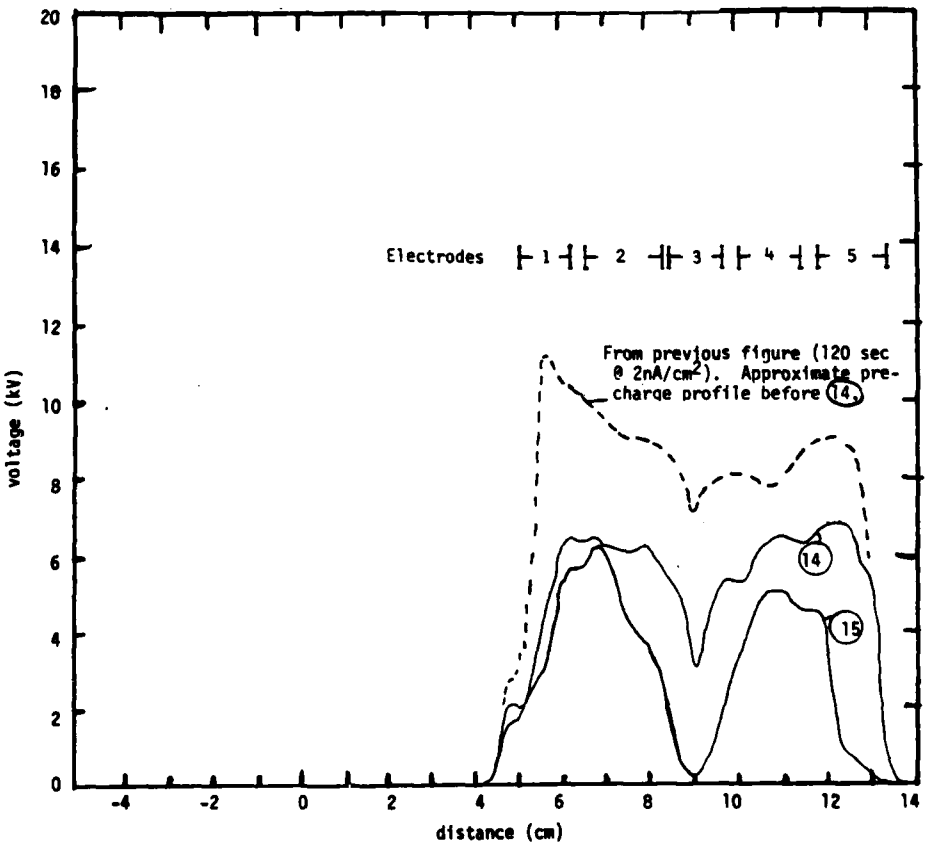

Figure 103. Post-discharge profiles for 0.020 cm second surface mirrors after events 11:52 and 12:09. Estimate of profile before event 11:52.

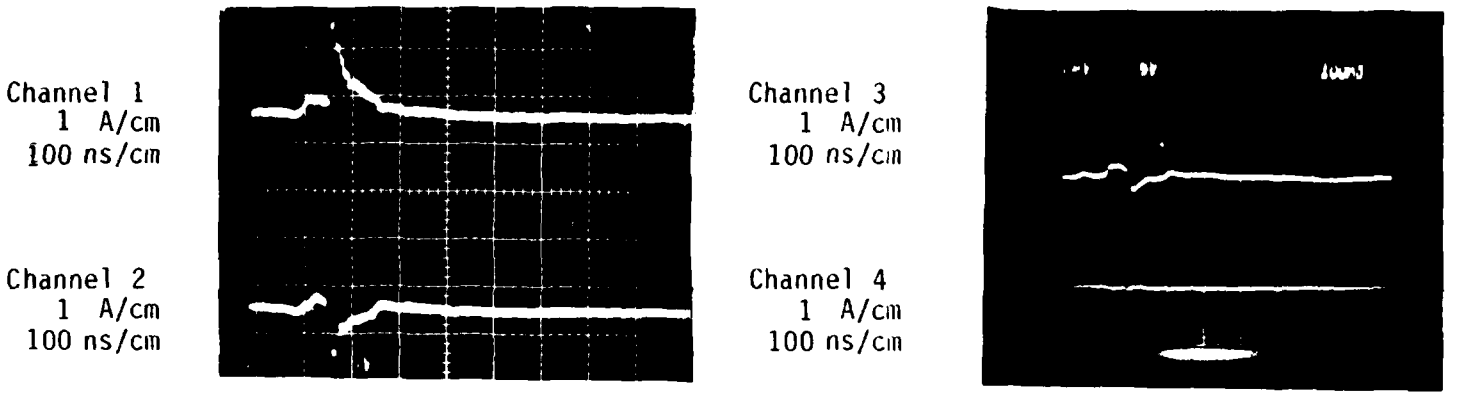

Material: Solar Mirror
Charging Voltage: 16 kV

Date: 5/4/82
Time: 11:52

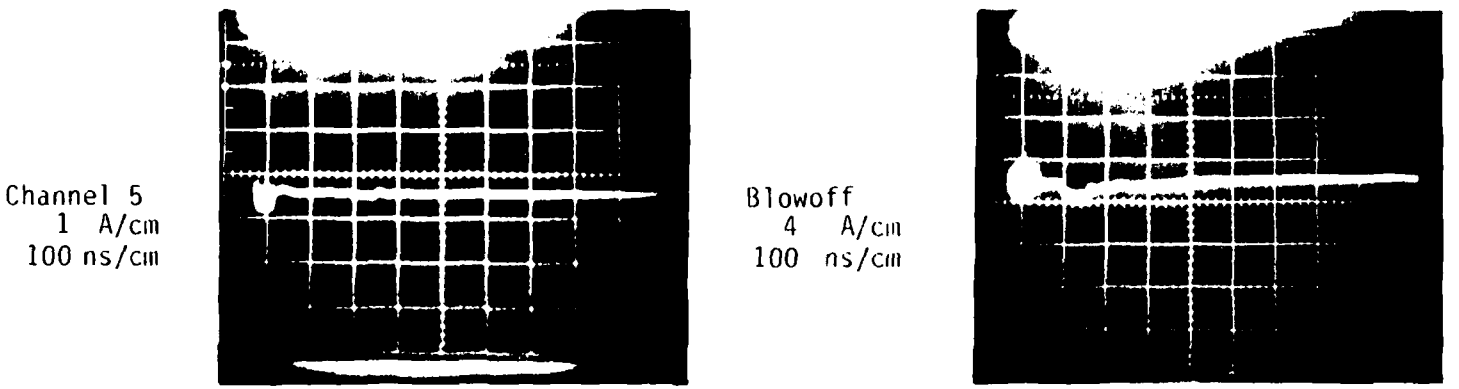

Figure 104. Transient record of discharge 11:52 on 0.020 cm second surface mirrors exposed to 16 kV electrons.

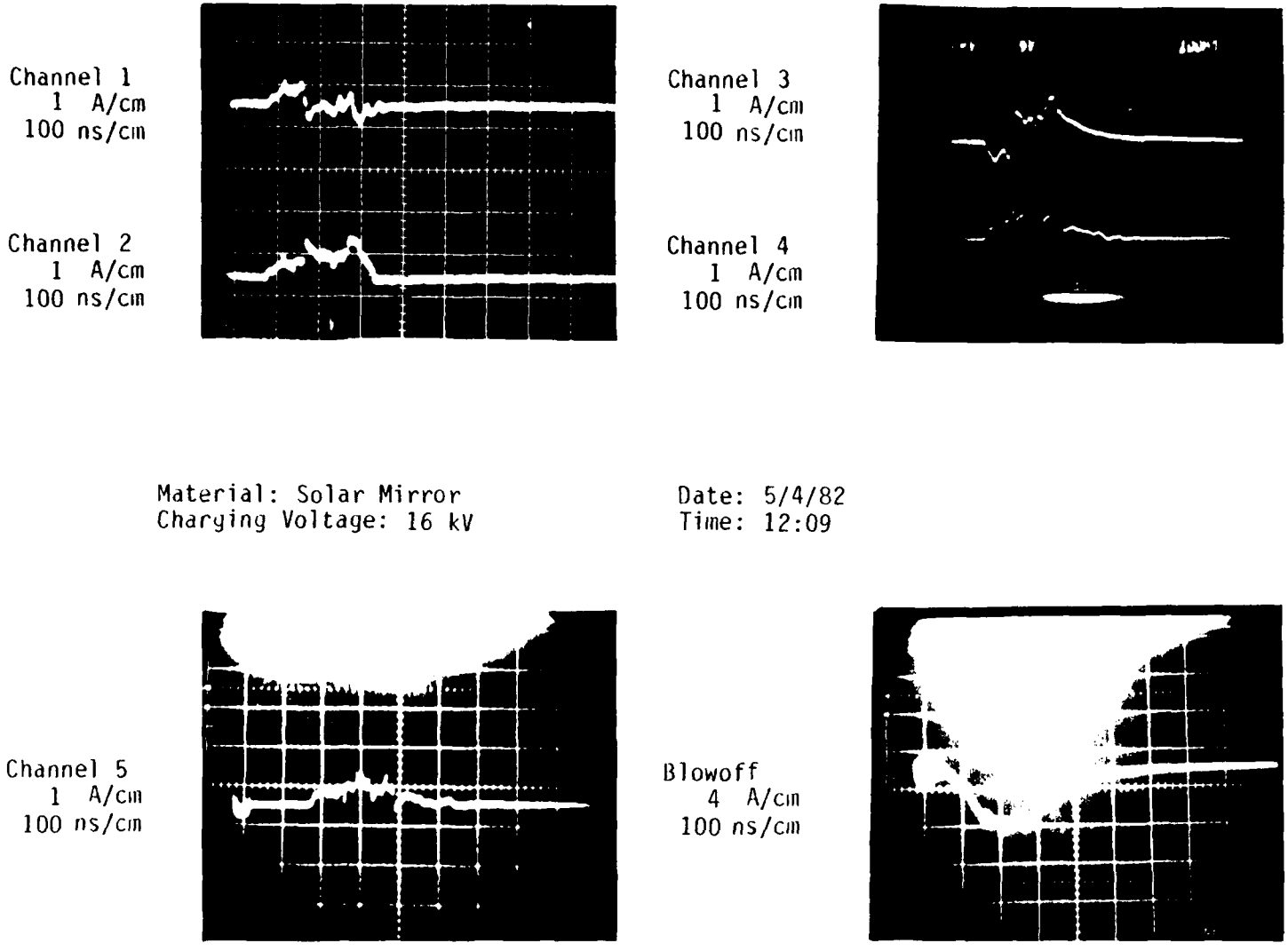

Figure 105. Transient record of discharge 12:09 on 0.020 cm second surface mirrors exposed to 16 kV electrons.

than compensate for the blow-off happening on mirror 2. Channel 1 shows the coupling from the early (60 ns) "punch-through" on Channel 3, followed by a net-zero signal for the duration of the event. Since 2 and 3 show positive during this late stage, we infer that Channel 1 has a combination of charge moving directly to the electrode, and charge blown off, which balance out to about zero. Visually, this event appeared as bright points of light along the edges of the mirrors and the joint between them.

Figure 106 shows the decay of voltage on the sample after leaving it 38 hours without charging. The voltage has dropped about 100 V out of 8200, which implies a conductivity of 3×10^{-20} ohm^{-1} cm^{-1}. No conductivity was observed to be large enough to be measured in less than 10 hours. Hence, if there is any field-enhanced, photo-enhanced, or radiation-generated conductivity, the change in conductivity due to any of these effects is less than an order of magnitude and the resultant conductivity is still very small compared to that of the other materials.

Figure 107 shows another decay of voltage over several days. The middle profile was taken 138 hours after the upper, and shows a conductivity of $\approx 9 \times 10^{-20}$ ohm^{-1} cm^{-1}. The lower profile was taken 71 hours after the middle, implying a conductivity of $\approx 5 \times 10^{-20}$ ohm^{-1} cm^{-1}. One final profile was taken 46 days later, where the peak voltage had decayed from 11,050 V to 8400 V, which implies a conductivity of 2×10^{-20} Ohm^{-1} cm^{-1}.

Figure 108 shows a good example of a "flash-over" or "punch-through" directly onto the back surface electrode. We said before that an event of this type should produce a signal, on the electrode where charge is arriving from the buried charge layer, which is negative and 60% of the total charge which actually moved. The adjacent channel should show a positive 40% signal, and channel 3 (which is only half covered by that mirror) should show a positive 20% of the total charge released. This is almost exactly what we see here. Channel 1 is off scale negative at more than 5A, Channel 2 shows

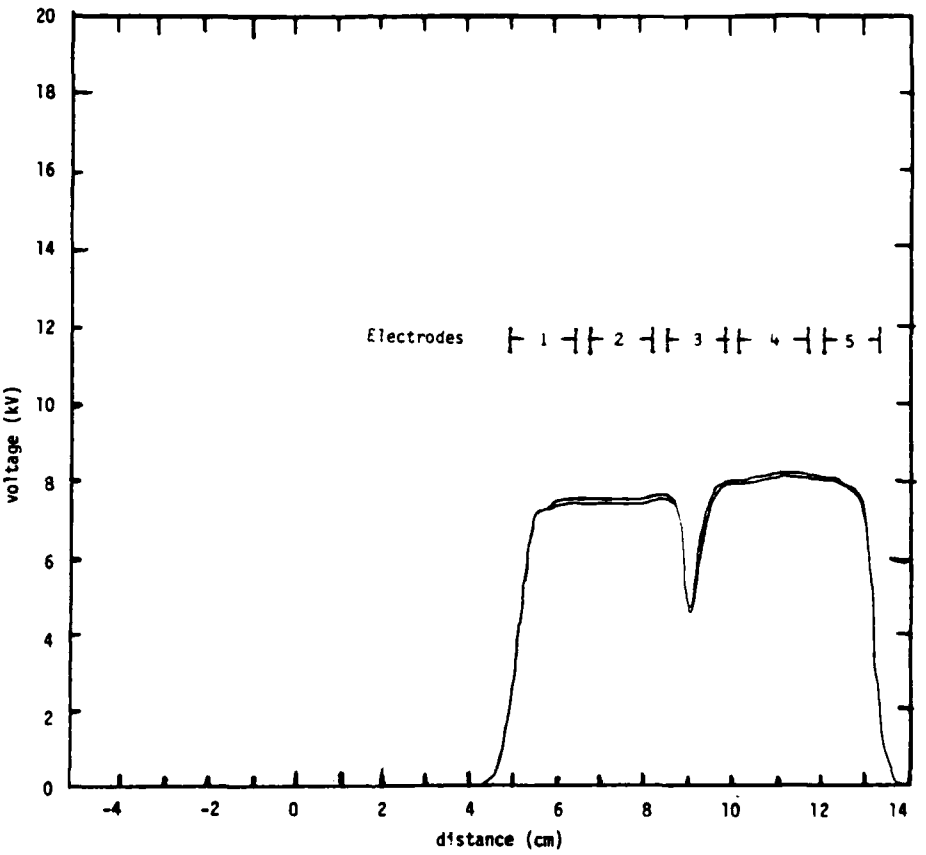

Figure 106. Decay of voltage profile on 0.020 cm second surface mirrors after 38 hours.

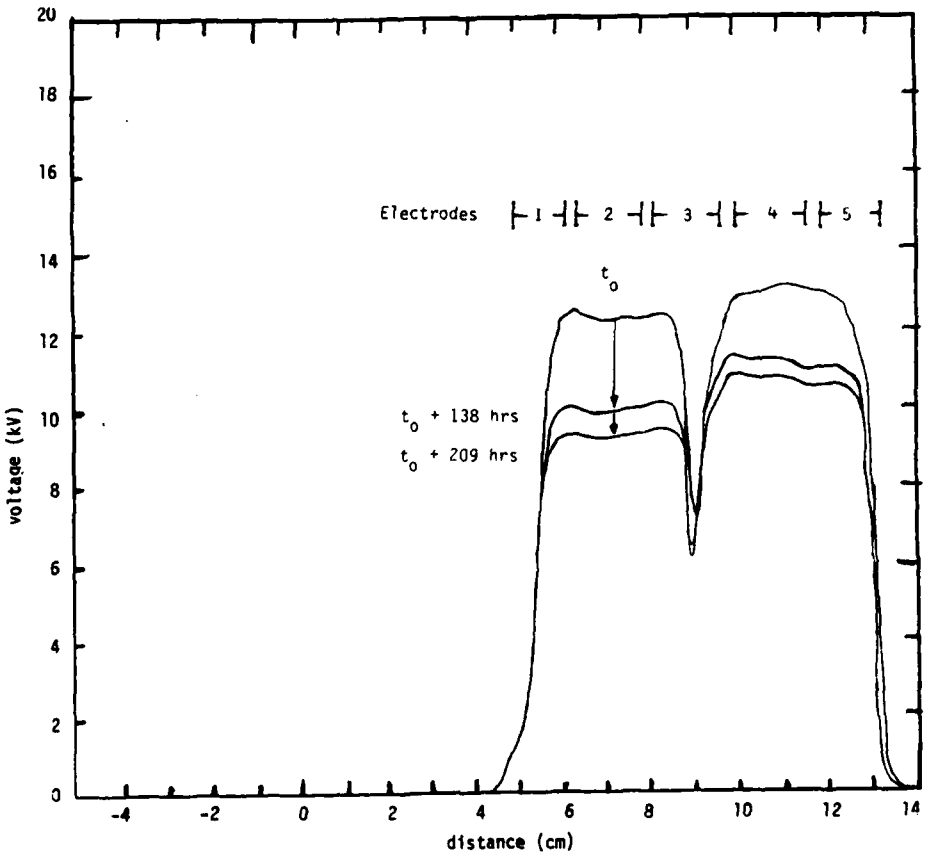

Figure 107. Decay of voltage profile on 0.020 cm second surface mirrors over 138 hours, then 71 hours.

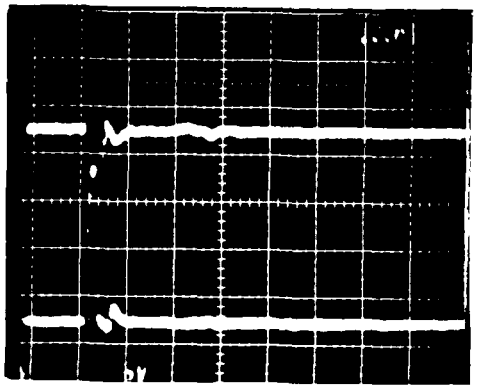

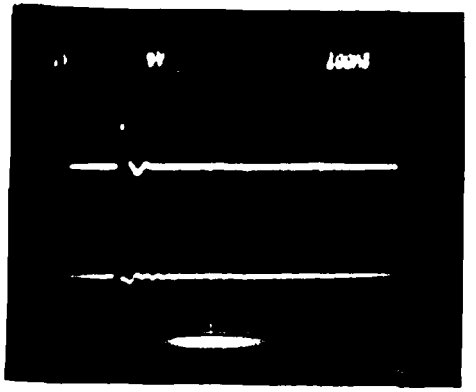

Material: Solar Mirror
Charging Voltage: 16 kV

Date: 5/3/82
Time: 11:47

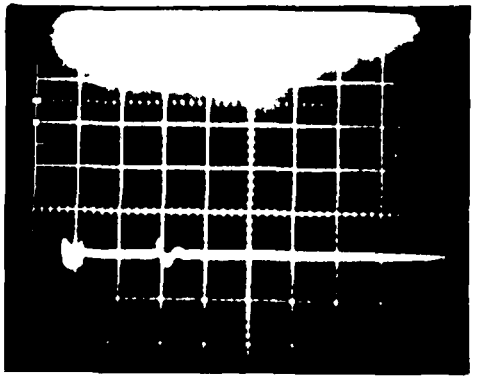

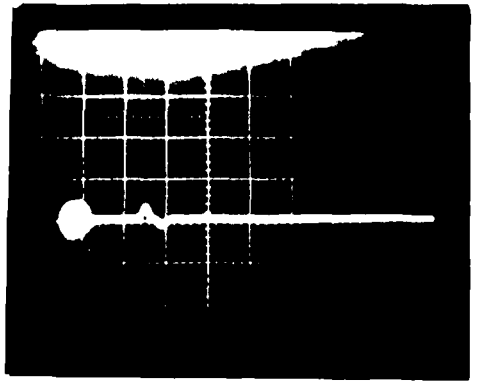

Figure 108. Transient record of discharge 11:47 on 0.020 cm second surface mirrors exposed to 16 kV electrons. We believe this is a punch-through or flash-over to the substrate, with no blow-off.

a peak of positive 3 A and Channel 3 shows 2 A. Channels 4 and 5, and the blow-off collector apparently did not participate, and show a net zero current. A post-discharge profile shows charge missing from everywhere on the sample so we speculate that there must have been second discharge to remove charge from above 4 and 5 after the end of our scope sweeps, before we took the potential profile.

Figure 109 shows the plot of the current and voltage dependence of breakdown initiation. The X-axis represents the current density of the electron beam and the Y-axis represents the energy of the electrons. The circles indicate that the sample achieved an asymptotic profile without breakdown; the X's indicate that a breakdown occurred. Since the asymptotic profiles were virtually independent of current density, the figure shows that the conditions necessary for breakdown depend on current density of the beam, as well as the voltage profile to which the sample has charged. In fact, we have reason to believe that at the data point labeled A on Figure 109 the sample discharged when its voltage profile was lower than what had previously been a stable level. That is, at point A, the sample discharged after charging to around 9±2 kV (See Figure 103), where before it had been stable at an equilibrium potential of ≈13 kV (See Figure 102).

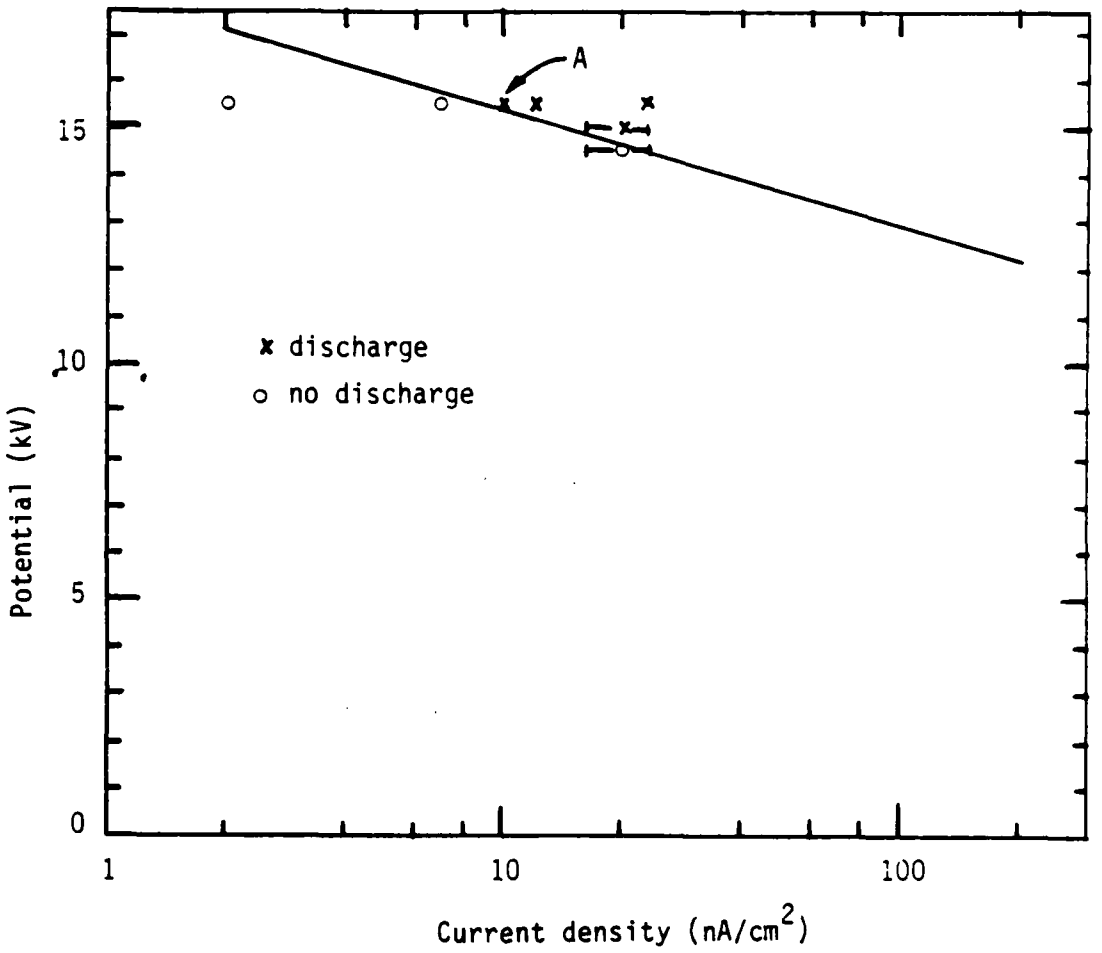

Figure 109. Stability of breakdown as a function of beam current and energy. Second surface mirrors.

SECTION IV
SUMMARY OF RESULTS

The data accumulated in this effort adds to an existing data base that has been accumulating for the past decade. We have no intention of slighting other investigations and/or data, or of duplicating effort but, there are literally thousands of papers and presentations related to spacecraft charging, electron caused electromagnetic pulse (ECEMP), and systems generated electromagnetic pulse (SGEMP). We also know from personal communications that a lot of unpublished data exists, and that significant contributions exist in obscure locations. There is presently controversy throughout the SCC/SGEMP community about the significance and/or relevance of various conditions and observations.

This work was constructed to create and measure the charging and discharge characteristics of selected dielectrics under conditions perceived to be representative of space. Recent data from SCATHA (Spacecraft Charging at High Altitudes) and the results of multi-beam experiments (Ref. 13) which suggest surface potentials need not be very high to induce discharges may challenge some of our perception. Nevertheless, dielectrics were charged to spontaneous breakdown and the discharges characterized. Discharge propagation velocities of from 2×10^7 to 6×10^7 cm/s were measured for the organic dielectrics. This is basically in accord with the velocities

13. P. Coakley, M. Treadaway and B. Kitterer, "Charging and Discharging Characteristics of Dielectric Materials Exposed to Low- and Mid-Energy Electrons," IEEE N.S.R.E. Conference, Las Vegas, July 1982.

previously inferred from discharge pulse-width scaling observations, and with more recent independent optical observations (Ref. 14). This investigation demonstrated discharges which either propagate at very high velocities ($v > 3 \times 10^8$ cm/s) or initiate simultaneously over distances of several cm [in Mylar and silicates (glass and silica)]. These events were not observable in earlier investigations. To the best of our knowledge this is a new and unpredicted observation.

Table 5 is a summary of the discharge observations of this report. Numerous other records associated with charging (potentials and gradients) and discharging (including conductivity measurements) may be found in the text.

14. K.G. Balmain, M. Gossland, R.D. Reeves and W.G. Kuller, "Optical Measurements of the Velocity of Dielectric Surface Arcs, IEEE N.S.R.E. Conference, Las Vegas, July 1982.

TABLE 5. SUMMARY OR CATALOG OF EVENTS (KAPTON).

	Description	Interpretation	Figure
Transient Signals	Discharge signals lasting ≈100 ns appearing sequentially on neighboring electrodes	Surface flashover or subsurface burrowing, propagating across sample at a fairly consistent rate. Probably intiated by high lateral fields, or maybe by tiny punch-through. No tracks found with microscope examination	17, 20 26, 27 29, 31
Potential Profiles	Charge uniformly missing over entire sample		18, 19 25, 28
Visual	Lichtenberg or tree-like pattern to light emitted (no damage)		
Transient Signals	Discharge signals lasting ≈500 ns appearing about simultaneously accompanied by blow-off	Discharge located between electrodes propagating parallel to the electrodes	22, 24 29, 30
Potential Profiles	Charge preferentially lost from low capacitance areas between electrodes		23, 28
Visual	Faint tree-like pattern, or simple strip of glow, between electrodes		

TABLE 5. SUMMARY OR CATALOG OF EVENTS (TEFLON).
(Continued)

	Description	Interpretation	Figure
Transient Signals	≈100 ns signals appearing sequentially on neighboring electrodes with blow-off ≈CΔV from potential profile	Surface flash-over or subsurface burrowing, propagating across sample at a fairly consistent rate. Probably initiated by high lateral fields, or maybe by tiny punch-through. No tracks found with microscope examination	36, 37 39, 43 45, 47 49, 50
Potential Profiles	Charge removed uniformly from all parts of the sample		38, 42 44, 46 48
Visual	Lichtenberg or tree-like glow (no damage)		
Transient Signals	200-500 ns signals	Discharge located between electrodes propagating parallel to the electrodes	34
Potential Profiles	Charge preferentially missing from areas between electrodes where the pre-event potential was greatest		35
Visual	Faint and concentrated between electrodes		

TABLE 5. SUMMARY OR CATALOG OF EVENTS (MYLAR).
(Continued)

	Description	Interpretation	Figure
Transient Signals	Positive signals lasting ≈100 ns, appearing sequentially on neighboring electrodes - blow-off ≈ $\int Idt \approx C\Delta V$	Propagating discharge either a burrowing lichtenberg or surface flashover (brush fire) event	52, 53 55, 56
Potential Profiles	Charge emission uniformly over entire sample		54, 57
Visual	Appeared as Lichtenberg or dendritic pattern	Microphotographs show "tree" structure	73-76
Transient Signals	Positive signals appearing simultaneously on all electrodes, presisting 100-200 ns	A discharge initiated simultaneously over the entire sample surface, but requiring time to remove charge	60, 61 66, 67
Potential Profiles	Show charge missing over entire sample		68
Transient Signals	Negative signals on some electrodes, positive on others	Punch-through	66
Potential Profiles	Charge lost uniformly		68
Visual	Bright points of light with or without Lichtenberg patterns associated		
Transient Signals	Positive signals lasting ≈100-200 ns but <u>not</u> sequentially on adjacent electrodes	a. two nearly simultaneous discharges b. a single discharge that doesn't remove all the charge in certain areas on the first pass c. very discontinuous propagation	58, 59 69

TABLE 5. SUMMARY OR CATALOG OF EVENTS (MYLAR).
(Continued)

	Description	Interpretation	Figure
Transient Signals	Very large blow-off collection when the collector is biased +200 v	Collection of real blow-off plus conduction through a neutral plasma	60, 61
Transient Signals	Bipolar blow-off when collector is biased -200 v	Collection of energetic blow-off electrons followed by conduction through a neutral plasma	65

TABLE 5. SUMMARY OR CATALOG OF EVENTS (GLASS).
(Continued)

	Description	Interpretation	Figure
Transient Signals	Discharge signals initiate simulatneously and persist 200-400 ns with blow-off	Discharge propagation velocity greater than 3×10^8 cm/s (simultaneous)	87, 89 91, 93
Potential Profiles	Charge lost pretty uniformly. $C\Delta V$ equal to integral of current	With some current limiting mechanism	86, 88 90, 92
Visual	Bright spots, especially on the sample edges	Not propagating like Teflon, Kapton and Mylar	

TABLE 5. SUMMARY OR CATALOG OF EVENTS (SECOND SURFACE MIRRORS).
(Continued)

	Description	Interpretation	Figure
Transient Signals	Discharge signals persisting less than 100 ns, some positive (charge removal) some negative (charge collection) with negligible blow-off	Punch-through or discharge around edge (Notice the metallization on the back of the mirrors reduces resolution of the measurement) Several discharges happening in conjunction	104, 108
Potential Profile	Charge removed from all of sample		103
Visual	Bright spots at edge of sample		
Transient Signals	Discharge signals of both polarities persisting 100 to 300 ns, accompanied by blow-off	Combination of flash-over and punch-through or discharge around edge	99,104 105
Potential Profile	Charge removed from all of the sample		98,103
Visual	Bright spots at edge of sample		

REFERENCES

1. J.D. Riddell, V.A.J. van Lint, B.C. Passenheim, "Charging and Discharging of Satellite Dielectrics," Mission Research Corporation Report, MRC/SD-R-70, January 1981.

2. M. Gossland, K.G. Balmain and M.J. Treadaway, "Surface Flashover Arc Orientation on Mylar Film," IEEE Trans. Nuc. Sci., NS-28, 4535 (1981).

3. L.J. Amore and A.E. Eagles, "Materials and Techniques for Spacecraft Static Charge Control," pg. 621 of the Proceedings of the Spacecraft Charging Technology Conference, AFGL-TR-77-0051, February 1977.

4. K.G. Balmain, M. Cuchanski and P.C. Kremer, "Surface Micro-Disharges on Spacecraft Dielectrics," pg. 519 of the Proceedings of the Spacecraft Charging Technology Conference, AFGL-TR-77-0051, February 1977.

5. R.L. Gardner, C. Longmire, J.L. Gilbert, and M.H. Frese, "Nuclear Lightning," AFWL-TR-81-192 (2 Vol.) February 1982.

6. B.C. Passenheim and V.A.J. van Lint, "Charging and Discharging Teflon," pg. 52 in the 1980 Spacecraft Charging Technology Conference Proceedings, NASA pub. 2182, AFGL-TR-81-0270.

7. G.T. Inouye, "Brushfire Arc Discharge Model," pg. 133 of the 1980 Spacecraft Charging Technology Conference Proceedings, NASA pub. 2182, AFGL-TR-81-0270.

8. V. Adamec and J.H. Calderwood, "Electrical Conduction in Dielectrics at High Fields," J. Phys. D., 8, 551, (1975).

9. A.R. Fredrickson, "Bulk Charging and Breakdown in Electron-Irradiated Polymers," pg. 33 of the 1980 Spacecraft Charging Technology Conference Proceedings, NASA pub. 2182, AFGL-TR-71-0270.

10. J. Wilkenfeld, presentation at the 1980 Spacecraft Charging Technology Conference (not published in the proceedings).

11. B. Gross, G.M. Sessler, J.E. West, "Charge Dynamics for Electron Irradiated Polymer Foil Electrets," J. Appl. Phys. 45, 3841, (1974).

12. J. A. Wall, E.A. Burke, and A.R. Fredrickson, "Results of Literature Search on Dielectric Properties and Electron Interaction Phenomena Related to Spacecraft Charging," pg. 581 of the 1977 Proceedings of the Spacecraft Charging Technology Conference, AFGL-TR-77-0051 or NASA TMX-73537.

REFERENCES (Concluded)

13. P. Coakley, M. Treadaway and B. Kitterer, "Charging and Discharging Characteristics of of Dielectric Materials Exposed to Low- and Mid-Energy Electrons, IEEE N.S.R.E. Conference, Las Vegas, July 1982.

14. K.G. Balmain, M. Gossland, R.D. Reeves and W.G Kuller, "Optical Measurements of the Velocity of Dielectric Surface Arcs," IEEE N.S.R.E. Conference, Las Vegas, July 1982.

APPENDIX

GLOSSARY OF TECHNICAL TERMS

Anisotropic: Not isotropic, having physical properties (such as velocity and conductivity) which vary according to the direction in which they are measured.

Backscatter: When particles impinge on a solid, some are scattered through angles great enough to escape back into the hemisphere they came from.

Charged Particle Spectrum: The flux of particles with energies between ε and $\varepsilon + \Delta\varepsilon$.

Conductivity: The ability to conduct current. $\sigma = J/E$.

Dielectric: A material whose conductivity at room temperature is less than about 10^{-9} $(\Omega cm)^{-1}$ (semiconductors range from about 10^{-9} to 10^{+2} $(\Omega cm)^{-1}$ and conductors have conductivity greater than 10^{2} $(\Omega cm)^{-1}$)

ECEMP: Electron Caused Electromagnetic Pulse. An electromagnetic pulse caused by spontaneous discharge of a satellite charged by space radiation.

Faraday Cage: A complete conductive enclosure used to eliminate external electric fields from the enclosed space.

Flux: Particles crossing a unit area per unit time. Time deravitive of fluence.

Image Charge: When a real charge is located near a conducting surface, charge is induced on the conductor. It is often convenient to think of the fields and potentials as being created by the primary charge and one or more suitably placed charges of appropriate magnitude external to the region of interest that result in the required boundary conditions. There are image charges.

Joule Heating: Conversion of electrical energy to heat. The integral of current density J time electric field E over volume.

Lichtenberg Figures: A tree like discharge pattern produced by the rapid discharge of space charge in a dielectric (plastic).

Monoenergetic: A collection of items that all have the same energy.

PREVIOUS PAGE IS BLANK

GLOSSARY OF TECHNICAL TERMS (Continued)

Photoemission:	Electrons emitted from a solid by absorbing energy (HV) from a photon (Einstein's relation $mv^2/2 = h\nu - W$, where m is the electron wars, v is its velocity, h is planks constant, ν is the frequency, and W is the materials work function.
Plasma:	Highly ionized gas, with nearly equal densities of ions and electrons.
Rastered:	Simultaneous sweeping a small beam from side to side and up and down at different frequencies to produce (quasi) uniform illumination of an area larger than the beam.
SCATHA:	Spacecraft Charging at High Altitudes. An experimental satellite designed to measure spacecraft charging and discharging.
SCC:	SpaceCraft Charging (by charged particles in the space radiation).
Secondary Electron:	As energetic electrons (keV to MeV) pass through material they are slowed down by numerous electron electron collisions. The low energy electrons (10-100 eV) produced by these interactions are secondaries.
SGEMP:	Systems Generated Electromagnetic Pulse. An electromagnetic pulse created by photoemission of electrons from a spacecraft (or other system) exposed to an x-ray radiation pulse.
Stepped Leader:	Cloud to earth natural lightning is thought to be intiated by an ionized track extending from earth to the cloud, composed of a number of field-induced short ionization avalanche steps. The main strokes are then channeled along this leader's path.
Vacuum Ultraviolet:	Light with wavelengths between about 2 and 2000 Å (0.2 to 200 nm) having photon energies of 6 to 5000 eV.

DISTRIBUTION LIST

DEPARTMENT OF DEFENSE

Defense Communications Agency
ATTN: DWSE-E, B. Hoff
ATTN: WWMCCS Sys Engr

Defense Communications Engineer Center
ATTN: Code R401, T. Ellington
ATTN: Code R410, N. Jones

Defense Intelligence Agency
ATTN: DB-4C, Rsch, Phys Vuln Br

Defense Nuclear Agency
4 cy ATTN: TITL
4 cy ATTN: RAEV

Defense Technical Information Center
12 cy ATTN: DD

Dep Under Secretary of Defense
Comm, Cmd, Cont & Intell
ATTN: Comm Sys
ATTN: Surveillance & Warning Sys
ATTN: C3IST&CCS

Field Command, DNA
Det 1
Lawrence Livermore Lab
ATTN: FC-1

Field Command, DNA
Det 2
Los Alamos National Lab/DST
ATTN: MS-635 FC-2

Field Command
Defense Nuclear Agency
ATTN: FCTT, W. Summa
ATTN: FCTP
ATTN: FCTXE
ATTN: FCTO
ATTN: FCLMC, H. Putnam
ATTN: FCPR

Joint Chiefs of Staff
ATTN: C3S Evaluation Office, HDOO
ATTN: GD10 J-5 Nuc & Chem Div

Joint Strat Tgt Planning Staff
ATTN: JLKS
ATTN: JPTM
ATTN: JLK, DNA Rep

National Communications System
ATTN: NCS-TS

National Security Agency
ATTN: J. Hilton

Under Secy of Def for Rsch & Engrg
ATTN: AE
ATTN: C3I
ATTN: Strategic & Space Sys, OS

DEPARTMENT OF THE ARMY

BMD Advanced Technology Center
ATTN: ATC-O

BMD Systems Command
ATTN: BDMSC-H

Dep Ch of Staff for Rsch Dev & Acq
ATTN: DAMA-CSS-N

Harry Diamond Laboratories
ATTN: DELHD-NW-RH, R. Gilbert
ATTN: DELHD-TA-L

US Army Communications Sys Agency
ATTN: CCM-AD-LB, Library

US Army Foreign Science & Tech Ctr
ATTN: DRXST-IS-1

USAMICOM
ATTN: Documents Section

DEPARTMENT OF THE NAVY

Naval Electronic Systems Command
ATTN: PME-106
ATTN: PME-106-1

Naval Research Laboratory
ATTN: Code 4720, J. Davis
ATTN: Code 6701
ATTN: Code 6707, K. Whitney

Naval Surface Weapons Center
ATTN: Code F31

Strategic Systems Project Office
ATTN: NSP

DEPARTMENT OF THE AIR FORCE

Air Force Communications Command
ATTN: XOT

Air Force Geophysics Laboratory
ATTN: PH, C. Pike

Air Force Weapons Laboratory
ATTN: NTN
ATTN: SUL

Air University Library
ATTN: AUL-LSE

Assistant Chief of Staff
Studies & Analysis
ATTN: AF/SASC, C. Rightmeyer

Deputy Chief of Staff
Research, Development & Acq
ATTN: AFRDQI
ATTN: AFRDS, Space Sys & C3 Div

DEPARTMENT OF THE AIR FORCE (Continued)

Deputy Chief of Staff
Plans and Operations
ATTN: AFXOX, C2 & Telecom
ATTN: AFXOKS

Office of the Secretary of the Air Force
ATTN: Director

Rome Air Development Center
ATTN: ESR/ET, E. Burke

Space Command
ATTN: ADCOM DE

Space Division
ATTN: XR, Plans
ATTN: YDE
ATTN: YEZ
ATTN: YGJ
ATTN: YH
ATTN: YKF
ATTN: YKM
ATTN: YNV

Strategic Air Command
ATTN: XPFS
ATTN: NRI-STINFO Library

OTHER GOVERNMENT AGENCIES

Central Intelligence Agency
ATTN: OSWR/STD/MTB

Department of Commerce
National Oceanic & Atmospheric Admin
ATTN: F. Fehsenfeld

NASA, Lewis Research Center
ATTN: Library
ATTN: C. Purvis
ATTN: N. Stevens

DEPARTMENT OF ENERGY CONTRACTORS

University of California
Lawrence Livermore National Lab
ATTN: Technical Info Dept Library

Los Alamos National Laboratory
ATTN: Reports Library

Sandia National Laboratories
ATTN: T. Dellin

Sandia National Laboratories
ATTN: Org 9336, D. Allen
ATTN: Tech Lib 3141

DEPARTMENT OF DEFENSE CONTRACTORS

Aerospace Corp
ATTN: P. Hansen
ATTN: D. Schmunk
ATTN: V. Josephson
ATTN: H. Phillips
ATTN: Library

DEPARTMENT OF DEFENSE CONTRACTORS (Continued)

AVCO Systems Division
ATTN: Library

BDM Corp
ATTN: D. Shaeffer

Beers Associates, Inc
ATTN: B. Beers

California Institute of Technology
ATTN: P. Robinson

Computer Sciences Corp
ATTN: A. Schiff

Dikewood Corporation
ATTN: Technical Library

Dikewood Corporation
ATTN: K. Lee

EG&G Wash Analytical Svcs Ctr, Inc
ATTN: Library

Electro-Magnetic Applications, Inc
ATTN: D. Merewether

EOS Technologies, Inc
ATTN: B. Gabbard

General Electric Co
ATTN: D. Tasca
ATTN: J. Peden
ATTN: H. ODonnell

General Research Corp
ATTN: A. Hunt

Hughes Aircraft Co
ATTN: Technical Library

Hughes Aircraft Co
ATTN: L. Darda
ATTN: E. Smith
ATTN: W. Scott
ATTN: A. Narevsky

IRT Corp
ATTN: N. Rudie
ATTN: B. Williams
ATTN: Library

JAYCOR
ATTN: W. Radaski

JAYCOR
ATTN: R. Stahl
ATTN: Library
ATTN: E. Wenaas

JAYCOR
ATTN: E. Alcaraz
ATTN: R. Sullivan

JAYCOR
ATTN: R. Poll

DEPARTMENT OF DEFENSE CONTRACTORS (Continued)

JAYCOR
ATTN: M. Bell

Johns Hopkins University
ATTN: P. Partridge

Kaman Sciences Corp
ATTN: D. Osborn
ATTN: Library
ATTN: W. Rich
ATTN: N. Beauchamp

Kaman Tempo
ATTN: DASIAC
ATTN: W. McNamara

Kaman Tempo
ATTN: DASIAC

Lockheed Missiles & Space Co, Inc
ATTN: L. Chase

Lockheed Missiles & Space Co, Inc
ATTN: Dept 85-85

Martin Marietta Corp
ATTN: B. Broulik
ATTN: J. Casalese

McDonnell Douglas Corp
ATTN: R. Kloster
ATTN: R. Andrews

McDonnell Douglas Corp
ATTN: S. Schneider

Mission Research Corp
ATTN: M. Scheibe
ATTN: C. Longmire
ATTN: R. Stettner

New Technology, Inc
ATTN: D. Divis

Pacific-Sierra Research Corp
ATTN: H. Brode, Chairman SAGE

DEPARTMENT OF DEFENSE CONTRACTORS (Continued)

Mission Research Corp
ATTN: Library
4 cy ATTN: J. Riddell
4 cy ATTN: B. Passenheim
4 cy ATTN: V. van Lint
4 cy ATTN: B. Kitterer
4 cy ATTN: J. Vahldieck
4 cy ATTN: N. Hall
5 cy ATTN: Doc Con

Physics International Co
ATTN: J. Shea

R&D Associates
ATTN: S. Siegel
ATTN: Technical Information Center
ATTN: P. Haas

R&D Associates
ATTN: C. Rogers

Rockwell International Corp
ATTN: Library

S-CUBED
ATTN: Library
ATTN: A. Wilson

Science Applications, Inc
ATTN: W. Chadsey
ATTN: J. Tigner

SRI International
ATTN: Library

SRI International
ATTN: A. Padgett

TRW Electronics & Defense Sector
ATTN: Technical Information Center
ATTN: D. Clement

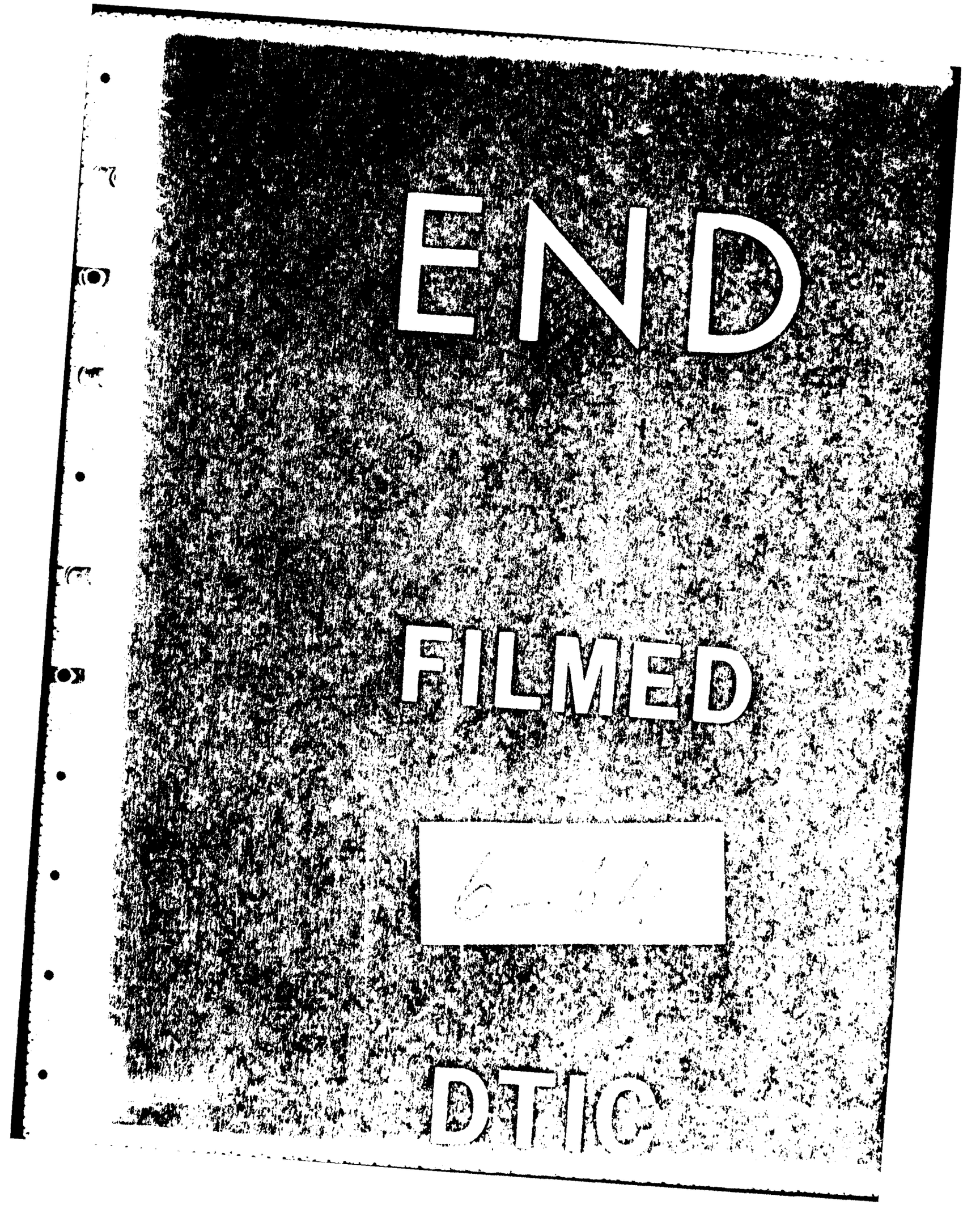
END
FILMED
DTIC